LOCALIZED CORROSION OF NICKEL AND NICKEL-MOLYBDENUM ALLOYS

LOCALIZED CORROSION OF NICKEL AND NICKEL-MOLYBDENUM ALLOYS

BY

MOHAMMED ZAMIN, M.Eng.

A Thesis

Submitted to the School of Graduate Studies

in Partial Fulfilment of the Requirements

for the Degree

Doctor of Philosophy

McMaster University

January 1976

DOCTOR OF PHILOSOPHY (1976) McMASTER UNIVERSITY
(Metallurgy and Materials Science) Hamilton, Ontario

TITLE: Localized Corrosion of Nickel and Nickel-Molybdenum Alloys

AUTHOR: Mohammed Zamin, B.Tech. (Hons) (Indian Institute of Technology, Kharagpur).
D.I.I.T. (Indian Institute of Technology, Kharagpur).
M. Eng. (McMaster University).

SUPERVISOR: Professor M. B. Ives

NUMBER OF PAGES: xix,287

ABSTRACT

This investigation is concerned with the study of the localized corrosion of nickel and the effect of the addition of molybdenum on its corrosion properties. To this end, alloys containing up to 30 wt % Mo have been studied in 1N H_2SO_4 and chloride containing environments by potentiostatic and galvanostatic techniques and 'in-situ' microscopic observations.

The anodic oxidation of nickel has been studied by the galvanostatic technique. The experimental results have been used to develop the kinetic equation describing the film growth on nickel. It has been shown that an inverse logarithmic behaviour is obtained in that the film growth current density is inversely proportional to the charge stored in the film. The resistivity of the film has been calculated and its value suggests that the film is pure and almost stoichiometric NiO.

The significance of the Flade potential of nickel in 1N H_2SO_4 solution is discussed in view of the results obtained and those existing in literature. The implications of the critical potential for determining the susceptibility to pitting corrosion of metals and alloys has been investigated for Ni and Ni-Mo alloys. It is concluded that the critical potential does not adequately describe the electrochemical conditions required for the pitting corrosion of Ni and Ni- Mo alloys in sulfuric acid solutions containing chloride ions.

The passive electrode has been treated as a metal-semiconductor system and justification has been provided for the assumption of a 100% efficiency for the current density during cathodic reduction.

The charge required to reduce the film formed on Ni and Ni-Mo alloys in 1N H_2SO_4 and in the presence of chloride ions is reported. Some information is provided on the nature of the film on the Ni-Mo alloys in chloride containing solutions. Studies are reported on the polarization behaviour of the Ni-Mo alloys in synthetic sea water and on the corrosion morphology obtained after 30 day immersion in synthetic sea water and an acidic chloride containing solution.

It is proposed that the improved resistance to corrosion of Ni-Mo alloys in naturally corroding systems is due to a sluggish anodic reaction imparted by a slow hydration of the metallic ions, while under anodic polarization in the presence of chloride ions it is due to the presence of a diffusion barrier film of MoO_3. The results obtained on the Ni-Mo alloys have been explained on the basis of a defect model for the passive film on the alloys.

ACKNOWLEDGEMENTS

My sincerest thanks and gratitude to my supervisor, Dr. M. B. Ives, for his guidance, encouragement and counsel throughout the duration of my graduate work. His sensitiveness to the problems that beset one, both academically and personally, can only be paralleled by his warm friendship. I shall always cherish my association with him.

My thanks also to Dr. W.W. Smeltzer and Dr. O. E. Hileman who served as members of my Ph.D. Supervisory Committee. I deeply appreciate their keen interest, advice and guidance throughout my Ph.D. research.

I thank Dr. R. Kelly for bringing to my attention the solid-state implications of simple electrode processes, for his candid comments and enlightening discussions. I am grateful to Dr. G.R. Purdy for his help towards the x-ray diffraction part of this work. His eager involvement and insight were invaluable.

I owe my thanks to the technical staff of both the Department of Metallurgy and Materials Science and the Institute for Materials Research - in particular to Mr. Frank Gibbs, Mr. Fred Smith, Mr. Fred Pearson and Mr. Martin Van Oosten. I also gratefully acknowledge the expertise of Mr. Rudy Palme, the university glass blower. I appreciate the help offered by Mr. Henry Behmann, Department of Chemical Engineering in obtaining the atomic absorption analysis for the nickel in solution.

The manuscript was typed with skill and remarkable patience by Mrs. Helen Kennelly, to whom I give special thanks. The figures were drawn with precision by Mr. David Hodgson, whose general expertise and constant help I gratefully acknowledge.

My heartfelt thanks to two of my special friends who saw me through the ups and downs of graduate study. To Mrs. Angela Manolescu and Mr. Satinder Vig my gratitude for their understanding, friendship and moral support.

I thank the following for providing the financial assistance - McMaster University, in the form of a graduate assistantship, and the Defense Research Board and the National Research Council, in the form of research grants to Dr. Ives.

Last and by no means least, my thanks to a very special person. In the short time that I have known her, her friendship and counsel, kindness and sincerity, and above all, her love and understanding have shown me an entirely new aspect of life and made the last and most difficult days of graduate work more enjoyable. To Catherine Jean Good, my deepest gratitude.

Finally, there are many others who, either directly or indirectly, were involved at various stages of this work. They are too numerous to mention by name, yet have been too kind to be completely forgotten. To all of them, I remain deeply indebted.

TABLE OF CONENTS

LIST OF ILLUSTRATIONS

LIST OF TABLES

CHAPTER I

INTRODUCTION

The progress of modern technology places extraordinary demands on material properties. Among them, improved resistance to corrosion, the destruction or deterioration of a material by chemical or electrochemical reaction with its environment, is second perhaps only to mechanical properties.

Almost all materials corrode in one environment or another. A combination of material and environment that does not result in corrosion is usually quite specific - the material having been developed for the particular application. Unfortunately, this places considerable restraints on the versatility of engineering materials.

A metal or alloy may undergo many different forms of corrosion depending upon its metallurgical nature and its environment. If a large portion of the surface is affected, the attack is said[1] to be 'General Corrosion'; if only small areas, it is called 'Localized Corrosion'. Specific cases such as crevice corrosion, pitting corrosion, intergranular corrosion, selective leaching and even stress corrosion have come to be regarded as forms of localized corrosion.

1.1 Significance of Localized Corrosion

The importance of the form of localized corrosion which a metal or alloy experiences depends upon the particular

application. For example, Wilde[2] has pointed out that for stainless steels in sea water applications crevice corrosion is the most important form. In general, crevices cannot be avoided in engineering structures and are therefore a reality which every corrosion engineer must accept. Without undermining their importance, in instances where no crevices are present and no stresses involved, the two most important forms of localized corrosion are probably pitting and intergranular corrosion.

Although many definitions of pitting are available, it may simply be defined[1] as 'corrosion confined to small points so that definite holes are produced in an otherwise almost unattacked surface'. Pitting may be regarded as an intermediate stage between general corrosion and corrosion resistance. If a material is in the corrosion resistant state, the entire surface of the material is inert and no corrosion occurs. However, if this resistance breaks down at discrete places, these exposed areas become anodic to some regions of the surface which are cathodic. Owing to the unfavourable area ratio, corrosion at the exposed points is extremely high resulting in pitting of the surface. Various metals including nickel, iron, chromium, aluminum, copper, zinc, tin and many of their alloys are prone to this form of corrosion attack.

Intergranular corrosion, as the name implies, is corrosion confined to the grain boundaries. A drastic deterioration in mechanical properties may occur due to intergranular corrosion because the grooves formed result in areas of stress concentra-

tion. The failure of austenitic stainless steels as a result of sensitization occurs through intergranular corrosion[3]. Sensitization (heating in the temperature range of 600-700°C for some time followed by slow cooling) results in the precipitation of carbides along the grain boundaries[3]. This is detrimental in two ways. First, it uses up the chromium leaving a 'chromium-depleted zone' on either side of the grain boundaries, and secondly, the carbides are cathodic to the depleted zone which further aids corrosion. A parallel effect is encountered with nickel-base alloys. In alloys which have a small amount of carbon, carbides are precipitated along the grain boundaries. For example, Hastelloy B (see Table 1-1) in the annealed condition (1150°C) contains randomly distributed M_6C type carbides of approximate composition Ni_3Mo_3C[4]. If the temperature is increased (a necessity during welding) there is a tendency for the molybdenum content of the M_6C to increase, for example to Ni_2Mo_4C, and for Mo_2C to form. Intergranular corrosion is then attributed to preferential attack of molybdenum depleted zones adjacent to high molybdenum M_6C and Mo_2C with the latter probably playing the major role[4]. Susceptibility in material exposed to temperatures of about 800°C can again be attributed to molybdenum depletion[4], in this case adjacent to the intermetallic compound Ni_4Mo predicted from the nickel-molybdenum phase diagram. Segregation of solute atoms along grain boundaries without the formation of another phase has also been shown to produce intergranular corrosion[5].

Although corrosion is undesirable in any form, general corrosion is the preferred alternative over any form of localized corrosion. It might be said that general corrosion becomes more dangerous the more restricted the area on which it is concentrated.

1.2 Development of Nickel-Base Alloys - Status of the Hastelloys

Pure metals are not practical engineering materials. Apart from the fact that they are prone to corrosion, their greatest drawback is their low strength. As the demands on the mechanical properties of a material increase, a pure metal is alloyed to produce a simple binary, ternary or quartenary alloy. Often other elements are added in minor quantities thus making the alloy a complex system not only metallurgically but also from a corrosion view point. A knowledge of the metallurgical nature of an alloy is necessary to understand fully and to predict its corrosion behaviour.

Nickel is more noble than iron and less so than copper in the electromotive series[6]. It does not readily discharge hydrogen from any of the common non-oxidizing acids so a supply of some oxidizing agent such as dissolved air is necessary for appreciable rates of corrosion. As a general rule, oxidizing conditions favour corrosion of nickel while reducing conditions retard corrosion[7]. Nickel is resistant to corrosion by sea water when it is in motion, rates of attack being usually less than 30 mdd*. However, it may suffer pitting under conditions

*mdd ≡ milligrams per square decimeter per day

of stagnant exposure[8].

Alloying nickel with copper moderately improves the resistance to corrosion under reducing conditions. The nickel-copper alloys find their greatest use in sea water under conditions of high velocity, although they tend to pit under stagnant exposure[7]. Their uses also include the holding of boiling sulfuric acid solutions (in concentrations of less than 20% by weight) and of non-oxidizing acids such as hydrochloric, hydrofluoric and phosphoric when deaerated. However, oxidizing acids such as nitric and nitrous severely attack the alloys[8].

A noticeable increase in corrosion resistance is achieved by substituting chromium for copper. These alloys, containing 60-80% nickel and 13-20% chromium with the remainder mostly iron are referred to as Ni-Cr alloys. Of these, the 79.5% Ni-13% Cr-6.5% Fe alloy (called Inconel) is the most widely used for corrosion resistant purposes. The most significant differences in the performance of these alloys are, on the one hand, in very strongly oxidizing solutions such as nitric acid (except those of oxidizing halogens), where higher chromium content is usually most effective, and, on the other hand, in reducing acids such as hydrochloric, where increased nickel content is usually beneficial. However, the oxidizing effect of dissolved air alone is not sufficient to insure complete passivity and freedom from attack in air-saturated mineral acids. The Ni-Cr alloys are moderately resistant to rapidly flowing sea water, but may be prone to pitting under stagnant exposure[8].

Interest in the Ni-Mo alloys for resistance to corrosion began about 1920 in an attempt to utilize the excellent resistance to corrosion that molybdenum offers in non-oxidizing acids. However, little use was made of the binary Ni-Mo alloys because of the difficulty of preparing them free from other metallic elements[8]. Although the corrosion resistance of these alloys, particularly in hydrochloric acid, is excellent, the cost of preparation was too great to warrant their commercial use.

The development of the Ni-Mo alloys for industrial use was started about 1927. In an attempt to compromise corrosion resistance, cost, and workability, part of the molybdenum was substituted with iron and later with chromium[9]. These alloys, which were designated as Ni-Mo-Fe-(Cr) alloys, were given the name Hastelloys*. Although many different grades of the Hastelloys are available on the market, the composition of the three most common grades is given[7] in Table 1-1. Hastelloy B is usefully resistant to hydrochloric acid of all concentrations and temperatures up to the boiling point[7]. Its resistance to boiling sulfuric acid is good up to 60% H_2SO_4, but its resistance to oxidizing acids, eg HNO_3, or to oxidizing metal chlorides, eg $FeCl_3$, is extremely poor[7]. Hastelloy C offers excellent resistance to corrosion in oxidizing media such as nitric acid, chromic acid, and acid mixtures such as nitric-sulfuric acid

*Trade mark of the Haynes Stellite Co.

Table 1-1

Nominal Composition (wt %) of the Hastelloys*

	Ni	Mo	Co	Cr	W	Fe	Si	Mn	C	Others
Hastelloy B	61 approx.	26-30	2.5 max	1.0 max	-	4-7	1.0 max	1.0 max	0.05 max	-
Hastelloy C	54 approx.	15-17	2.5 max	14.5-16.5	3.0-4.5	4-7	1.0	1.0 max	0.08 max	-
Hastelloy F	46 approx.	5.5-7.5	2.5	21-23	1.0 max	20	1.0 max	1-2	0.05 max	Cb+Ta 1.75-2.50

*Trademark, Haynes Stellite Co.

as well as ferric chloride[7,8]. It has good resistance to attack by hydrochloric acid at room temperature and offers excellent resistance to pitting and weight loss in sea water[8]. Hastelloy F containing about 2% Cb and some Ta is resistant under oxidizing as well as reducing conditions[7].

One of the major drawbacks of these alloys has been their susceptibility to intergranular corrosion if improperly heat treated. The temperatures producing susceptibility are in the range of about 500°-700°C. In this range, grain boundary precipitation occurs in short times, that is, in less than a few minutes[4]. Intergranular corrosion has been detected in a variety of acid media (sulfuric acid-ferric sulfate, hydrochloric acid and chromic acid)[4]. Small amounts of columbium have been helpful in stabilizing the alloys with respect to intergranular corrosion by preventing carbide precipitation. However, the best method for avoiding intergranular attack in these alloys is to use them in the water quenched condition (from about 1200°C).

1.3 Aims of the Present Investigation

The aims of the present investigation are to study the effects of molybdenum addition on the corrosion properties of nickel. There are two reasons for the choice of the Ni-Mo system for this investigation. First, the Hastelloys are essentially Ni-Mo alloys and, therefore, a complete and clear understanding of the binary system up to about 30% molybdenum is needed to better understand the corrosion behaviour of the Hastelloys. Secondly, molybdenum does not exhibit the typical

active-passive polarization behaviour of nickel whereas the alloys do. It would,therefore, be interesting to examine the mechanism by which these alloys retard corrosion. Furthermore, the extent of corrosion is greatly affected by the metallurgical structure. The Ni-Mo binary also provides a convenient system where solid solution effects on corrosion can be studied by employing appropriate heat treatments.

As will be evident in later chapters, information on the corrosion characteristics of nickel in 1N H_2SO_4 is substantial. Since previous work on nickel in this laboratory had been performed in 1N H_2SO_4, the extension of the investigations to the Ni-Mo alloys H_2SO_4 seemed the obvious choice of medium. It became clear that this was a good choice when it was found that all data in the literature on the corrosion properties of the Ni-Mo system are confined to acid solutions (HCl, HBr, and H_2SO_4). An acid solution thus provided a means of comparison of the results with existing data. H_2SO_4 also provided a large concentration of hydrogen ions (whose presence is known to be detrimental in corrosion[6]) without providing the aggressive chloride ions (whose concentration could be adjusted by appropriate additions of 1N NaCl). Thus a broader range of environments could be studied.

1.4 An Outline of the Presentation which Follows

In the presentation which follows,Chapter II will deal with the principles of the electrochemistry of corrosion and the existing knowledge of the metallurgy and corrosion characteristics

of nickel and nickel-molybdenum alloys. Chapter III will outline the experimental techniques and procedures employed. Chapter IV will deal with the corrosion behaviour of nickel and examine film thickness and galvanostatic film growth in 1N H_2SO_4. Chapter V will be devoted to alloy characterization and the corrosion behaviour of Ni-Mo alloys in 1N H_2SO_4 and in chloride containing solutions. Finally, Chapter VI will examine the kinetics and mechanisms of the passive film formation on nickel along with the significance of the Flade potential. It will discuss the importance of the critical potential and the validity of film thickness measurements, and examine the effect of molybdenum addition on the corrosion properties of nickel.

CHAPTER II

REVIEW OF LITERATURE

THE ELECTROCHEMISTRY OF CORROSION

2.1 The Concept of Anodic Polarization

A material may be polarized (anodically or cathodically) by means of a potentiostat. However, before a detailed description of the consequences of anodic polarization is undertaken, it is important to understand the function of a potentiostat and the meaning of the terms anodic reaction and polarization.

A potentiostat is an electronic device which is capable of adjusting the current in a corrosion cell so as to maintain the potential (present with respect to a reference electrode) constant. An anodic reaction is one where ions of a metal are removed from the lattice sites and passed into solution. For instance

$$Ni \rightarrow Ni^{2+} + 2e$$

is an anodic reaction. Naturally the reverse reaction, ($Ni^{2+} + 2e \rightarrow Ni$) which involves the consumption of electrons, is a cathodic reaction. In an acid solution the normal cathodic reaction is,

$$2H^{+} + 2e \rightarrow H_2\uparrow \ .$$

The term polarization may be understood in the following manner. When a material is introduced in an aqueous environment it

attains a certain potential and corrodes at a certain rate. After some time, a steady state potential is attained (known as E_{corr}) which implies a steady state corrosion rate. At this stage, the rates of the anodic and cathodic reactions are equal. However, if by an external means, for example a potentiostat, the equilibrium situation is disturbed, the material is said to be polarized. If the impressed source shifts the potential to a value which is more positive or noble than the steady state corrosion potential, the material is said to be anodically polarized whereas if the potential shift is in the negative or active direction the material is considered to be cathodically polarized.

When a material is anodically polarized, i.e. its electrode potential is made more positive than its corrosion potential, the dissolution rate increases exponentially. The corrosion product is normally a salt of the metallic ion and the anion in solution and tends to form as a deposit on the metal surface. Local very high current densities occur at discontinuities in this deposit and it gradually spreads over the whole surface. In materials which are capable of exhibiting an active-passive transition, a certain stage is reached when the dissolution rate falls markedly, and the material is said to be passivated. The passivation occurs due to the formation of a thin film. The potential at which the passivation occurs is known as the primary passive potential, E_{pp}, and the critical anodic current maximum at

this potential is designated by i_c. If the polarization of the material is continued further, there is no appreciable increase in the corrosion current. At this stage two processes occur simultaneously on the surface of the specimen - the formation of the passive film due to the anodic control of the electrode and dissolution of the film due to the bulk solution. As long as the rate of film formation is greater than (or at least equal to) the rate of film dissolution, the electrode remains passive. The current in this region is known as the 'passive current' and is designated by i_p. It is many orders of magnitude lower than i_c and, in many instances, is independent of potential over a certain range. On still further polarization, a potential is reached after which the anodic current again begins to increase. This potential is termed the 'critical potential', E_c. There are various beliefs as to the phenomenon occurring in this region. The evolution of oxygen is certainly one of them. Among others, the increase in the anodic current is attributed to the oxidation to a higher state of the previous film or the increased ability of the metal ions to pass through the film due to high fields. Thus, based upon the manner in which the material behaves, the anodic polarization curve (Figure 2-1) exhibits three regions, called 'active', 'passive' and 'transpassive'. If the polarization direction is reversed in the transpassive region, the curve may or may not follow its original path.

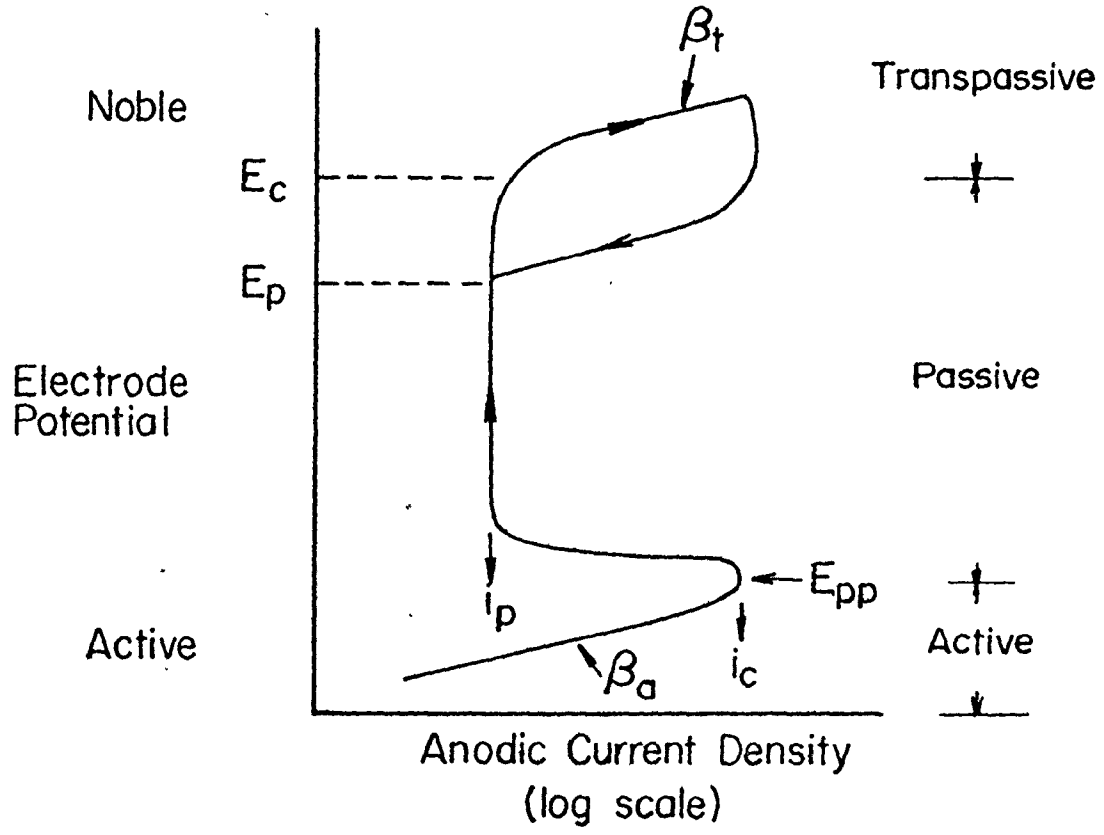

Figure 2-1. Schematic representation of an anodic polarization curve. Various symbols used in the text are also shown.

The point of intersection of the reverse scan with the curve in the passive region yields another potential known as the 'protection potential', E_p. The significance of this potential and its cause will be dealt with later.

The processes occurring in the transpassive region are different in the presence and absence of chloride ions. In this investigation, however, any variation in the critical potential is considered to arise as a result of the processes occurring during the breakdown of the passive film in the presence of chloride ions, and the subsequent development of localized attack.

The rate of an electrochemical reaction is represented by the current density. Since an anodic reaction cannot occur in complete isolation and requires a cathodic reaction to sustain it, the total current density (i) in a corroding system is composed of the anodic and cathodic current densities. In obtaining the value of the total current density, the partial anodic and cathodic current densities are added algebraically (which means that if the anodic current density is considered to be positive then the cathodic current density is taken to be negative). The relationship between the potential and the total current density is given by the following equation

$$i = i_o[\exp(\frac{\alpha F}{RT}\eta) - \exp(-(\frac{\alpha' F}{RT}\eta)] \qquad (2\text{-}1)$$

where i_o = the corrosion current density, i.e. the current density corresponding to the stage when the rates of the anodic and cathodic reactions are equal to each other without any impressed potential or current.

η = overvoltage = $E-E_{corr}$, the difference between the impressed potential and the corrosion potential (or the spontaneous potential)

α = a kinetic constant, sometimes called the Tafel constant for the anodic reaction

α' = a kinetic constant (the Tafel constant) for the cathodic reaction.

T = temperature in °K

R = Universal gas constant

F = Faraday, 96500 Coulombs.

Equation (2-1) is a modification of the Butler-Volmer equation which is central to electrode kinetics and the derivation of which may be found in any standard electrochemical text[10,11]. The first term in Eqn. (2-1) is the contribution to the current density of the forward reaction aided by the overvoltage while the second term is the contribution of the reverse reaction in a direction opposed by the overvoltage.

Although many specific cases arise in simplifying equation (2-1), only one of them will be dealt with here owing to its specific relevance to corroding systems. When the irreversibility of the electrode process is high, i.e. $\eta > 50$ mV, then the rate of the reaction in the direction opposed by the overvoltage is reduced to negligible proportions. Thus, the second term on the right hand side of Eq. (2-1) can be neglected. Hence,

$$i = i_o \exp\left(\frac{\alpha F}{RT}\,\eta\right) \qquad (2\text{-}2)$$

and by taking logarithms and transposing,

$$\eta = \left(-\frac{2.303\ RT}{\alpha F}\right) \log i_o + \left(\frac{2.303\ RT}{\alpha F}\right) \log i$$

or

$$\eta = a + \beta \log i \qquad (2\text{-}3)$$

which is known as Tafel's Law.

The terms $a = \left(-\frac{2.303\ RT}{\alpha F}\right) \log i_o$ and $\beta = \left(\frac{2.303\ RT}{\alpha F}\right)$ are constants for a particular system. The term β is known as the Tafel slope and a subscript 'a' or 'c' is generally used to refer to the anodic or cathodic Tafel slope.

An alternate manner of defining the Tafel slope is by differentiating Eqn. (2-3). Then,

$$\beta = \frac{\partial \eta}{\partial \log i} \quad . \qquad (2\text{-}4)$$

Consequently, the unit of β is mV/decade (or simply mV). Since it is more convenient to plot the polarization curve as potential vs current density, the definition of β is slightly modified and the overvoltage term in Eqn. (2-4) is replaced by the potential term. Then,

$$\beta = \frac{\partial E}{\partial \log i} \quad . \qquad (2\text{-}4(a))$$

It is evident that a large value of β implies a sluggish reaction rate whereas small values of β correspond to highly corroding systems.

Often, though not always, the increase in the current density in the transpassive region (beyond E_c) is also exponen-

tial. Thus, on lines similar to those just discussed for the 'active region', a transpassive slope β_t, may be defined as,

$$\beta_t = \left(\frac{\partial E}{\partial \log i}\right)_{\text{transpassive}} . \qquad (2\text{-}4(b))$$

In the present analysis, β_a has been calculated by fitting the best straight line to points in the active region lying between the potential limits $(E_{corr}+50)$ mV and $(E_{corr}+200)$ mV where as β_t has been estimated in a similar manner to points lying between the limits (E_c+50) mV and (E_c+200) mV.

The terms E_{pp}, E_c, i_p, i_c, β_a etc. will be referred to as the anodic polarization parameters. Extensive use will be made of these parameters in comparing the performance of the alloys during later chapters.

2.2 The Phenomenon of Passivity

The phenomenon of metallic passivity has fascinated scientists and engineers since the days of Faraday. The phenomenon itself is rather difficult to understand because of its complex nature and the specific conditions under which it occurs.

Notwithstanding the comparatively frequent and readily observed manifestations of passivity, no all-inclusive definition of this phenomenon has been advanced. Many investigators do not provide a concrete defintion of passivity but instead substitute a description of the phenomenon. However, on the basis of the theory of electrochemical corrosion, the phenomenon of passivity of metals is most rationally defined in the following manner:[12]

> "Passivity is a state of high corrosion resistance of metals or alloys (under conditions when their reactions are thermodynamically possible) caused by inhibition of the anodic process, that is, a passive state is a state of corrosion resistance caused by an increased anodic control."

This definition includes the ennoblement of potential observed in most cases of passivity and is not confined only to a particular positive shift of potential.

2.2.1 Theories of Passivity

Many theories of passivity have been put forward and numerous modifications of the basic theories have been proposed.

The most fundamental and generally accepted theories at present are those explaining the passive state on the basis of a film or adsorption mechanism accounting for inhibition of anodic dissolution.

2.2.1(a) Generalized Film Theory

While considering the behaviour of iron in concentrated nitric acid, the mechanism of passivity was proposed by Faraday[13] more than 100 years ago in the following terms" "The surface of iron is oxidized ... or is in such relation to the oxygen of the electrolyte as to be equivalent to oxidation ...". The first theory of passivity was propounded by Evans[14]. This theory considers the passive state as the appearance of a very thin, often invisible protective film of products formed by reaction of the environment with the metal. Very often this thin film represents some form of metallic oxide.

In a number of cases, besides films that inhibit the anodic process and that have thickness of hundred or even tens of atomic layers, thinner monomolecular protective adsorption layers of oxygen, oxidant or other substances can exist and produce passivity - that is,cause a so-called adsorption passivity.

Although the concept of adsorption was developed by Uhlig[8] as a separate means of explaining the phenomenon of passivity, it is best to look upon adsorption as the stage prior to film formation. The adsorption of oxygen atoms (and sometimes other species) leads to a reorganization or shift

of the electrode potential in the double layer which strongly inhibits metal dissolution. Hence, anodic inhibition emerges as an electrochemical mechanism.

Some workers[15] believe that the establishment of passivity requires at least a continuous coverage of the surface with an adsorbed monomolecular layer of oxygen atoms. Others[16], however, think that it is only necessary to have oxygen adsorption on the more actively dissolving surface area.

In recent years, it has been pointed out that in addition to the purely electrochemical adsorption mechanism, consideration must also be given to the formation on the surface of adsorbed (chemisorbed) compounds, and the formation of electric dipoles as a result of partial ionization of the oxygen atom by an electron from the metal which changes the chemical and electrochemical reactivity of the metal.

A generalized view of the phenomenon of passivity invokes the idea that the first step towards passivity is the adsorption of the oxidant on the initially bare metal surface followed by thickening of the film with time. For as the adsorbed film in the process of thickening gradually transforms into an oxide film, the retardation of the anodic process promoted by a change in the double layer structure will also be supplemented by the greater difficulty encountered by ions passing through the protective film.

2.2.1(b) Electron Configuration Theory

This theory, which accounts quantitatively for critical passivity concentrations, was outlined by Uhlig and Wulff[17,18]. According to this theory, the ease in forming a passive state is associated with noncomplexity of the internal shells of a metal, as, for instance, the easily passivated transition metals of the periodic table (chromium, nickel, cobalt, iron, molybdenum and tungsten), which have incomplete levels in the metallic state.

Adsorption of oxygen or oxidant results in passivity, because the adsorption of the oxidant leads to the incorporation of electrons from the metal resulting in unfilled electron levels in the metal. Adsorption of hydrogen or reducing agents in general, on the contrary, provides electrons to the metal, filling the d level and converting the metal into the active state.

The corrosion behaviour of Ni-Cu alloys has provided considerable support to this theory. When nickel with 0.6 electron holes per atom in the d band, is alloyed with a non-transitional metal, e.g. copper (with no d-electron holes), electrons from copper contribute to the unfilled d-electron levels of nickel. The alloy retains the transitional metal characteristics of nickel so long as the d-electron holes are not completely filled. Specific heat and magnetic measurements of the Ni-Cu alloys show that the d band of energy levels is filled at about 60 atom % or 58 wt % Cu and is

unfilled at lower copper compositions. The alloys therefore are expected to be passive and to behave like nickel below 60 atom % Cu (> 40% Ni), but to be active and to behave more like copper at higher copper compositions. Corrosion rate and anodic polarization data[19,20] confirm that lowest corrosion occurs in alloys containing a minimum of about 40-50% nickel.

Several other alloy systems exhibit critical compositions for passivity[21]. Examples are the Ni-Mo, Co-Cr, and Ni-Cr alloys for which the critical alloy compositions as determined from the lowest value of i_c comes at values specific to each alloy. Critical alloy compositions for passivity have also been observed[18,22] in the three- or four-component alloy systems, e.g., Fe-Ni-Mo, Cr-Ni-Fe and Fe-Cr-Ni-Mo.

Many objections have been levied against the electron configuration theory. Properties of metals depend on the internal structure of the atoms and consequently on the electron configuration in the metal. But passivity is determined not only by the metal but to a large extent also by the environmental conditions. Therefore, it is difficult to believe that the passive state is explained by the electron configuration only.

Actually the electron configuration theory does not explain all the aspects of the passive state that are not covered by the generalized film theory. The major objection

to this theory is that the capability of transition into a passive state is a property not only of the transition metals but also of aluminum, magnesium, beryllium and many others. Under suitable conditions almost all metals can be rendered passive, including those that do not have any free electron levels. However, in all fairness, credit must be given to the theory in its ability to explain the passive behaviour of the transition metals. To quote Evans[23] "... Probably an impartial judge would say that, although further work is needed to establish the contention, the balance of evidence is in its favour."

2.3 The Phenomenon of Localized Corrosion

The occurrence of corrosion is the direct consequence of an anodic reaction where atoms from the metal lattice enter solution aided by other ions from the solution. The dynamic viewpoint is that the extent of corrosion on a metal surface depends on the active anode/cathode site ratio, being higher if this ratio is large and vice versa. If the sites are mobile, general corrosion is encountered, whereas if they are fixed, localized corrosion results. It might be said that localization of the anodic reaction results in localized corrosion and that a combination of large cathode and small anode is always favourable to a high intensity of local attack. Among factors that tend to aid the unfavourable area ratio and to localize the anodic reaction are imperfections - whether these be in the metal or in the passive film. These imperfec-

tions may be scratches, dislocations, structurally disturbed regions such as grain boundaries and slip traces, inhomogeneity in composition, microsegregation of solute and dominant residual impurities, inclusions and precipitation of second phase particles. The extent of localization of the anodic reaction and its origin will determine whether the attack is pitting or intergranular corrosion. Intergranular corrosion may be regarded as an advanced stage of grain boundary pitting.

2.3.1 Theories of Localized Corrosion

There is, perhaps, no general theory that covers all the known forms of localized corrosion. The similarity among them ends at the fact that they all result in a high intensity of localized attacks. Therefore, in dealing with this section the theories of pitting will be dealt with at first, followed by the theory of intergranular corrosion and a brief comment on the two forms of localized corrosion.

2.3.1.1 Theories of Pitting Corrosion

The phenomenon of pitting corrosion occurs in two distinct stages; first, nucleation of pits and, secondly, growth of pits. It is not possible to categorize the several divergent views that have been advanced. Nevertheless, two broad divisions may be made.

2.3.1.1(a) Penetration Theory

This theory owes its origin to Hoar[24]. It is proposed

that the initiation of pits might be due to the adsorption of aggressive anions on the surface of the oxide film followed by the penetration of ions through the film. Anion entry, without exchange, into the film is postulated as producing a greatly induced ionic conduction in the contaminated oxide film, which thus becomes able (at certain points) to sustain high current density and to produce brightening by random removal of cations. When the field across the film/solution interface reaches a critical value, pitting occurs.

Later, Hoar suggested two modifications of the basic theory[25,26]. Except for elaborating on the details of the mechanism, the basic concept still remains the same.

2.3.1.1(b) Displacement Theory

On the basis of the adsorption concept of passivity, the formation of pits is described as a result of a competitive adsorption of chloride ions and oxygen. Pits develop on the spots where oxygen adsorbed on the metal surface is displaced by chloride ions. Kolotyrkin[27] presumes that even during the dissolution of a passivated metal, irregular distribution of the current does exist on the metal surface, since the latter is never quite homogeneous. On some spots occur a stronger adsorption of chloride ions and a more rapid dissolution of the metal. According to this theory, the breakdown potential represents that minimum electrode potential value, at which the aggressive anions become capable of producing a reversible displacement of the passivating oxygen

from the metal surface.

A consequence of the localization of the anodic and cathodic reaction is, first of all, a noticeable difference in the composition of the solution near the active area from its composition at other sections of the surface and in the bulk. The production of acidity at an anode has been definitely established[28] and occurs as a result of the hydrolysis of the metal chloride produced. It is,therefore, reasonable to conclude that the reaction of displacement of the passivating oxygen takes place only on those sections of the metal surface near which the concentration of the aggressive anion reaches a certain critical value, greater than its bulk concentration. This increase in concentration of aggressive anions near separate areas of the metal surface, leading to depassivation of these sections, can be affected by means of anion transport by the current. This hypothesis is supported by the results of Engell and Stolica[29] who showed that the activating influence of the chloride ions is not observed immediately after their addition into the solution but only after a certain period of time which is longer the lower the concentration of the chloride ions in solution.

2.3.1.2 Theory of Intergranular Corrosion

Owing to the wide range of applications that the stainless steels have been used for, most existing theories on intergranular corrosion have been specifically advanced to explain this phenomenon in stainless steels. The most

plausible and general treatment of the accepted viewpoint follows.

Intergranular corrosion susceptibility (in stainless steels as well as nickel-molybdenum alloys) increases as the carbon content increases.Whereas the carbon is soluble during high temperature annealing, it has very restricted solubility at lower temperatures. Rapid cooling from the annealing temperature results in supersaturation of carbon in solution. Subsequent holding in the sensitization range enables this carbon to precipitate out as alloying element rich carbides along the grain boundaries. Since carbon is an interstitially diffusing species, it has a very high diffusion coefficient and the diffusion occurs uniformly all over the matrix. The alloying element,on the other hand, is invariably substitutional and therefore has a much lower diffusion coefficient. Its diffusion is confined to very narrow regions along the grain boundaries. This situation manifests itself in four different ways:

a) An alloying element depleted zone exists on either side of the grain boundary.
b) The precipitation of the carbide leads to a build-up of strain.
c) The carbide is more noble to the depleted zone - galvanic effect.
d) The depleted zone is more active with respect to the matrix - galvanic effect.

If one combines all the above effects, particularly the alloy depletion and galvanic corrosion concepts, there is feasibly quite a large potential difference between the carbide and the anodic depleted zone. In the presence of a corroding medium, this will result in intergranular corrosion.

In many instances, neither second phase particles nor alloy depleted zones are present along the grain boundaries, yet the grain boundaries are preferentially attacked.

In order to explain this behaviour, two concepts have been advanced. First, that the grain boundaries are attacked because they are high energy regions[30,31] and secondly, that elements segregated at grain boundaries result in a chemical difference between the boundary and the matrix, and this serves as the driving force for corrosion[32]. Attempts have been made to combine the two theories on the basis that the high-energy regions are those most likely to show segregation. However, the very fact that high-purity steels are not susceptible to attack, supports the segregation theory as opposed to that dependant solely on grain boundary energy. Interestingly enough however, the work of Uhlig et al[33] on Ni-Mo alloys in boiling 10% HCl seems to support the grain boundary energy concept. They found that there was a tendency towards intergranular attack in a few of the low-molybdenum alloys for which the corrosion rate was the highest. This tendency was found to persist even in the pure alloys prepared from spectroscopically pure molybdenum and decarburized nickel.

2.3.2 Comments on the Theories of Localized Corrosion

The theories of pitting corrosion are sufficiently qualitative in that no rigid experimental evidence has ever been provided to either support or contradict them. The experimentally observed manifestations of the phenomenon of pitting corrosion conform to the broad framework of the theories which has been the only reason for their existence.

The most convincing experimental evidence regarding the initiation of pitting corrosion has been provided by Kruger and co-workers[34,35]. In studying the phenomenon on iron in buffered sodium tetraborate - boric acid solution (pH = 8.4) Ambrose and Kruger[34] found that the thickness of the film is not the sole factor in influencing the time to breakdown. Their results indicate that adsorption followed by completed penetration by the chloride ions to the metal surface is necessary to initiate pitting. In further support of these conclusions, the work of McBee and Kruger[35] points to a mechanism for passive film breakdown on iron that requires a penetration of chloride ions via lattice defects, possibly anion vacancies.

The importance of the nature of the oxide film covering a metal substrate has been examined in detail by Bianchi et.al.[36] who studied the pitting susceptibility of 19Cr-10Ni steel in $AlCl_3$+LiCl glycerol-ethanolic solutions. They found that the chloride content weakly influences the pitting corrosion process of the naturally oxidized samples

(in air at 25°C for 2 hrs) whilst it markedly increases the pit nucleation on samples oxidized at 300°C for the same time. According to them, this difference in behaviour is due to the defect nature of the oxide film. From Tafel slope measurements they concluded that high susceptibility to pitting is connected with n-type conductivity while low susceptibility to pitting corresponds to p-type conductivity of the oxide film.

The theory of intergranular corrosion as outlined in the previous section has a firmer experimental basis. However, the theory has not gone unchalleneged. Specifically for the case of austenitic stainless steels, Sticker and Vinckier[37] found that the width of the groove at the grain boundary was much greater than could be attributed to the corrosion of the chromium depleted material. This cannot be regarded as convincing evidence against the theory since the possibility exists that once corrosion starts in depleted material it could spread to 'good' material, that is, the alloy content of the steel might be sufficient to maintain the passivity of an air formed protective film but not enough to passivate a more actively corroding surface.

The main disadvantage of the alloy depletion theory has been the lack of direct evidence for the depleted zone. A depleted layer has been detected in some cases[38], but the data are inconclusive. Recent calculations by Strawström and Hillert[39] and Tedmon et.al.[40] indicate a very narrow depleted zone which is consistent with the practical problems

experienced in detecting it.

Although most of the theoretical and experimental work on intergranular corrosion has been confined to the stainless steels, the basic concepts of the alloy depletion theory can be adapted to include the intergranular corrosion of nickel-base alloys as discussed in Chapter 1. The experimental observations amply justify this.

METALLURGY OF THE NICKEL-MOLYBDENUM SYSTEM

2.4 The Binary Phase Diagram

The first phase diagram on the Ni-Mo system was published by Grube and Schlecht[41] in 1938. This diagram was the result of a combination of the work of many previous investigators along with their own work. Since the nickel-rich end at lower temperatures remained uncertain, Grube and Winkler[42] sought to complete the diagram. In the form in which it was published then, it contained all the phases known today. The phase diagram as it is known today was published by Ellinger[43] in 1942. It differed significantly from the previous one in that it established the nature of the reactions by which the various phases are formed. The most recent investigation of the system was performed by Guthrie and Stansbury[44]. Their version of the phase diagram (nickel-rich end) is presented in Figure 2-2. Its basic features are essentially similar to that of Ellinger's and it differs only in its limits of the

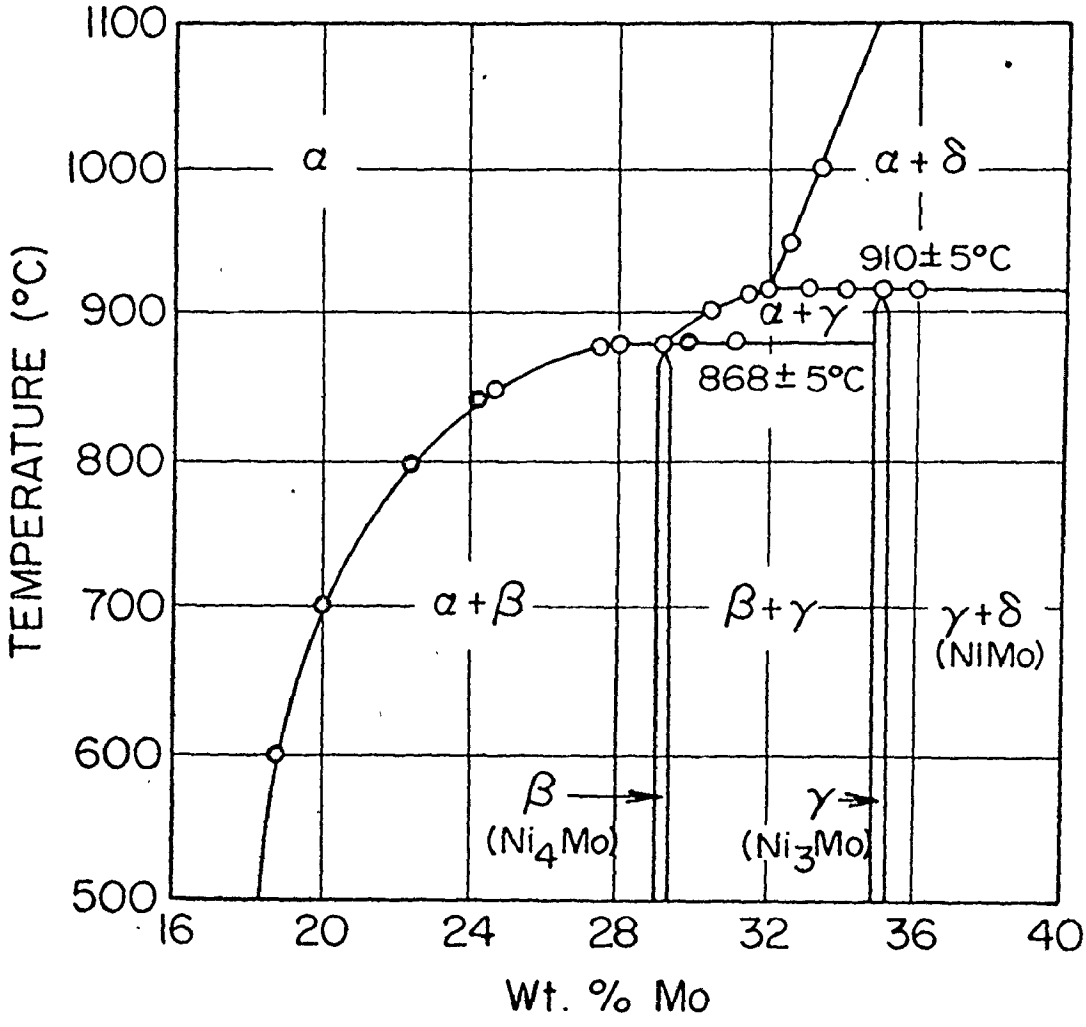

Figure 2-2. The nickel-rich end of the Ni-Mo phase diagram at lower temperatures.[44]

phase boundaries and the transformation temperatures. The characterization of the alloys in the present investigation has been based on this diagram.

2.5 Phases and Structures of the System

2.5.1 The α-phase. The α-phase is the solid solution of molybdenum in nickel and therefore possesses a face-centered cubic structure. The dissolution of molybdenum has a very marked effect on the lattice parameter of nickel. The lattice parameter variation determined as a function of molybdenum content from powder metallurgy specimens is given in Figure 2-3. In fact, Gethrie and Stansbury[44] considered this plot a very convenient means of determining the correct molybdenum content of their other alloys.

2.5.2 The β-phase. The β-phase has a composition Ni_4Mo and according to the diagram is the equilibrium phase after about 18.5% Mo. According to Harker[45] it results from a slight tetragonal distortion of the cubic lattice. This new cell has a volume 2.5 times that of the distorted face-centered cubic cell with a_o = 5.720 Å, c_o = 3.564 Å and c/a = 0.6231.

If the alloy of composition Ni_4Mo is quenched from the α-phase field (above 868±5°C), then the face-centered cubic structure of the α is retained. Such a structure will be referred to as $(Ni_4Mo)_\alpha$. Harker[45] found that for $(Ni_4Mo)_\alpha$ quenched from 1200°C, a_o = 3.612 Å.

2.5.3 The γ-phase. The composition of the γ-phase is Ni_3Mo and its structure can be considered as a superstructure of

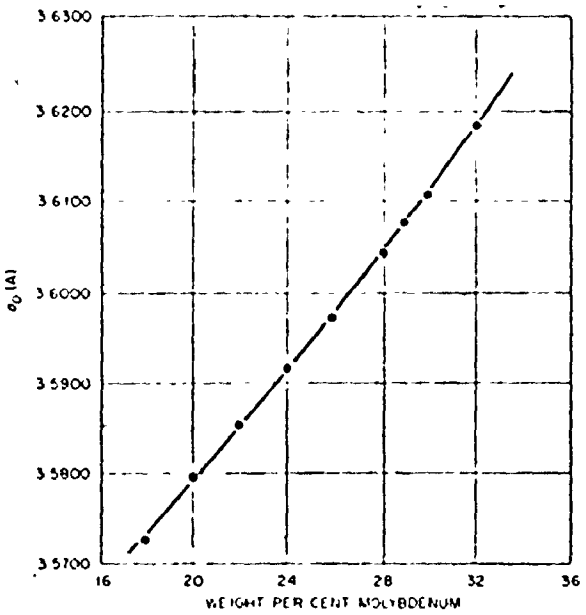

Figure 2-3. The variation of lattice parameter of the α-solid solution (a_o) as a function of molybdenum content for Ni-Mo alloys.[44]

the hexagonally close-packed structure[46]. In the close packed plane the molybdenum atoms are arranged on a rectangular lattice. As a result the crystal becomes orthohombic with lattice parameters, a_o = 5.064 Å, b_o = 4.448 Å and c_o = 4.224 Å.

2.5.4. The δ-phase. Although the δ-phase is known to possess a composition NiMo, only one indication of its structure in the literature could be found[47] which describes the δ-phase as possessing a tetragonal unit cell with a_o = 9.108 Å and C_o = 8.852 Å. In their investigation Guthrie and Stansbury[44] merely mention that "the x-ray pattern of this specimen (δ-phase with 62.01 wt % Mo) showed numerous diffraction lines indicating a complex structure even more complex than that of β or γ".

The ordering reactions of the various phases have been the subject of many investigations[46-50,44,51,52]. During these studies, the existence of metastable phases has been encountered. Due to their lack of relevance with the present investigation, the details of these studies will not be reviewed here.

CORROSION CHARACTERISTICS OF NICKEL AND NICKEL-MOLYBDENUM ALLOYS

2.6 Corrosion of Nickel

2.6.1 Passivation Behaviour

A substantial amount of information exists on the corrosion properties of nickel in acid and alkaline solutions. Nickel is a transition metal and possesses the ability to

passivate. A typical potentiostatic anodic polarization curve for nickel in an aqueous solution is an s-shaped curve which shows that nickel dissolution occurs in the 'active region' but is inhibited at more anodic potentials. The importance of water, and hence probably an oxide film, in the passivation of nickel has been noted, passivation being absent in anhydrous acetonitrile solutions[53]. The oxide film is believed to inhibit nickel dissolution by forming a physical barrier between the metal and solution, thus preventing bare metal from being in contact with the solution[54-57]. However there is some question as to whether the physical presence of the oxide is, by itself, sufficient for passivation since a large potential drop across the oxide film may allow continued dissolution through field-assisted metal cation migration. In this case passivation would occur when the potential gradient across the oxide is too small to allow cation migration - a condition which could arise by either a thickening of the oxide or an increase in its electronic conductivity. Among the earlier mechanisms regarding the passivation of nickel, it was suggested[58,59] that the essential step in the passivation process is the conversion of a precursor, nonprotective, oxide film into an electronic conductor through the introduction of non-stoichiometry.

Two mechanims have been suggested for the oxide formation on nickel: i) dissolution-precipitation mechanism[58,60,61];

ii) direct oxidation of the metal surface[54,55,57,62-64].

In the first case, it is postulated that oxide formation can occur when the solubility of $Ni(OH)_2$ in solution near the electrode is exceeded, thus resulting in a precipitation of the $Ni(OH)_2$ onto the electrode. Dependence of the induction time for oxide formation on the rate of solution stirring has been used as support for the mechanism[61]. However, in direct contradiction of this result, Armstrong and Henderson[65] found no dependence of the potential-current density curve on the rotation speed on a circular nickel electrode in 0.5 M H_2SO_4 solutions. According to them, the dissolution precipitation model is inappropriate.

The second mechanism of oxide formation involves a reaction of the form $Ni + H_2O \rightarrow NiO + 2H^+ + 2e$, where a direct electrochemical reaction between the nickel electrode and water from solution is the cause of the oxide formation. A search through the literature reveals that the maximum support and no contradiction exists for this mechanism. The most recent of these studies is that of MacDougall and Cohen[64]. They found that when a nickel electrode is subjected to a passive potential in a pH 8.4 Na_2SO_4 solution, the current decay rate is independent of solution stirring and added nickel (10 μgm/ml Ni^{2+}). This shows that Ni^{2+} ions in solution are not an important factor in the oxide formation reaction. Hence, the cause of nickel passivation is a direct electro-

chemical reaction between water and metal to form essentially anhydrous NiO.

A glance at the potential-pH diagram (Figure 2-4) for the nickel-water system at 25°C reveals[66] that the possibility exists for the formation of many different oxides on nickel. These oxides have been identified to range from NiO to Ni_2O_3, their formation depending only upon the potential and pH of the solution[67]. For instance, in alkaline solutions it has been shown[68] that the final oxidation state on the nickel electrode corresponds to a non-stoichiometric oxide NiO_x, (where x = 1.7 - 1.9). Yahalom and Weisshaus[69] observed a film covering the pits formed in phosphate buffer solution by chloride ions in thin nickel foils. From electron diffraction data they concluded that the film was NiO.

The constituents of the passive film in acid solutions are evidently quite different. Sato and Okamoto[67] proposed that the potential for the onset of passivity is the potential for the transformation from NiO to the higher oxide Ni_3O_4 when the concentration of the nickel in solution is small. Polarization to higher potentials leads to oxidation and conversion of this oxide (Ni_3O_4) to Ni_2O_3. Thus, the passive oxide film on nickel may be taken to consist of either a single higher oxide Ni_3O_4 or the duplex oxide NiO and Ni_3O_4. The results of Cowan and Staehle[56] support the presence of a single oxide Ni_3O_4. In cases where the nickel electrode is directly subjected to a passive potential in 1N H_2SO_4 solution, the passive film has been assumed[70] to be composed of NiO.

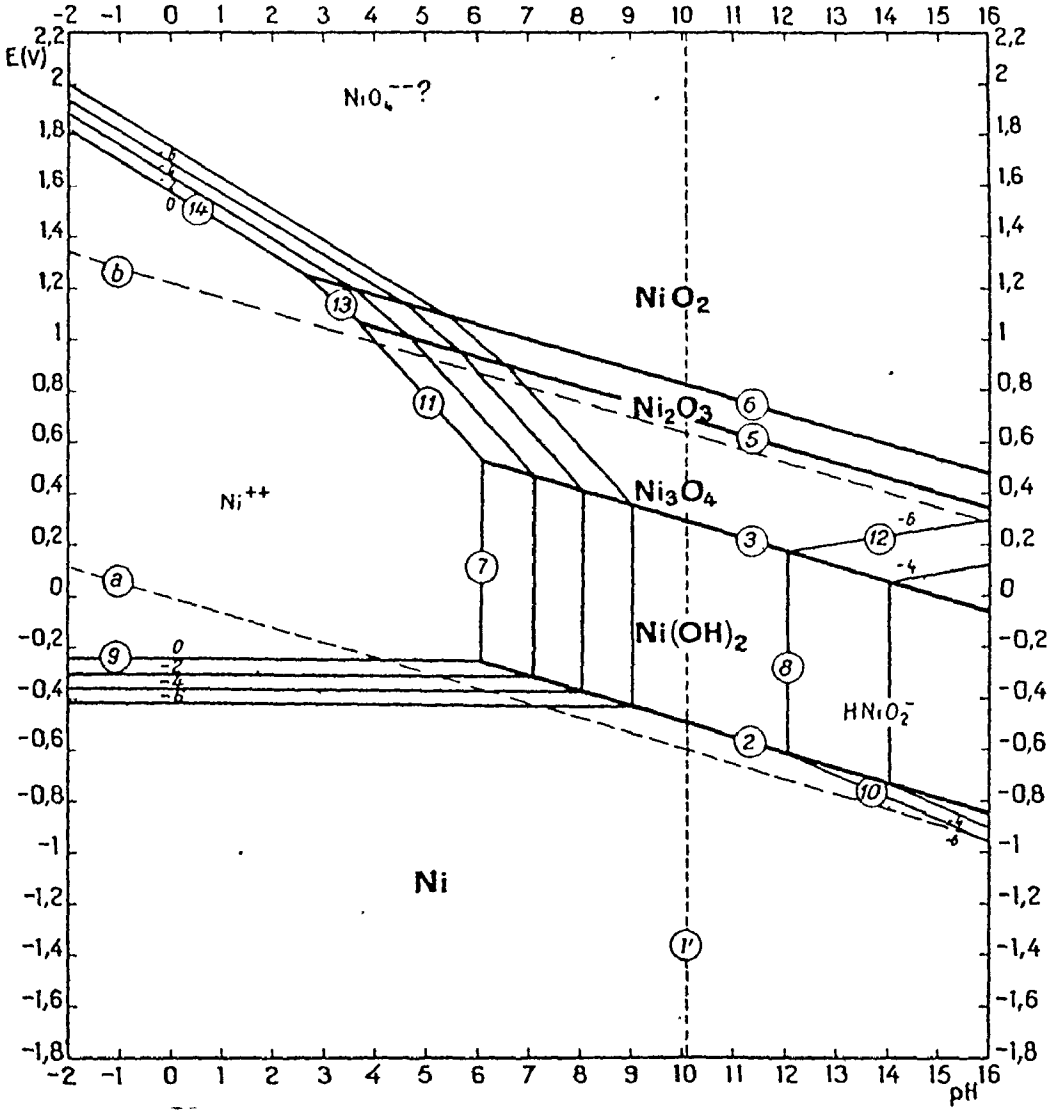

Figure 2-4. The potential-pH diagram for the nickel-water system at 25°C[66].

The earlier estimates of the thickness of the anodic passive films on nickel were rather high[58,71,72]. For instance, Tronstad[71] estimated 50-80 Å for nickel passivated anodically in acid sulfate solutions whereas Bockris et al[58] found the thickness to range between 70-100 Å for a pH 3.1 H_2SO_4 solution. Pfisterer et al[73] were probably the first to report only 15 Å thickness for the passive films on very thin nickel foils. Recent work[64,74] reveals that anodic passive films on nickel are typically 6-16 Å thick.

No rate law has been derived to describe the kinetics of the passive film formation on nickel. Possibly the earliest indication regarding the nature of the events involved in the film growth of nickel in 1N H_2SO_4 came from Okamoto et al[75]. On the basis of measurements of capacitance vs. potential and temperature, they concluded that the film thickness is proportional to the potential; therefore, the electric field remains constant throughout the film. A similar conclusion has been drawn by Ammar and Darwish[76] from galvanostatic polarization studies. Later, Okamoto and Sato[77] suggested that if the motion of the ions in the passive film is due to a high electric field, then a linear relation between film thickness and potential would be expected because the strength of the electric field, which is constant with the current, is inversely proportional to film thickness. Their results showed this to be true[77]. Recently, Sato et al[74] found that an inverse logarithmic relation was obeyed for the anodic film growth

on nickel in 0.3 Na_2CO_3 solution (pH = 11.49). This conclusion necessarily implies field-assisted growth. The potentiostatic data has merely been fitted to an inverse logarithmic rate law, and no derivation has been presented.

2.6.2 Localized Corrosion Behaviour

The passive film on nickel is known to be an oxide and the inhibition of corrosion is due to the presence of this protective film. The presence of certain anions, particularly chloride, destroys passivity and leads to localized corrosion, which in many cases takes the form of pitting. Whatever be the mode by which the chloride ion acts, its importance in destruction of passivity cannot be doubted. The presence of hydrogen ions has also been found to promote corrosion[6,70] although its mode of attack is unclear. This necessarily implies that for the same concentration of chloride ions, an acid solution is more aggressive than an alkaline solution[78].

Many detailed studies have been conducted to investigate the effect of Cl^- ions on the passivity of nickel. Postlethwaite[79] studied solutions with sodium chloride additions over the temperature range 25° to 275° C. He found that the critical Cl^-/OH^- ratio for breakdown (1:1) increased with OH^- concentration. The attack changed from pitting at lower temperatures to a general attack at elevated temperatures. Ammar and Darwish[70] observed that nickel passivated in 1N H_2SO_4, but Cl^- ion addition caused pitting which occurred after an induction

period that depended on both potential and Cl^- concentration. A very small effect on the passive behaviour of nickel over a 24 hr period was observed[70] for a Cl^- concentration of 0.001 N; the attack increased with Cl^- concentration and became vigorous above 0.06 N. Smialowska[80] has suggested that higher Cl^- concentrations and potentials lead to the formation of a more aggressive solution within the pits and to the dissolution of the oxide film covering their orifices.

Although any existing theory of pitting corrosion requires the existence of a protective film or a passive state as a precursor to pitting, Hodge and Wilde[81] found that a pure nickel specimen did not passivate in 1N NaCl + 1N H_2SO_4 solution, since the anodic current density increased continuously with potential. From an examination of the structure of the specimen, they concluded that the metal had undergone pitting corrosion. However, in a later study[82] designed to study the effect of Cl^- ion concentration on the anodic dissolution behaviour of nickel, it was found that a critical concentration of the aggressive ion exists upto which the breakdown of the passive film on nickel is localized resulting in pitting. Beyond this concentration, the area of attack increases giving rise to general corrosion. From 'in situ' microscopic observations during polarization and the surface structure after each run, the attack in 1N NaCl + 1N H_2SO_4 solution was re-interpreted as general corrosion. That a high concentration of Cl^- ions can lead to general corrosion has also been shown by Smialowska[83]

who has found that after pitting, the amount of nickel estimated analytically in solution is higher than that calculated mathematically from the volume of the pits formed. The excess nickel has been attributed to general corrosion.

There does not seem to be any information regarding the mechanism of the initiation process of pitting in nickel. On the basis of the observations that covered pits were found on nickel held at constant passive potential and that a bulge was observed in the passive film prior to the appearance of a crack that revealed the presence of a deep pit below, it was suggested[84] that, similar to the case of iron[34,35], penetration of the Cl^- ions through the passive film to the nickel surface is required to initiate pitting. Ammar and Darwish[70] suggest that the first step leading to the formation of pits is associated with Cl^- ions which have access to the Ni^{2+} ions either by means of normal corrosion reactions of the passive film if the latter is pore-free or through active patches in the form of grain boundaries and lattice imperfections which may result during crystallization of the pseudomorphic oxide[75].

Smialowska[80] suggests that pits nucleate at non-metallic inclusions which dissolve chemically or electrochemically in the given solution forming microcrevices visible as small dots on the metal surface. The Cl^- ions diffuse through the crevices dissolving the active metal more and more severely. Tokuda and Ives[85] working with polycrystalline nickel found that pits nucleated at scratches and grain boundaries.From polarization

curves they concluded that the active sites for pitting are identical with the dissolution sites in the 'active' polarization condition.

Pit nucleation at imperfections in the passive film does not seem too improbable in view of the fact that for pitting corrosion to occur a 'border-line passivity' is essential. Since the passive film forms by the anodic dissolution of the metal, it seems reasonable to suppose that the passive film around a defect, such as inclusion, dislocation or a grain boundary where the lattice is strained, is imperfect. Naturally enough, such sites are those favouring pit nucleation. Cold working would increase the dislocation density and consequently increase the susceptibility to pitting corrosion as evidenced by a decrease in the critical potential. The work of Garz and Häfke[86] on nickel single crystals shows this to be true. However, cold working up to 40% was found[87] to have no effect on either the critical potential or pit density of polycrystalline nickel in 1N H_2SO_4 with 0.02 M Cl^- ions.

When a metal is subjected to a potential in the passive region, the anodic current increases momentarily. Apart from transient phenomenon in the vicinity of the critical potential (which can be attributed to repassivation effects) the current-time curves have uniformly ascending shapes. Engell and Stolica[29] have shown that the rate of development of pits, characterized

by the increase of the current at a constant potential is given by

$$i = kt^b \qquad (2\text{-}5)$$

where t is the time and k is a constant dependant upon the concentration of Cl^- ions. The exponent b equals 2 when the number of pits, N, is constant in time, and equals 3 when the pit number is proportional to t. The basic assumptions underlining the above equation are that the pits are hemispherical in shape and that the current density in the pit is constant and uniform. If this is true, then the radius of the pits, r, should increase linearly with time.

The validity of the above equation has been confirmed many times. However, the exponent b is not always 2 or 3, and also a linear dependence of r upon t and N upon t is not always observed. For instance, exponent b smaller than 2 has been noticed by Garz et al[88] who performed electrochemical and metallographic studies of nickel single crystals anodically polarized in 0.5 M $NiCl_2$. They found that the increase of the current during pitting occurs in agreement with Engell and Stolica's equation, but the exponent b is less than 2 and depends upon the crystallographic orientation for {100} and {110} planes. They obtained b values of 0.6 and 0.3 respectively, whereas for the {111} plane, the value was 1 when the pits are triangular and 1.5 when they are hexagonal. They always obtained crystallographic pits and not hemispherical

ones for which Engell and Stolica deduced the equation.

Investigations[80] of the pitting corrosion of nickel in solutions containing different concentrations of SO_4^{2-} and Cl^- ions at various pH values showed that within the range of equivalent Cl^-/SO_4^{2-} ratios from 0.15 to 2.5, the current increases in accordance with equation (2-5), but the values of b are either higher (at a low ratio of Cl^-/SO_4^{2-}) or lower than 1 (at higher ratios of Cl^-/SO_4^{2-}), independent of the pH of the given solution.

Ammar and Darwish[70] found that for polycrystalline nickel in 1N H_2SO_4, the exponent b decreased with increasing potential and was almost independent of Cl^- ion concentration over the range studied (0.02 N - 0.06 N Cl^-). Specifically, b = 3.0 at 1000 mV (SCE) and b = 1.8 at 1500 mV (SCE) at 0.02 N Cl^-. This behaviour was interpreted on the basis that at higher potentials pits are diminishingly small in area and comparatively large in number such that they rapidly fuse together making the surface very rough and resulting in a lower intensity of attack.

2.7 Corrosion of Nickel-Molybdenum Alloys

Although enough information for material evaluation exists on the corrosion characteristics of the Hastelloys[7,8], data on the corrosion properties of the binary nickel-molybdenum alloys is rather limited. Parr's development in 1915 of a complex hydrochloric-acid resistant alloy known as 'illium'

is possibly the earliest use of nickel and molybdenum in an alloy[89]. However, the first work on the binary nickel-molybdenum system is that of Field[9] who studied the weight loss of the alloys in 10% HCl at 70°C with molybdenum varying from 5 to 47 wt %. It was found that the corrosion rate dropped from 4080 mdd for a Ni-5Mo alloy to less than 240 mdd for a Ni-15Mo alloy. There was no loss of weight for a Ni-47Mo alloy. While the alloys with more than 15% Mo were satisfactory from a corrosion viewpoint, they had the disadvantage of being rather expensive and difficult to work. Since Field's work was confined to the development of acid resistant alloys, further research on the nickel-molybdenum binary system was abandoned in order to investigate to what extent other elements, such as chromium and iron, might be substituted to reduce the cost and improve workability.

More detailed work on the binary system came many decades later when Uhlig et al[33] studied the corrosion and passivity of alloys containing upto 25% Mo in 10% HCl at 25°, 70° and 102°C (the boiling point). They found that aeration of the acid considerably increases the loss of weight. For instance at 25°C in aerated acid, the average corrosion rate of the alloys at and above 3% Mo was 65 mdd; in deaerated acid the rates were lower becoming extremely small above 10% Mo and Zero within the experimental accuracy of the measurements at 19.1% Mo and above. In deaerated acid, a minimum rate was

reached at or about 20% Mo at 70° and 102°C. Since the corrosion potentials in deaerated acid are not noble but close to or equal to the potential of the hydrogen electrode indicating marked polarization of the anode areas on the alloy surface and also because molybdenum has little effect on the hydrogen overvoltage, it was concluded[33] that the alloys corroded under anodic control. Although anodic control is typical of all materials exhibiting an active passive transition and hence corroding through a passive film, the case with the nickel-molybdenum alloys has been considered to be very different. This is because the corrosion potentials, unlike values for the passive chromium alloys, are more active than the corresponding Flade potentials at which the passive film is established[33,80], implying that the increased anodic polarization (and consequently the corrosion resistance) is related most likely to a sluggish hydration of metal ions imparted by molybdenum or alternatively to a porous diffusion-barrier film of molybdenum oxide.

The alloys used by Uhlig et al[33] were water quenched from 1000°C and, therefore, from a metallurgical viewpoint would have a single phase structure comprising the α-solid solution; although alloys containing more than about 18% Mo would be considerably saturated.

The importance of the metallurgical structure of the alloy has been brought out by the work of Pavlov and Svistunova[91]

who have shown by weight loss measurements that Ni-rich alloys of the nickel-molybdenum system are susceptible to corrosion by boiling in HCl after heating at temperatures between 600° and 900°C. Within this temperature range the nickel-rich nickel-molybdenum alloys undergo order-disorder transitions. Extensive transmission electron microscopic studies have been performed of the substructures which form during order-disorder processes[46-50].

In correlating the importance of the metallurgical structure and the corrosion properties of Ni-Mo alloys, the work of Ruedl[92,93] needs special mention. He studied the corrosion of a Ni-33Mo alloy in HBr exposed at 130°C for 24 hrs. Specimens were heat treated to obtain three different structures. The weight loss was in general small (less than 50 mdd) but was dependent upon the thermal pretreatment. A relatively large loss of weight was observed for short-range ordered samples quenched from the α-solid solution region[92]. Scanning electron microscope studies revealed a uniform attack of the grains and also a selective attack of some boundaries.

For specimens of Ni-33Mo alloy cooled rapidly from 950°C, the structure consists of the disordered α-phase (with 20 at.% Mo) and the ordered δ-phase (containing 50 at.% Mo). Corrosion tests revealed that the α-phase was simultaneously attacked at the grain boundaries and within the grains whereas the δ-phase was much more resistant[93]. The structure of

specimens held at 840°C for 10 days after being cooled rapidly from 950°C was found[93] to consist of the β-phase, retained α and a metastable X of a structure that is not yet described in the literature. This phase was found to contain approximately 50 at % Mo and thus a content of molybdenum similar to the δ-phase but of a different structure. Corrosion tests showed that the phase with the higher molybdenum content (phase X) was most resistant to attack. Grains corresponding to the β-phase were corroded in a regular pattern, but to a lesser degree. Holes were found corresponding to the regions where the disordered α-phase was present. Transmission electron microscopy revealed that the β-phase consists of numerous domains and attack on the domain boundaries was responsible for the regular pattern of corrosion observed.

Although Uhlig[7] believes that the alloys of the nickel-molybdenum system are not passive in the sense that their electrochemical behaviour does not approach that of an appreciably less active or noble metal, electrochemical studies[94,95] have shown this to be untrue. Greene[94] studied the passivity of the alloys containing upto 25% Mo in 1N H_2SO_4 at 25°C. All alloys containing 20% Mo or less exhibited typical active-passive curves. The critical current density maximum occurring at -100 mV (SCE) increased and then decreased as the molybdenum content was increased. Current density in the passive region (ie between 200 mV to 1000 mV (SCE)) increased with increasing molybdenum content. Finally at 25% Mo,

the material demonstrated very little of the original electrochemical behaviour of nickel. Only a small current density maximum remained at approximately -200 mV (SCE) while the original passive region had disappeared entirely. The polarization characteristics of pure molybdenum were interesting. It did not exhibit an active-passive curve; instead the current density increased with increase in potential (an activation-controlled dissolution process) with a Tafel slope of 50 mV/decade. Alloys of this investigation were water quenched from 1160°C and would therefore have a single phase structure of the α-solid solution.

The ability of nickel-molybdenum alloys to passivate has also been demonstrated by Chassaing and Kinh[95]. Potentiodynamic polarization curves (continuous potential scan at 2000 mV/hr) and galvanostatic techniques were used to study the passivity of nickel, molybdenum and a Ni-25Mo alloy in 1N HCl. While nickel showed no tendency for passivation, molybdenum passivated spontaneously; the Ni-25Mo alloy was in between the two extremes. For the Ni-25Mo alloy, the corrosion current, i_{corr}, decreased linearly and the corrosion potential, E_{corr}, linearly became more noble as a function of pH in normal chloride solutions. The total quantity of charge Q used during the passivation time t_p may be taken to consist of two terms[96]

$$Q = Q_f + Q_o = Q_f + \int_o^{t_p} i_o dt = Q_f + i_o t_p \qquad (2\text{-}6)$$

where Q_f represents the charge necessary for the formation of the passive film, Q_o and i_o correspond to the maintenance of the passive film. To a first approximation i_o can be considered constant during the time of passivation. Extrapolation to $t_p = 0$ of the $Q - t_p$ curve permits the evaluation of Q_f. It was found that for Mo, $Q_f = 0.9 - 1.0$ mC/cm^2 in 1N-6N HCl while for the Ni-25Mo alloy, $Q_f = 5.7$ mC/cm^2 in 0.01 N-0.1 N HCl. Although no interpretation is given to these Q_f values, they do demonstrate the existence of a passive film. In fact, Chassaing and Kinh[95] conclude that the resistance to corrosion of the nickel-molybdenum alloys in HCl is linked to a passive state.

CHAPTER III

EXPERIMENTAL TECHNIQUES AND PROCEDURE

3.1 Materials and Specimen Preparation

The alloys used in this investigation were graciously supplied by Dr. L. A. Morris, Metallurgical Laboratories, Falconbridge Nickel Mines Limited, Thornhill, Ontario. The alloys were made from good purity materials whose qualitative analysis is shown in Table 3-1. The impurity levels are claimed to be closer to the lower end of the range indicated.

The alloys were supplied as 75 gm buttons. It was claimed that they were homogeneous having been remelted five times during their preparation. In all, five alloys containing 5, 10, 15, 22 and 30 per cent molybdenum by weight were supplied. No separate chemical analysis for the composition of the alloys was performed and the suppliers claim that the actual composition was very close ($\sim \pm 0.2\%$ by wt.) to the nominal values indicated was accepted.

The nickel used was 'low-oxygen nickel' and was also supplied by Dr. L. A. Morris. It was received as cold-rolled sheets prepared directly from the refined cathode material. Its composition is given in Table 3-2. The molybdenum used in the study (only that used as pure molybdenum and not that used in alloy preparation) had a purity of 99.97% and was obtained from Ventron Corporation, Aldrich Chemicals, Montreal, in the form

Table 3-1

Qualitative spectrographic analysis of Nickel and Molybdenum used for the preparation of the alloys

Element	Range in weight %	
	Ni	Mo
Aluminum	0.01 -0.10	0.003-0.03
Calcium	0.0003-0.003	0.001-0.01
Chromium	-	0.001-0.01
Cobalt	0.001 -0.01	0.003-0.03
Copper	0.0001-0.001	-
Iron	0.003 -0.03	0.01 -0.1
Magnesium	0.001 -0.01	0.001-0.01
Molybdenum	-	MC
Nickel	MC	0.1 -1.0
Silicon	0.001 -0.01	0.003-0.03

MC - main component

Table 3-2

Analysis of the cold-rolled sheets of nickel prepared directly from cathode material

Element	Analysis in ppm by weight
Aluminum	< 1
Calcium	3
Carbon	15
Chromium	< 0.6
Cobalt	60
Copper	8
Iron	40
Lead	8
Magnesium	< 1
Manganese	< 0.7
Phosphorus	< 2
Silicon	5
Sulfur	5
Titanium	< 1
Hydrogen	1.5
Nitrogen	2
Oxygen	14

of a 0.25 mm thick sheet.

In order to be usable for specimen preparation, the alloys were required to be in a sheet form of approximately 1 mm thickness. This was achieved by rolling. As a starting point, the alloys were given another homogenizing anneal at 1250°C for 100 hrs. For this and for all heat treatments employed for all material in this investigation, the alloys were sealed in a quartz tube under a vacuum of better than 10^{-5} torr. Following the homogenizing treatment, the alloy buttons were cold rolled with intermediate annealing at 950°C for various periods up to 8 hrs. Considerable caution was exercized during the earlier stages of the cold rolling operation and the alloys were annealed after two light passes through the rolls. However, once the 'as cast' structure was broken, the rolling operation became rather simple. Considerable difficulty was encountered during the rolling of the Ni-30Mo alloy and therefore once a thickness of 0.6 cm was attained, the rolling was stopped. Wafers of approximately 1 mm thickness were cut from the button by a multiple wire-saw.

Samples of 0.6 cm × 0.6 cm were cut from the rolled sheet by a Micro-matic Precision Wafering Machine. The sample was given the selected heat treatment after which a lead wire was attached in the centre on one side by Pb-Sn solder. The sample mount consisted of a Tygon* ring of 10 mm diameter and 8 mm thickness. The soldered sample was mounted on this ring

---

*Brand name for flexible plastic tubing manufactured by most companies dealing in plastics.

with epoxy resin such that soldered face and all edges were covered with epoxy leaving only one face exposed. This assembly fitted snugly into the specimen holder.

The possibility of the presence of crevices cannot be completely ruled out. As has been pointed out by Wilde[2], the presence of crevices leads to premature breakdown of passivity and, therefore, is prejudicial to material evaluation. In the present investigation, the test specimen was thoroughly checked under an optical microscope for crevices prior to its insertion into the cell. After completion of an experiment, the specimen surface was again checked, and in cases where crevice corrosion had taken place the data was disregarded. However, with careful specimen preparation, crevice corrosion did not pose any problems throughout this investigation. In fact, one in every hundred specimens had to be discarded owing to the presence of crevices.

The alloys were heat treated according to the schedule given in Table 3-3. The purpose of the heat treatment was to relieve the stresses and to obtain a medium grain size (around 0.02-0.04 mm). The Ni-30Mo alloy was heat treated to obtain three different structures in order to enable a study of the effect of metallurgical structure on corrosion. Particular difficulty was encountered with molybdenum. The recommended full annealing temperature for molybdenum is 2200°F (1204°C) with a time of 1 hr for each inch of section[97]. It is mentioned that annealing raises the ductile-brittle transition temperature

Table 3-3

Heat treatment schedule for Ni, Mo and Ni-Mo alloys

Alloy	Heat Treatment Schedule	
Ni	775°C for 5 hrs.	FC
Ni-5Mo	600°C for 3 hrs.	AC
	800°C for 1-1/2 hrs.	FC
Ni-10Mo	800°C for 7-1/2 hrs.	FC
Ni-15Mo	850°C for 57 hrs.	FC
Ni-22Mo	900°C for 124 hrs.	FC
Ni-30Mo-1	950°C for 8 hrs.	FC
Ni-30Mo-2	800°C for 50 hrs.	AC
Ni-30Mo-3	800°C for 1200 hrs.	AC
Mo	900°C for 1 hr.	AC

FC - Furnace Cooled

AC - Air Cooled

of the molybdenum with nearly a complete loss of ductility at room temperature. During the course of annealing the molybdenum it was found that fully annealed specimens were very difficult to handle with a marked tendency for chipping at the edges during mechanical polishing: As a standard procedure for molybdenum therefore, specimens were only stress relieved according to the recommended procedure given in Table 3-3.

Specimens were mechanically polished through 220, 320, 400, 600 grit silicon carbide papers using water as lubricant followed by final polishing on 6 μm and 1 μm diamond wheels with kerosene as lubricant. Specimens were washed with water, rinsed in methanol, dried in a jet of air and stored in a desiccator. Prior to their use, all specimens (except the Ni-30 Mo alloys which were used in the mechanically polished condition) were electropolished in 60% H_2SO_4 according to the schedule given in Table 3-4. This schedule was taken as the standard procedure of electropolishing the specimens. Complying with the earlier practice[84], the acid was ice-cooled and the specimen was vigorously mechanically stirred to eliminate etch pitting. A stainless steel plate of approximately 8 cm^2 area was used as the cathode.

A different procedure was adopted for the surface preparation of molybdenum. The final surface was obtained by anodizing and stripping the film formed. The anodizing solution[98] was such that each litre of glacial acetic acid contained 0.02 M $Na_2B_4O_7 \cdot 10\ H_2O$ and 1.0 mole of water. The cathode was a

Table 3-4

Electropolishing schedule for Ni and Ni-Mo alloys

Alloy	Voltage V	Current Density A/cm^2	Time mins
Ni	5.0	0.50	1
	7.5	1.00	2
Ni-5Mo	5.0	0.56	1
	7.5	0.89	1
	10.0	1.22	1
Ni-10Mo	5.0	0.61	1
	7.5	1.03	1
	10.0	1.42	1
Ni-15Mo	5.0	0.61	1
	7.5	1.06	1
	10.0	1.44	1
Ni-22Mo	5.0	0.61	1
	7.5	1.14	1
	10.0	1.69	1

Pt-wire gauze cylinder 6.0 cm long with an inside diameter of 2.5 cm. The stripping solution was 1 gm/litre of KOH. The anodizing solution is hygroscopic and was discarded after the polishing of two specimens. Specimens were anodized for a period of 4 mins. at 100 volts. The film formed was dissolved in the KOH solution. Specimens were then rinsed in methanol, dried with a filter paper and again anodized. In all, each specimen was anodized six times for a total anodizing time of 24 mins. This treatment has been assumed[98] to provide a reproducibly flat surface of constant area.

The characterization of the specimen surface was performed with the aid of a scanning electron microscope and surface replicas observed in transmission by an electron microscope. The surface of specimens electropolished according to the standard schedule and observed at magnifications up to 38,000× was found to be very flat.

It has long been believed that as a result of electropolishing, a thin film is formed on the surface of metals. However, it was not till recently that MacDougall and Cohen[64] pointed out that the oxide obtained by electropolishing nickel in H_2SO_4 solution is a result of the subsequent air exposure of the wet nickel electrode, the electropolishing itself mainly stripping nickel from the surface in a uniform manner and leaving the surface essentially free from oxide. Since in this investigation electropolishing was performed separately and then the specimen was introduced into the corrosion cell assembly a film

would be present on the surface. In order to always start from a bare surface and to obtain reproducibility, it was found necessary to remove this film. This was achieved by cathodic reduction in 1N H_2SO_4 at -1500 mV (SCE) for 10 mins. Except in instances where it is especially mentioned, the cathodic reduction treatment was incorporated as a standard step in the specimen preparation technique.

All solutions were prepared from reagent grade materials meeting A.C.S. specifications using distilled water. The potassium chloride solution used for the Saturated Calomel Reference electrode was especially prepared for the purpose by Fisher Scientific Company and saturated at 20°C. The synthetic sea water was made by dissolving 41.95 gms of sea-salt in distilled water to make one litre. Sea-salt is an ASTM trade mark for a simulated salt mix containing elements found in natural sea salt in quantities greater than 0.004% (composition is given in Table 3-5). It is granular, colorless and has a density of 1.025 at 15°C. It was obtained by the courtesy of Lake Products Company, Inc., St. Louis, Missouri.

All solutions were deaerated by bubbling pure dry nitrogen for a minimum period of two days prior to their use. In order to be able to obtain large volumes of solutions at any instant, solution deaeration was performed continuously in a 4 litre conical flask. This flask was connected to a 500 ml flask which was calibrated to measure solution volumes. Nitrogen was bubbled through this flask as well. From this flask,

Table 3-5

Composition of sea-salt

Compound	%
NaCl	54.490
$MgCl_2 \cdot 6H_2O$	26.460
Na_2SO_4	9.750
$CaCl_2$	2.765
KCl	1.645
$NaHCO_3$	0.477
KBr	0.238
H_3BO_3	0.071
$SrCl_2 \cdot 6H_2O$	0.095
NaF	0.007

the solution could be drawn through a Tygon tube to the corrosion cell where deaeration was continued throughout an experimental run. Thus, transfer of solution was always carried out under a nitrogen atmosphere. The importance of solution deaeration cannot be sufficiently emphasized. It might suffice to say that electrochemical studies are apparently extremely sensitive to dissolved oxygen in solution. It was found during the course of this investigation that insufficiently deaerated electrolytes produced irreproducible results during cathodic reduction studies. This aspect will be described in more detail later.

3.2 Description of Apparatus

3.2.1 Corrosion Cell Assembly

The polarization of a specimen requires, apart from the specimen itself which serves as the working electrode, an auxiliary or counter electrode and a reference electrode with respect to which all potentials are measured. The working electrode and the auxiliary electrode are introduced directly into the corroding solution whereas the reference electrode is placed in a separate compartment and is connected to the corrosion cell by means of a salt bridge.

The corrosion cell for electrochemical studies consisted of a cylindrical glass container with a removable cover (Figure 3-1). The cell capacity was 300 ml. A thin optical glass window was incorporated in the bottom of the cell to permit observation and photomicroscopy 'in situ', if required, when the

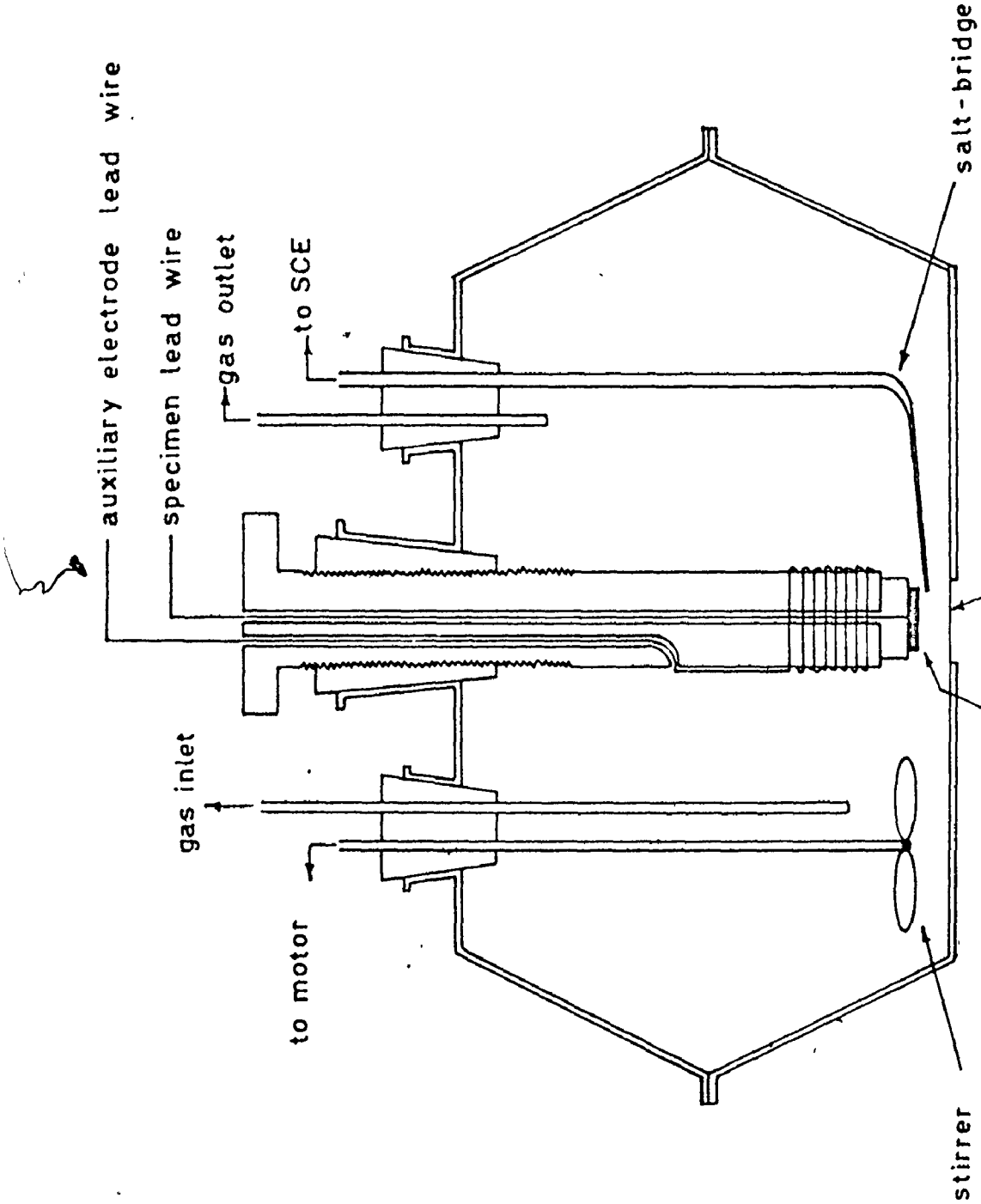

Figure 3-1. Schematic diagram of the corrosion cell. The window for 'in-situ' microscopic observations is at the bottom.

cell was placed on the stage of a Zeiss Inverted Metal Microscope. The top cover was fixed by means of springs. There were openings in the cover to accomodate the specimen holder, salt bridge, gas inlet and the stirrer.

The specimen holder for all the alloys except molybdenum was made of Teflon* and fitted the cell in such a way that it could be raised or lowered by screwing in or out. The specimen could be snugly fitted at the lower end and when placed in the corrosion cell allowed the flat polished surface to be parallel to the glass window. The auxiliary electrode was a platinum wire wound at the lower end of the holder. The lead wires for electrical connections passed through the holder out of the cell.

During film formation studies, when the chloride containing solution had to be removed from the cell and more fresh solution was required to be added, a cell of similar features but with a larger capacity (500 ml) and no optical window was used. This cell incorporated a tap placed at the side about 5 mm above the cell base. Opening of the tap resulted in the discharge of the solution from the cell leaving behind about 75 ml of the original solution. Since the volume of the fresh solution added was constant, this arrangement resulted in a constant amount of dilution during different experimental runs.

---

*Trademark of Du Pont Chemical Co. Inc., for Polytetrafluoroethylene (PTFE)

The specimen holder for the molybdenum was different. Since the molybdenum specimens were in the form of strips 3.5 cm × 0.6 cm (and 0.25 mm thick), the specimen holder consisted of a brass rod 5 mm in diameter forked and with a screw at the end. The rod passed through a Teflon stopper which fitted the cell opening. The specimen was inserted between the fork, tightened with the screw and when inserted in the cell dipped the molybdenum strip about 5 mm into the electrolyte. The auxiliary electrode which also passed through the Teflon stopper consisted of a 1 mm thick platinum disc with a 12 mm diameter attached to a 1 mm platinum wire.

The cell for weight loss determinations was similar to the one used by Bond and Uhlig[99] and is shown in Figure 3-2. The specimens for weight loss measurements consisted of 25 mm × 10 mm × 1 mm coupons with a 1 mm diameter hole near one edge. Specimens were suspended in the corrosion cell by means of a glass hook. The 10% HCl solution was continuously deaerated with pure dry nitrogen at the rate of 20 ml/min measured by a flowmeter (Matheson of Canada Ltd., Model 702BBX W72).

3.2.2 Potential Measuring Device

All potential measurements were carried out versus the Saturated Calomel Electrode (SCE) using an agar-agar salt bridge. Care was taken to see that the 'pick-up' end of the salt bridge was within a few millimeters from the specimen surface. All values of potentials reported are as recorded

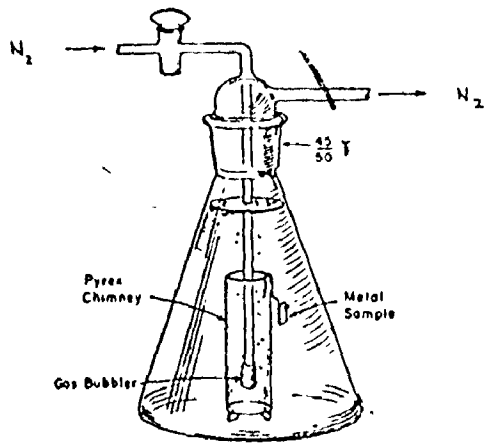

Figure 3-2. Schematic diagram of the cell for the determination of corrosion rates by weight loss measurements.[33]

with no corrections being incorporated for any junction potentials.

3.2.3 Purification of Nitrogen

All solutions were deaerated by bubbling pure dry nitrogen for a minimum period of two days. The atmosphere within the corrosion cell was maintained inert by bubbling nitrogen. Pure nitrogen* was further purified by passing it over copper wool at 450°C, cooled in a coiled glass water column, dried by passing through silica gel, drierite (anhydrous $CaSO_4$) and a molecualr sieve before entering the corrosion cell. The amount of oxygen remaining in solution after deaeration was determined by a Chemtrix Type 30 Oxygen Meter (with a detection accuracy of ± 0.2 ppm) and found to be 1.2 ppm.

3.2.4 Electrical Circuit

A potentiostatic circuit and a galvanostatic circuit, integrated by means of many switches, were used for the various experiments of this investigation. Although the actual circuitry was complicated mainly because of its versatility to switch from one potentiostat to the other or from galvanostatic to potentiostatic mode, the basic concept behind the circuits is shown in Figure 3-3.

Two Wenking potentiostats were used in the potentio-

---

*Canadian Liquid Air Ltd. 'Certified Grade' Purity 99.99% oxygen 20 ppm max.; argon 80 ppm; moisture < 10 ppm.

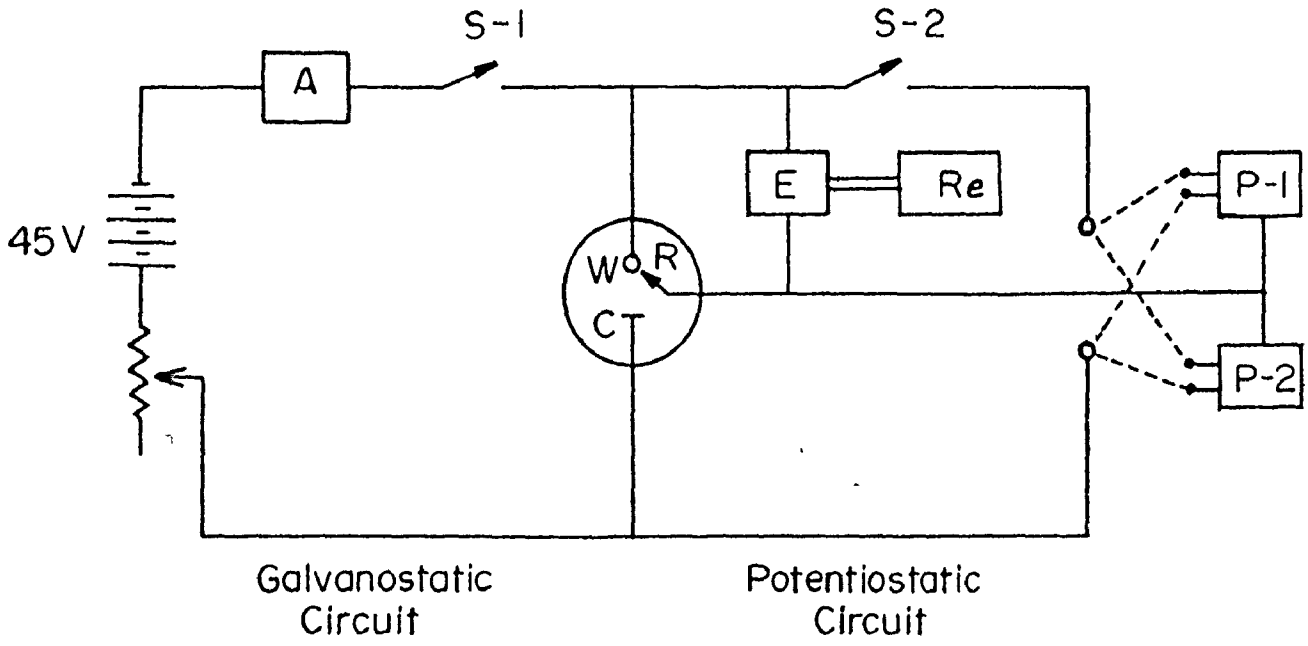

Figure 3-3. Schematic circuit diagram of the polarization circuit[100]

W - working electrode (specimen); C - auxiliary electrode (Pt); R = reference electrode (SCE);
A - Keithley Digital Multimeter, Model 160;
E - Keithley Electrometer, Model 610C;
Re- Brinkman Servogor Recorder, Model 2574;
P-1, Wenking Potentiostat, Model 62TRS;
P-2, Wenking Potentiostat Model 70EC3;
S - Switch.

static circuit only for convenience. Potentials were measured versus a Saturated Calomel Electrode (SCE) using a Keithley Electrometer. The potential and current outputs of the potentiostats were connected to a Brinkman Servogor Recorder. The recorder was a two pen linear/log model with integrator on one channel. Thus, when the current output from the potentiostat was connected to this channel, the current was integrated with respect to time and yielded the amount of charge which had passed. Current was followed by measuring the potential drop across a precision resistor (0.1%). In the case of Model 62 TRS the resistor had to be placed externally while for Model 70HC3 it was incorporated within its own circuitry.

The galvanostatic circuit was composed of a 45 volt stabilized D.C. power supply and a set of high resistors (> 10^6 ohms) to yield various current density values. The current in this circuit was measured by a Keithley Digital Multimeter claiming a sensitivity of 0.01 μA. The stability in this circuit was excellent since the current remained constant during any galvanostatic experiment.

3.3 Experimental Techniques

3.3.1 Potentiostatic Polarization

Specimens were anodically polarized from -300 mV with potentiostatic steps of 25 mV/min (the potential was changed by 25 mV and the resulting current was noted after an interval of 1 min) to different potentials, depending upon the nature of the experiment. The potential scan rate was chosen arbitrarily. However, it was found that although after 1 min at a potential the current was

still decreasing slowly, it was steady enough to allow unambiguous recording.

The potentiostatic polarization of all specimens in solutions of varying concentrations of chloride ions was performed in the following manner. Specimens were mechanically polished up to 1 μm diamond, electropolished in 60% H_2SO_4, cathodically reduced in a separate cell at -1500 mV for 10 mins in 1N H_2SO_4 and then held at a cathodic galvanostatic current density of 5.8 $\mu A/cm^2$ for 5 mins with occasional specimen stirring to remove the hydrogen bubbles. The specimen was put on open circuit and quickly transferred to the corrosion cell filled with 200 ml of the chloride-containing solution. It was allowed to stand undisturbed in the solution for 10 mins after which the potential was noted. This was taken to be the value of the corrosion potential, E_{corr}. The auxiliary lead was then connected and the specimen potentiostatically polarized. In-situ observation was performed throughout the scan.

3.3.2 Potentiostatic Activation

Specimens were directly subjected to a potential in the passive region in 1N H_2SO_4 solution and maintained in that condition for a certain period of time. They were activated by the addition of different volumes of 1N NaCl solution.

Specimens for potentiostatic activation studies were mechanically polished up to 1 μm diamond, electropolished in 60% H_2SO_4 and then introduced into the cell containing 150 ml 1N H_2SO_4. They were cathodically reduced at -1500 mV for 10 mins, switched to a cathodic galvanostatic current density of 5.8 $\mu A/cm^2$ for 5 mi[illegible] the specimen to

disperse the gas bubbles from the surface. They were then potentiostatically passivated at +400 mV for 30 mins. After 30 mins, chloride ions were added while stirring the solution and the current-time (i-t) curve was recorded. Four concentrations of chloride ions were employed, namely 0.02 M, 0.047 M, 0.13 M and 0.20 M.

3.3.3 Film Formation Study

This study was not involved with the formation of the film on a bare surface but concerned with film growth at later stages. Therefore, an initial film was formed potentiostatically and its growth studied by galvanostatic means. The study was performed only on nickel.

Specimens were electropolished and cathodically reduced in the standard way. They were then given a preliminary oxidation treatment at +400 mV for 3 mins in 1N H_2SO_4 after which they were switched to an appropriate anodic current density. The growth of the film was evident by the decrease in current with time at the constant potential during the preliminary oxidation and later by the increase in potential with time at the constant growth current density.

3.3.4 Cathodic Reduction Studies

These studies were used to determine the charge consumed in the cathodic reduction of the anodically formed film. The basic process consists of holding the specimen anodically at a constant passive potential for a certain period of time

and then cathodically reducing the film at a constant current density until the corrosion potential, E_{corr}, of the specimen is reached. The time involved in the reduction of the film multiplied by the current density yields the charge density. The record of the potential change with time permits the analysis of the data for plateaus corresponding to the various surface species.

The film was formed at a constant potential of +600 mV for 15 mins, 30 mins and 60 mins and cathodically reduced at a current density of 2.7 $\mu A/cm^2$. When the growth of the film was carried out in 1N H_2SO_4 the standard procedure was employed. Specimens were electropolished and cathodically reduced as before in the corrosion cell. They were held anodically at +600 mV for the various times and then cathodically reduced. The potential trace was recorded. However, when film formation was performed in chloride containing solutions, the procedure was slightly modified. After the standard electropolish, specimens were introduced in the cell containing 150 ml 1N H_2SO_4 and then cathodically reduced in the standard manner. They were switched to a galvanostatic cathodic current density of 5.8 $\mu A/cm^2$ for 4 mins, occasionally stirring the specimen to remove the gas bubbles from the surface. While still under galvanostatic cathode control, 1 ml 1N NaCl was now added to the cell and the solution stirred for 2 mins for thorough mixing. This yielded a chloride concentration of 0.007 M. Specimens were then anodically oxidized at +600 mV for various times. After

the time, the tap on the side of the cell was opened and 75 ml of the solution was allowed to drain out. 400 ml of fresh deaerated 1N H_2SO_4 was added (resulting in the reduction of the chloride concentration to 0.001 M) and the reduction performed cathodically.

In actual practice, the galvanostatic circuit (switch S-1, Figure 3-3) was closed before the potentiostatic circuit (switch S-2, Figure 3-3) was opened, the potentiostat compensating for the small cathodic current introduced by the reduction circuit[100]. This ensured that reduction of the film would begin instantaneously with no possibility of side reactions during time at open circuit.

3.3.5 Repassivation Studies

For the most part these studies were similar to the potentiostatic polarization ones. Electropolished specimens were polarized from -300 mV to different potentials in the transpassive region. However, when a current density of 3.0 mA/cm^2 was reached for the Ni, Ni-5Mo , Ni-10Mo and Ni-15Mo alloys and 5.5 mA/cm^2 for the Ni-22Mo alloy, the direction of the potentiostatic scan was reversed although the rate (25 mV/min) was not changed. The reverse scan was continued to various lower potentials depending upon the particular experimental run. Experiments were performed in 1N H_2SO_4 and in 0.02 M and 0.09 M chloride containing solutions.

3.3.6 Anodic-Cathodic Polarization

These studies were aimed at exploring the effect of molybdenum on the anodic and cathodic partial processes in 1N H_2SO_4 by the measurement of the respective Tafel slope (β_a, β_c). The procedure was as follows. Specimens were electropolished and then cathodically reduced in the corrosion cell. They were then put on open circuit and allowed to attain the steady state corrosion potential (E_{corr}). The potentiostatic scan was performed starting at just above the corrosion potential for cathodic polarization and just below (more negative) the corrosion potential for anodic polarization. The cathodic polarization curve for each specimen was determined first. The cathodic overvoltage was increased to about 400 mV. The specimen was disconnected from its electrical connections and allowed to attain E_{corr}. It was then polarized anodically to potentials just below its E_{pp}. It was found that using separate specimens for each part of the experiment did not alter the results. Thus, the same specimen was used to obtain both sections of the curve.

3.3.7 Weight Loss Measurements

Specimens for weight loss measurements were only mechanically polished up to 600 grit silicon carbide paper, rinsed in methanol and air dried. They were suspended in the corrosion cell by a glass hook to avoid any galvanic corrosion effects. The test solution of 10% HCl was used in order to provide

measurable weight loss. Specimens were removed once a day from the cell, washed thoroughly in water, rinsed in methanol and air dried. They were weighed on a gravimetric balance with an accuracy of ±2 micrograms (Mettler, Model M-5) after which they were re-introduced in the corrosion cell. The experiment was performed for 8 days and the reported values for the corrosion rates are steady state values determined from the slope of the weight loss-time curves. The corroding 10% HCl solution was saturated with nitrogen before immersion of the specimens and bubbling of nitrogen was continued throughout the duration of the test.

3.4 General Techniques

3.4.1 Metallography

The metallographic structure of all specimens was determined by mechanically polishing them up to 1 μm diamond followed by an electropolish in 60% H_2SO_4 according to the schedule of Table 3-4 (the Ni-30 Mo alloys were never electropolished) and then by etching them electrolytically in a solution containing 2 parts 20% HCl and 1 part H_2O_2 at a current density of 0.05 A/cm^2 using a stainless steel cathode[43]. All specimens removed from the corrosion cell after potentiostatic polarization had their structure clearly revealed and did not require any etching All structures were photographed on a Zeiss inverted metal microscope.

3.4.2 Replication

A two-stage replication procedure was adopted. Parlodion* was deposited on the specimen surface and allowed to dry overnight. The parlodion was stripped from the specimen surface, taped to a microscope glass slide and shadowed with gold at an angle of about 20°. A thin film of carbon was deposited over the shadowed replica from an arc. The parlodion was cut into small squares and placed on 200 mesh electron microscope grids. The parlodion was dissolved in iso-amyl acetate solution leaving behind the carbon film with the shadowed gold on the grid. A Philips EM 300 electron microscope operating at 80 kV was used in transmission to examine the replicated surface.

3.4.3 Electron Microscopy

The Philips EM 300 electron microscope was used to obtain the diffraction pattern of the film collected from a Ni-5Mo alloy. A thin foil of gold was used for calibration purposes.

A Cambridge Scanning Electron Microscope (Mark 2A) equipped with a Kevex-ray detector and appropriate electronics was used to map out the distribution of nickel and molybdenum in the various specimens. The scanning electron microscope was also employed to obtain the photographs of the fractured surface (fractographs) of some of the alloys.

---

*A highly purified form of non-explosive cellulose nitrate.

3.4.4 X-ray Diffraction

A Philips x-ray diffractometer was used for lattice parameter determination and phase identification of the alloys. A copper target with no filter was used since the Geiger counter was equipped with a crystal monochromator. The tube was operated at 30 kV with a filament current of 30 mA. Specimens were in the form of sheets about 3 cm × 3 cm. They were scanned at a rate of $2\theta = 1°/2$ mins from $2\theta = 5°$ to $2\theta = 150°$.

3.4.5 Atomic Absorption Spectroscopy

Atomic absorption spectrophotometry was used to determine the quantity of nickel and molybdenum in solution. For the analysis of solutions after potentiostatic polarization of the alloys in chloride containing environments, a Perkin-Elmer Atomic Absorption Spectrophotometer (Model 303) with a gas flame was employed. The accuracy of detection is 0.15 ppm for nickel using an air-acetylene flame and 0.60 ppm for molybdenum employing a nitrous oxide-acetylene flame.

The determination of nickel in 1N H_2SO_4 solution for the film formation study was performed using a Varian Techtron Atomic Absorption Spectrophotometer (Model AA6) with a carbon rod atomizer (Model 63). The accuracy of detection by this method is better than 0.005 ppm.

3.5 Reproducibility of Results

The experiments reported in this investigation were repeated up to five times to check for reproducibility. In

general, the results were found to be quite reproducible, the limits of reproducibility varying with type of equipment and are therefore represented differently. Error bars are shown on weight loss measurements whereas the limits are numerically indicated in cathodic reduction experiments. For all other experiments the presented curve is the record of one particular experimental run and is typical of the system for potentiostatic polarization studies (including repassivation), the results were reproducible to within ± 5%. The active region of the curve was almost exactly reproducible although some scatter was found in the passive region. The results of the galvanostatic oxidation were reproducible to better than 5%. The maximum scatter was found in the potentiostatic activation studies (± 10%). However, the trend of the results (of one chloride concentration for all the alloys or all chloride concentrations for one alloy) was found to be the same.

CHAPTER IV

RESULTS: THE CORROSION BEHAVIOUR OF NICKEL

4.1 Introduction

In order to prevent a metal from corroding, a barrier is required between the metal and the environment. For a 'passivated' metal, it has generally been assumed that this barrier consists of a very thin, often invisible protective film of products formed by reaction of the environment with the metal. Very often this film represents some form of metallic oxide and is generally referred to as the 'passive film'.

Nickel is a transition metal and is capable of exhibiting an active-passive transition in many environments including H_2SO_4 solution. The passive film on nickel in acid solution is believed to be either a single oxide[56,67,69] (NiO or Ni_3O_4) or a duplex oxide[67] (NiO + Ni_3O_4). In an attempt to understand the effect of molybdenum addition to nickel-molybdenum alloys and to provide a basis for comparison, an investigation was undertaken on polycrystalline nickel with an average grain size of 0.035 mm. The studies reported in this chapter contain the determination of film thickness with time of film formation, kinetics of film growth under galvanostatic conditions and an examination of the significance of the critical potential for determining the susceptibility of nickel to pitting corrosion.

4.2 Passive Film Thickness and Cathodic Reduction Behaviour

When nickel is potentiostatically subjected to a potential in the passive region - anodic oxidation - the formation of the film proceeds by the anodic dissolution of the nickel. The current density (at constant potential) decreases with time signifying the growth of the film. The charge stored in the film, which is proportional to film thickness, can be calculated by integrating the current density with respect to time, if it is assumed that all the current is involved only in film growth.

A large amount of charge is consumed during the anodic oxidation of nickel even in the passive region. For instance, during 3 mins of preliminary potentiostatic oxidation in 1N H_2SO_4 at +400 mV, an average of 6.12 mC/cm^2 is consumed. If the film is assumed to be NiO, then the thickness of the film can be calculated from the equation[74] -

$$\text{Thickness, } x = \frac{Q_f\, M}{nfDr}, \qquad (4\text{-}1)$$

where M = molecular weight of NiO = 74.7 gms

D = density of NiO = 6.83 gm/cm^3

f = Faraday = 96500 C

$Q_f = \int_0^t i_p dt$ = total charge consumed = 6.12±0.02 mC/cm^2

n = oxidation number = 2

r = surface roughness factor, assumed = 1

which for a charge 6.12 mC/cm^2 yields,

$$x = \frac{74.7 \times 6.12 \times 10^{-3} \times 10^{8}}{2 \times 96500 \times 6.83} \text{ , } \mathring{A} = 34.7 \mathring{A} \text{ .}$$

Actually, as was pointed out earlier, passive films on nickel are typically 6-16 $\mathring{A}$ thick. It, therefore, seems unlikely that all the charge associated with the anodic oxidation process corresponds to film growth. If only a part of the charge is involved in film growth, then considering the mass balance, the remainder of the charge must be associated with nickel dissolution. It thus appears that nickel dissolution is a major and important aspect of nickel passivation.

It is, therefore, apparent that in order to determine the thickness of the film on nickel, the fraction of the charge corresponding to nickel present in solution must be accurately known. This charge, when subtracted from the total charge consumed during the anodic oxidation process, will yield the charge stored in the film and hence film thickness.

The amount of nickel that passes into solution during anodic oxidation can be estimated provided an analytical technique sensitive enough to detect the minute concentrations is available. The atomic absorption spectrophotometer using a carbon rod atomizer is capable of detecting nickel with a sensitivity of 0.005 ppm. This technique was employed to determine the nickel that remained in solution after the nickel electrode was withdrawn. Nickel electrodes were anodically oxidized for periods of 15 mins, 30 mins and 60 mins at +600 mV in 100 ml of 1N H_2SO_4 solution. After the appropriate time,

the electrode was quickly withdrawn from the solution while still under potentiostatic control. The solution in the cell was collected in a volumetric flask and later analyzed by the atomic absorption spectrophotometer. The quantity of nickel dissolved during the cathodic pretreatment could not be detected (ie. it was less than 0.005 ppm from a 0.36 cm^2 nickel electrode). Hence, the charge stored in the film, Q_f, is simply the total charge involved in the anodic oxidation process, Q_T, less the calculated charge corresponding to the quantity of nickel detected in solution, Q_{Ni} (ie. $Q_f = Q_T - Q_{Ni}$) and is presented in Table 4-1. The error in the estimation of Q_T is about 4% while that in the determination of Q_{Ni} is about 6%. Hence, the uncertainty in the tabulated value of Q_f is about 7%. The thickness of the film has been calculated using Eqn. (4-1) assuming that the film is uniform and is composed entirely of the oxide NiO.

There is another, and perhaps simpler, method of evaluating the film thickness on nickel. This method, which is direct, consists in determining the charge required to cathodically reduce at constant current density the anodically formed film. This charge then is the charge stored in the film and can be converted to film thickness using equation (4-1).

The charge consumed during anodic oxidation at +600 mV and subsequent cathodic reduction at 2.7 $\mu A/cm^2$ is presented in Table 4-2. Once again, film thickness has been calculated

Table 4-1

The charge stored in the film during anodic oxidation of Ni in 1N H_2SO_4 at +600 mV for various times

Time mins	Q_T mC/cm^2	Q_{Ni} mC/cm^2	Q_f mC/cm^2	x* Å	Charge in Film** %
15	24.06	22.88	1.18	6.7±0.3	4.9
30	32.58	29.90	2.68	15.2±0.7	8.2
60	43.46	40.63	2.83	16.1±0.8	6.5

*Film thickness assuming film to be uniform and composed of NiO

**As percentage of the total anodic charge involved in film growth.

Table 4-2

Charge consumed during anodic oxidation of Ni in 1N H_2SO_4 at +600 mV and subsequent cathodic reduction at 2.7 $\mu A/cm^2$

	Passivation Time		
	15 mins	30 mins	60 mins
Anodic Oxidation	23.7 mC/cm^2	33.7 mC/cm^2	43.5 mC/cm^2
Cathodic Reduction	1.03±0.11 mC/cm^2	2.50±0.04 mC/cm^2	1.77±0.01 mC/cm^2
Film Thickness*	5.8 ±0.6 Å	14.2±0.2 Å	10.1±0.1 Å
Charge in Film**	4.4%	7.4%	4.1%

*Assuming film to be uniform and composed of NiO.

**As percentage of the total anodic charge involved in film growth

from equation (4-1) assuming the oxide to be uniform and composed of NiO. It is evident that cathodic reduction experiments provide a true and realistic estimate of the passive film thickness. It is interesting to note that only a small fraction of the total charge involved in the anodic oxidation process goes towards film formation.

The cathodic reduction curve as obtained from the recorder is a potential trace as a function of time. Since the reduction current density is constant and known, the time axis can be redesignated to represent the charge consumed in reduction. Cathodic reduction curves are normally drawn with the electrode potential along the ordinate and charge along the abscissa. The cathodic reduction curves for nickel are given in figure 4-1. These curves exhibit the following arrest plateaus:

15 mins - one arrest at -50 mV (SCE) = +192 (SHE)

30 mins - two arrests at -50 mV (SCE) and -170 mV (SCE) = +72 mV (SHE)

60 mins - one arrest at -160 mV (SCE) = +82 mV (SHE).

Each arrest is due to the reduction of a particular species. In this case, the arrest at +72 mV (SHE) is found to correspond to the reaction

$$Ni + H_2O \rightleftharpoons NiO + 2H^+ + 2e. \qquad (4\text{-}2)$$

For this reaction from Nernst's equation[66],

$$E_1 = 110 - 59\ [pH],\ mV\ (SHE)$$

and at the pH of the solution (= 0.4).

$$E_1 = +86\ mV\ (SHE).$$

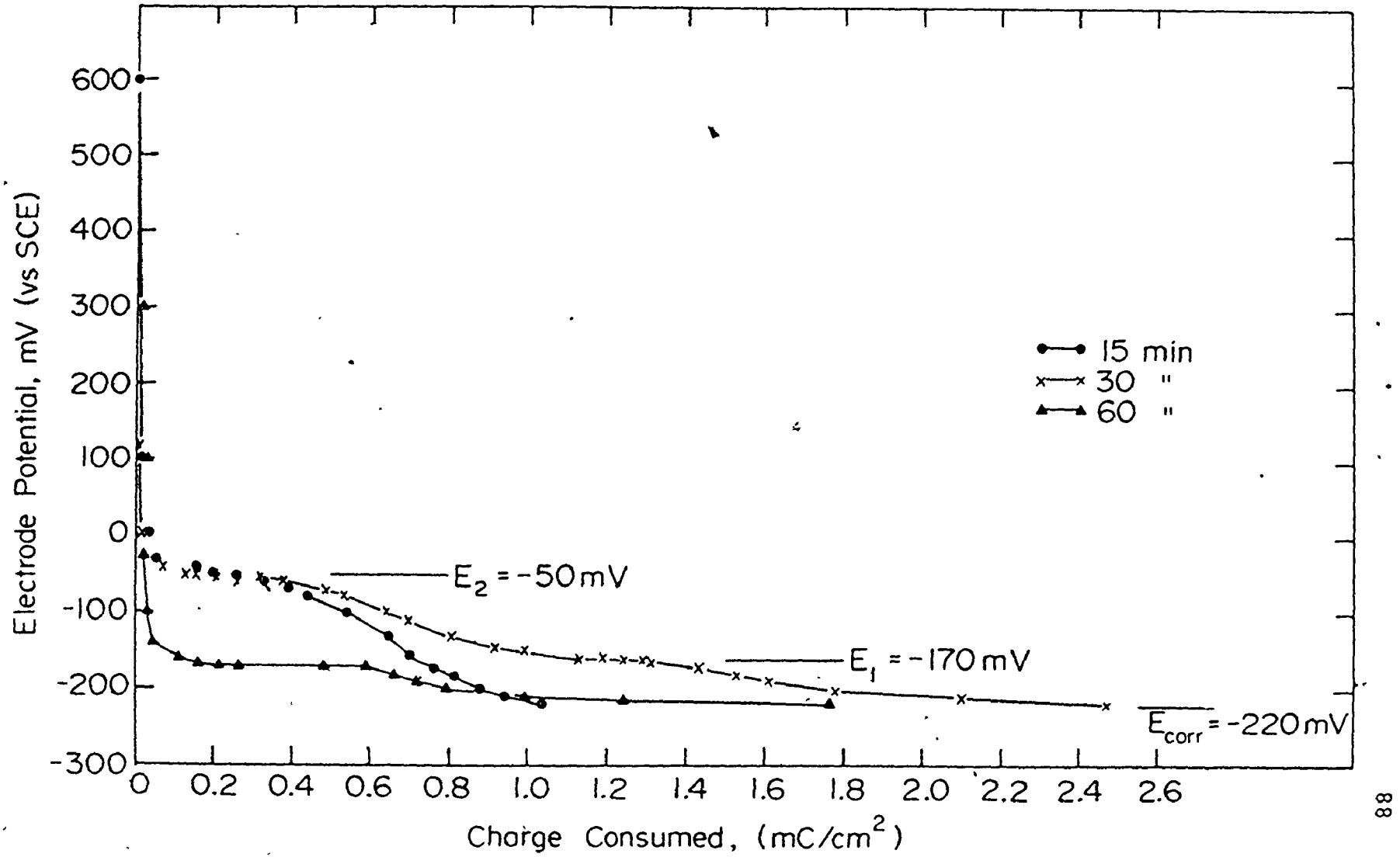

Figure 4-1. Cathodic reduction curves for nickel at 2.7 $\mu A.cm^2$ in 1N H_2SO_4 for various times of anodic oxidation at +600 mV.

Although it has not been possible to accord any reaction scheme to the other arrest potential, it is possible that the arrest is due to a metastable complex.

4.3 Galvanostatic Film Growth

It is believed by some investigators[101] that the dissolution rate of NiO in 1N H_2SO_4 is potential dependent, increasing with increase in potential. However, contrary to this belief Sato and Okamoto[67] and the results of this investigation (Figure 5-8) indicate that during potentiostatic polarization in 1N H_2SO_4 the current density in the passive region (i_p) becomes independent of potential (E). It is believed[102] that at this stage a steady state sets in implying that film formation and film dissolution proceed at equal rates, ie.

$$i_f = i_d = i_p \qquad (4\text{-}3)$$

where i_f and i_d are the film formation and film dissolution current densities. However, potentiostatic oxidation curves (current density-time curves at constant potential) show that equilibrium does not set in until after about 4 mins at the potential[67]. Therefore, even though the dissolution current may be considered independent of potential, there is little doubt that it is dependent upon time.

If the oxidation is carried out under constant current density conditions (galvanostatic), the potential increases with charge consumed. At any particular potential, the thickness of the film (measured as the charge stored in the film)

should be characteristic of that potential and the measured growth current density. That is to say, the fraction of the charge involved in the growth of the film should be constant.

The galvanostatic oxidation curves for nickel in 1N H_2SO_4 at four different current densities are presented in Figure 4-2 in the form of Potential-Total charge consumed ($E - Q_T$). It has already been shown that nickel dissolution is an important aspect of anodic oxidation and the present galvanostatic curves are no exception. In fact, as can be seen by the numerical values of the abscissa, the charge involved is extremely high, thereby suggesting very thick films if it is assumed that all the charge is involved only in film growth. Thus, a correction is required for the nickel dissolved into solution. As has been found by Okuyama and Haruyama[103] if such a correction is applied the shape of the anodic curve does not change, although the values on the abscissa may be significantly different.

Weil[104] has suggested a method whereby the galvanostatic oxidation curves can be corrected for nickel dissolution. This method, which was later used by Sato and Okamoto[77] states that the actual growth current density, i_{growth}, is given by

$$i_{growth} = i_g - i_d \qquad (4-4)$$

where, i_g = the measured galvanostatic growth current density

i_d = the potential-independent dissolution current density (= 17.0 $\mu A/cm^2$, as found in this investigation).

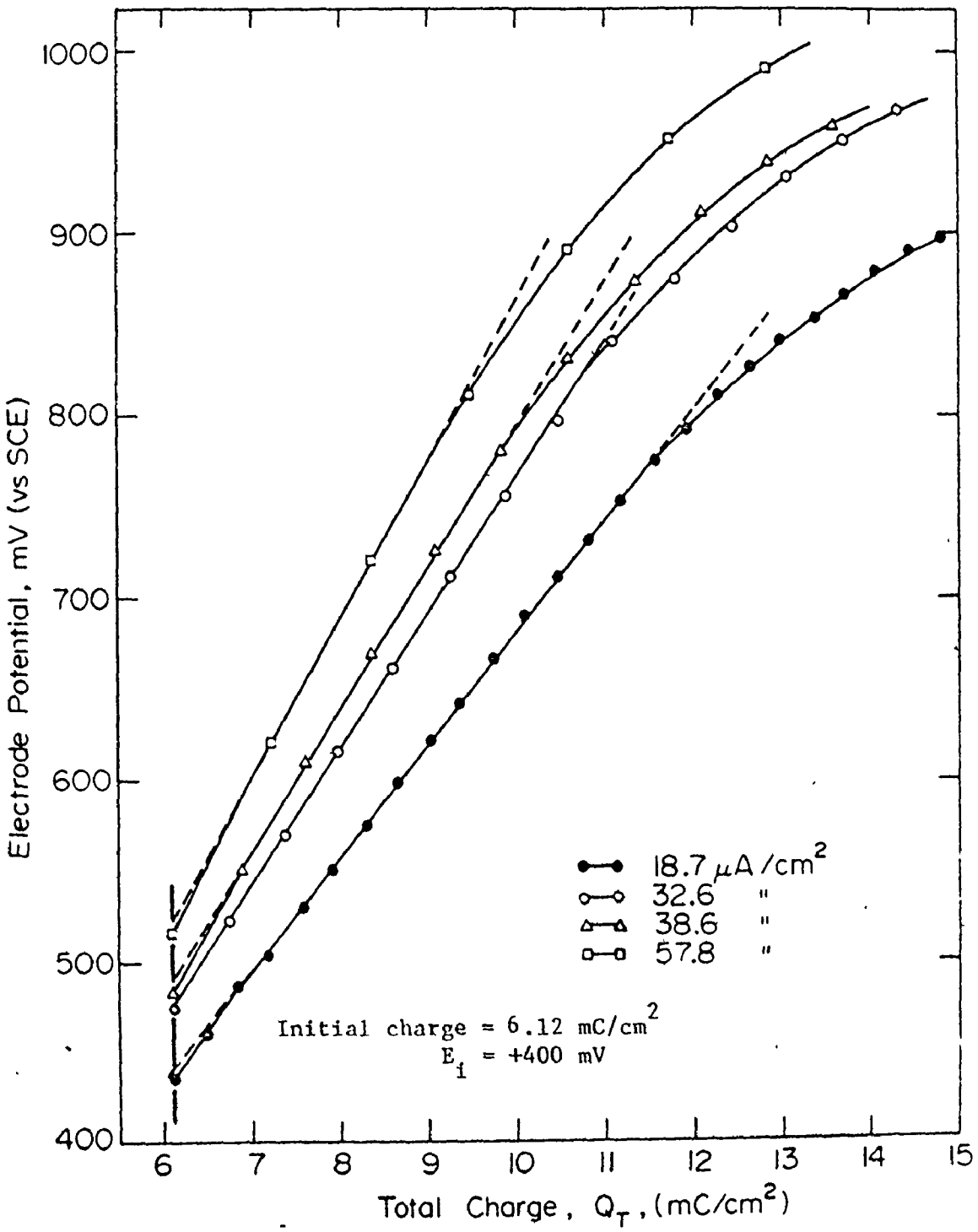

Figure 4-2. Electrode potential - total charge consumed ($E-Q_T$) curves for nickel in 1N H_2SO_4 at various growth current densities. The curves are uncorrected for dissolution.

And therefore, charge stored in the film is,

$$Q_g = (i_g - i_d)t \qquad (4\text{-}5)$$

where, t = growth time.

If this analysis is applied to the present results, it is found that sections of the E - Q_g curves at constant Q_g yield Tafel lines (ie. E-log i lines) with negative slopes. This obviously is not meaningful. A closer examination of equation (4-5) indicates that the answer to the problem lies in the product $i_d t$ which must be smaller than $i_g t$. This implies that either the dissolution current density must be very small as compared to the growth current density so that the reverse reaction rate is negligible (as was the case for Sato and Okamoto[77]) or that the time of growth be very large so that the dissolution current density can become independent of time and steady state can set in (as was the case with Weil[104]). In the present case, i_d is comparable to i_g and t is not very large. Thus, the analysis cannot be applied as it stands. A slight modification of the same basic procedure follows.

The growth times involved in the lowest growth current density (viz 18.7 $\mu A/cm^2$) are about that reaching equilibrium. Hence, the 'true growth' curve for this current density can be drawn based on the method of Weil[104]. The fraction of the charge used in film growth can be calculated from

$$f = \left(\frac{Q_g}{Q_T}\right)_i \qquad (4\text{-}6)$$

where $Q_T = Q_g + Q_d$

= total charge consumed up to that instant.

The growth curves for the other current densities can now be obtained by multiplying f by the value of the total charge consumed at various constant potentials.

Based on this procedure, the results obtained are presented in Figure 4-3. It can be seen that the shape of these curves is not different from those of Figure 4-2, although the abscissa numerical values are significantly lower. The extrapolated curves of Figure 4-3 meet at +225 mV (SCE) or +467 mV (SHE) (as do those of Figure 4-2). This potential has been related to the Flade potential* (E_F) by Weil[104]. For nickel in 1N H_2SO_4, Sato and Okamoto[77] found that E_F= +435 mV (SHE).

Sato and Okamoto[77] have shown that (see Appendix B for a derivation of this equation)

$$E - E_F = K\{(i_g - i_d)t + Q_i\} \qquad (4\text{-}7)$$

---

*There is no general agreement on the exact nature of the Flade potential (E_F). One belief is that it corresponds to an equilibrium potential (in a potentiostatic polarization scan) at which electrochemical production of a protective film (oxide or adsorbed) is thermodynamically possible by a reaction of the type

$$M + H_2O \rightarrow MO + 2H^+ + 2e \ .$$

Hence E_F can be more negative than the passivation potential (E_{pp}). Others[11] suggest that E_F and E_{pp} are synonymous. Yet others prefer to identify E_F with a potential more positive than E_{pp} at which passivation is complete.

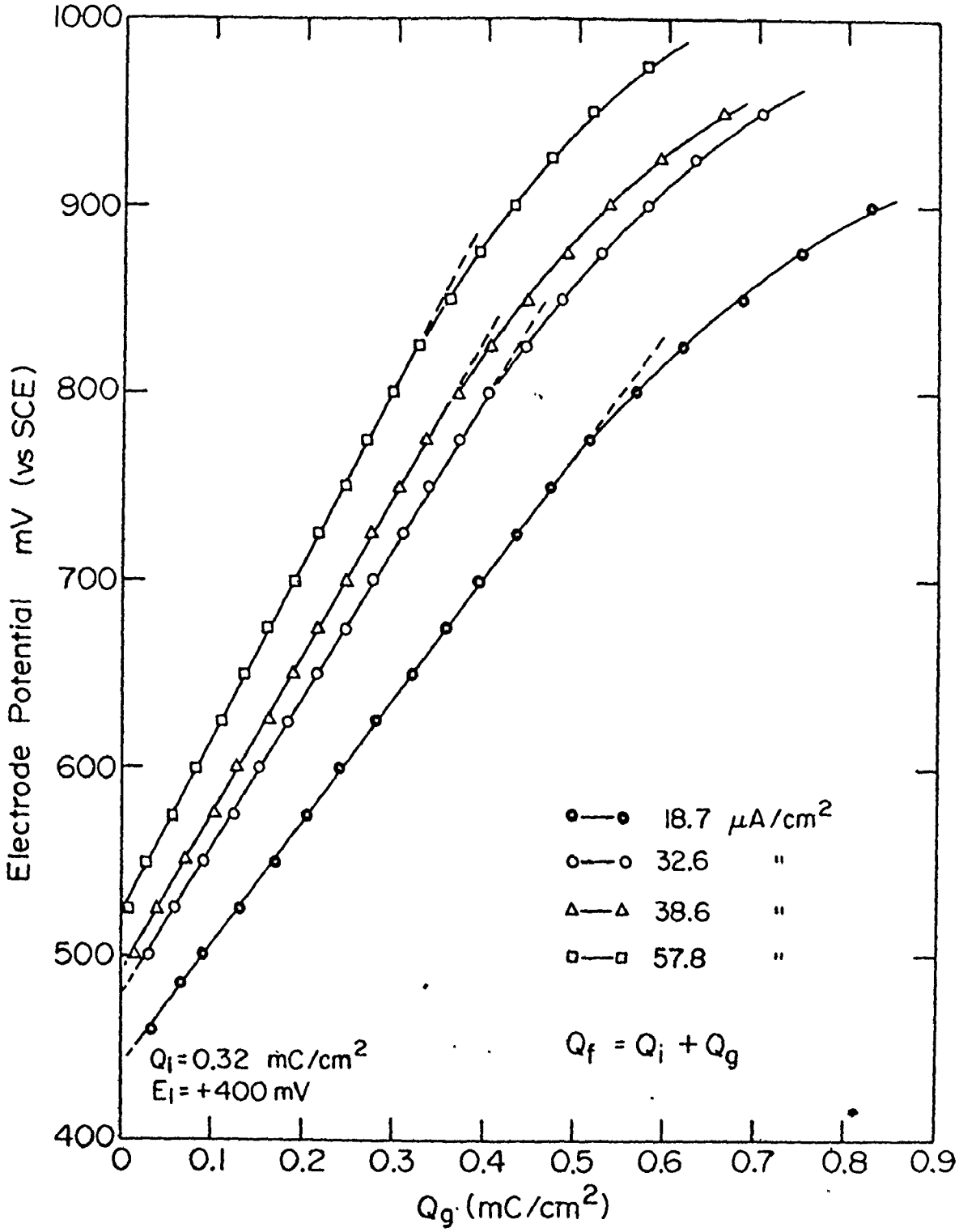

Figure 4-3. Electrode potential - charge stored in film ($E-Q_f$) curves for nickel in 1N H_2SO_4 at various growth current densities. The curves are corrected for dissolution.

$$= K(Q_g + Q_i) \qquad (4\text{-}8)$$

$$= KQ_f \qquad (4\text{-}9)$$

where $Q_f = Q_g + Q_i$

= total charge in the film (and consequently a measure of film thickness)

and,

E = initial oxidation potential

K = a constant = $\frac{\partial E}{\partial Q_f}$ = slope of the growth curve

Q_i = charge stored in the film during the initial oxidation (ie., initial film thickness).

Now, the initial oxidation was performed potentiostatically at +400 mV (SCE) for 3 mins. Thus,

$$E = +400 \text{ mV (SCE)}$$

$$E_F = +225 \text{ mV (SCE)}.$$

Hence, the charge during initial oxidation can be calculated from equation (4-7) knowing the slopes of the growth curves and their intercept on the abscissa at the various growth current densities. These results are given in Table 4-3.

The average value of Q_i = 0.32 mC/cm^2. Potentiostatic measurements yield that the total charge consumed during 3 mins of anodic oxidation at +400 mV is 6.12 mC/cm^2 (of which only 0.32 mC/cm^2 - 5.25% - goes towards film formation). Thus, about 95% of the charge during initial oxidation in 1N H_2SO_4 goes for Ni dissolution.

Table 4-3

Estimation of the charge stored in the passive film on Ni in 1N H_2SO_4 during 3 mins of anodic oxidation at +400 mV

i_g $\mu A/cm^2$	Q_g mC/cm^2	K $mV/mC/cm^2$	Q_i mC/cm^2
18.7	-0.060	675	0.32
32.6	-0.103	800	0.32
38.6	-0.112	840	0.32
57.8	-0.133	925	0.32

Average, Q_i = 0.32 mC/cm^2

4.4 The Critical Potential

The anodically formed passive film is the only barrier that exists between the nickel surface and the solution. Any damage or breakdown of the film results in corrosion. The presence of chloride ions has always been detrimental to the film and has been responsible for corrosion, which in many cases takes the form of pitting. It has generally been believed[105-107] that metals undergo pitting corrosion only beyond a certain critical potential (E_c). This potential has served as one of the fundamental electrochemical criteria characterizing the susceptibility of metals to pitting corrosion. It is believed[108] that at more negative potentials than E_c the metal exists in a passive state, while above E_c, active and passive states coexist on the metal surface giving rise to pitting corrosion. The implication is that the more positive the value of E_c, the more resistant is the metal to pitting corrosion. The validity of this concept was examined for nickel in a 0.02 M Cl^- containing solution by studying the effect of grain size and polarization procedure on E_c.

The anodic polarization curves for eight specimens with grain size ranging from 0.025 to 0.330 mm. are shown in Figure 4-4. All specimens exhibit an active-passive transition. The anodic dissolution parameters, the anodic Tafel slopes (β_a), and the slopes in the transpassive region (β_t) are summarized in Table 4-4. It can be seen that the value of the critical

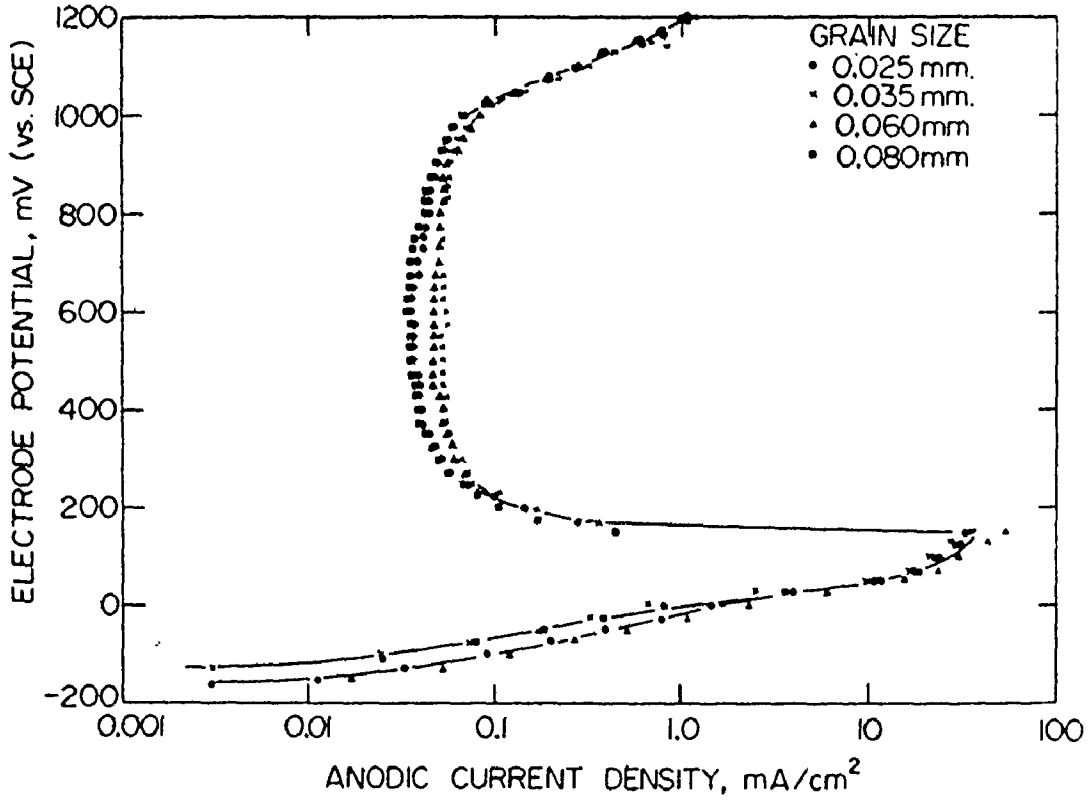

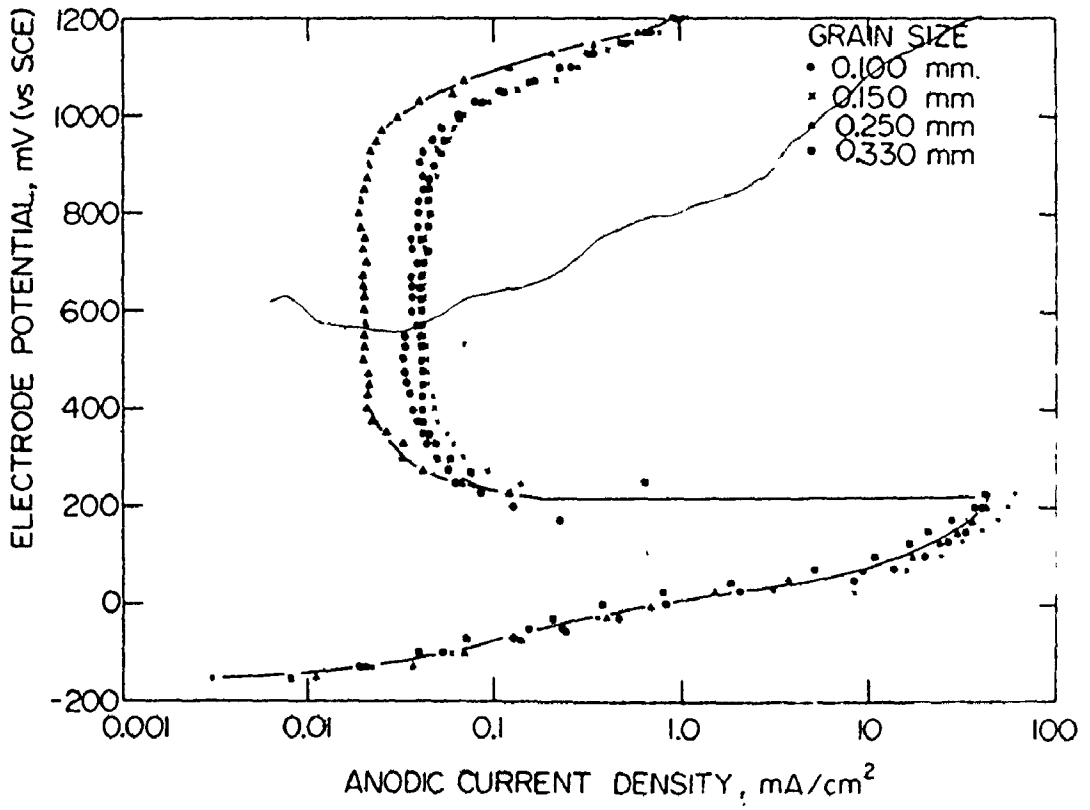

Figure 4-4. Anodic polarization curves for nickel of
in M Cl^- solution (pH=0.4).

Table 4-4

Anodic polarization parameters for nickel with varying grain size in 0.02 M Cl^- solution

Grain Size Average grain diameter	E_{corr} mV	E_{pp} mV	i_c mA/cm^2	i_p* mA/cm^2	E_c mV	β_a mV/decade	β_t mV/decade
0.025	-170	+150	33.3	0.036	+950	80	160
0.035	-130	+150	36.7	0.053	+950	80	165
0.060	-190	+150	52.8	0.047	+950	75	165
0.080	-135	+125	28.3	0.036	+950	70	160
0.100	-165	+150	33.3	0.033	+950	80	158
0.150	-175	+225	61.1	0.042	+950	82	160
0.250	-170	+200	41.9	0.019	+950	95	152
0.330	-220	+225	43.5	0.041	+950	85	172

*Lowest recorded value

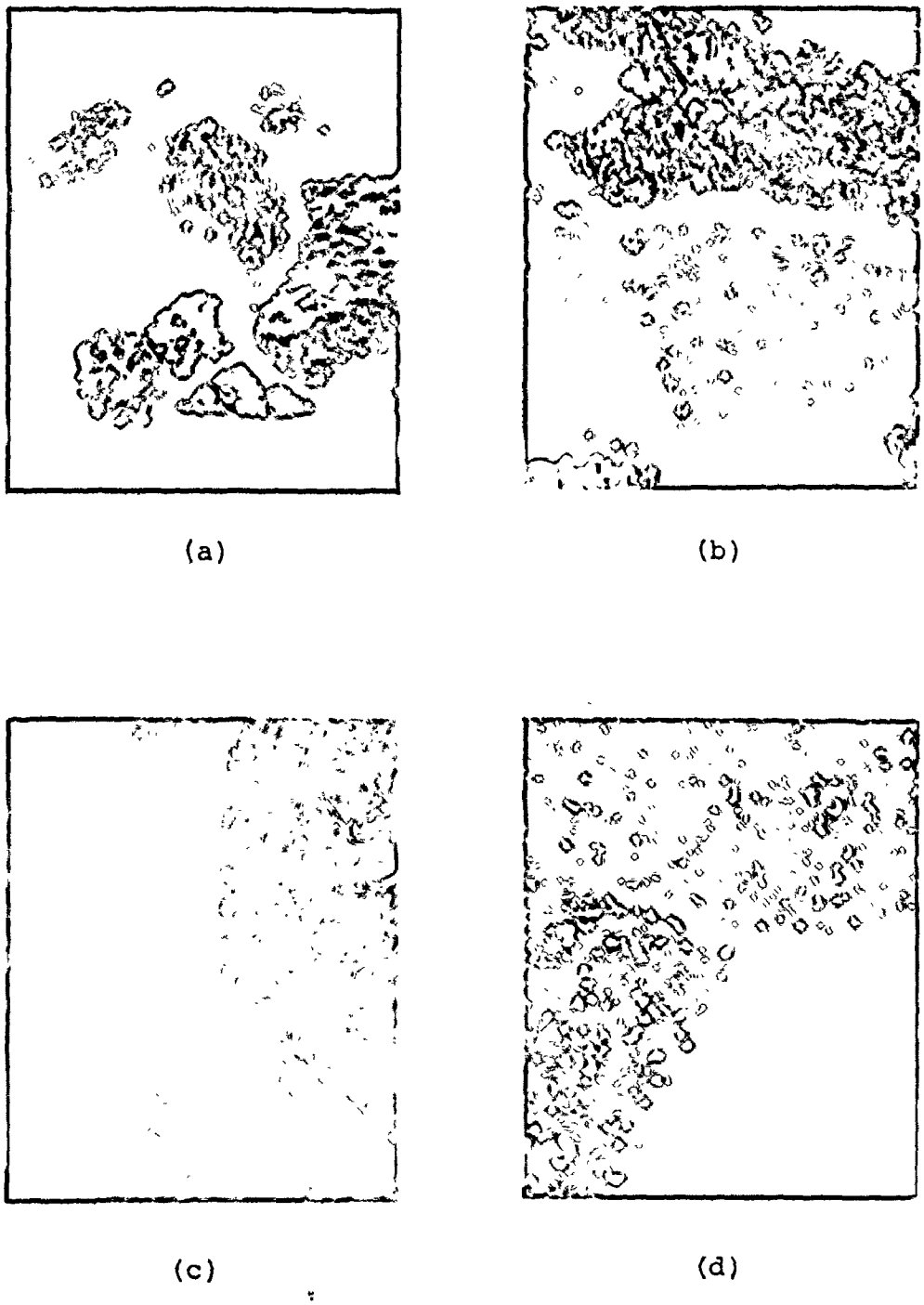

Figure 4-5. Nature of attack on polycrystalline nickel with varying grain size in 0.02 M Cl^- solution after polarization to +1200 mV
(a) Grain size = 0.025 mm, 500×
(b) Grain size = 0.060 mm, 500×
(c) Grain size = 0.100 mm, 250×
(d) Grain size = 0.330 mm, 250×
The arrows indicate some regions of localized attack.

potential (E_c) is the same in every case and, within the limits of experimental error, the values of the other parameters do not change significantly over the grain size range.

A definite trend was observed in the nature of the attack in these specimens. At lower grain sizes (0.025-0.035 mm) pits were formed only along the grain boundaries (Figure 4.5(a)). As the grain size increased to 0.060 mm both grain boundary and grain interior pitting occurred (Figure 4-5(b)). At grain sizes larger than 0.080 mm, pits were formed only within the grains, and their density increased with increasing grain size (Figures 4-5(c) and (d)).

'In-situ' microscopic examination of the specimen surface was performed throughout each polarization run. Photomicrographs showing the surface morphology at various stages of polarization and the relevant polarization curve for a 0.060 mm grain size specimen are given in Figures 4-6 and 4-7. It can be seen that most of the attack develops in the 'active region', i.e. before the onset of passivity, and at higher (more anodic) potentials only increases slightly in intensity.

In order to understand better the significance of the critical potential, specimens of grain sizes 0.025, 0.100 and 0.330 mm were subjected to a passive potential of +400 mV for 28 mins (time taken for a normal potentiostatic sweep from -300 mV to +400 mV) in 1N H_2SO_4 followed by the addition of 0.02 M Cl^- as 1N NaCl and polarization continued up to +1200 mV. The results are presented in Figure 4-8. The anodic current

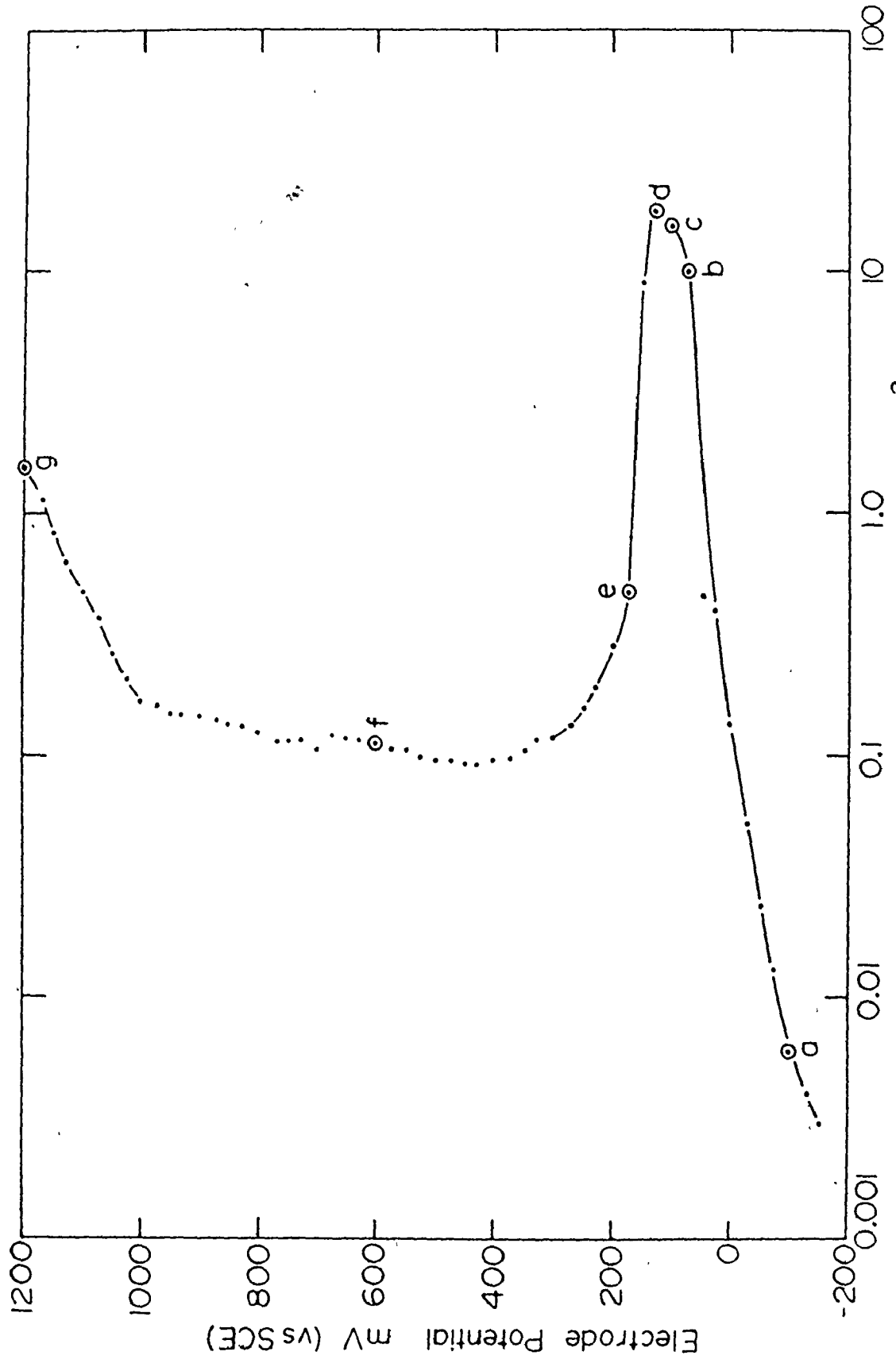

Figure 4-6. Anodic polarization curve for nickel in 0.02 M Cl solution (pH = 0.4). (a), (b)....(g) refer to stages at which optical micrographs were taken to record the development of corrosion morphology shown in Figure 4-7.

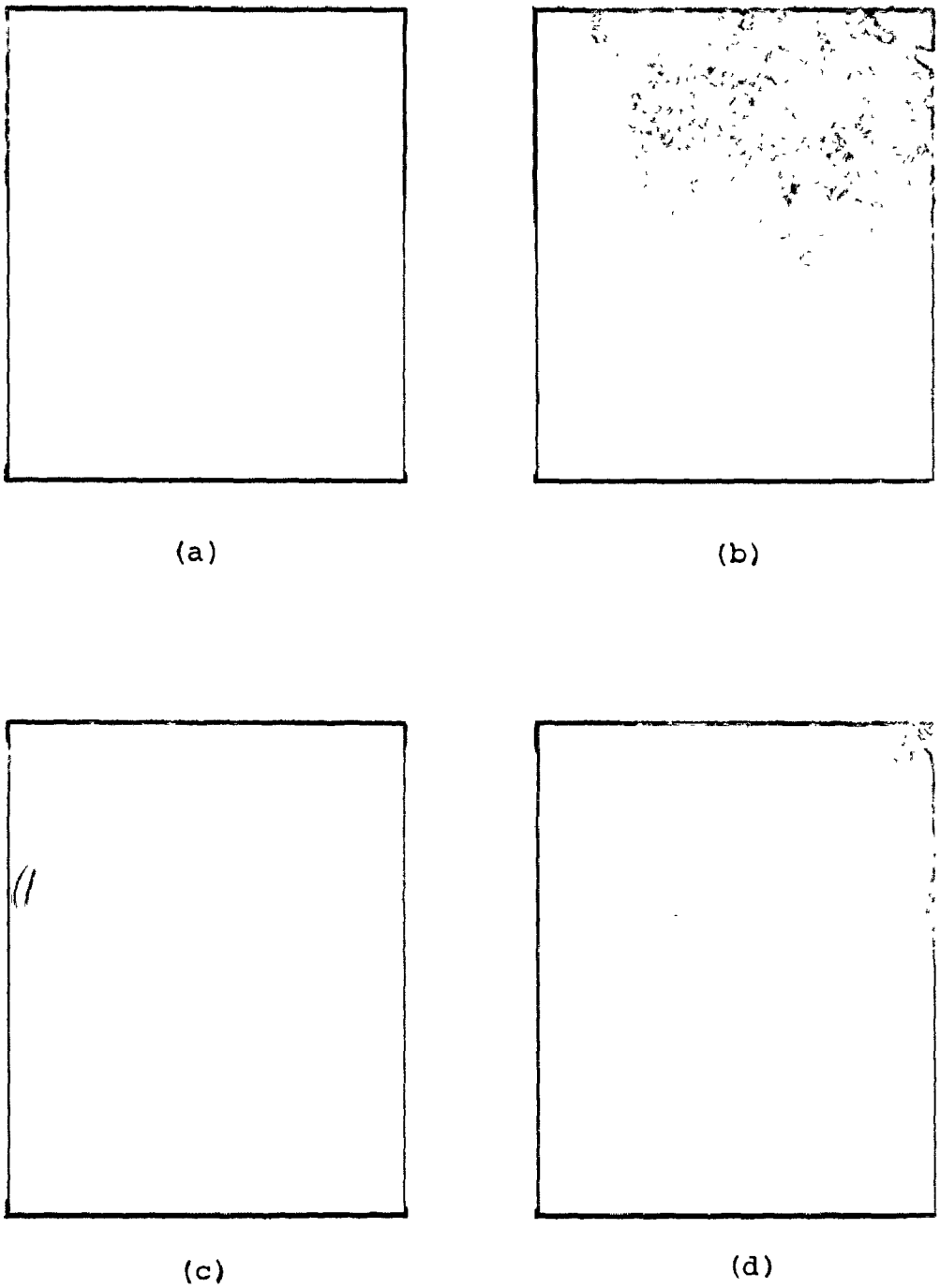

Figure 4-7. 'In-situ' optical micrographs showing the development of surface morphology on a nickel specimen polarized in 0.02 M Cl^- solution (pH=0.4). The potentiostatic polarization curve is shown in Figure 4-6 and the micrographs refer to stages shown on the curve. 600×

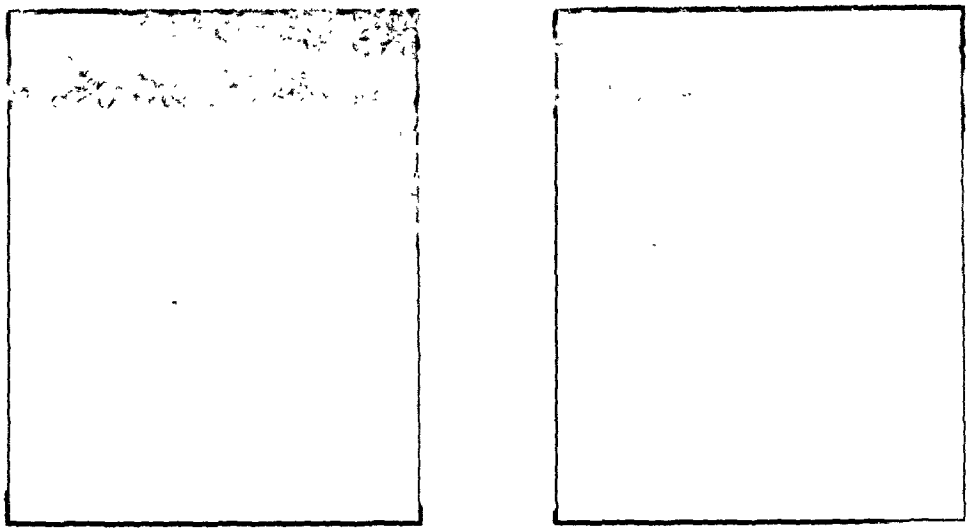

(e) (f)

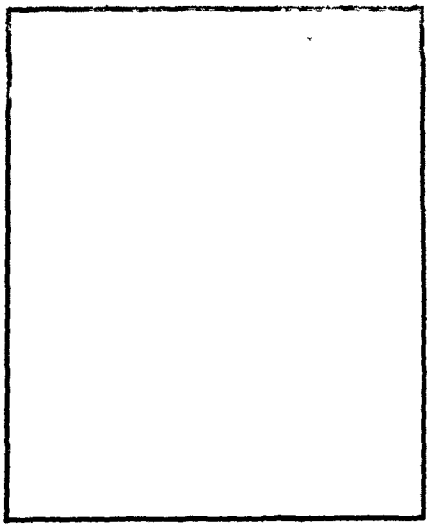

(g)

Figure 4-7 (cont'd). 'In-situ' optical micrographs showing the development of surface morphology on a nickel specimen polarized in 0.02 M Cl^- solution (pH=0.4). The potentiostatic polarization curve is shown in Figure 4-6 and the micro graphs refer to stages shown on the curve. 600×

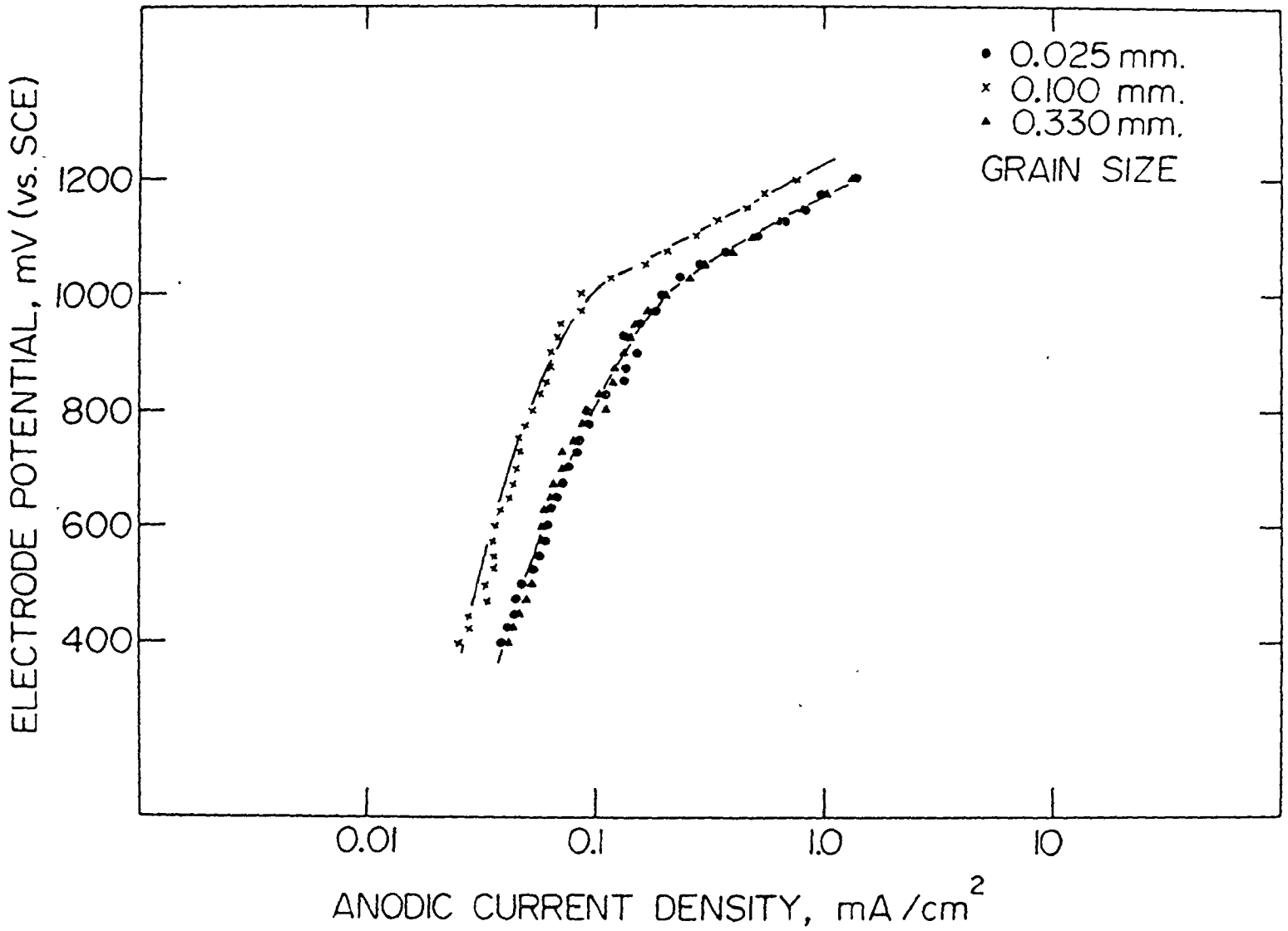

Figure 4-8. Potential--current density curves for nickel of varying grain size after being held at +400 mV for 28 mins in 1N H_2SO_4 followed by the addition of Cl^--ions to yield a 0.02 M Cl^- solution.

density increases with increase in potential and a change in slope occurs between +950 and +1000 mV. The number of pits decreased with grain size even though pit distribution followed the trend shown in Figure 4-5. The surface of every specimen remained bright until the addition of Cl^- ions, after which most of the surface remained in this visual condition (even though pits nucleated) while a small area of the specimen tarnished and by the end of polarization, a faint outline of the grain structure was visible.

Further, a specimen of 0.100 mm grain size was polarized in 1N H_2SO_4 from -300 to +1200 mV. The solution was removed and a fresh,previously deaerated 1N H_2SO_4 solution was introduced into the corrosion cell. The specimen was subjected to a potential of -300 mV, held at this potential for 30 mins, polarized again up to +400 mV, and then 0.02 M Cl^- ions added as 1N NaCl and polarization continued up to +1200 mV. Very few pits were formed, all within the grains and they nucleated in the passive potential region. The critical potential in the two cases was almost the same, viz. +1000 mV in the former instance and +950 mV in the latter.

4.5 Summary

A large amount of charge is consumed during the anodic oxidation of nickel in 1N H_2SO_4. It is, of course, possible to analytically estimate the nickel in solution and correct the total anodic charge to obtain film thickness. An easier and

equally effective method is to estimate the charge for the galvanostatic cathodic reduction of the anodically formed passive film. In fact, galvanostatic cathodic reduction is a powerful tool to estimate film thickness. It has one great advantage over the analytical method of film thickness determination - it provides valuable information regarding the nature of the surface species being reduced. Films on nickel are about 6-16 Å thick.

Galvanostatic oxidation of nickel suggests that film growth occurs under the influence of an electric field which remains constant at constant current density. In view of the field assisted growth, the kinetics of anodic oxidation of nickel in 1N H_2SO_4 may be speculated to be an inverse logarithmic type.

The critical potential (E_c) of nickel in a dilute chloride containing solution (0.02 M Cl^-), shows no change with variation in grain size from 0.025 to 0.330 mm or with different polarization techniques. E_c has been found[82] to be dependent on the composition of the solution (Cl^--ion concentration).

The critical potential, which has been taken to designate the susceptibility of metals and alloys to pitting corrosion, becomes more noble with the addition of certain alloying elements, notably Cr and Mo. The difficulty encountered in 'breaking the film', yielding a high value for E_c, could be due to many factors. Among them stability and thickness of the passive film, inherent sluggishness of the anodic reaction, the

ability to repassivate are only a few possibilities. In order to investigate the effect of molybdenum addition to nickel, these possibilities are examined in the next chapter.

CHAPTER V

RESULTS: CHARACTERIZATION AND CORROSION BEHAVIOUR OF NICKEL-MOLYBDENUM ALLOYS

5.1 Characterization of the Alloys

Various techniques were employed for a complete characterization of the alloys used in this investigation. Optical microscopy was used to obtain a knowledge of the metallographic structure. X-ray diffraction was employed for lattice parameter determination and phase identification. A scanning electron microscope equipped with a Kevex-ray detector was used for obtaining X-ray images of nickel and molybdenum in order to reveal their distribution.

The optical micrographs of Figure 5-1 show the metallographic structure of the alloys. It can be seen that the Ni, Ni-5Mo, Ni-10Mo and Ni-15Mo alloys appear to be single phase structures. This is also supported by the binary phase diagram (Figure 2-2). However, contrary to what the micrographs show, the Ni-22Mo and Ni-30Mo alloys are not single phase structures. The presence of the second phase particles although unobservable by optical microscopy was detected by X-ray diffraction and observations of fractured surfaces. The Ni-30Mo alloy in the two conditions of heat treatment (Figure 5-1(h) to (k)) is a multiphase alloy with a duplex structure.

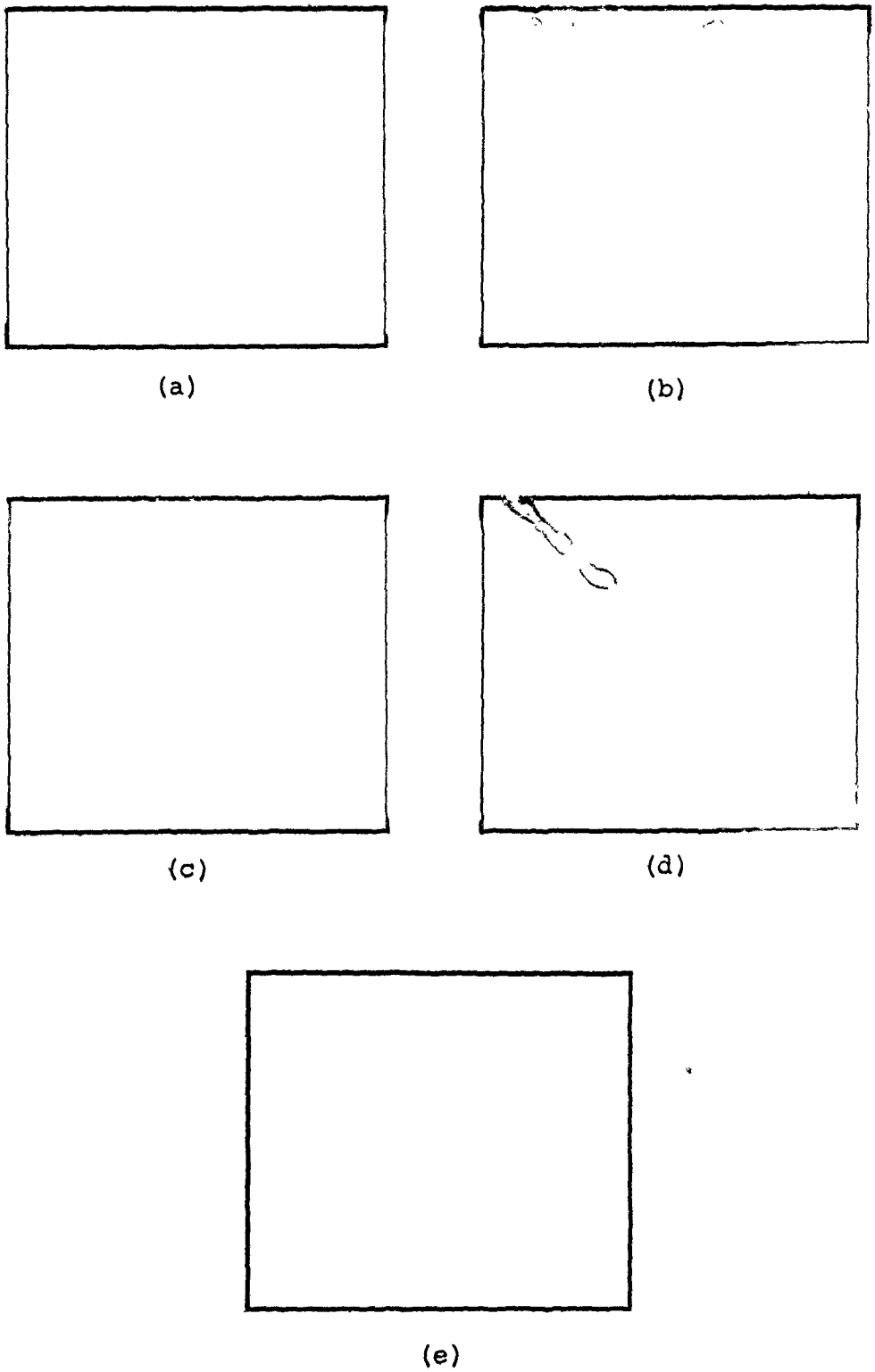

Figure 5-1. Optical photomicrographs of the surface of the alloys. (a) Nickel, 300× (b) Ni-5Mo alloy, 600× (c) Ni-10Mo alloy, 600× (d) Ni-15Mo alloy, 300× (e) Ni-22Mo alloy, 300× . Etched electrolytically in 20% $HCl-H_2O_2$ (2:1 by volume) at 0.05 A/cm^2

(f)

(g)

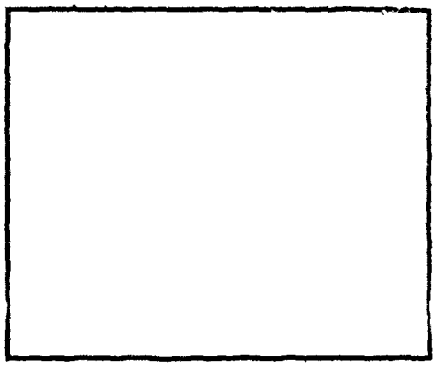

(h)

(i)

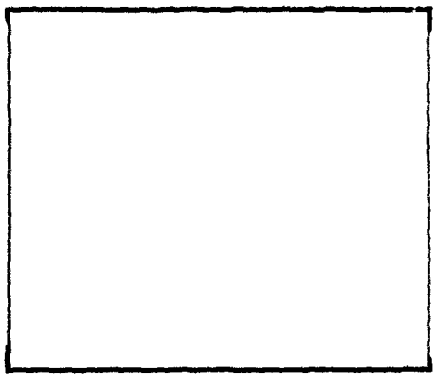

(j)

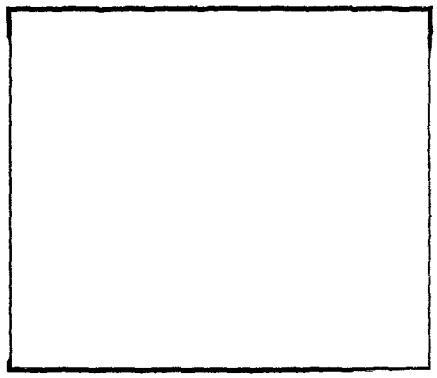

(k)

Figure 5-1 (contd.) Optical photomicrographs of the surface of Ni-30Mo alloy in various heat treated conditions. (f) Ni-30Mo-1 alloy, 950° for 8 hrs, furnace cooled, 150×, (g) same as (f), 600×. (h) Ni-30Mo-2 alloy, 800°C for 50 hrs, air cooled, 150× (i) same as (h), 600× (j) Ni-30Mo-3 alloy 800°C for 1200 hrs, air cooled, 600× (k) same as (j), 600× . Etched electrolytically in 20% HCl-H_2O_2 (2:1 by volume) at 0.05 A/cm^2

The lattice parameter of the α solid solution determined from the X-ray diffraction results (Appendix A) is given in Figure 5-2 as a function of the molybdenum content. It can be seen that the point for the Ni-22Mo alloy falls away from the line joining the other alloy compositions. It is of course possible that this shift is due to the experimental error. However, the sensitivity of the X-ray technique employed can be demonstrated by a comparison of the data of this investigation with that existing in the literature. Reference to the ASTM index card (no. 4-0850) for nickel shows that a_o = 3.5238 Å. The lattice parameter of nickel estimated in this investigation gives a_o = 3.5240 Å. A further check is provided by comparing a_o for one of the alloys. Spruiell and Stansbury[52] found that for a Ni-16.37Mo alloy a_o = 3.5696 Å. Taken from Figure 5-2 for an alloy of the same composition, a_o = 3.5694 Å. It is, therefore, concluded that the shift in the lattice parameter of the Ni-22Mo alloy is due to the fact that the α solid solution is already supersaturated and that the precipitation of the second phase has commenced. A glance at the Ni-Mo phase diagram (Figure 2-2) shows that the equilibrium structure of a Ni-22Mo alloy is a two phase structure containing α and β(Ni_4Mo).

The point of intersection of the horizontal line through the Ni-22Mo alloy point with that through the others should not be taken as the limit of the phase boundary separating the single phase α region from the two phase α+β region. This is because the specimen for X-ray diffraction was not quenched from 900°C

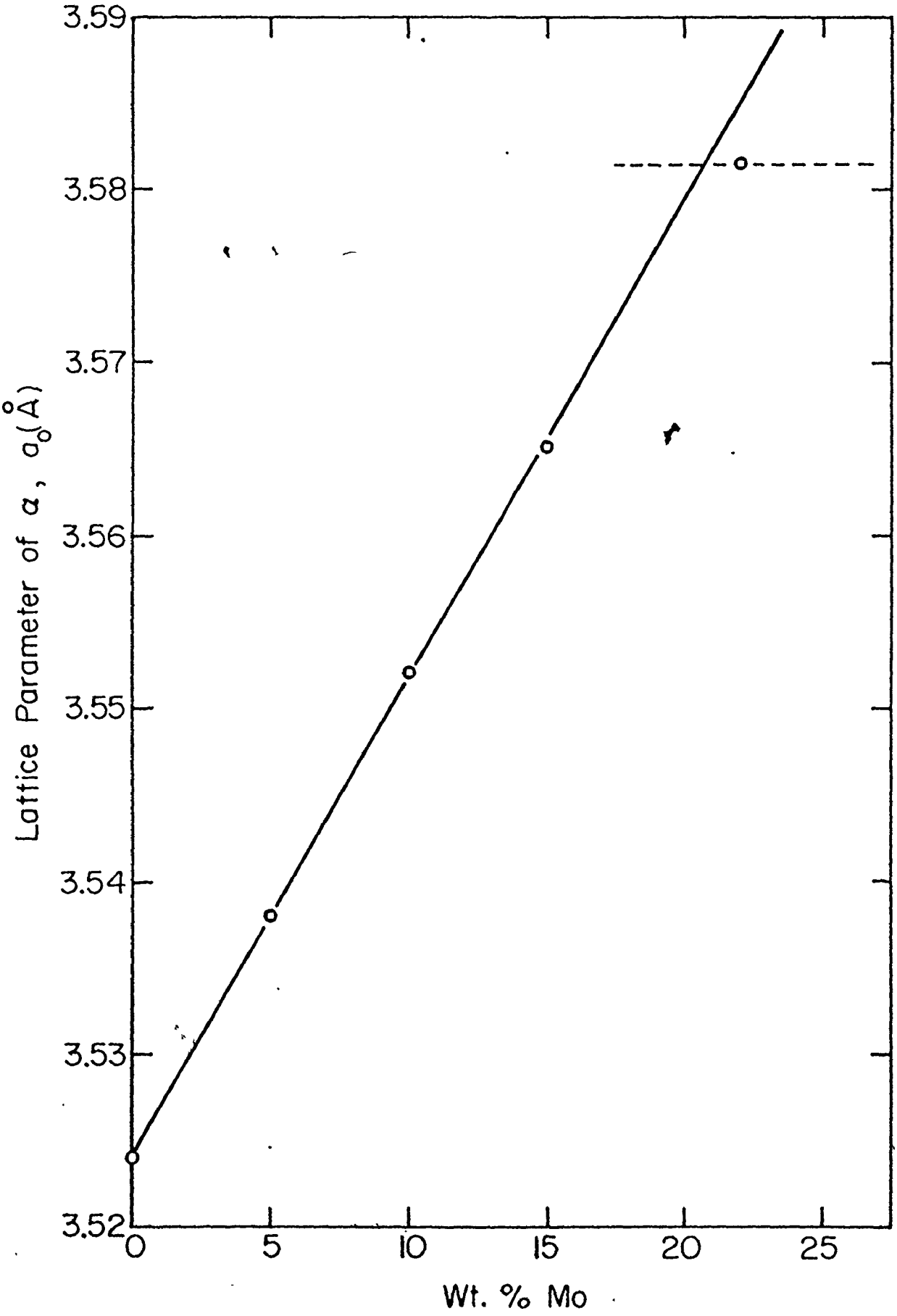

Figure 5-2. The variation of lattice parameter of the α-solid solution (a_o) as a function of molybdenum content for

but merely introduced in the furnace at this temperature (in order to obtain a fine grain size) and then slowly cooled.

The X-ray diffractometer trace for the Ni-5Mo, Ni-10Mo and Ni-15Mo alloys showed the usual peaks for the face centered cubic α solid solution. The only difference in their trace lay in the fact that the peaks shifted to lower angles as the molybdenum content increased, thereby suggesting an expansion of the lattice. However, although the trace for the Ni-22Mo alloy contained the usual face centered cubic peaks, three extra peaks at low angles were also observed (Figure 5-3). Although the planar spacings calculated from these peaks do not match satisfactorily with those of Ni_4Mo (the β phase) taken from the ASTM index card (no. 3-1036), reference to the original work[45] based on which the card was prepared reveals that the composition of the alloy used was 27.3%Mo, corresponding to a formula of $Ni_{4.065}Mo_{0.935}$. It is possible that greater non-stoichiometry is associated with the Ni_4Mo in the present case which would account for the large differences in the planar spacings. This could be more so if the β were to be precipitated as a coherent precipitate in the α-matrix. It might be mentioned in passing that the diffraction results are generally considered less reliable at lower angles. In fact, for precise lattice parameter determinations, values of θ taken are generally greater than 60°.

Peak broadening has been observed in materials and been attributed to the presence of either very fine particles

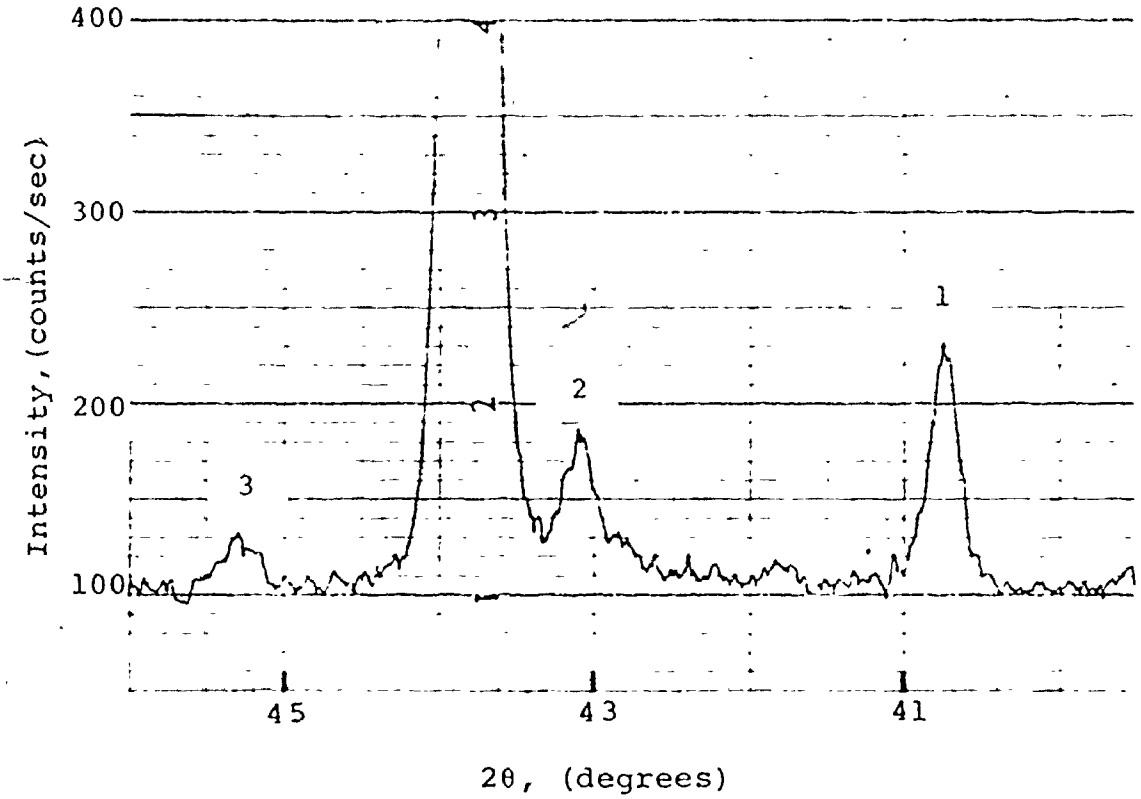

Figure 5-3. X-ray diffractometer trace for Ni-22Mo alloy showing the low angle extra peaks associated with the alloy.

or non-uniform strain[109]. The Scherer formula which describes the line broadening due to particle size is[109]

$$B = \frac{0.9\ \lambda}{t \cos \theta}$$

where B is the peak width at half the maximum intensity, λ is the wavelength of the X-rays, t is the particle size and θ is the Bragg angle. It is evident that B will be greater at higher angles since $\cos\theta$ will be smaller. The effect of strain, both uniform and non-uniform, on the X-ray diffraction profile is schematically shown in Figure 5-4. The diffraction peak from the unstrained crystal is shown in (a). If the crystal is given a uniform tensile strain such that the planar spacing becomes larger than its original value of d_o, then the diffraction peak shifts to lower angles but does not otherwise change (b). If the grain is bent and the strain is non-uniform (c), on the top (tension) side the plane spacing exceeds d_o, on the bottom (compressive) side it is less than d_o, and somewhere in between it equals d_o. This grain may be imagined as composed of a number of small regions in each of which the planar spacing is substantially constant but different from the spacing in adjoining regions. These regions cause various sharp diffraction peaks indicated on the right of (c) by dotted curves. The sum of these sharp lines, each slightly displaced from the other, is the broadened line shown by the full curve. The broadening due to a fractional variation in plane spacing ($\Delta d/d$) is given by[109],

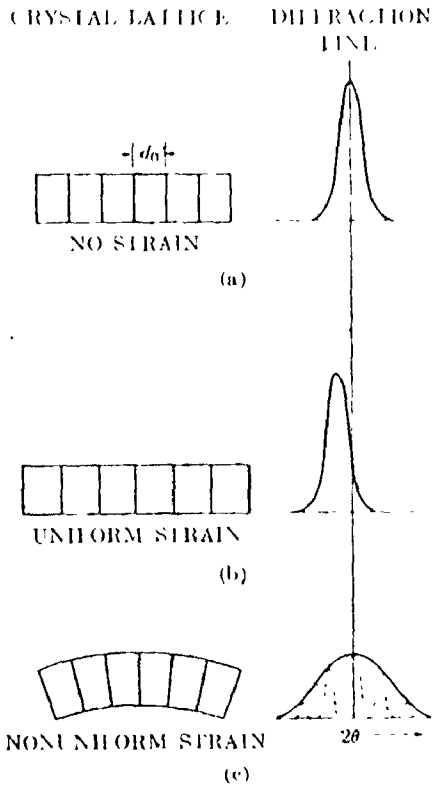

Figure 5-4. Schematic representation of the effect of lattice strain on the Debye-line width and position[109].

$$B' = \Delta 2\theta = -2 \frac{\Delta d}{d} \tan\theta.$$

Once again, it can be seen that the value of B' increases as θ increases. The combination of both the effects described, small particle size and non-uniform strain (as for example will result from coherent precipitation of a second phase in a matrix), evidently will lead to peak broadening, better observable at higher angles.

The X-ray diffraction trace for a Ni-15Mo alloy and a Ni-22Mo alloy showing high angle peak broadening is given in Figure 5-5. It is, therefore, concluded that the Ni-22Mo alloy is a two phase alloy with coherent precipitation in an α-matrix.

The Ni-30Mo alloy was used in three different conditions of heat treatment. In the first case, it was heated at 950°C for 8 hrs and furnace cooled. This structure will be referred to as Ni-30Mo-1. In the second instant, it was aged at 800°C for 50 hrs followed by air cooling. This condition will be designated as Ni-30Mo-2. In the third case, it was aged at 800°C for 1200 hrs and then air cooled. This state will be referred to as Ni-30Mo-3. The three structures are shown in Figure 5-1(f) to (k).

Although the optical micrographs of the Ni-30Mo-1 alloy show large equiaxed grains suggesting a single phase alloy, there are two aspects of its history that make this difficult to accept. First, the alloy was found to be very brittle

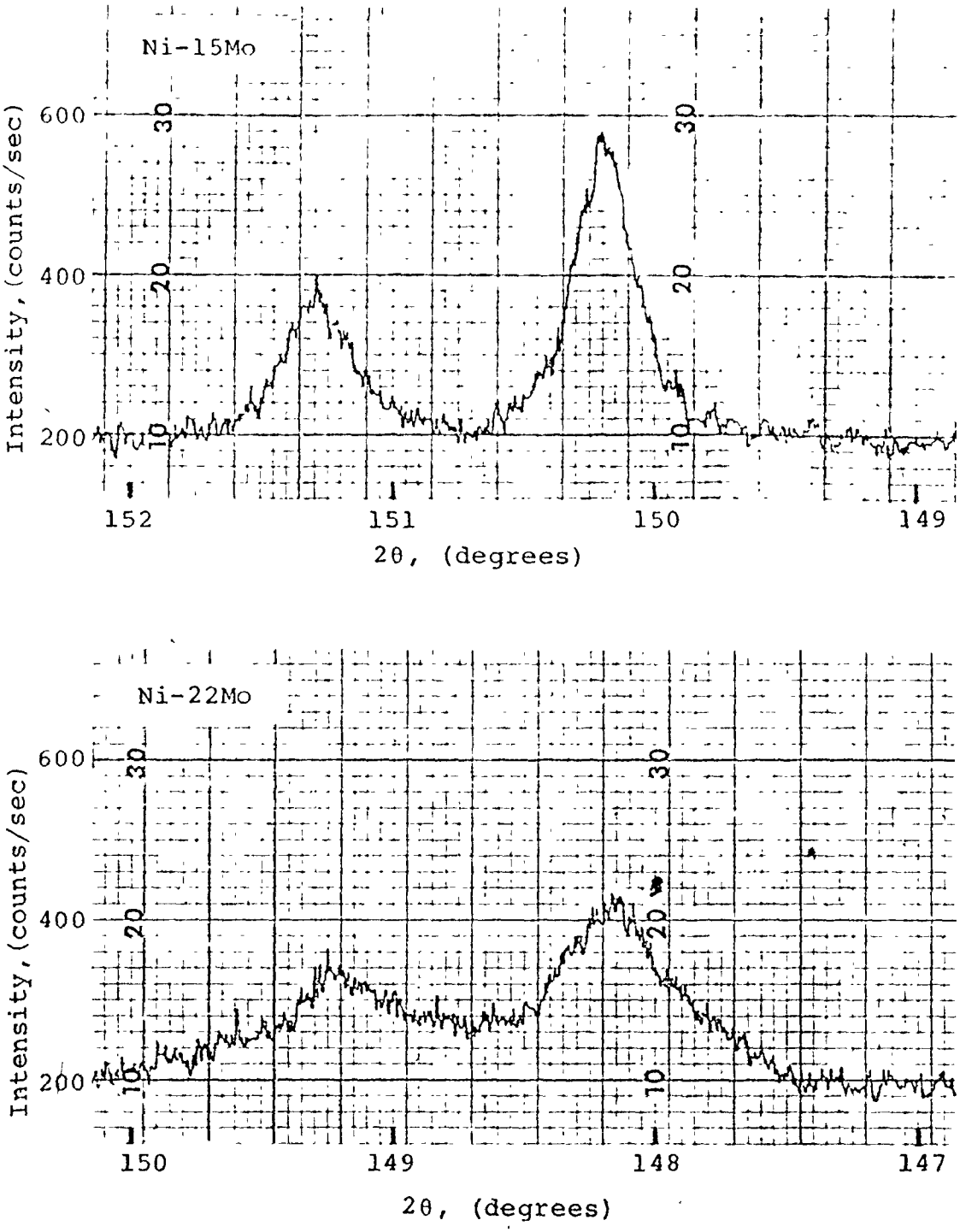

Figure 5-5. X-ray difractometer trace for Ni-15Mo alloy (single phase) and Ni-22Mo alloy (two phase) showing high angle peak broadening, possibly suggesting coherent precipitation in an α-matrix.

for cold rolling purposes as was mentioned in the previous chapter and secondly, the X-ray diffractometer trace showed considerable peak broadening at higher angles. To further complicate matters, the X-ray diffraction data could be indexed as Ni_4Mo (Table A-6, Appendix A). As a matter of fact, the analytical indexing method assuming the structure to be Ni_4Mo gives a_o = 5.699 Å, c_o = 3.579 Å, c/a = 0.628. The ASTM index card (no. 3-1036) states a_o = 5.720 Å, c_o = 3.564 Å, c/a = 0.623. However, in view of the peak broadening and its brittleness, this was thought unlikely. Some of the peaks in the diffractometer trace can be re-indexed as belonging to a supersaturated α solid solution with 30% Mo while the remaining ones can be designated as due to the β and γ phases (Table A-7, Appendix A). The value of the lattice parameter calculated from the α peaks yields a_o = 3.6075 Å. This value falls at 30% Mo on the extrapolated line in Figure 5-2. As will be discussed later, SEM fractographs of the surfaces of the alloy showed the presence of second phase particles. It is, therefore, concluded that the Ni-30Mo-1 alloy is a supersaturated α solid solution of composition Ni_4Mo with precipitation of β and possibly γ (Ni_3Mo) at the grain boundaries.

Heat treating the α-alloy at 800°C for 50 hrs yields more support for its initial supersaturated nature. The micrographs in Figure 5-1(h)-(i) clearly show the presence of other phases at the grain boundaries. X-ray diffraction data (Table

A-8, Appendix A) reveals that the alloy contains α, β and γ. The high angle peaks are found to be split into multiple peaks corresponding to α, β and γ. In the example of Figure 5-6, the original α peak now splits into two peaks, one corresponding to α (still supersaturated and metastable but considerably relieved of lattice strains) and the other to β. The values of the lattice plane spacings for the α-phase have been calculated using a_o = 3.6075 Å obtained from the X-ray diffraction data of the Ni-30Mo-1 alloy.

In an attempt to obtain the equilibrium structure of β+γ, the alloy was heated at 800°C for 1200 hrs. The microstructure given in Figure 5-1(j)-(k) shows that all three original phases (α,β and γ) are still present, although their proportions are different. The X-ray diffraction data confirmed this conclusion. Although the β and γ peaks were more numerous, the α peaks were nonetheless present (Table A-9, Appendix A). Apparently, the transformation of the α to β + γ is a very sluggish reaction. However, the strains in the cubic lattice are highly relaxed as can be seen by a comparison of the X-ray diffractometer trace for the three conditions of heat treatment (Figure 5-6).

The effect of these second phase particles on the impact properties is important. Although the specimens were too small to permit the use of conventional impact testing techniques, a simple test was performed. Specimens were gripped in

Figure 5-6. X-ray diffractometer trace for Ni-30Mo alloy in various heat treated conditions.

a) Heated at 950°C for 8 hrs and furnace cooled.

   High angle peak broadening, which, along with the extra lines observed in the diffraction pattern and the SEM fractograph, suggests a supersaturated α phase with the presence of $\beta(Ni_4Mo)$ and $\gamma(Ni_3Mo)$ at the grain boundaries.

b) Aged at 800°C for 50 hrs and air cooled.

   The previous peak now splits up and the new peaks correspond to α (still supersaturated) and metastable but considerably relieved of lattice strains) and β.

c) Aged at 800°C for 1200 hrs and air cooled.

   The peaks are much sharper with the doublet being completely resolved.

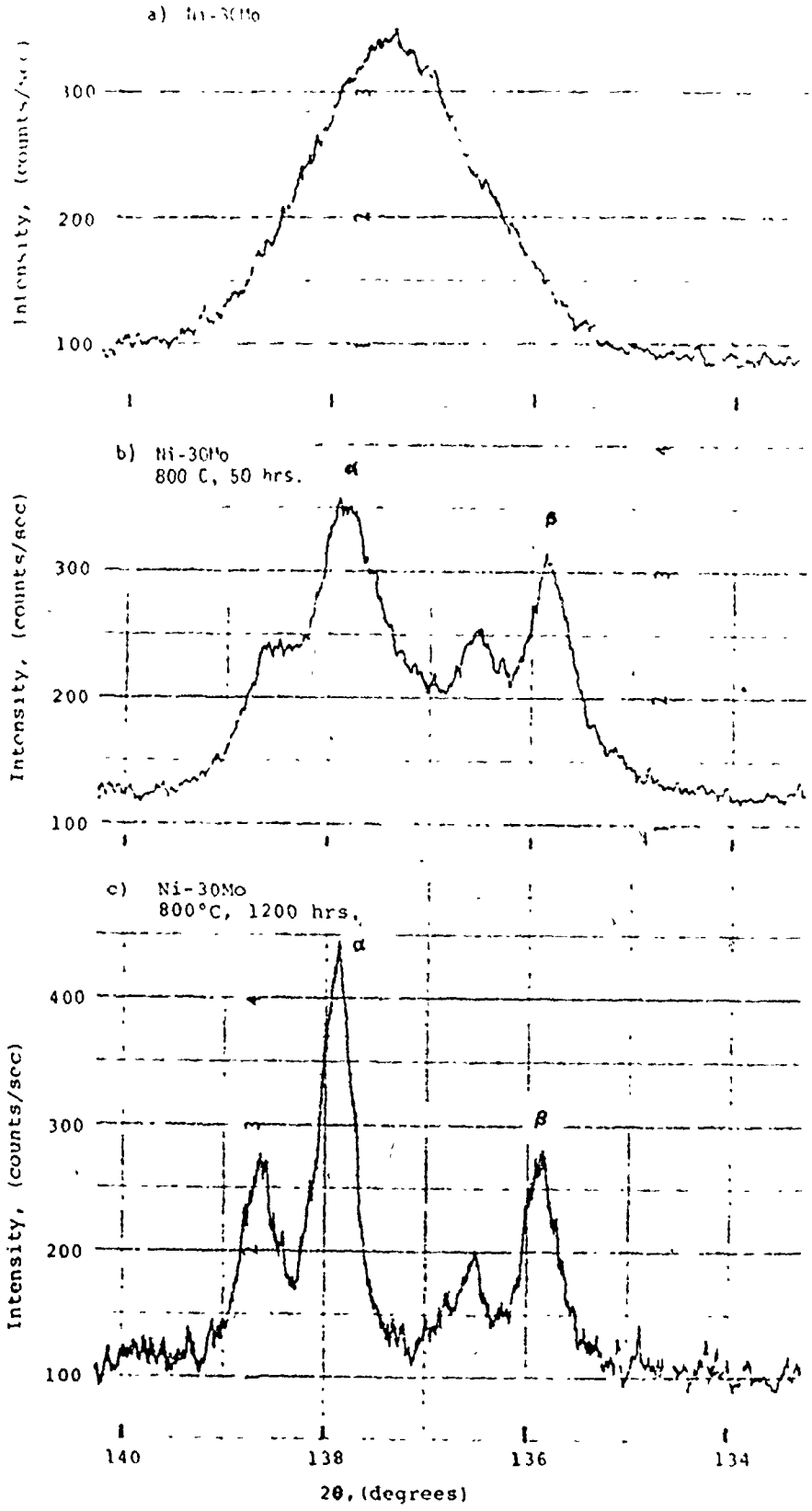
a) Ni-30Mo
300
200
100
b) Ni-30Mo
800 C, 50 hrs.
α
β
Intensity, (counts/sec)
300
200
100
c) Ni-30Mo
800°C, 1200 hrs.
α
β
Intensity, (counts/sec)
400
300
200
100
140
138
136
134
2θ, (degrees)

Figure 5-6

a bench vise and bent with a pair of pliers. The Ni-22Mo alloy was found to be quite tough. In order to obtain an observable fractured surface, a notch had to be made with the edge of a file and then the alloy bent many times before it fractured. The SEM fractograph shown in Figure 5-7(a) is typical of ductile failures. This further supports the contention that in this alloy, the second phase is not precipitated along any grain boundary or any preferred plane but is uniformly coherently precipitated throughout the entire matrix.

None of the Ni-30Mo alloys showed any ductility at all. The Ni-30Mo-1 alloy showed a very shiny and coarse fractured surface. The SEM fractograph (Figure 5-7(b)) shows a surface which is typical of an intergranular brittle fracture. The presence of second phase particles along the grain boundaries is evident. The fractured surface of the other two Ni-30Mo alloys were shiny, but fine grained. Their fractographs do not provide any extra information (Figure 5-7(c) and (d)). They both show that the second phase particles are small and distributed throughout the grain boundary. Although the fractographs for Ni-30Mo-3 alloy (Figure 5-7(d)) look very similar to that of Ni-22Mo alloy (Figure 4-7(a)), it must be remembered that while the former was extremely brittle, the latter showed considerable ductility.

The X-ray images obtained for nickel and molybdenum did not reveal any segregation of the two elements in any of the alloys. Within the limits of detection, the distribution was

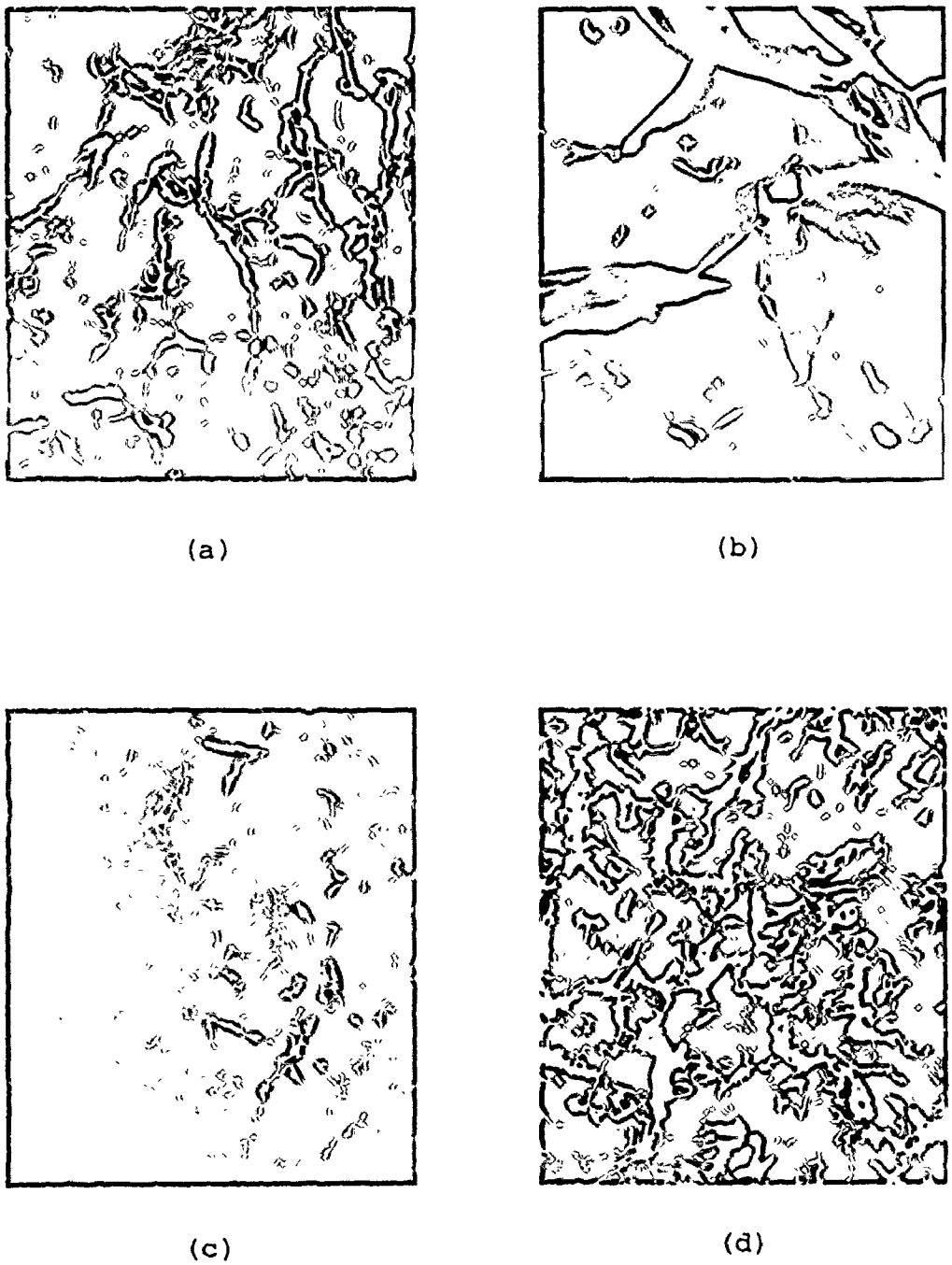

(a) (b)

(c) (d)

Figure 5-7. SEM fractographs (a) Ni-22Mo alloy, 610× (b) Ni-30Mo-1 alloy, 525× , (c) Ni-30Mo-2 alloy, 570× (d) Ni-30Mo-3 alloy, 600×

very uniform. A point to point scan of the grain boundaries and the grain interiors also failed to reveal any variation in distribution. Some deviation was found in the Ni-22Mo alloy as regards the concentration of molybdenum at the grain boundaries. The X-ray counts for molybdenum were much lower (half to even less) at the grain boundaries when compared with those of the grain interiors. The nickel counts were the same. Although this contention is qualitative, it seems that there are grain boundaries in the Ni-22Mo alloy which are somewhat depleted in molybdenum. An overview of the nature of the alloys resulting from their characterization is given in Table 5-1.

The mechanical properties of the alloys up to 22 wt % molybdenum were determined by tensile testing flat specimens. These results are presented in Appendix C. It was found that the presence of molybdenum significantly increases the yield strength and the ultimate tensile strength of the alloys with no detectable loss in ductility. Thus, the addition of molybdenum to nickel has a beneficial effect on the mechanical properties of the alloys.

5.2 The Corrosion Behaviour of Nickel-Molybdenum Alloys

5.2.1 Sulfuric Acid Environment

The non-aggressive environment consisted of 1N H_2SO_4. Experiments were conducted in this solution to provide a basis for comparison of the results with those of nickel and enable the determination of the effect of molybdenum addition on the anodic polarization characteristics, film thickness and growth and the anodic and cathodic partial processes.

Table 5-1

Summary of the metallurgical nature of Ni and Ni-Mo alloys used in the investigation

Alloy	Grain Size Av.Gr. Dia. (mm)	Phase and Structure
Ni	0.035	single phase, fcc
Ni-5Mo	0.021	single phase, α-ss, fcc
Ni-10Mo	0.020	single phase, α-ss, fcc
Ni-15Mo	0.040	single phase, α-ss, fcc
Ni-22Mo	0.046	two phase, α + coherent precipitation of β
Ni-30Mo-1	0.073	three phase, supersaturated α with some evidence of β and γ at the grain boundaries
Ni-30Mo-2	0.100	three phase, β and γ precipitated at the α-grain boundaries
Ni-30Mo-3	-	three phase, mostly aggregate of β and γ with some retained α

fcc - face-centred cubic

α-ss - α-solid solution

5.2.1.1 Anodic Polarization Characteristics

The anodic polarization curves for the alloys are shown in Figure 5-8 and the anodic polarization parameters are summarized in Table 5-2. A glance at Table 5-2 brings out the following points:

i) The Ni-5Mo alloy exhibits the highest critical current density, i_c (almost an order of magnitude greater than the other alloys). It is interesting to note that Uhlig et al[33] also found that the highest corrosion rate (determined from weight loss experiments in 10% HCl solution) was experienced by a Ni-7Mo alloy.

ii) The primary passive potential, E_{pp}, does not show any trend with increasing Mo-content.

iii) The nature of the substrate has no effect on the oxygen evolution reaction, ie. the transpassive region is independent of alloy content.

iv) The current density in the passive region, i_p, increases with Mo content, and finally reaches a stage where the ability to passivate is completely lost. Apparently, molybdenum does not have a beneficial effect on the corrosion of nickel in the passive region. However, increasing Mo-content decreases the corrosion rate in the 'active region'.

'In-situ' microscopic observations revealed that for all alloys investigated the surface was etched and the grain structure

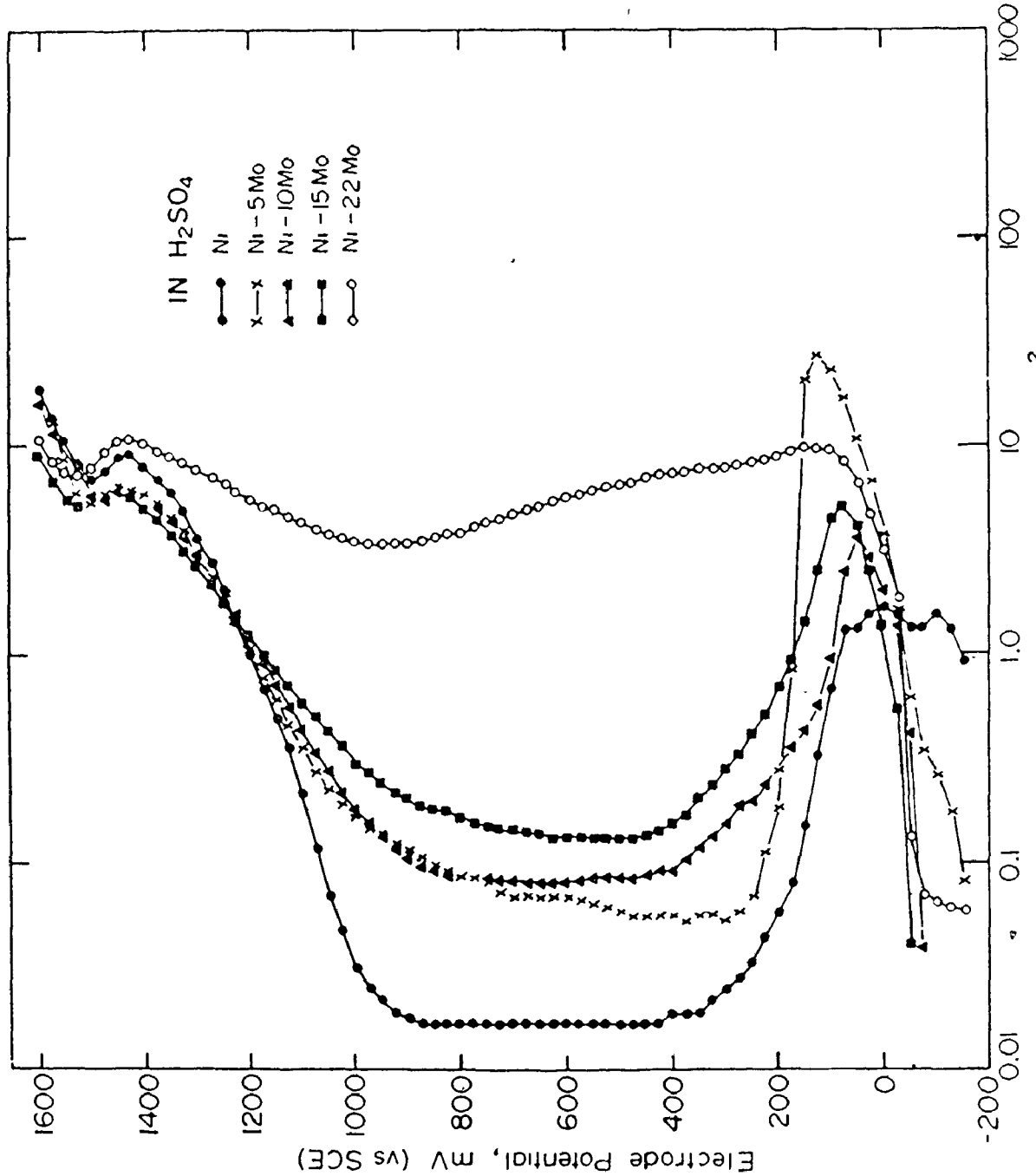

Figure 5-8. Anodic polarization curves for Ni and Ni-Mo alloys in 1N H_2SO_4 .

Table 5-2

Anodic polarization parameters for Ni-Mo alloys in 1N H_2SO_4 solution

Alloy wt %	E_{corr} mV	E_{pp} mV	i_c mA/cm^2	$(i_a)^*_{-75}$ mA/cm^2	i_p^{**} mA/cm^2	E_c mV	β_a mV/decade	β_t mV/decade
Ni	-220	0	1.7	1.4	0.02	950	50	118
Ni-5Mo	-180	125	26.7	0.34	0.07	900	95	220
Ni-10Mo	-140	50	3.6	0.04	0.18	900	30	245
Ni-15Mo	-102	100	4.4	0.01	0.14	900$^+$	28	340
Ni-22Mo	-110	125	9.4	0.04	4.0	1000^{++}	35	870
Ni-30Mo-1	-126	NO PASSIVE REGION		0.05	-	-	-	-
Mo	+ 42	NO PASSIVE REGION		-	-	-	-	-

*Anodic current density in the 'active region' at -75 mV (SCE)
**Lowest recorded value
+Approximate value of E_c, since curve gradually bends over
++Value of E_c to be taken with caution (refer to Figure 5-8)

was clearly visible when the polarization reached the passivation potential. No significant change in this structure was observed at later stages of polarization.

5.2.1.2 Film Thickness Measurements

Alloy anodic oxidation produces results which are essentially similar to those obtained for nickel. Dissolution of the alloys is a major contribution to the charge consumed during film formation as is evident by the large amounts of charge involved. For example, after 3 mins of anodic oxidation in 1N H_2SO_4 at +400 mV the charges consumed are:

Alloy	Charge
Ni-5Mo	8.2 mC/cm^2
Ni-10Mo	46.1 mC/cm^2
Ni-15Mo	52.8 mC/cm^2 .

Hence, once again, galvanostatic cathodic reduction was resorted to as the technique to determine the charge stored in the film. It may be pointed out that it is not possible to determine the thickness of the passive film because its composition is unknown and possibly changes with time of anodic oxidation. There are reasons to believe that the dissolution of the alloy is selective in that nickel (the less noble of the two terminal metals) dissolves faster. This implies that the passive film, at least in the later stages, is richer in molybdenum.

In order to determine the reducibility of the passive

film on the alloys, the following two experiments were conducted.

i) The alloy was electropolished in the standard manner, cathodically reduced in 1N H_2SO_4 at -1500 mV for 10 mins, held at a cathodic current density of 5.8 $\mu A/cm^2$ for 5 mins and immediately polarized from -300 mV to +525 mV at 25 mV/min, after which the direction of the voltage scan was reversed. The results for the Ni-15Mo alloy are shown in Figure 5-9(a). The reactivation of the electrode on approaching E_{pp} is evident and is due to the reduction of the passive film.

ii) A sample of the alloy was electropolished and cathodically reduced as in (i) above and then immediately subjected to a passive potential of +600 mV for 60 mins. The film formed was cathodically reduced at a constant current density of 2.7 $\mu A/cm^2$ until the potential of the electrode reached -200 mV when the sample was immediately potentiostatically polarized from -200 mV to +525 mV at 25 mV/min. The results for Ni-15Mo are presented in Figure 5-9(b). The shape of the polarization curve is similar to that obtained in Figure 5-9(a) and suggests that the reduction of the film had occurred when the potential was -200 mV.

The charges consumed during anodic oxidation at +600 mV and subsequent cathodic reduction at 2.7 $\mu A/cm^2$ for the various times is given in Table 5-3. It can be seen on comparing with Table 4-2 that although the charge consumed during anodic oxi-

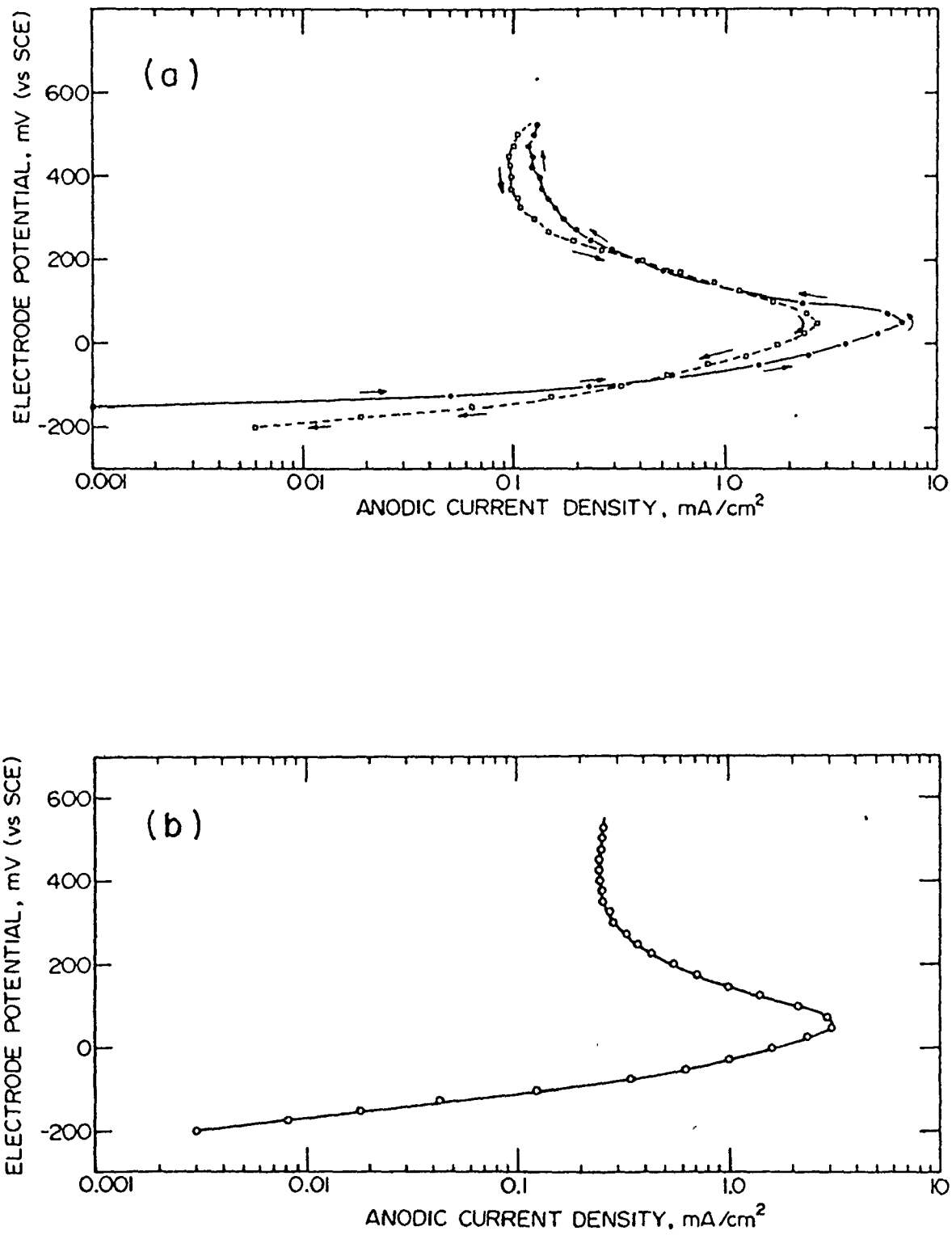

Figure 5-9. Determination of reducibility of the film on Ni-15Mo alloy.

Table 5-3

Charge consumed during anodic oxidation of Ni-Mo alloys in 1N H_2SO_4 at +600 mV and subsequent cathodic reduction at 2.7 $\mu A/cm^2$

Alloy	Experimental Mode	Charge Consumed, mC/cm^2 Passivation Time		
		15 mins	30 mins	60 mins
Ni-5Mo	Anodic Oxidn.	88.4	147.6	288.5
	Cathodic Redn.	1.43±0.00	1.79±0.23	2.0±0.44
Ni-10Mo	Anodic Oxidn.	96.7	164.9	406.2
	Cathodic Redn.	0.90±0.12	1.04±0.23	1.34±0.04
Ni-15Mo	Anodic Oxidn.	102.4	195.8	553.2
	Cathodic Redn.	0.47±0.00	0.46±0.03	0.45±0.11

dation of the alloys increases with the Mo-content, the passive film on the alloys becomes thinner with increasing Mo-content. The cathodic reduction curves for a Ni-5Mo alloy for the three times of anodic oxidation are given in Figure 5-10 while the curves for an oxidation time of 60 mins for the different alloys are presented in Figure 5-11. It can be seen that no arrests exist in the reduction curves for any of the alloys. The decay of potential is gradual, possibly suggesting that no single oxide layer or layers are formed making the composition of the film uncertain.

The surface of a Ni-15Mo alloy after the various electrochemical treatments is shown in Figure 5-12. It is evident that even after 15 mins at +600 mV in 1N H_2SO_4 the surface of the alloy is considerably roughened due to dissolution. This is even more evident after periods of time greater than 30 mins.

5.2.1.3 Anodic-Cathodic Polarization

The anodic and cathodic polarization characteristics of the alloys were studied in 1N H_2SO_4 only in order to determine the effect of molybdenum on the partial processes. Chloride containing solutions were excluded because of the occurrence of localized corrosion which tends to complicate the situation. The results are presented in Figure 5-13(a) where the current density is plotted against the overvoltage. It is apparent that molybdenum has no significant effect on the cathodic segment of the curve. This observation is similar to that of Uhlig[7] who has pointed out that the addition of molybdenum to nickel

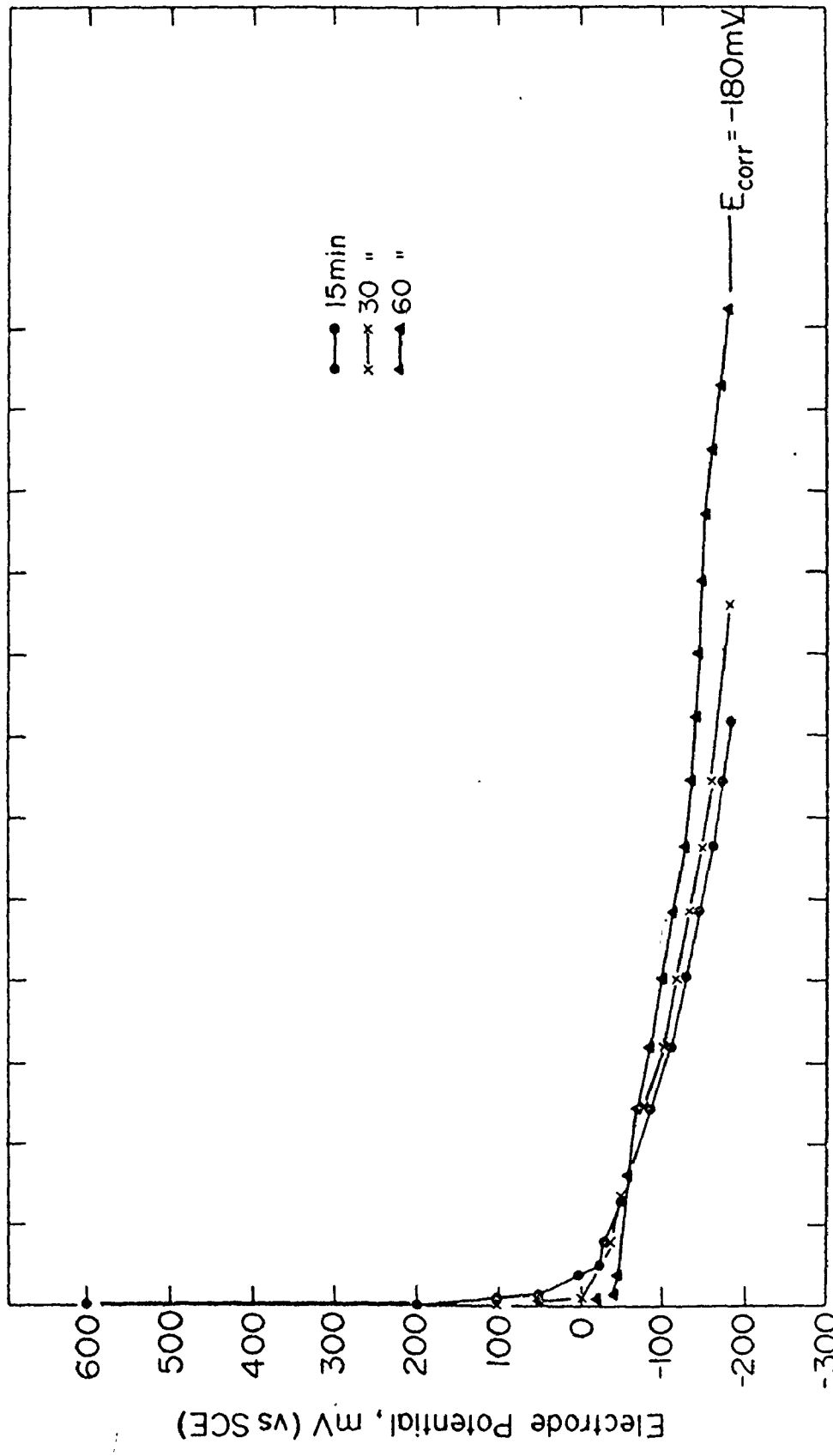

Figure 5-10. Cathodic reduction curves for Ni-5Mo alloy at 2.7 $\mu A/cm^2$ in 1N H_2SO_4 after various times of anodic oxidation at +600 mV.

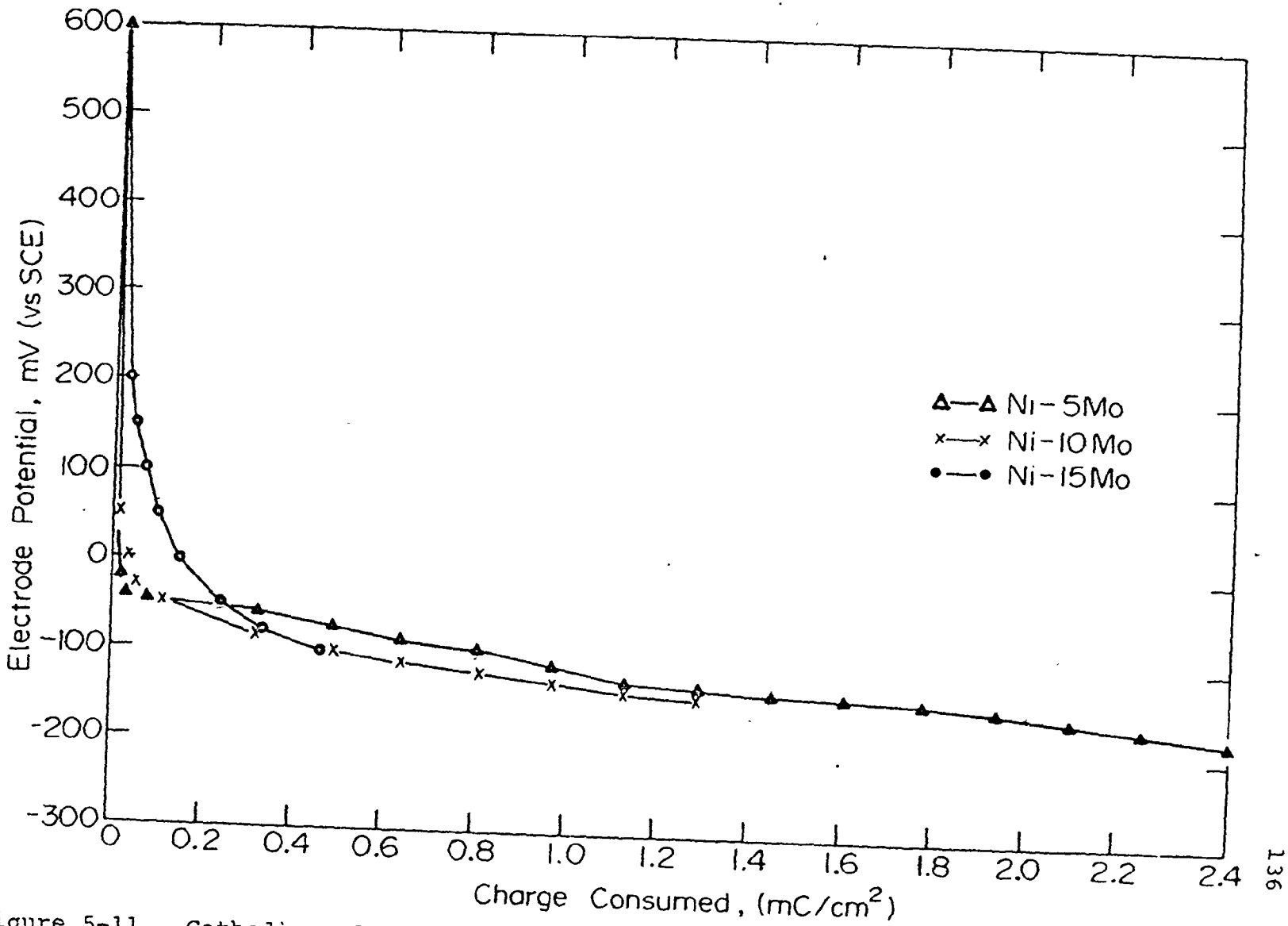

Figure 5-11. Cathodic reduction curves for Ni-5Mo, Ni-10Mo and Ni-15Mo alloys at 2.7 μA/cm² in 1N H_2SO_4 after 60 mins. of anodic oxidation at +600 mV.

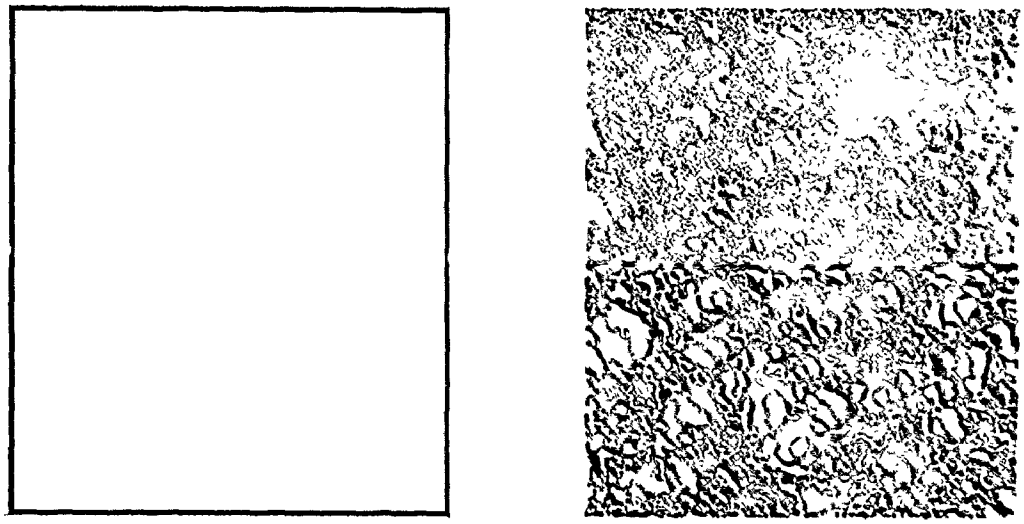

(a)

(b)

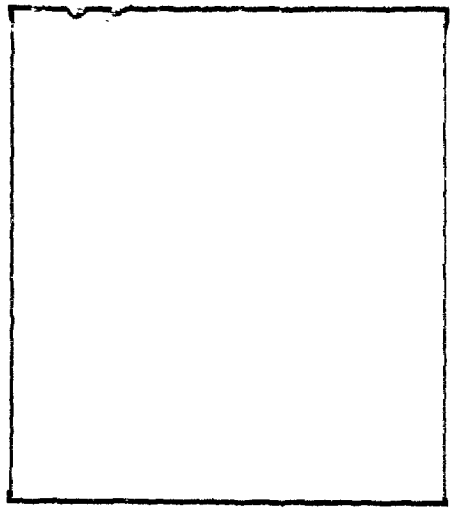

(c)

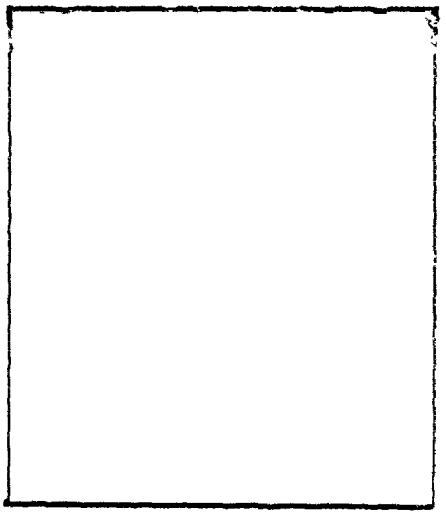

(d)

Figure 5-12. Transmission electron micrographs of two stage gold shadowed carbon replicas of surface of Ni-15Mo alloy after various electrochemical treatments. (a) electropolished (b) 15 mins at +600 mV in 1N H_2SO_4 (c) 30 mins at +600 mV in 1N H_2SO_4 (d) 60 mins at +600 mV in 1N H_2SO_4. All magnifications are 38,000×

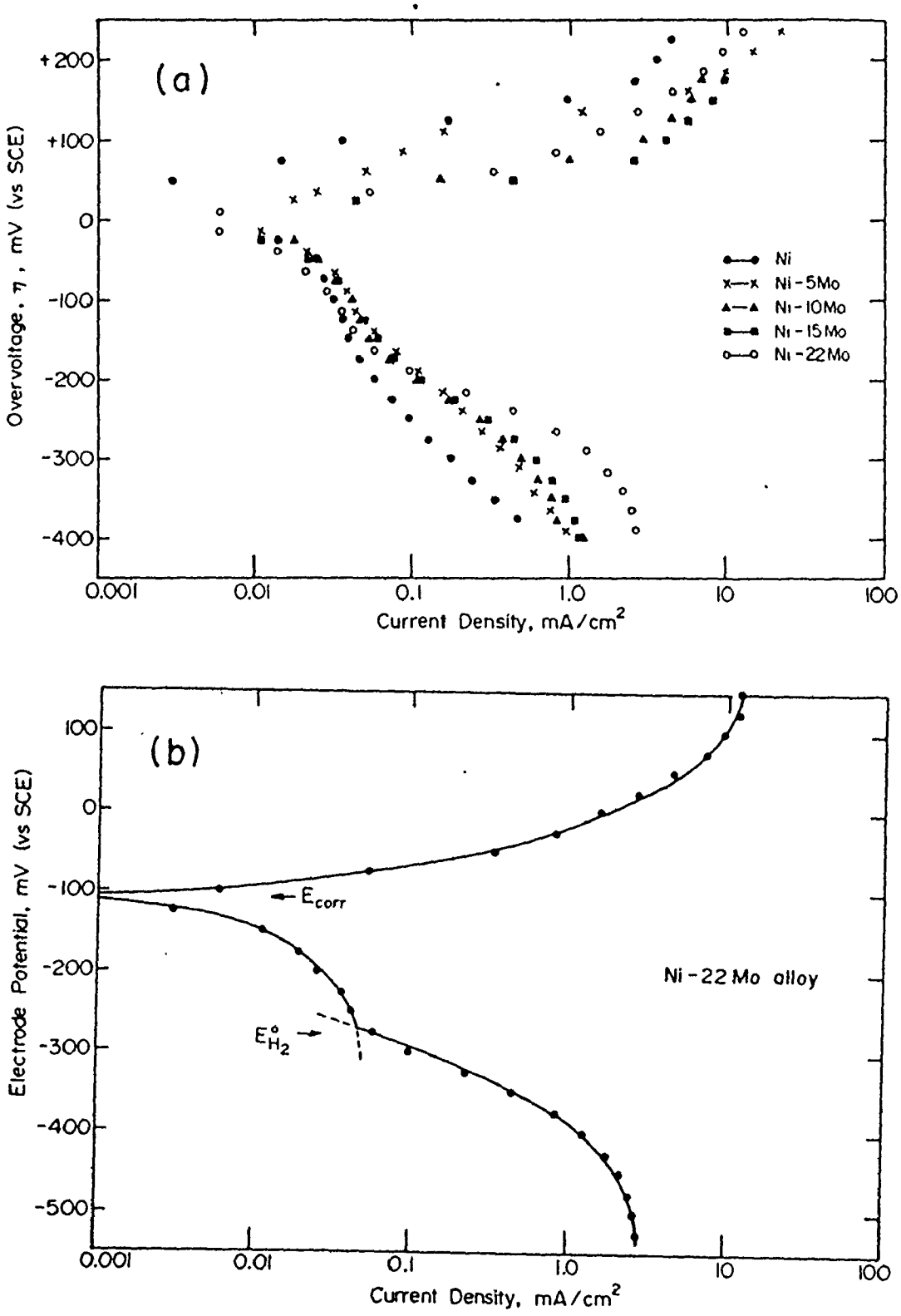

Figure 5-13. (a) Anodic-Cathodic polarization curves for nickel and Ni-Mo alloys in 1N H_2SO_4 (Overvoltage vs Current Density), (b) Anodic-Cathodic polarization curve for a Ni-22Mo alloy in 1N H_2SO_4 (Electrode potential vs Current Density).

has no effect on the hydrogen overvoltage.

All the original curves (electrode potential vs current density) from which the curves of Figure 5-13(a) have been drawn showed a discontinuity in the cathodic segment at a potential range of -270 mV to -290 mV (SCE) with the current density ranging between 3.6 to 6.0 mA/cm^2. As an example, the curve for a Ni-22Mo alloy is shown in Figure 5-13(b). Figure 5-13(a) also shows that the addition of molybdenum leads to a change in the anodic reaction. In general, the values of the anodic Tafel slope (β_a) increases (signifying a lower dissolution rate) with increase in molybdenum content. The values of β_a are tabulated in Table 5-2.

5.2.2 Chloride Containing Environments

The alloys were tested in three different aggressive environments. Most of the electrochemical work was conducted in 1N H_2SO_4 to which the chloride was added as 1N NaCl to yield different concentrations of the Cl^- ion. The alloys were also anodically polarized in synthetic sea water which was not deaerated. Finally, weight loss measurements were performed in deaerated 10% HCl solution. The results presented in the following sections include the effect of Cl^- ions on the anodic polarization characteristics (polarization parameters and corrosion morphology), the potentiostatic activation behaviour, film thickness and repassivation characteristics, anodic polarization behaviour in sea water and conventional weight loss

measurements.

5.2.2.1 Anodic Polarization Characteristics

The polarization characteristics were studied in solutions containing a wide range of Cl^- concentrations from 0.02 M to 0.50 M. Only the results of alloys containing up to 22% Mo are presented in this section. Results for the Ni-30Mo alloy in its three conditions of heat treatment will be presented later.

The anodic polarization curves for alloys up to 22% Mo are presented in Figures 5-14 to 5-19 while the anodic polarization parameters are summarized in Tables 5-4 to 5-9. The charge value indicated beside each curve is the total charge passed during polarization and has been obtained by multiplying the anodic current density by the time (60 secs) at that current density. The data for nickel has been taken from reference 82. A comparison of Figures 5-8 and 5-14 reveals that even a small concentration of the Cl^--ion (0 .02 M) has a drastic effect on the corrosion behaviour of Ni-5Mo and Ni-10Mo alloys. Not only does the critical current density increase significantly, a noticable decrease occurs in the critical potential, E_c. Even the transpassive slopes decrease, suggesting an overall increase in the corrosion rate in that region. For pure Ni, although an increase in i_p and i_c occurs no change in the E_c value is observed in 0.02 M Cl^-. In contrast the polarization curves for the Ni-15Mo and Ni-22Mo alloys in 1N H_2SO_4 and 0.02 M Cl^- are not significantly different. Figure 5-20 shows the optical micrographs of these

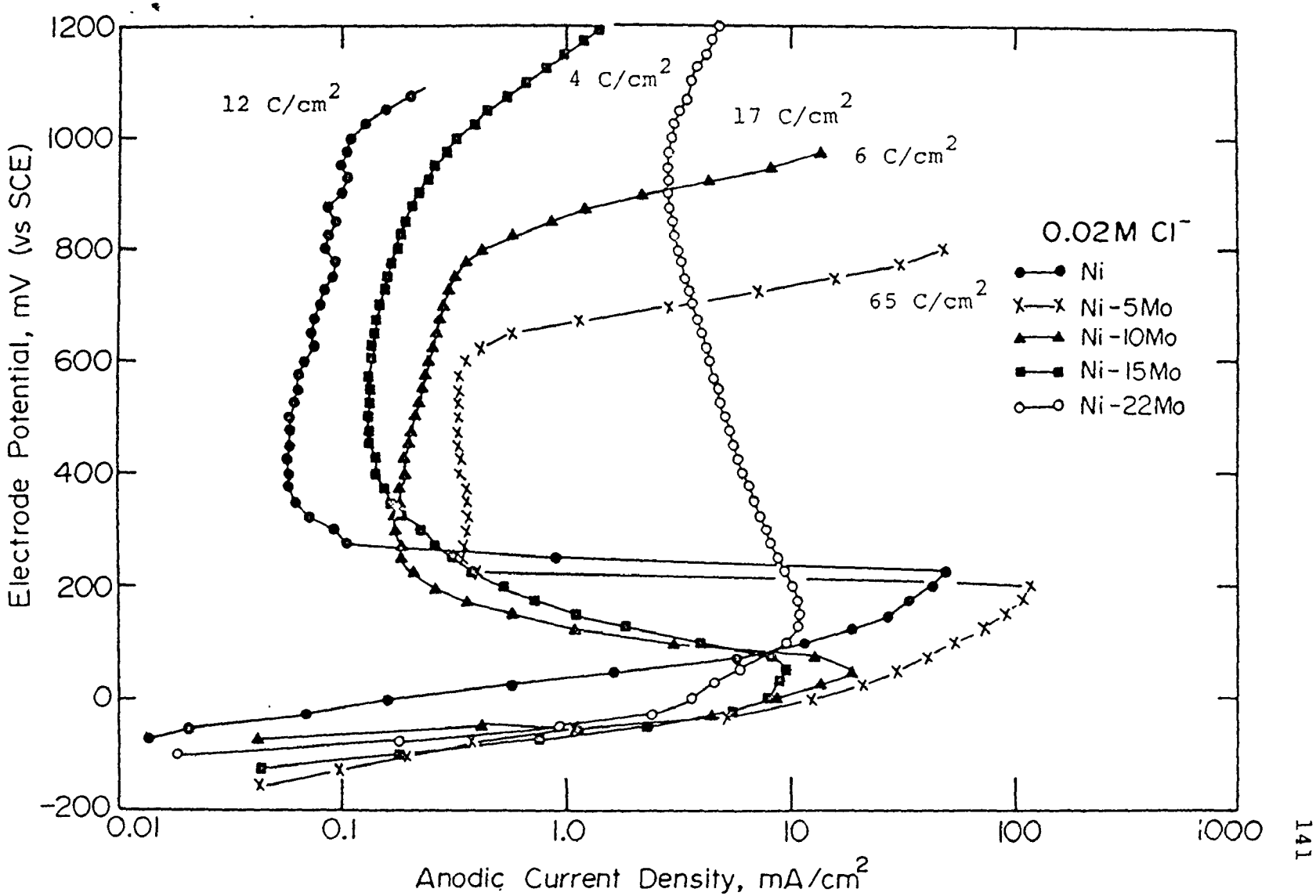

Figure 5-14. Anodic polarization curves for Ni and Ni-Mo alloys in 0.02 M Cl^- solution (pH = 0.4).

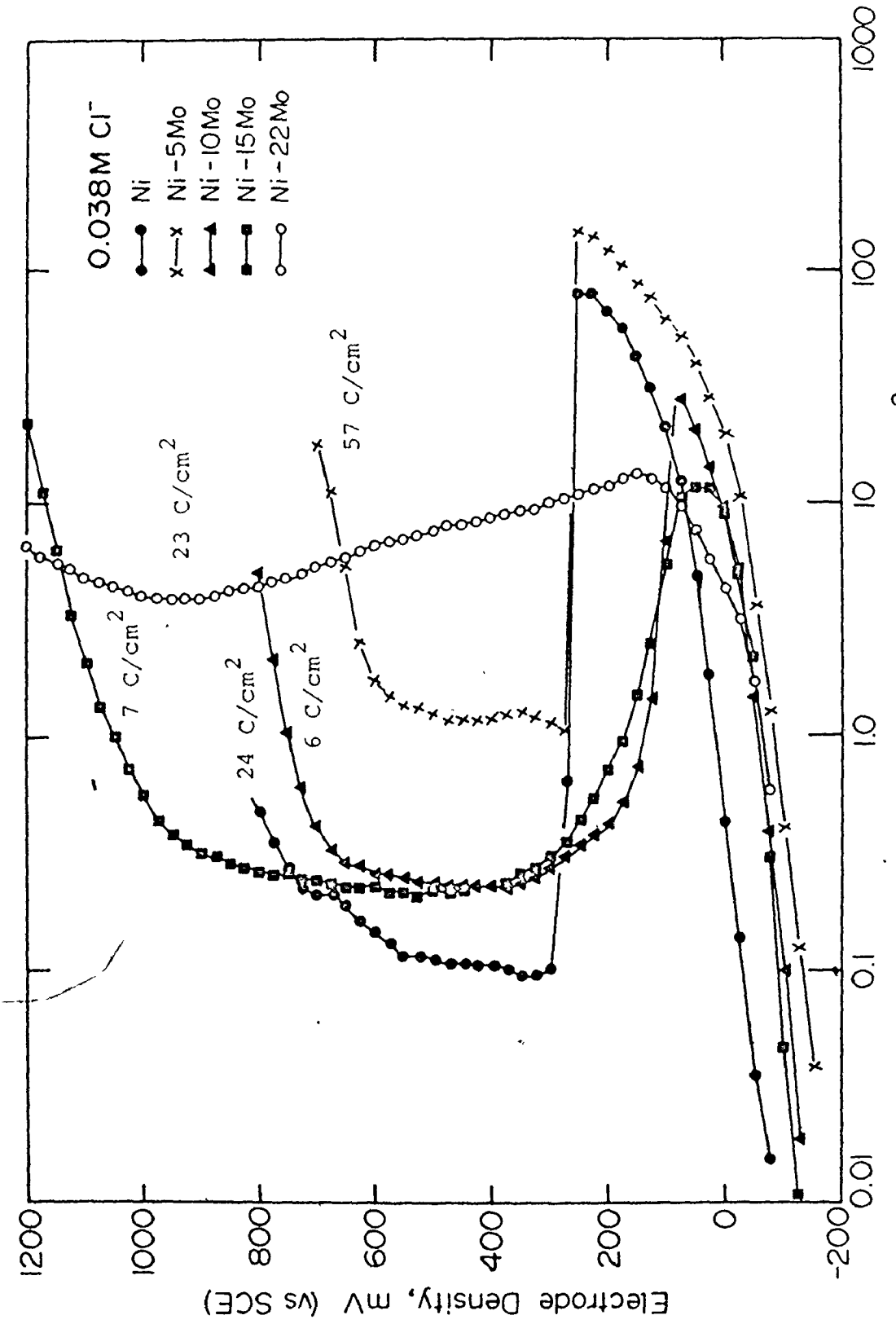

Figure 5-15. Anodic polarization curves for Ni and Ni-Mo alloys in 0.038 M Cl^- solution (pH = 0.4).

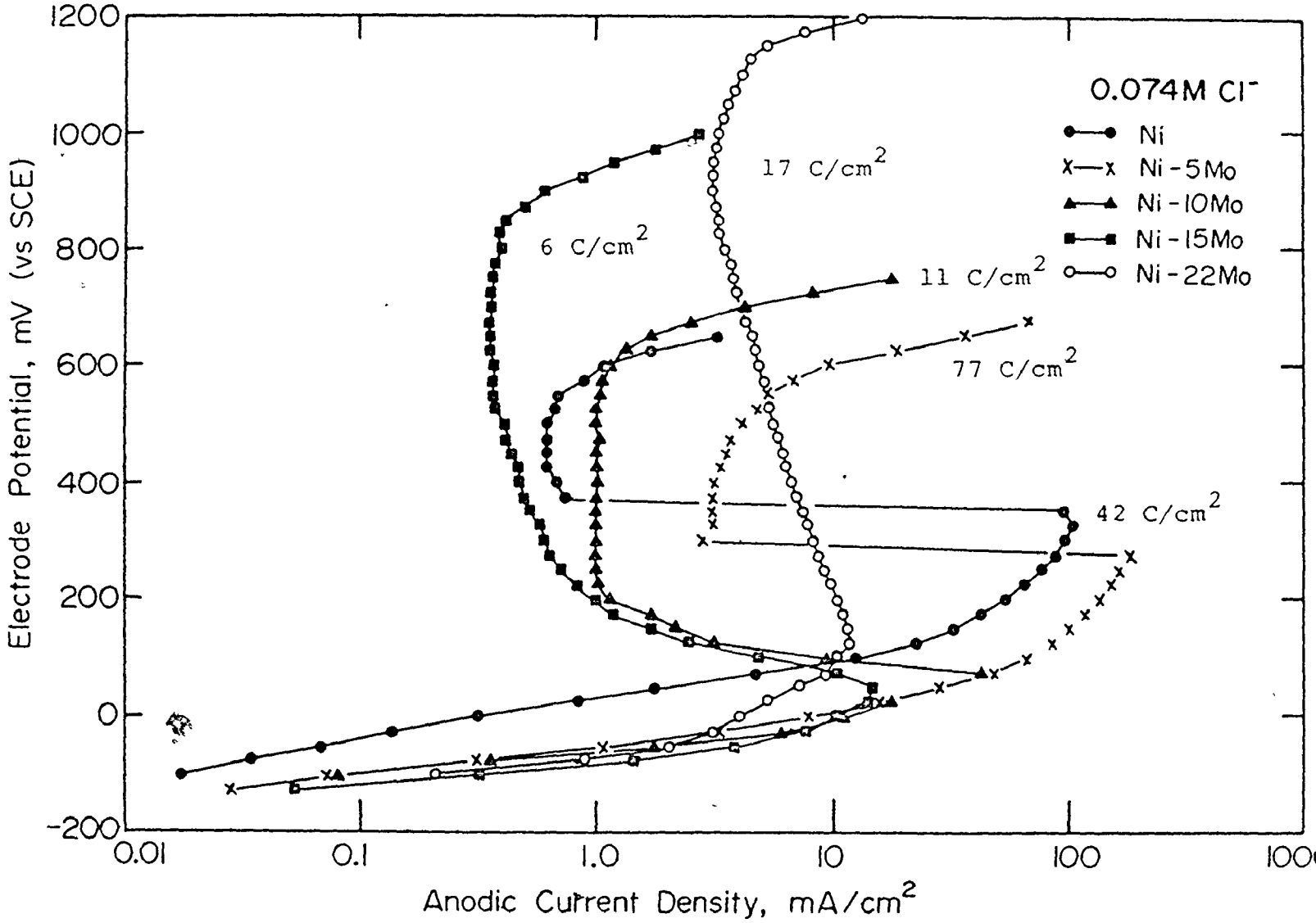

Figure 5-16. Anodic polarization curves for Ni and Ni-Mo alloys in 0.074 M Cl^- solution (pH = 0.4).

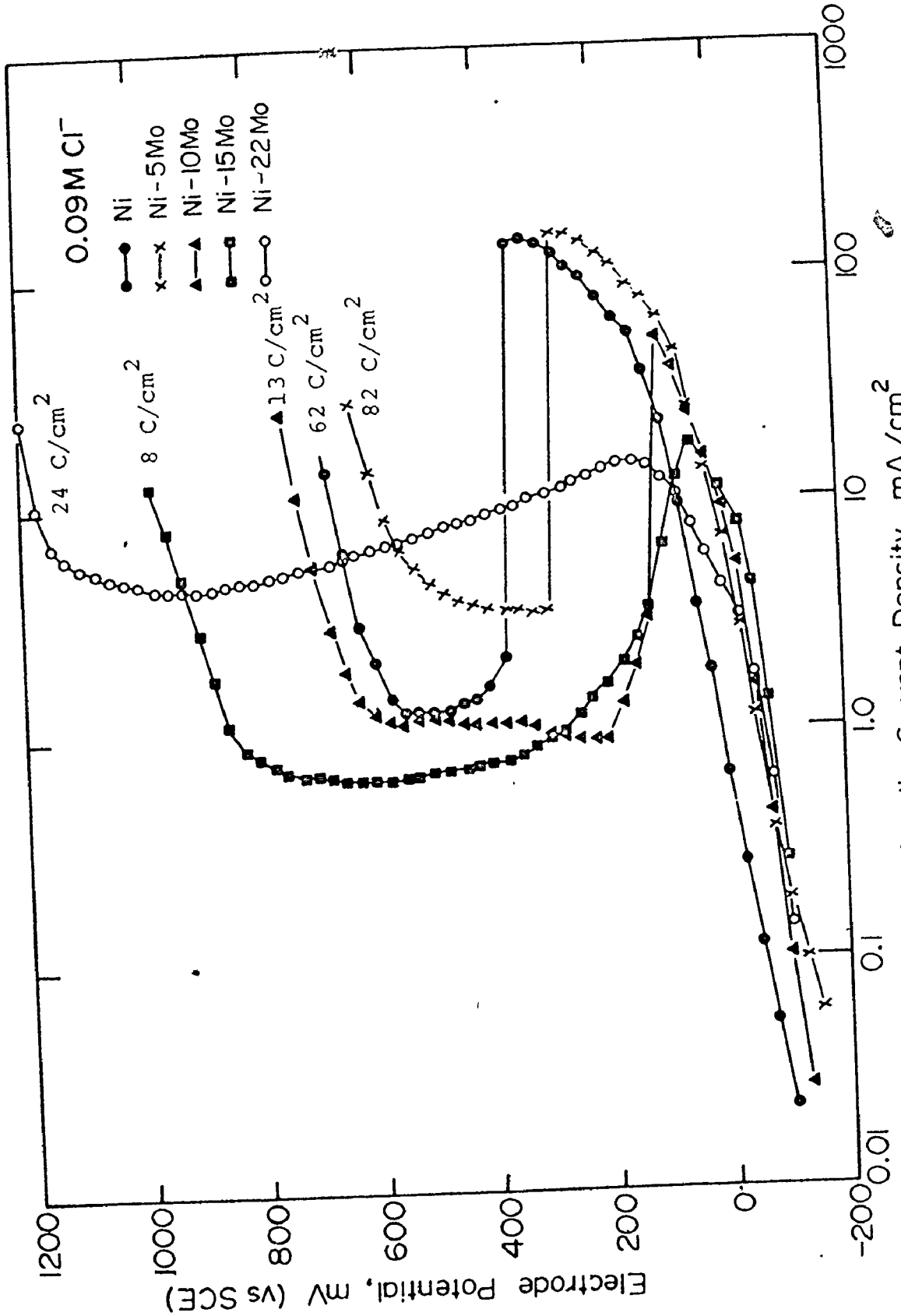

Figure 5-17. Anodic polarization curves for Ni and Ni-Mo alloys in 0.09 M Cl^- solution (pH = 0.4).

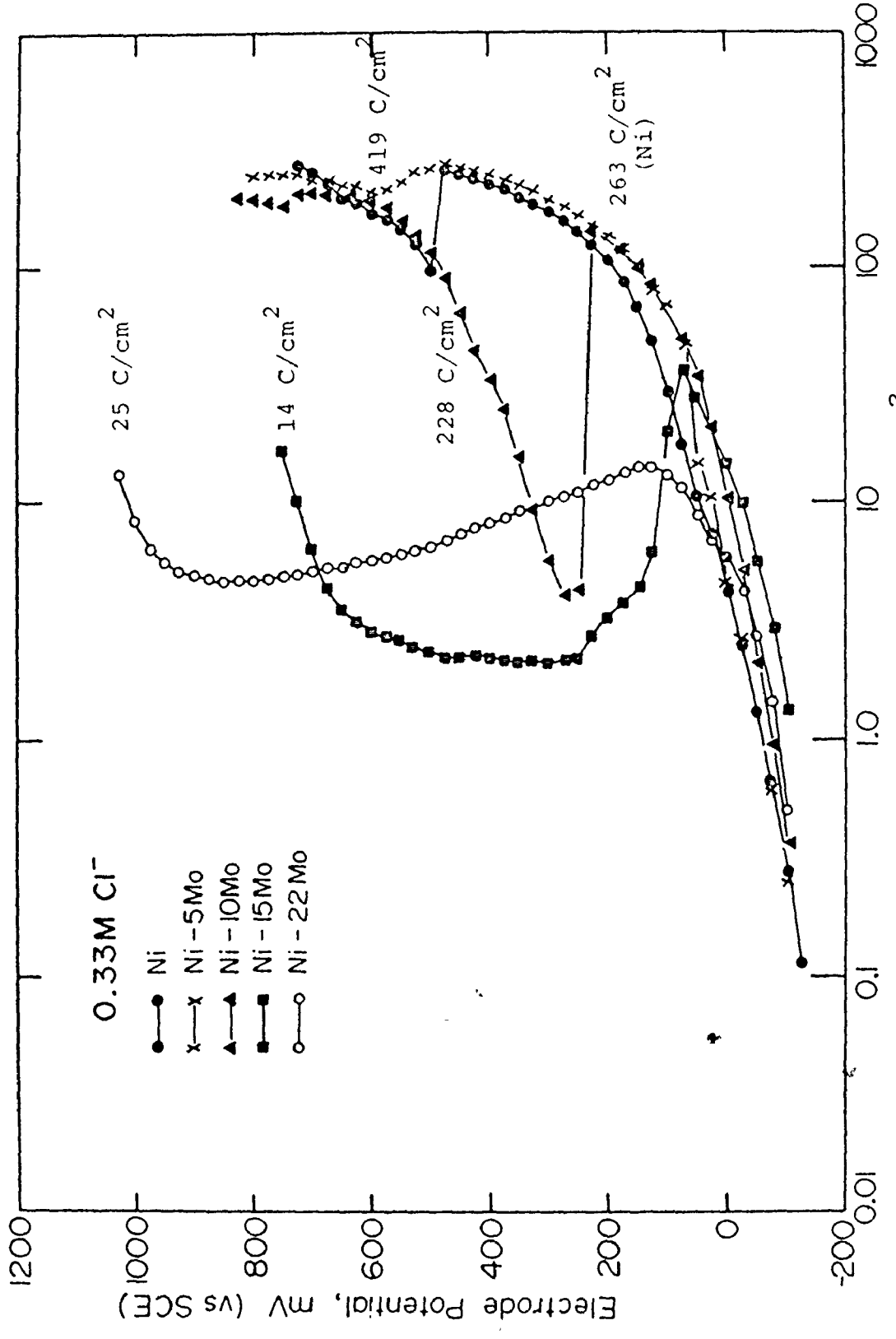

Figure 5-18. Anodic polarization curves for Ni and Ni-Mo alloys in 0.33 M Cl^- solution (pH = 0.4).

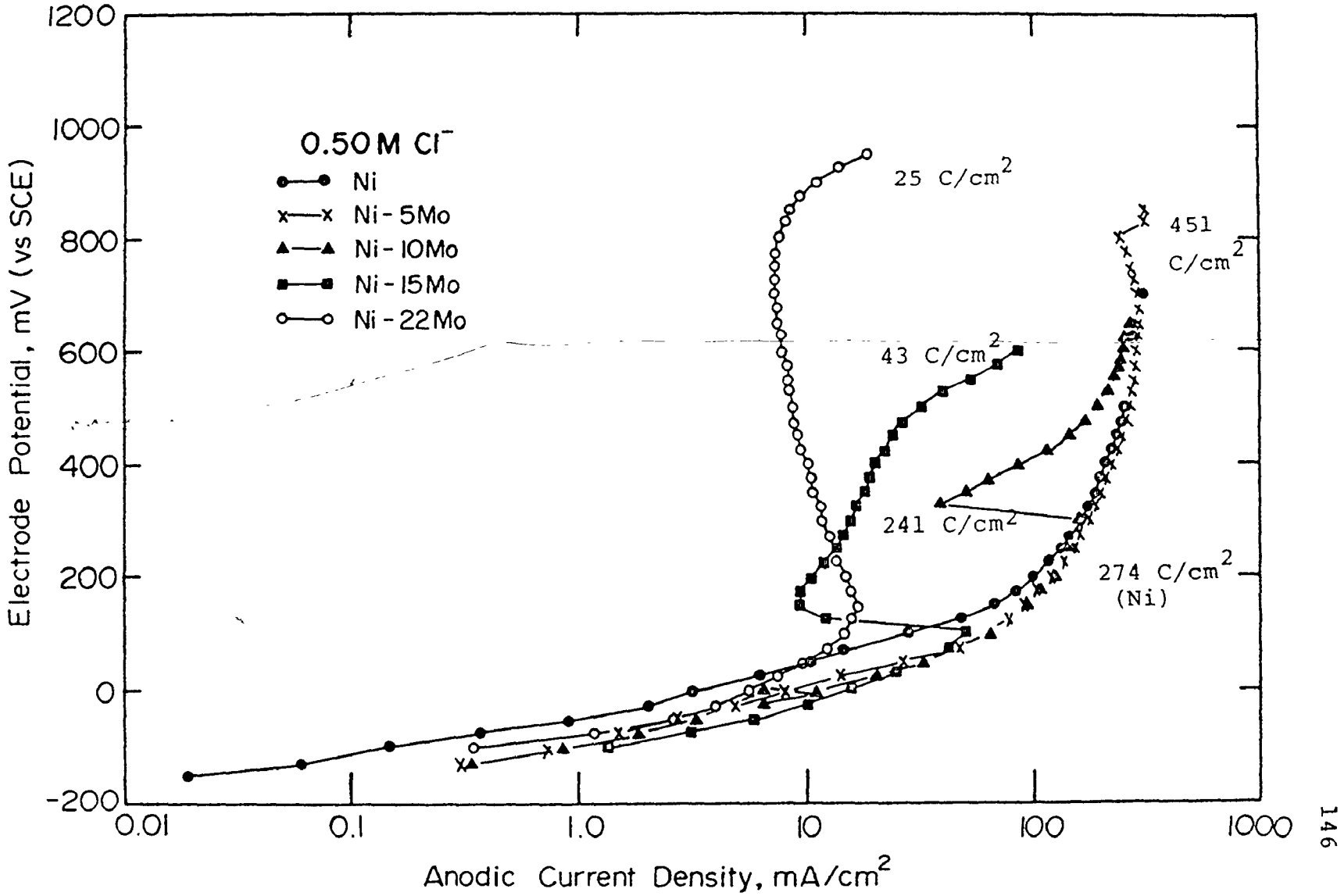

Figure 5-19. Anodic polarization curves for Ni and Ni-Mo alloys in 0.50 M Cl^- solution (pH = 0.4).

Table 5-4

Anodic polarization parameters for Ni-Mo alloys in 0.02 M Cl^- solution

Alloy wt %	E_{corr} mV	E_{pp} mV	i_c mA/cm^2	$(i_a)^*_{-75}$ mA/cm^2	i_p^{**} mA/cm^2	E_c mV	β_a mV/decade	β_t mV/decade
Ni	-	225	48.4	0.014	0.06	950	52	160
Ni-5Mo	-200	200	115	0.38	0.33	600	60	70
Ni-10Mo	-220	50	18.3	0.04	0.22	750	28	115
Ni-15Mo	-150	50	9.4	0.75	0.13	900$^+$	45	325
Ni-22Mo	-122	150	11.0	0.18	5.0	950^{++}	30	790
Ni-30Mo	-109	NO PASSIVE REGION			-	-	40	-
Mo	+ 23	NO PASSIVE REGION			-	-	45	-

*Anodic current density in the 'active region' at -75 mV (SCE)
**Lowest recorded value
+Approximate value, since curve exhibits gradual bend
++Value to be taken with caution (refer to Figure 5-14)

Table 5-5

Anodic polarization parameters for Ni-Mo alloys in

0.038 M Cl^- solution

Alloy wt %	E_{corr} mV	E_{pp} mV	i_c mA/cm^2	$(i_a)^*_{-75}$ mA/cm^2	i_p^{**} mA/cm^2	E_c mV	β_a mV/decade	β_t mV/decade
Ni	-	250	79	0.015	0.10	700	52	-
Ni-5Mo	-185	250	147	1.28	1.25	550	52	73
Ni-10Mo	-162	75	27.8	0.39	0.24	625	42	86
Ni-15Mo	-200	50	11.7	0.31	0.22	900+	33	110
Ni-22Mo	-200	150	13.1	0.58	7.5	900++	30	-
Mo	+ 44	NO PASSIVE REGION		-	-	-	50	-

*Anodic current density in the 'active region' at -75 mV (SCE)
**Lowest recorded value
+Approximate value, since curve exhibits gradual bend
++Value to be taken with caution (refer to Figure 5-15)

Table 5-6

Anodic polarization parameters for Ni-Mo alloys in 0.074 M Cl^- solution

Alloy wt %	E_{corr} mV	E_{pp} mV	i_c mA/cm^2	$(i_a)^*_{-75}$ mA/cm^2	i_p^{**} mA/cm^2	E_c mV	β_a mV/decade	β_t mV/decade
Ni	-	325	103	0.035	0.62	550	65	100
Ni	-210	275	181	0.31	2.8	475	48	90
Ni-10Mo	-190	75	42.2	0.36	1.0	575	43	83
Ni-15Mo	-210	50	14.4	1.47	0.36	850	35	160
Ni-22Mo	-153	150	11.7	0.89	3.1	900+	25	-
Mo	+ 44	NO PASSIVE REGION		-	-	-	50	-

*Anodic current density in the 'active region' at -75 mV (SCE)
**Lowest recorded value
+Value to be taken with caution (refer to Figure 5-16)

Table 5-7

Anodic polarization parameters for Ni-Mo alloys in 0.09 M Cl^- solution

Alloy wt %	E_{corr} mV	E_{pp} mV	i_c mA/cm^2	$(i_a)^*_{-75}$ mA/cm^2	i_p^{**} mA/cm^2	E_c mV	β_a mV/decade	β_t mV/decade
Ni	-	325	140	0.052	1.28	550	65	72
Ni-5Mo	-205	275	150	0.36	3.36	400	60	96
Ni-10Mo	-180	100	50	0.43	1.00	575	45	85
Ni-15Mo	-169	50	17.2	1.36	0.63	800	37	120
Ni-22Mo	-152	150	14.7	0.61	4.40	900+	36	-
Ni-30Mo-1	-109	NO PASSIVE REGION		0.01	-	-	38	-
Mo	+ 44	NO PASSIVE REGION		-	-	-	45	-

*Anodic current density in the 'active region' at -75 mV (SCE)
**Lowest recorded value
+Value to be taken with caution (refer to Figure 5-17)

Table 5-8

Anodic polarization parameters for Ni-Mo alloys in 0.33 M Cl^- solution

Alloy wt %	E_{corr} mV	E_{pp} mV	i_c mA/cm^2	$(i_a)^*_{-75}$ mA/cm^2	i_p^{**} mA/cm^2	E_c mV	β_a mV/decade	β_t mV/decade
Ni	-260	475	264	0.67	97	+	74	-
Ni-5Mo	-260	475	267	0.60	214	+	74	-
Ni-10Mo	-188	225	142	0.94	4.0	+	74	-
Ni-15Mo	-178	75	36.1	2.92	2.1	575	74	125
Ni-22Mo	-160	150	14.2	1.44	4.7	850++	73	-
Mo	+24	NO PASSIVE REGION	-	-	-	-	45	-

*Anodic current density in the 'active region' at -75 mV (SCE)
**Lowest recorded value
+No true value of E_c exists
++Value to be taken with caution (refer to Figure 5-18)

Table 5-9

Anodic polarization parameters for Ni-Mo alloys in 0.50 M Cl^- solution

Alloy wt %	E_{corr} mV	E_{pp} mV	i_c mA/cm^2	$(i_a)^*_{-75}$ mA/cm^2	i_p^{**} mA/cm^2	E_c mV	β_a mV/decade	β_t mV/decade
Ni	-315	NO PASSIVE REGION		0.14	-	-	65	-
Ni-5Mo	-220	675	292	1.5	286	+	68	-
Ni-10Mo	-195	275	158	1.8	40	+	75	-
Ni-15Mo	-265	100	51	3.1	9.3	400^{++}	78	230
Ni-22Mo	-165	150	16.4	1.17	7.2	750^{++}	73	-
Mo	+ 22	NO PASSIVE REGION		-	-	-	45	-

*Anodic current density in the 'active region' at -75 mV (SCE)
**Lowest recorded value
+No true value of E_c exists
++Value to be taken with caution (refer to Figure 5-19)

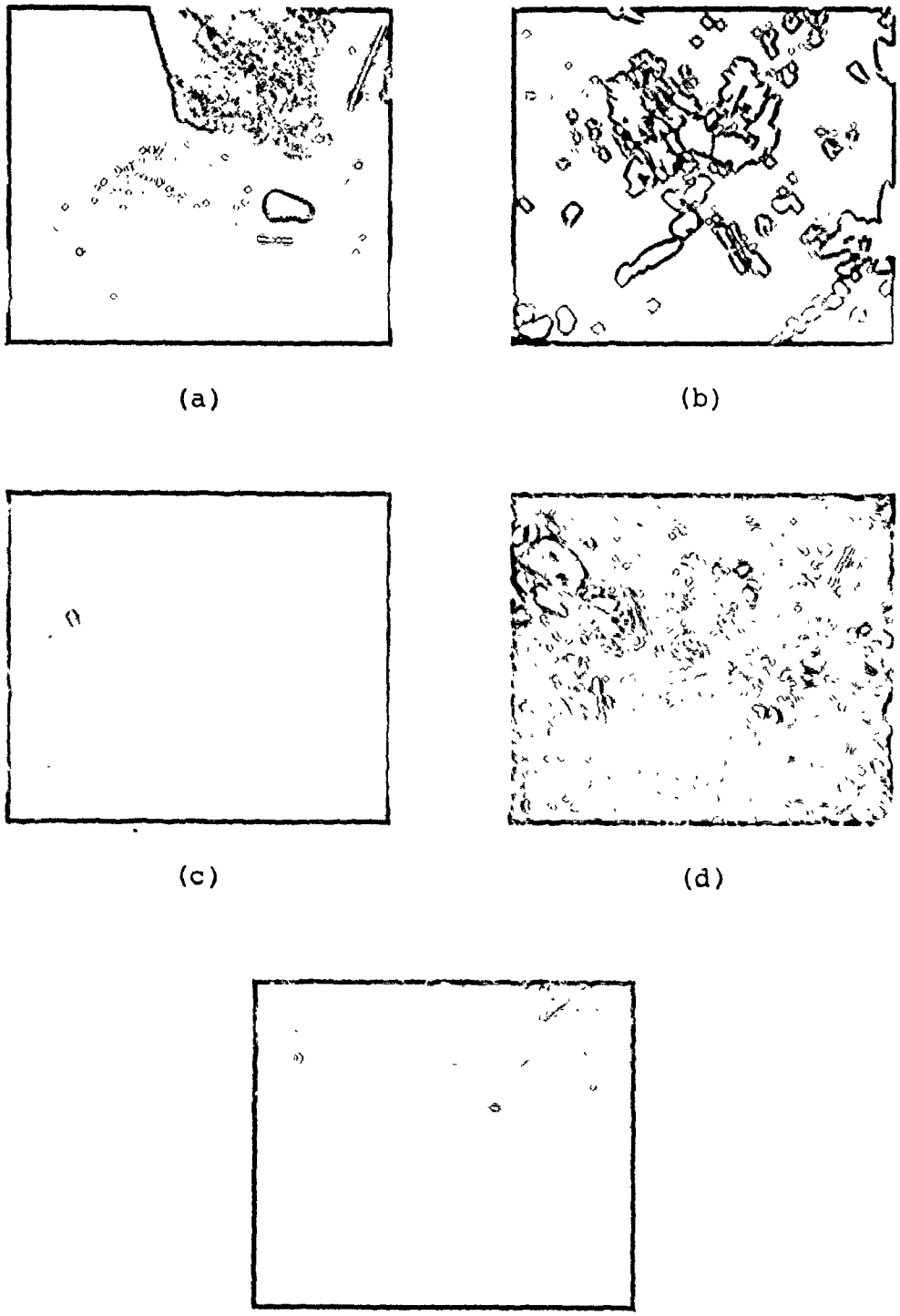

Figure 5-20. Surface morphology of the specimens after potentiostatic polarization in 0.02 M Cl^- solution (pH=0.4), Q = total charge passed up to end of polarization.
(a) Ni , E = +1100 mV, Q = 12 C/cm^2, 160×
(b) Ni-5Mo alloy , E = + 800 mV, Q = 65 C/cm^2, 600×
(c) Ni-10Mo alloy, E = + 975 mV, Q = 6 C/cm^2, 600×
(d) Ni-15Mo alloy, E = +1200 mV, Q = 4 C/cm^2, 300×
(e) Ni-22Mo alloy, E = +1200 mV, Q = 17 C/cm^2, 300×

specimens taken at the end of the polarization run. The charge consumed up to the instant of the photograph is also shown. It can be seen that while all the other materials show attack mainly along the grain boundaries, the attack in the Ni-5Mo alloy is so intense that a clear distinction between the grain boundary and grain interior corrosion is somewhat difficult. The high intensity of attack for the Ni-5Mo alloy is also evident from the amount of charge consumed. Whereas the charge for the other alloys varies between 4-17 C/cm^2, the Ni-5Mo alloy consumes a total charge of 65 C/cm^2. Note that whereas polarization in 1N H_2SO_4 revealed only the metallurgical structure of all specimens (except Ni-22Mo alloy which showed intergranular corrosion), even a small Cl^- ion concentration (as low as 0.02 M) produces intergranular corrosion in Ni-10Mo and Ni-15Mo alloys.

Increasing the Cl^- ion concentration further demonstrates the detrimental effect of this ion on the corrosion behaviour of Ni, Ni-5Mo and Ni-10Mo alloys. Figures 5-15 to 5-17 show that as the Cl^- ion concentration increases from 0.038 M to 0.09 M, the values of i_c and i_p increase while that of E_c decreases considerably. The passive region for the Ni-10Mo alloy is still well defined at 0.09 M Cl^- whereas that for Ni and Ni-5Mo alloy is less clear. Figure 5-21 shows the corrosion morphology of these specimens at the end of their polarization runs. A comparison of the charge consumed and the resultant surface morphology reveals that for pure Ni and Ni-5Mo alloy, a large charge is consumed and a heavily attacked surface, which may be taken to

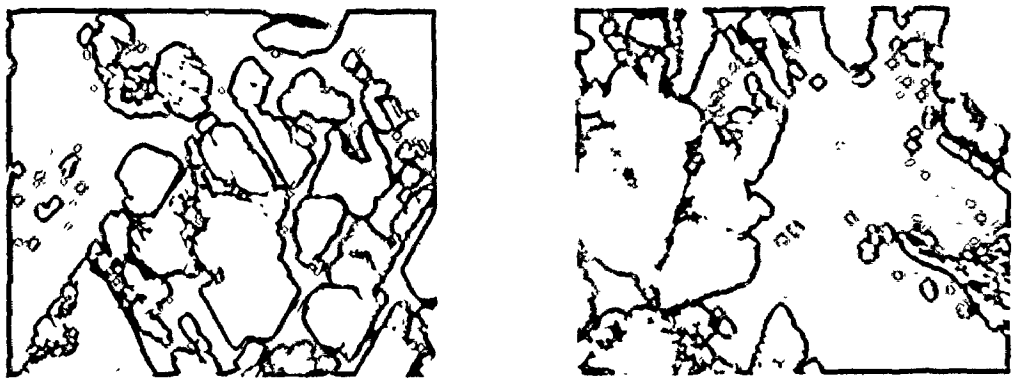

(a) (b)

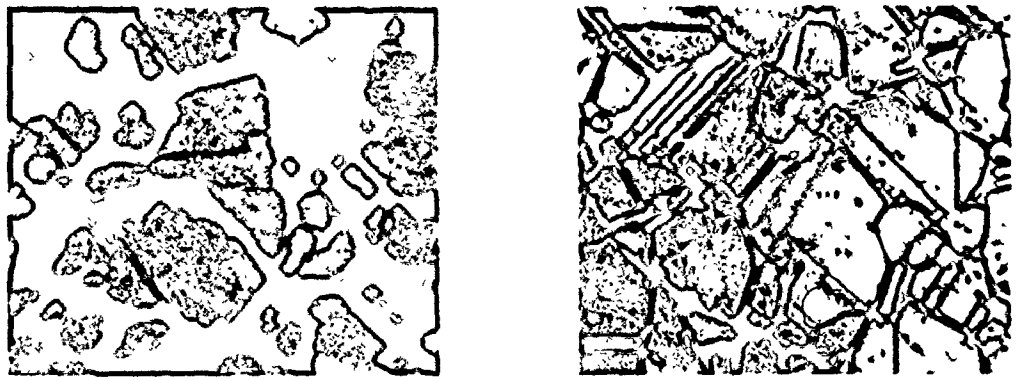

(c) (d)

(e)

Figure 5-21. Surface morphology of the specimen after potentiostatic polarization in 0.09 M Cl^- solution (pH=0.4). Q = total charge passed up to end of polarization

(a) Ni , E = + 675 mV, Q = 62 C/cm^2, 250×
(b) Ni-5Mo alloy , E = + 625 mV, Q = 82 C/cm^2, 600×
(c) Ni-10Mo alloy , E = + 750 mV, Q = 13 C/cm^2, 600×
(d) Ni-15Mo alloy, E = + 975 mV, Q = 8 C/cm^2, 300×
(e) Ni-22Mo alloy , E = +1200 mV, Q = 24 C/cm^2, 300×

be 'generally corroded' is produced. However, attack in the other alloys is still localized. The charge consumed has increased and the attack has spread considerably into the grain interior in the Ni-10Mo alloy but the individual grains are still distinguishable. Although the Ni-15Mo and Ni-22Mo alloys show little difference in corrosion morphology as compared to that of Figure 5-20 where the Cl^- ion concentration is only 0.02 M, the charge consumed has increased. Fluctuations in the passive current density (of the order of 0.03 mA/cm^2) were observed for all the alloys up to 15% Mo for Cl^--ion concentrations greater than 0.09 M.

The anodic polarization curves for Cl^--ion concentrations of 0.33 M and 0.50 M are given in Figures 5-18 and 5-19. It can be seen that the Ni, Ni-5Mo and Ni-10Mo alloys cannot be considered to truly passivate in these solutions. The Ni-15Mo alloy does exhibit a passive region in 0.33 M Cl^- but the region is considerably narrowed with a tendency towards disappearance when the Cl^--ion concentration is 0.50 M. The Ni-22Mo alloy is almost oblivious to the presence of Cl^--ions. The surface morphologies presented in Figures 5-22 and 5-23 show that all alloys up to 10% Mo consume very large charges and are heavily corroded. In fact, their corrosion may be considered to be general. However, the Ni-15Mo and Ni-22Mo alloys show a slight change in their corrosion morphology even when compared with Figure 5-20 where the Cl^--ion concentration is the lowest (0.02 M), although the charge consumed has increased considerably, es-

(a)

(b)

(c)

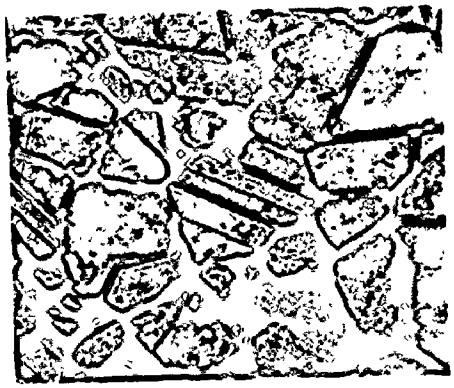

(d)

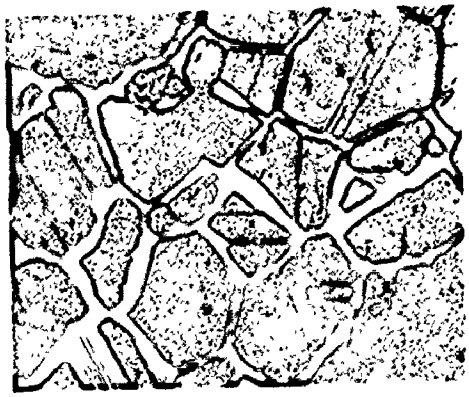

(e)

Figure 5-22. Surface morphology of the specimens after potentiostatic polarization in 0.33 M Cl^- solution (pH=0.4). Q = total charge passed up to end of polarization

(a) Ni , E = + 725 mV, Q = 263 C/cm^2, 600×
(b) Ni-5Mo alloy , E = + 800 mV, Q = 419 C/cm^2, 600×
(c) Ni-10Mo alloy , E = + 825 mV, Q = 228 C/cm^2, 600×
(d) Ni-15Mo alloy , E = + 750 mV, Q = 14 C/cm^2, 300×
(e) , E = +1025 mV, Q = 25 C/cm^2, 300×

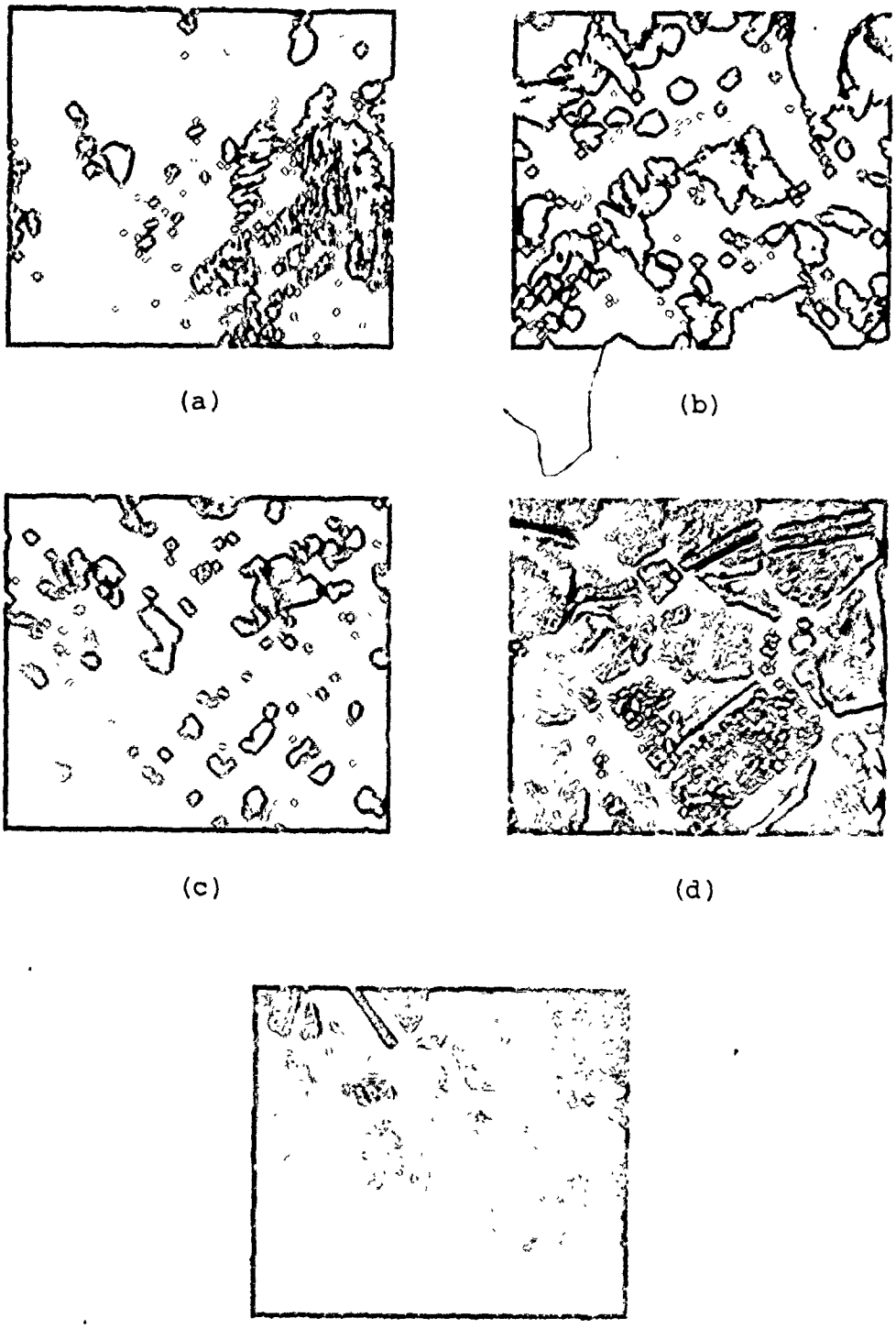

Figure 5-23. Surface morphology of the specimens after potentiostatic polarization in 0.50 M Cl^- solution (pH=0.4). Q = total charge passed up to end of polarization

(a) Ni , E = +700 mV, Q = 274 C/cm^2, 300×
(b) Ni-5Mo alloy , E = +850 mV, Q = 451 C/cm^2, 600×
(c) Ni-10Mo alloy , E = +650 mV, Q = 241 C/cm^2, 600×
(d) Ni-15Mo alloy , E = +600 mV, Q = 43 C/cm^2, 300×
(e) Ni-22Mo alloy , E = +950 mV, Q = 25 C/cm^2, 300×

pecially for the Ni-15Mo alloy. It is pointed out that although the charge consumed is an indication of the total amount of material removed from the specimen surface and provides a basis for comparison of the extent of corrosion, it does not provide any information on the nature of this attack - whether it is general or localized.

The surface of every specimen was continuously monitored by an optical microscope throughout the polarization runs. 'In-situ' microscopic observations revealed that in every case attack set in during the active region and increased in intensity at higher anodic polarization. At high concentrations of the Cl^--ion when the dissolution rate was high, it became impossible to observe the specimen surface (especially at higher anodic potentials) because the surface darkened and alloy dissolution produced solution stirring in the immediate vicinity making focussing of the microscope impossible.

A dark bluish-black film was found on the surface of the Ni-5Mo and Ni-10Mo alloys during polarization in solutions of 0.33 M and 0.50 M Cl^- concentrations. The film for the Ni-5Mo alloy was always thicker than that for the Ni-10Mo alloy. When the concentration of Cl^--ion was 0.33 M, the film was somewhat discontinuous and small pieces of the film flaked off and floated in the solution. A piece of this film from a Ni-5Mo alloy was collected on a copper grid and analyzed by transmission electron diffraction. The film was found to be quite thick and opaque to electrons except at the edges. Many dif-

fraction patterns were taken and using gold as a standard, the film was indexed as MoO_3 (Table 5-10). From the nature of the diffraction rings (Figure 5-24), it can be concluded that the film is crystalline with a large crystallite size.

When the Cl^--ion concentration was 0.50 M, the surfaces of the Ni-5Mo and Ni-10Mo alloys were covered with a very continuous film. In one specimen of the Ni-5Mo alloy, it was possible to completely float off this film from the specimen surface. The film readily dissolved in water during an overnight storage. In order to obtain some insight regarding the constituents of the film, the solution was analyzed for the presence of nickel, molybdenum, sulfate and chloride ions. A small amount of nickel and much larger amounts of molybdenum and sulfate was found. The chloride ion was found to be absent and did not respond even to tests designed for micro-quantities. Although these results are qualitative in that the amount of each constituent was judged by the quantity of the final precipitate obtained, they do establish the presence of nickel, molybdenum and sulfate ions.

The polarizing solutions containing 0.33 M and 0.50 M Cl^--ion concentrations were analyzed for metallic elements by atomic absorption spectrophotometry to determine the quantity of nickel and molybdenum present. The results are presented in Table 5-11 as the percentage weight fraction (Mo/Ni+Mo) of Mo in solution. It must be remembered that this ratio also incorporates the metals in solution due to film dissolution which,

Table 5-10

Diffraction analysis of film from a Ni-5Mo alloy polarized in 0.33 M Cl^- solution

Experimental (from the original of Figure 5-24)	MoO_3 (ASTM card no. 5-0508)	
d, Å	d, Å	I/I_o
out of	6.93	34
field	3.81	82
of view	3.463	61
3.317	3.260	100
3.017	3.006	13
-	2.702	19
-	2.655	35
-	2.607	6
-	2.527	12
2.353	2.332	12
-	2.309	31
-	2.271	18
2.126	2.131	9
-	1.996	4
-	1.962	13
-	1.960	17
1.858	1.849	21
-	1.821	11
-	1.771	5
-	1.756	5
-	1.733	17

(continued next page)

Table 5-10 (continued)

Experimental (from the original of Figure 5-24)	MoO_3 (ASTM card no. 5-0508)	
d, Å	d, Å	I/I_o
1.691	1.693	8
-	1.663	13
-	1.631	13
1.597	1.597	15
-	1.587	6
-	1.569	16
1.500	1.504	5
-	1.477	10
-	1.443	12
-	1.435	12
-	1.400	5
-	1.366	5
1.351	1.352	6
1.332		
1.213		
1.206		
1.080		
1.019		
0.919		
0.882		

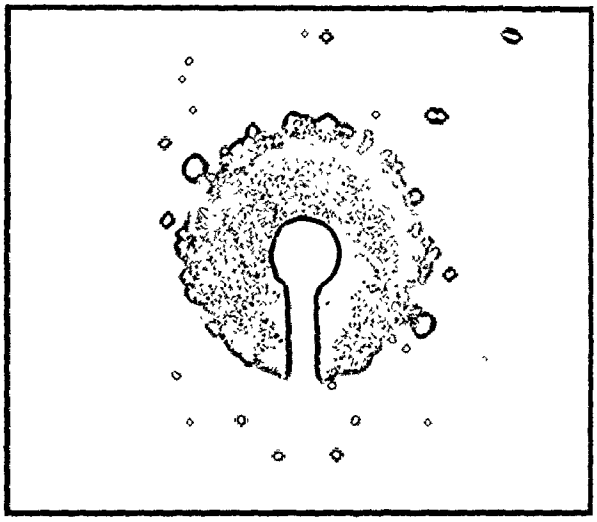

Figure 5-24. Electron diffraction pattern of the film formed on a Ni-5Mo alloy after potentiostatic polarization in 0.33 M Cl^- solution (pH=0.4). The pattern was indexed as MoO_3 (Table 5-10).

Table 5-11

Percentage weight-fraction of molybdenum in the alloy and in solution after potentiostatic polarization in chloride containing solutions

Alloy	$(\frac{Mo}{Ni+Mo})_{alloy}$	$(\frac{Mo}{Ni+Mo})_{solution}$	
		0.33 M Cl^-	0.50 M Cl^-
	%	%	%
Ni-5Mo	8.0	3.4	2.0
Ni-10Mo	15.6	7.8	4.5
Ni-15Mo	22.7	12.0	10.2
Ni-22Mo	31.9	16.6	21.2

especially at 0.33 M Cl^-, was quite high. It can be seen that the Mo/Ni+Mo ratio in solution is much lower than that calculated from the alloy composition. The low Mo/Ni+Mo ratio may be due to a higher rate of nickel dissolution, lower rate of molybdenum dissolution or a combination of both. In any case, it does establish that the film is richer in molybdenum.

5.2.2.2 Film Thickness Measurements

The purpose of this study was to determine the effect of the presence of Cl^--ions on the thickness of the passive film. In order to enable a direct comparison with the results of film growth in non-aggressive environments, the potential and times of anodic oxidation and the cathodic reduction current density were not altered. The film thickness (obtained as the charge required to cathodically reduce the passive film assuming it to be uniform) for films grown in the presence of 0.007 M Cl^--ion and reduced in diluted solutions (0.001 M Cl^-) is given in Table 5-12. On comparing with the corresponding values in non-aggressive environments (Table 4-2 and 5-3), it is seen that the films grown in the presence of Cl^--ions are much thinner. It is interesting to note that although film thickness in the presence of Cl^--ions are 1/4th to 1/10th their original value in the absence of these ions, the least affected are the film thickness values for the Ni-15Mo alloy.

During anodic oxidation, the current density vs time profiles are much flatter in most cases, suggesting that steady

Table 5-12

Charge consumed during the cathodic reduction at 2.7 $\mu A/cm^2$ of passive films formed in 0.007 M Cl^- at +600 mV for various times on Ni and Ni-Mo alloys

Alloy Wt %	Charge Consumed, mC/cm^2 Passivation Time 15 mins	30 mins	60 mins
Ni	0.74±0.08	0.37±0.09	0.36±0.00
Ni-5Mo	0.18±0.06	0.31±0.03	0.45±0.04
Ni-10Mo	0.07±0.01	0.06±0.01	0.19±0.00
Ni-15Mo	0.42±0.07	0.28±0.14	0.24±0.10

state (independence of current with time) sets in within the first 10-15 mins after which the current density becomes almost independent of time.

An experimental difficulty encountered during this study is worth mentioning here for it demonstrates the importance of solution deaeration in electrochemical studies. During the initial test runs, the previously deaerated 1N H_2SO_4 solution used for the dilution of the Cl^--containing solution was measured and stored in a beaker and later transferred to the cell by pouring through a funnel. The curve obtained during subsequent cathodic reduction showed peculiar characteristics. The potential decreased from +600 mV to about -150 mV and then became anodic increasing to about -50 mV and then decreased again. Although this peculiar form of the curve was not reproducible, a hump was always observed. However, when the diluting 1N H_2SO_4 solution was deaerated and transferred to the cell under a nitrogen atmosphere, the hump disappeared. Although the reasons for the occurrence of the hump have not been investigated, it is suggested that its occurrence has some relation to oxygen pick up during solution storage and pouring. Nevertheless, the importance of thorough solution deaeration is quite obvious.

5.2.2.3 Potentiostatic Activation

From Table 5-3 it can be seen that the thickness of the passive film in 1N H_2SO_4 decreases as the percentage of molybdenum increases. It has already been shown that film

thickness is even lower when a small concentration (0.007 M) of Cl^--ions is present (Table 5-12). If the film is considered to form a barrier against further attack, then its thickness would have an effect on the pitting corrosion of a specimen held at an anodic potential. This effect was investigated in the following experiments where specimens were subjected to a passive potential of +400 mV for 30 mins followed by the addition of Cl^--ions.

The results of the potentiostatic activation are shown in Figures 5-25 to 5-28. The addition of Cl^--ions leads to an increase in the anodic current density. In every case (up to 15% Mo) after the addition of Cl^--ions to the passive electrode, a certain time period was required before an increase in the anodic current density was observed. This observation of an induction or incubation period (τ) has been previously noted for many materials[29,106,110] including nickel[79]. The induction period has been interpreted as the time required for the transport of the Cl^--ions from the bulk of the solution to the passive film and their passage through it (passive film) to the metal surface. The induction periods observed in this study are given in Table 5-13 and were taken as the time at which the anodic current density increased by a value greater than 1/100th its initial value. Although it was never possible to entirely reproduce the curves, the trend was always the same. Therefore, the relative positions of the curves are to be considered more meaningful than their absolute positions.

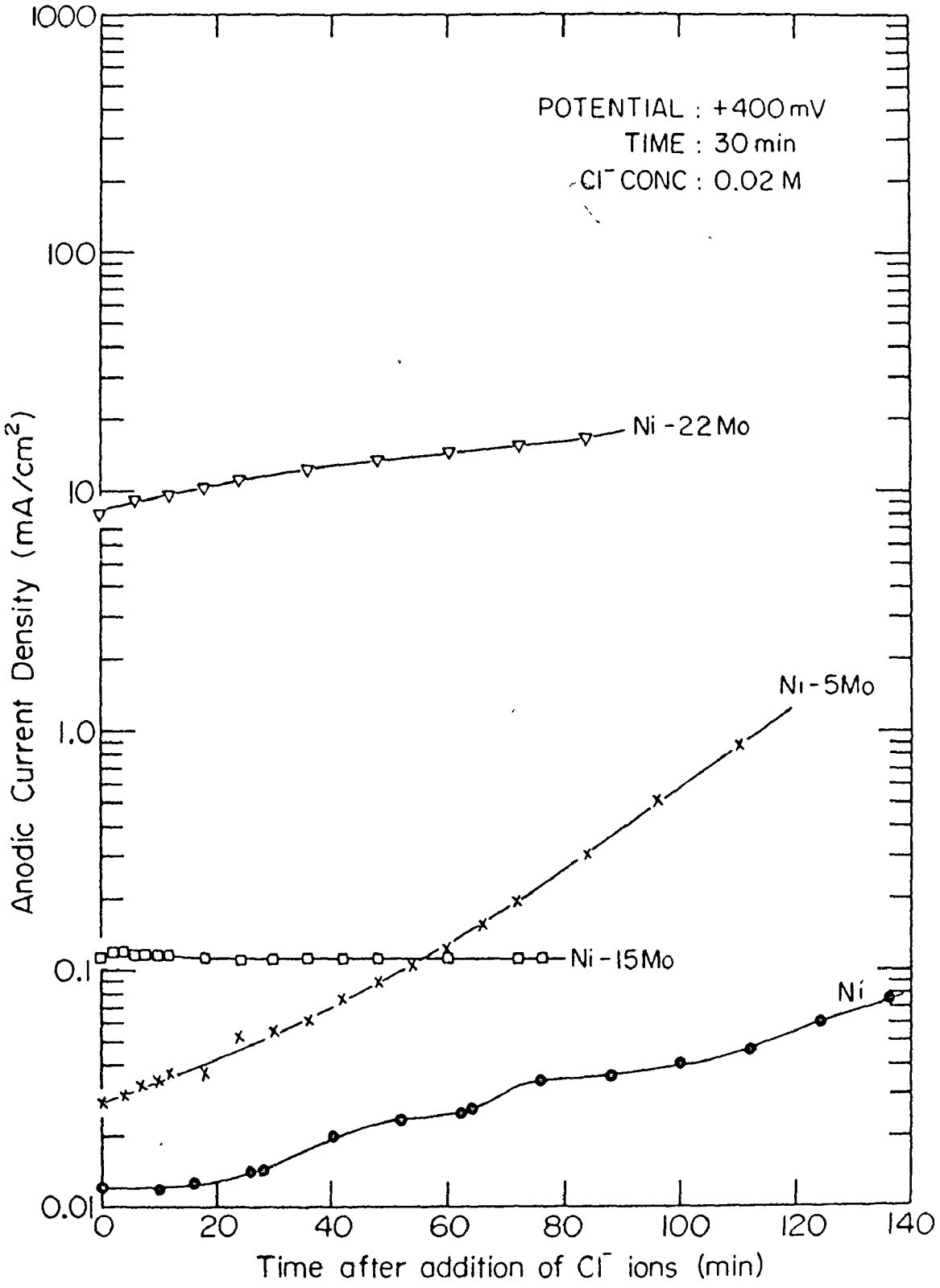

Figure 5-25. Anodic current density as a function of time after the addition of 0.02 M Cl^- ions at +400 mV for Ni and Ni-Mo alloys. Specimens were potentiostatically passivated at +400 mV for 30 mins in 1N H_2SO_4 before the addition of Cl^--ions.

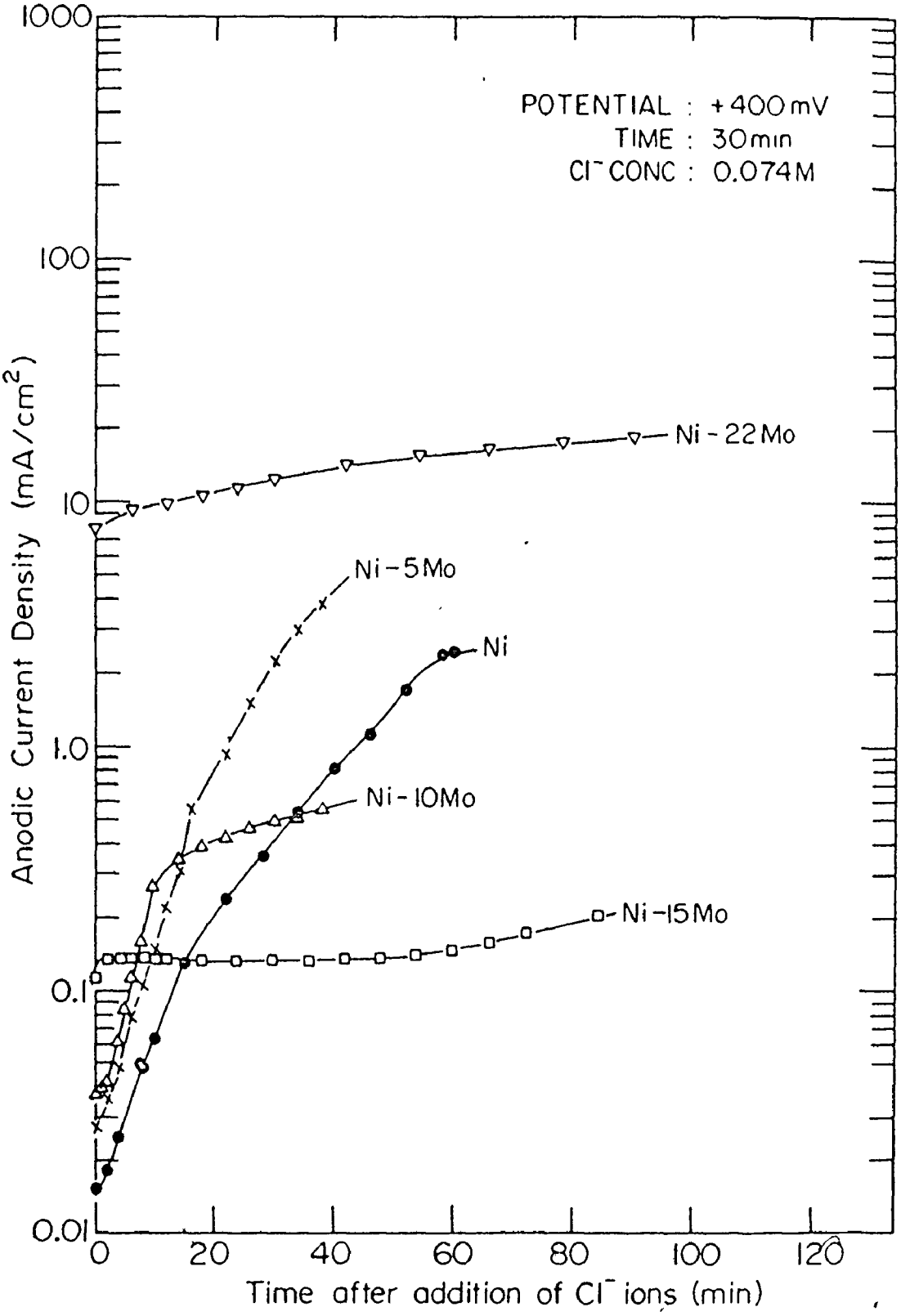

Figure 5-26. Anodic current density as a function of time after the addition of 0.074 M Cl^- ions at +400 mV for Ni and Ni-Mo alloys. Specimens were potentiostatically passivated at +400 mV for 30 mins in 1N H_2SO_4 before the addition of Cl^- ions.

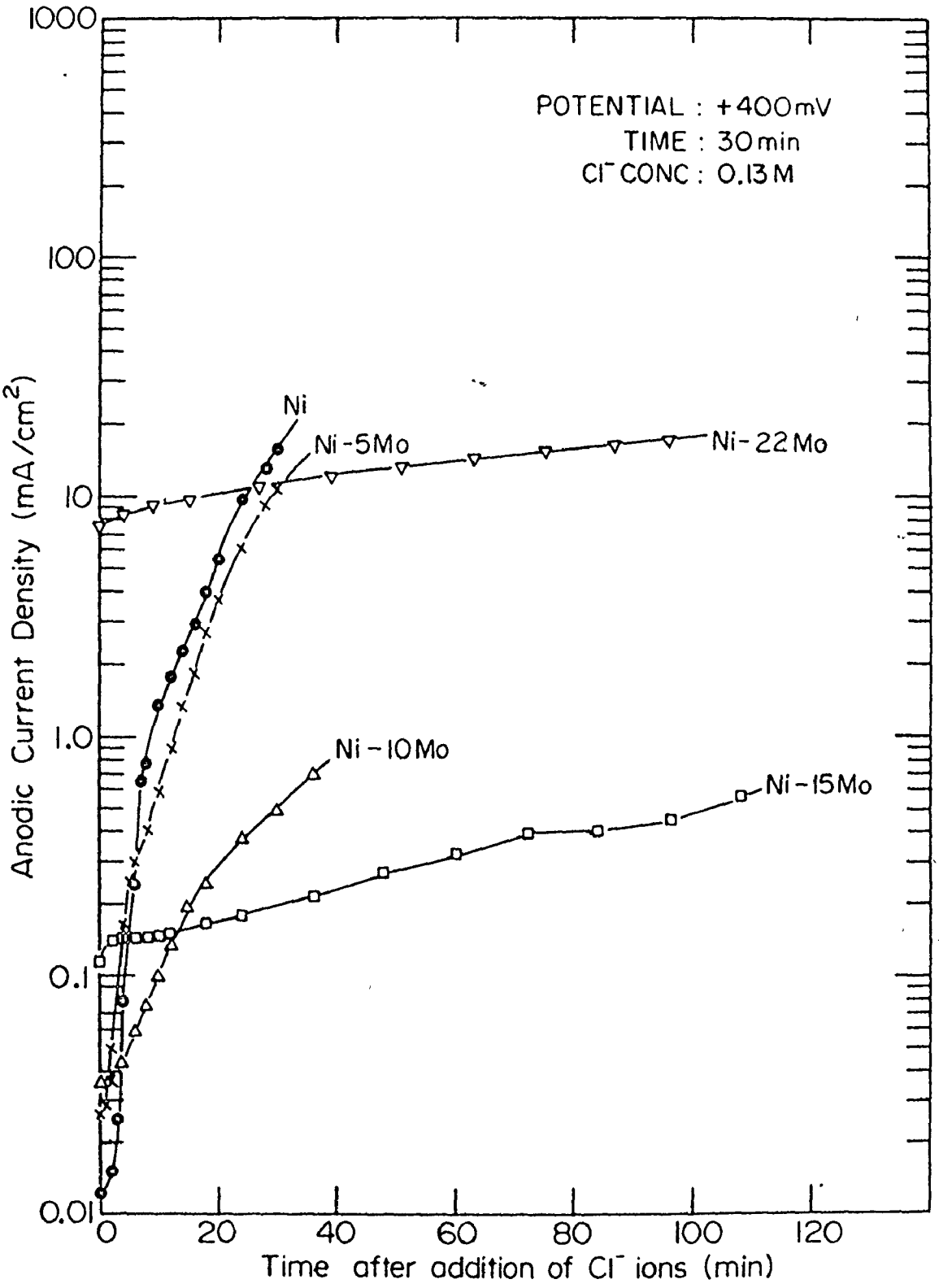

Figure 5-27. Anodic current density as a function of time after the addition of 0.13 M Cl^--ions at +400 mV for Ni and Ni-Mo alloys. Specimens were potentiostatically passivated at +400 mV for 30 mins in 1N H_2SO_4 before the addition of Cl^- ions.

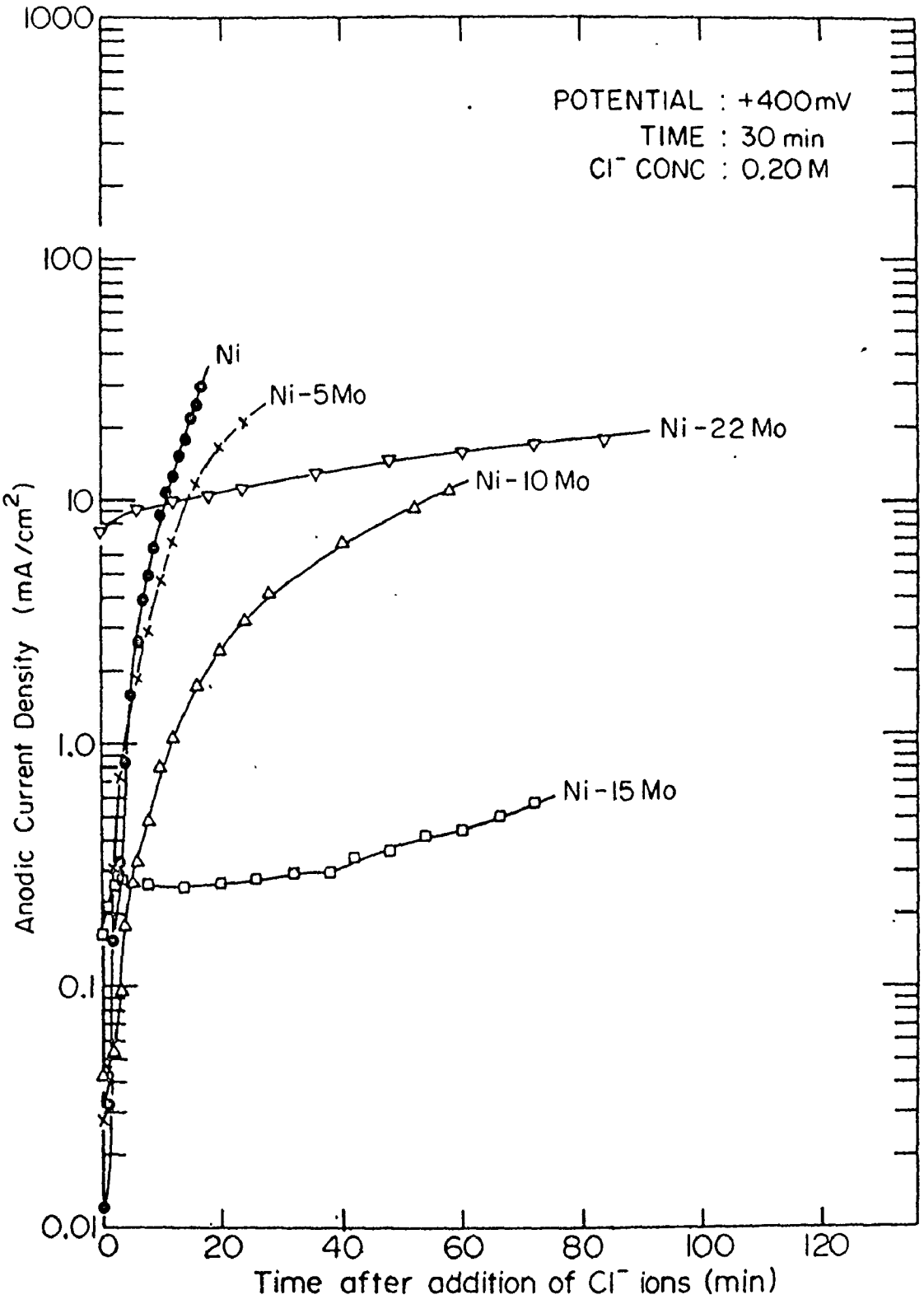

Figure 5-28. Anodic current density as a function of time after the addition of 0.20 M Cl^--ions at +400 mV for Ni and Ni-Mo alloys. Specimens were potentiostatically passivated at +400 mV for 30 mins in 1N H_2SO_4 before the addition of Cl^--ions.

Table 5-13

Induction times observed during potentiostatic activation of Ni and Ni-Mo alloys in various chloride concentrations at +400 mV after 30 mins of passivation

Alloy	Induction Time, mins			
	0.02 M Cl^-	0.074 M Cl^-	0.13 M Cl^-	0.20 M Cl^-
Ni	11.00	1.33	0.67	0.70
Ni-5Mo	2.50	0.72	0.33	0.33
Ni-10Mo	1.00	0.67	0.67	0.10
Ni-15Mo	0.20	0.20	0.20	0.07

Fluctuations in the anodic current density were observed in Ni and Ni-5Mo alloy particularly at low Cl^--ion concentrations. The plotted points are mean values. In such cases, the anodic current density increased, then dropped and then increased again A combination of this behaviour (fluctuations in current and drop in current density) was observed for the Ni-15Mo alloys where large cyclic fluctuations were found in the anodic current density, possibly bearing on the repassivation ability of the alloy.

The resultant corrosion morphology after removal of the specimen from the corrosion cell is described in Table 5-14. In general, lower Cl^- concentrations yielded more numerous very small pits while higher concentrations resulted in fewer large ones. 'In-situ' microscopic observations were not helpful in relating pit formation with the induction period, possibly because of the small pit sizes and low induction periods.

The behaviour of the Ni-22Mo alloys was very different from that of the single phase alloys just described. As will be seen from the polarization curve of this alloy in 1N H_2SO_4 (Figure 5-8), no true passive region exists and the current density at potentials more noble than +400 mV is still decreasing. Hence, when a Ni-22Mo alloy was subjected to a potential of +400 mV, the anodic current density momentarily increased to about 6 mA/cm^2, immediately dropped to about 5 mA/cm^2 and then began an almost linear rise to about 7.5-8.2 mA/cm^2

Table 5-14

Corrosion morphology of Ni and Ni-Mo alloys after potentiostatic activation at +400 mV in various chloride concentrations

Alloy	Morphology of the Surface			
	0.02 M Cl^-	0.074 M Cl^-	0.13 M Cl^-	0.20 M Cl^-
Ni	numerous very small pits all over surface	same as 0.02 M Cl^-	numerous pits bigger than 0.02 M Cl^- all over surface	numerous pits slightly larger than 0.13 M Cl^- with corrosion at edges
Ni-5Mo	numerous very small pits all over surface	same as 0.02 M Cl^- with tendency for corrosion at edges	numerous pits larger than 0.02 M Cl^- with corrosion at edges	much larger pits with pronounced corrosion at edges
Ni-10Mo	few large pits	more pits but smaller	same as 0.074 M Cl^- with still smaller pits; edge corrosion negligible	same as 0.13 M Cl^- but pronounced edge corrosion
Ni-15Mo	almost unattacked surface but few medium sized pits	same as 0.02 M Cl^-	same as 0.02 M Cl^-	similar to 0.02 M Cl^-; some corrosion along grain boundaries
Ni-22Mo	Highly corroded surface; grain boundary corrosion and pitting within grain.	same as 0.02 M Cl^-	same as 0.02 M Cl^-	same as 0.02 M Cl^-

after 30 mins. The addition of Cl^--ions had the immediate effect of increasing the anodic current density and it was never really possible to observe an induction period. Although no black film was formed on these specimens, the surface was dark and appeared corroded even to the naked eye. 'In-situ' microscopic observations revealed that an outline of the grain structure appeared within 2 mins and after 30 mins at +400 mV the basic trend in the attack - intergranular corrosion - had already set in. Addition of Cl^--ions resulted in the intensification of the attack with time, although very little difference could be found in the extent of localized attack with variation in Cl^--concentration.

If the potentiostatic activation results are presented for each alloy, the effect of the Cl^--ion concentration can be better emphasized. The results for Ni-5Mo, Ni-15Mo and Ni-22Mo alloys are given in Figures 5-29 to 5-31. The harmful effect of Cl^--ion on the Ni-5Mo alloy is evident. In fact, it is probably fair to say that this alloy is not an acceptable alloy for applications in Cl^--containing environments. Reference to Figure 5-30 reveals that the performance of the Ni-15Mo alloy is far superior to that of the Ni-5Mo alloy under the same conditions. The beneficial effect of the Ni-15Mo alloy towards corrosion and the complete indifference of the Ni-22Mo alloy towards the Cl^--ion are consistent with the results of potentiostatic polarization discussed before.

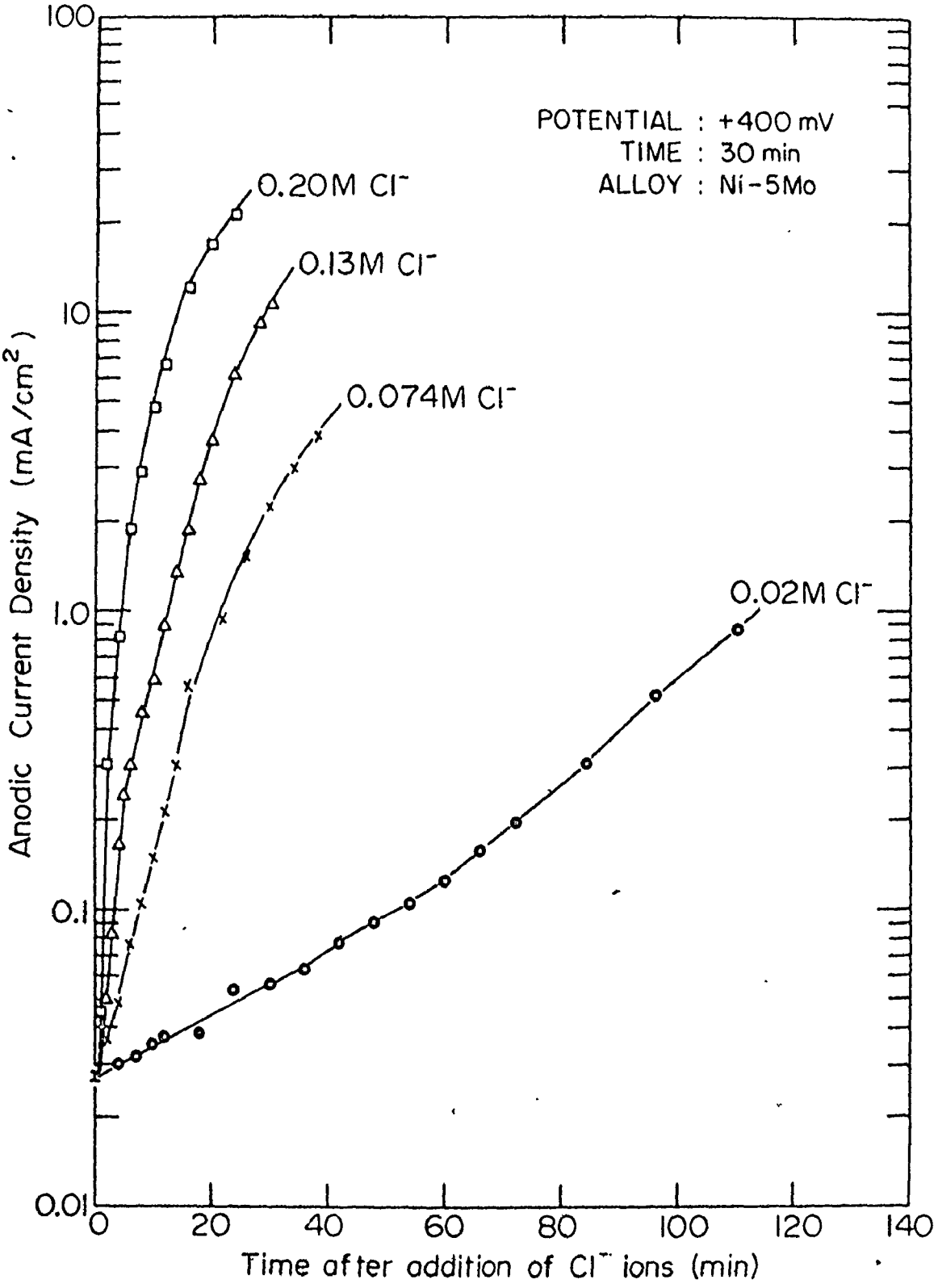

Figure 5-29. Effect of Cl^--ion concentration on the anodic current density as a function of time for Ni-5Mo alloy at +400 mV.

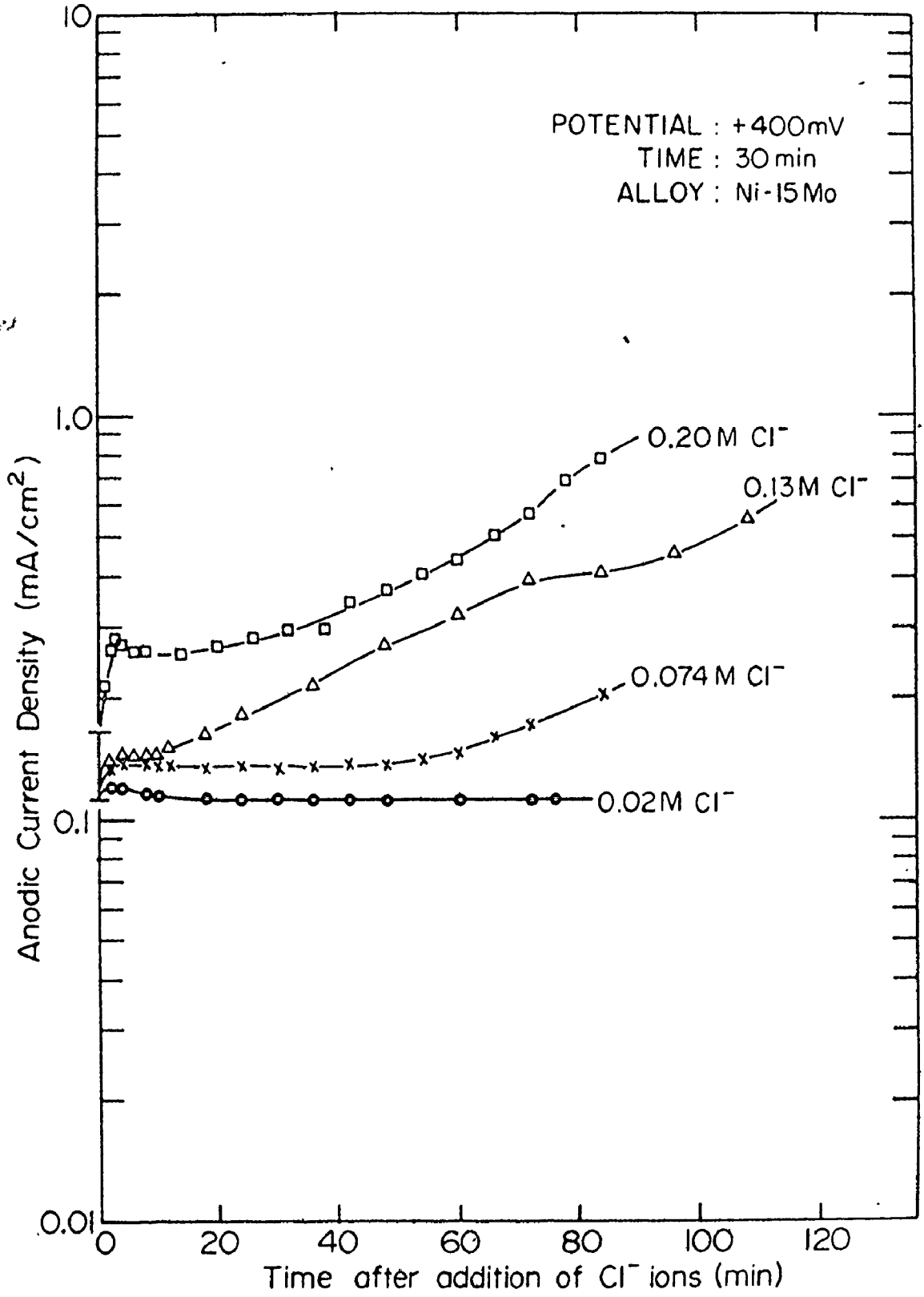

Figure 5-30. Effect of Cl^--ion concentration on the anodic current density as a function of time for Ni-15Mo alloy at +400 mV.

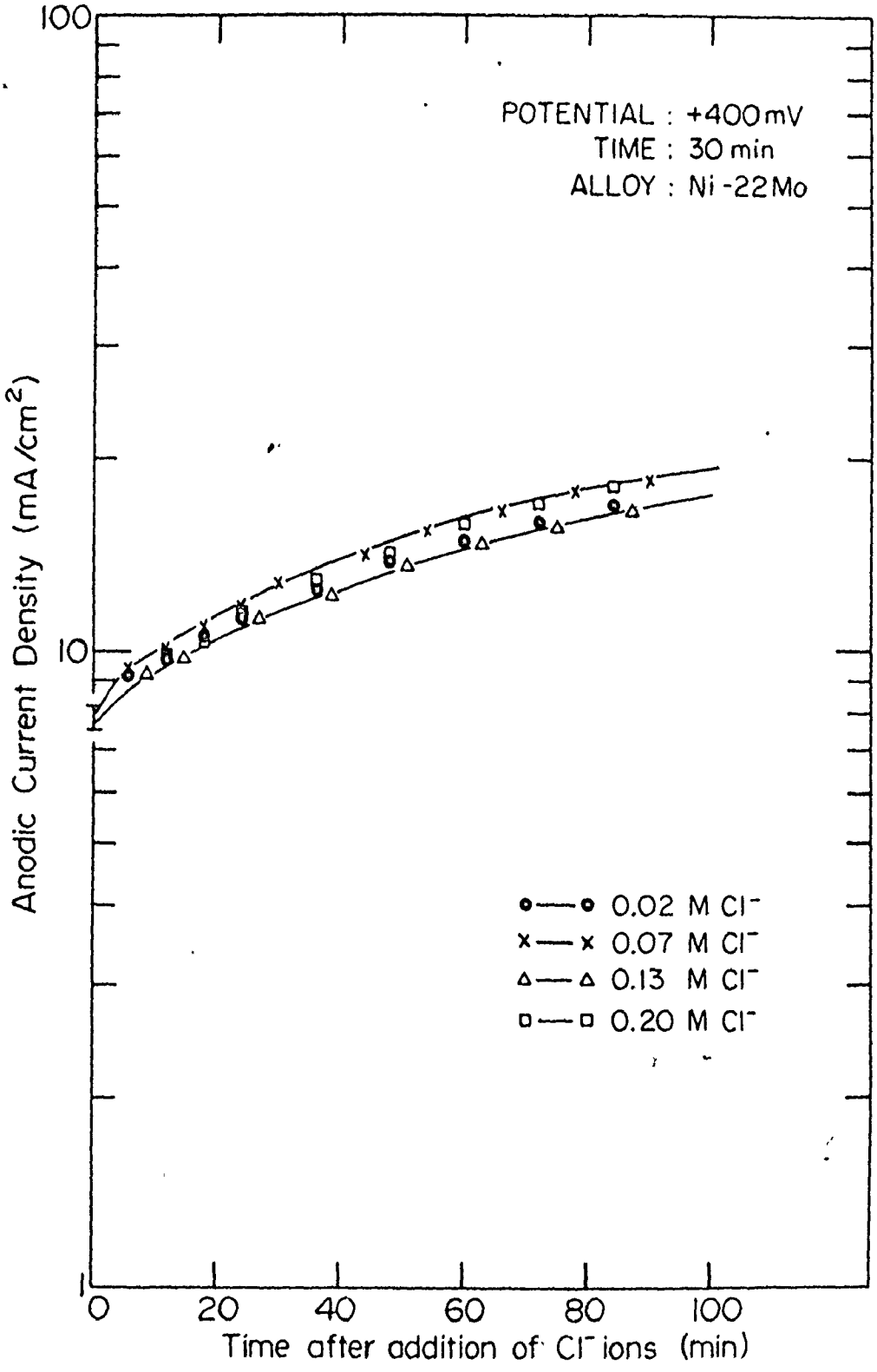

Figure 5-31. Effect of Cl^--ion concentration on the anodic current density as a function of time for Ni-22Mo alloy at +400 mV.

It was pointed out earlier that the rate of pit development of pits at a constant potential is given by[29]

$$i = kt^b$$

where t is the time and k is a proportionality constant. The numerical value of the exponent b provides an indication of the growth rate of the pits and is helpful in determining the aggressiveness of the environment. For, if b is large, pit growth is higher and the environment is aggressive. Since the above equation is based on the assumption that pits are hemispherical in shape so that the current density in the pit is constant, its validity in the present case where apart from pitting, intergranular corrosion also occurs may be doubtful. However, when the present data were plotted as logi vs logt, straight lines were obtained and the value of b could be estimated (Table 5-15). Thus, in the present case the meaning to the exponent b is different. It is taken to designate an overall corrosion phenomenon with the meaning that a low value of b implies lower corrosion while a high value of b signifies higher corrosion. Reference to Tables 5-14 and 5-15 reveals that indeed more corroded surfaces yield higher values of b.

5.2.2.4 Repassivation Characteristics

The increase in the current density in the presence of Cl^--ions is considered to be due to an anodic reaction resulting in metal dissolution. Any decrease in the current density would, therefore, be due to an inhibition of the anodic

Table 5-15

Value of the exponent b in the equation $i = kt^b$ for Ni and Ni-Mo alloys after potentiostatic activation at 400 mV

Alloy	Value of b at +400 mV Cl^--concentration			
	0.02 M	0.074 M	0.09 M	0.20 M
Ni	0.95	1.6	2.6	2.4
Ni-5Mo	0.19	2.6	2.0	1.9
Ni-10Mo	0.16	1.3	1.5	1.6
Ni-15Mo	0	0	0.08	0.08

anodic reaction. In the presence of active anodic dissolution, this decrease in the current density is most likely to be associated with a repassivation ability of the alloy. The sudden drops and cyclic fluctuations in the anodic current density observed during potentiostatic activation studies provided the basis of the results to be presented in this section. It is emphasized that the potential scan employed was not a continuous sweep (potentiodynamic) but a step-wise one (potentiostatic, 25 mV/min). It is felt that this method of testing is much harsher in that an alloy is held for a minute at a high anodic potential and then its potential stepped down. The ability for repassivation will be higher in the potentiodynamic method where the anodic reaction is continuously being suppressed by the reversed potential sweep. It is probably fair to conclude that an alloy which repassivates during the potentiostatic technique would certainly do so in the potentiodynamic one, although the reverse may not be true.

The results of the repassivation experiments are presented in Figures 5-32 to 5-36 for nickel and the alloys. It can be seen by comparing these Figures that the curves in 1N H_2SO_4, which provide a basis for comparison, possess little or no hysteresis. On the other hand an addition of a small amount of Cl^--ions (0.02 M) significantly affects the curves for Ni-5Mo and Ni-10Mo alloys (Figures 5-33 and 5-34) shifting the reverse scan to higher current density values. In fact, the hysteresis

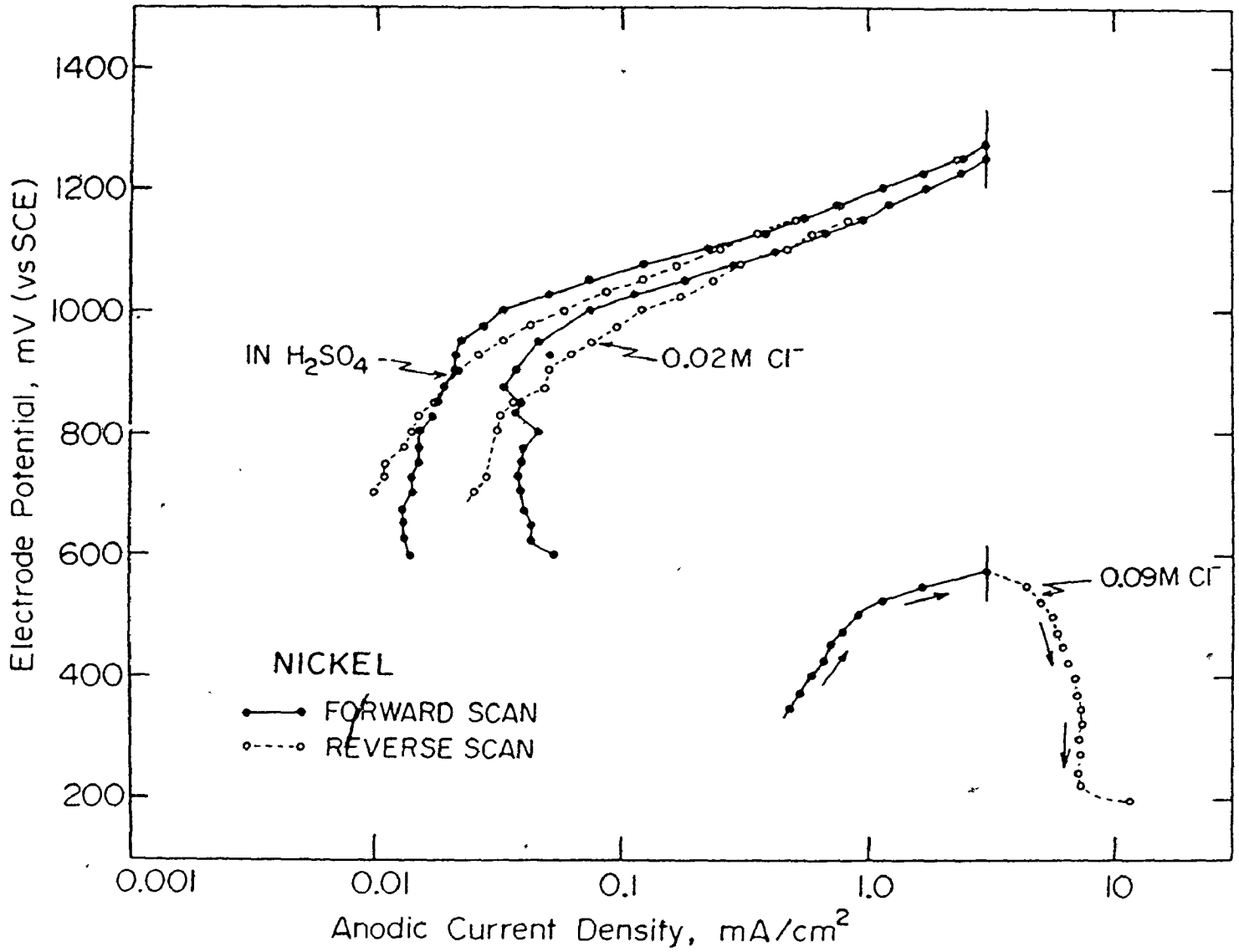

Figure 5-32. Effect of Cl^--ion concentration on the anodic current density during the potentiostatic forward and reverse scan for nickel.

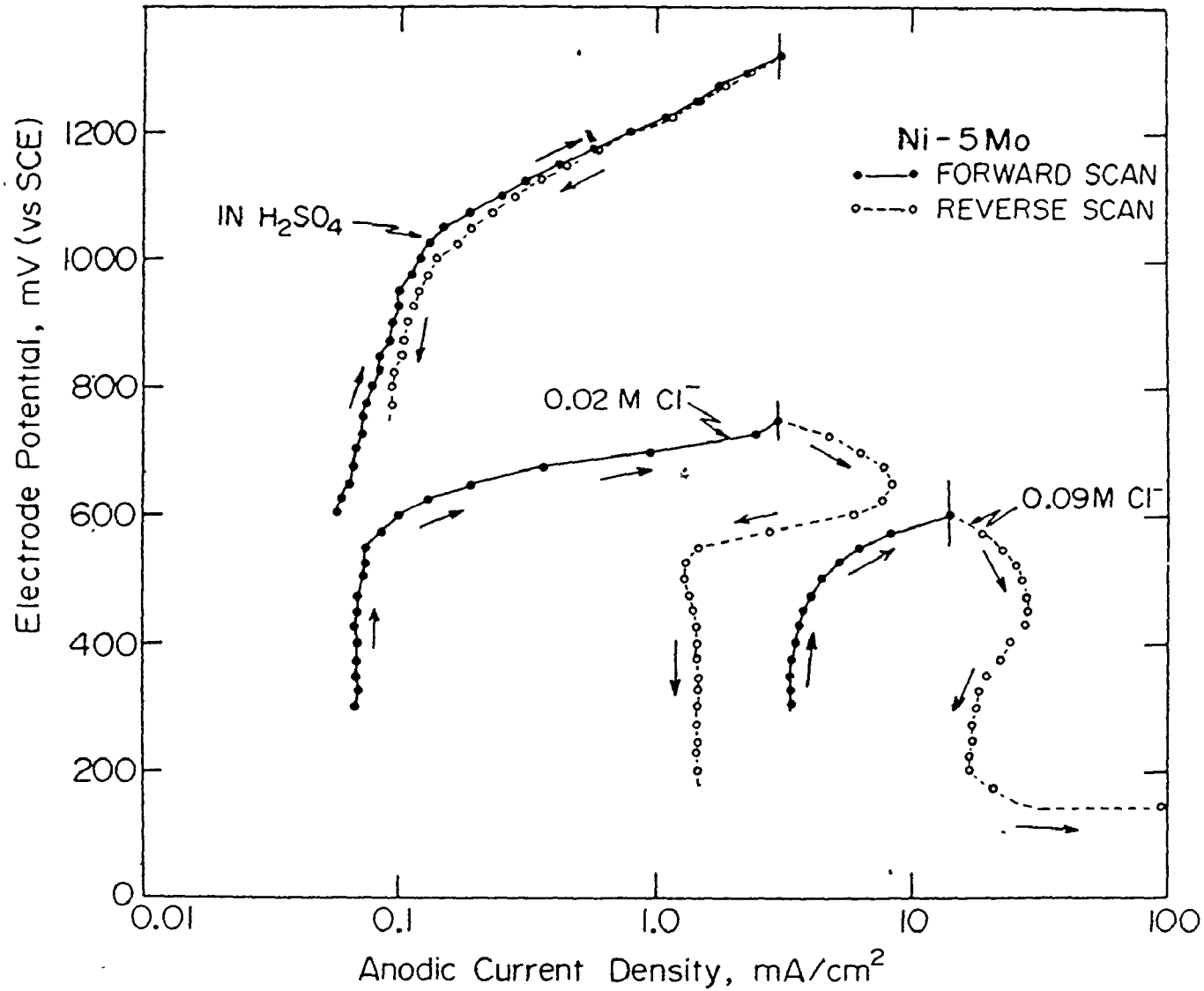

Figure 5-33. Effect of Cl^--ion concentration on the anodic current density during the potentiostatic forward and reverse scan for Ni-5Mo alloy.

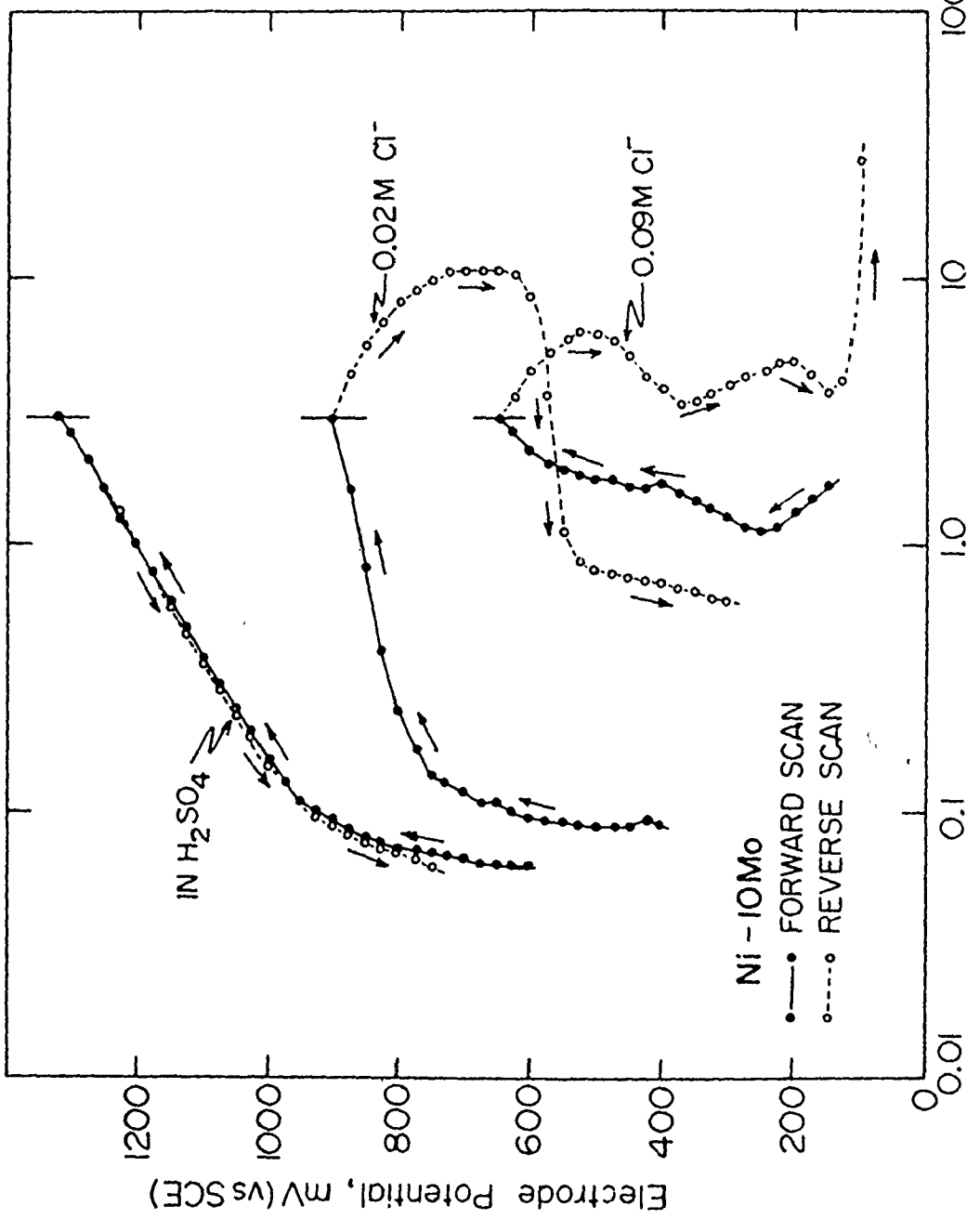

Figure 5-34. Effect of Cl^--ion concentration on the anodic current density during the potentiostatic forward and reverse scan for Ni-10Mo alloy.

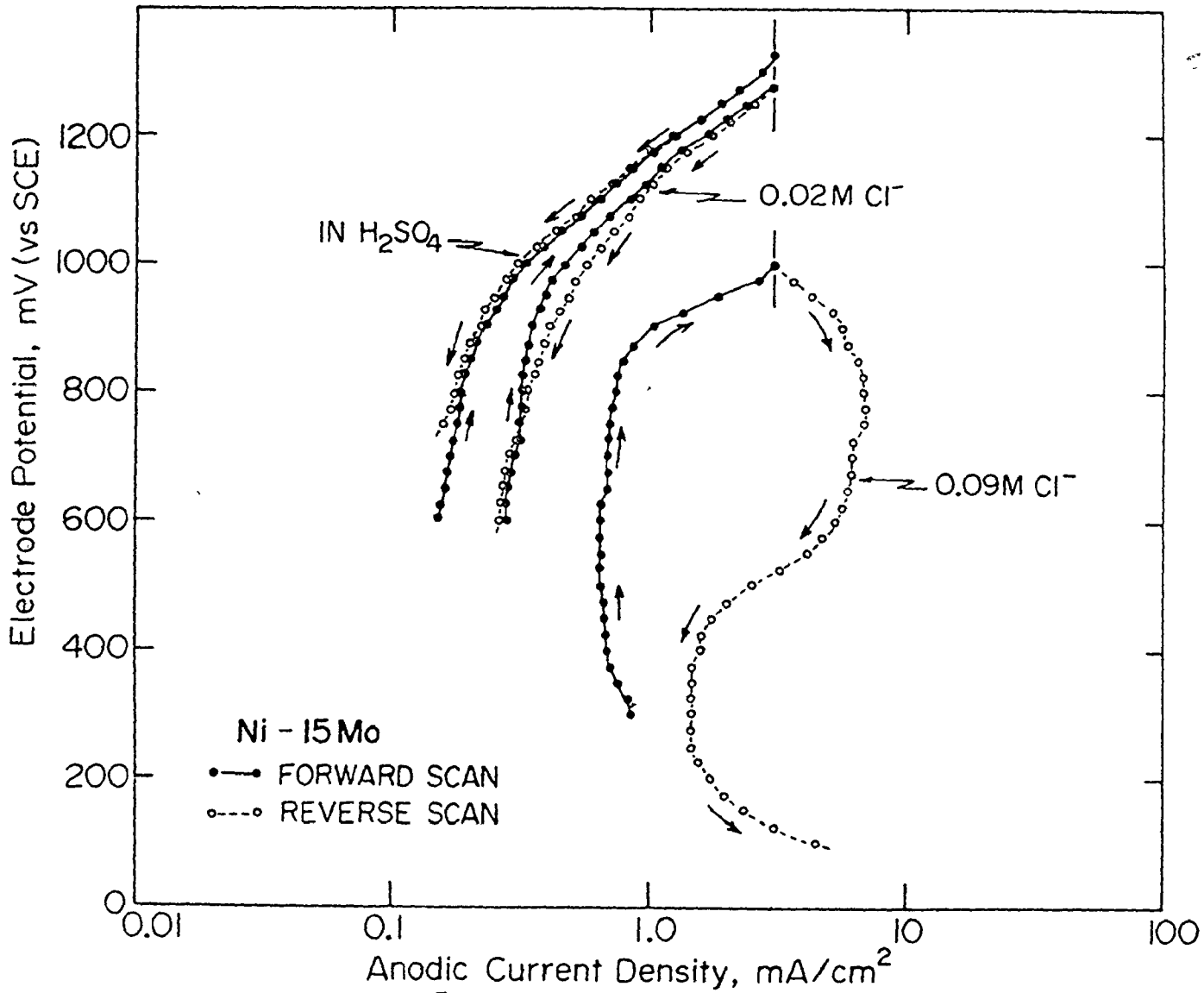

Figure 5-35. Effect of Cl^--ion concentration on the anodic current density during the potentiostatic forward and reverse scan for Ni-15Mo alloy.

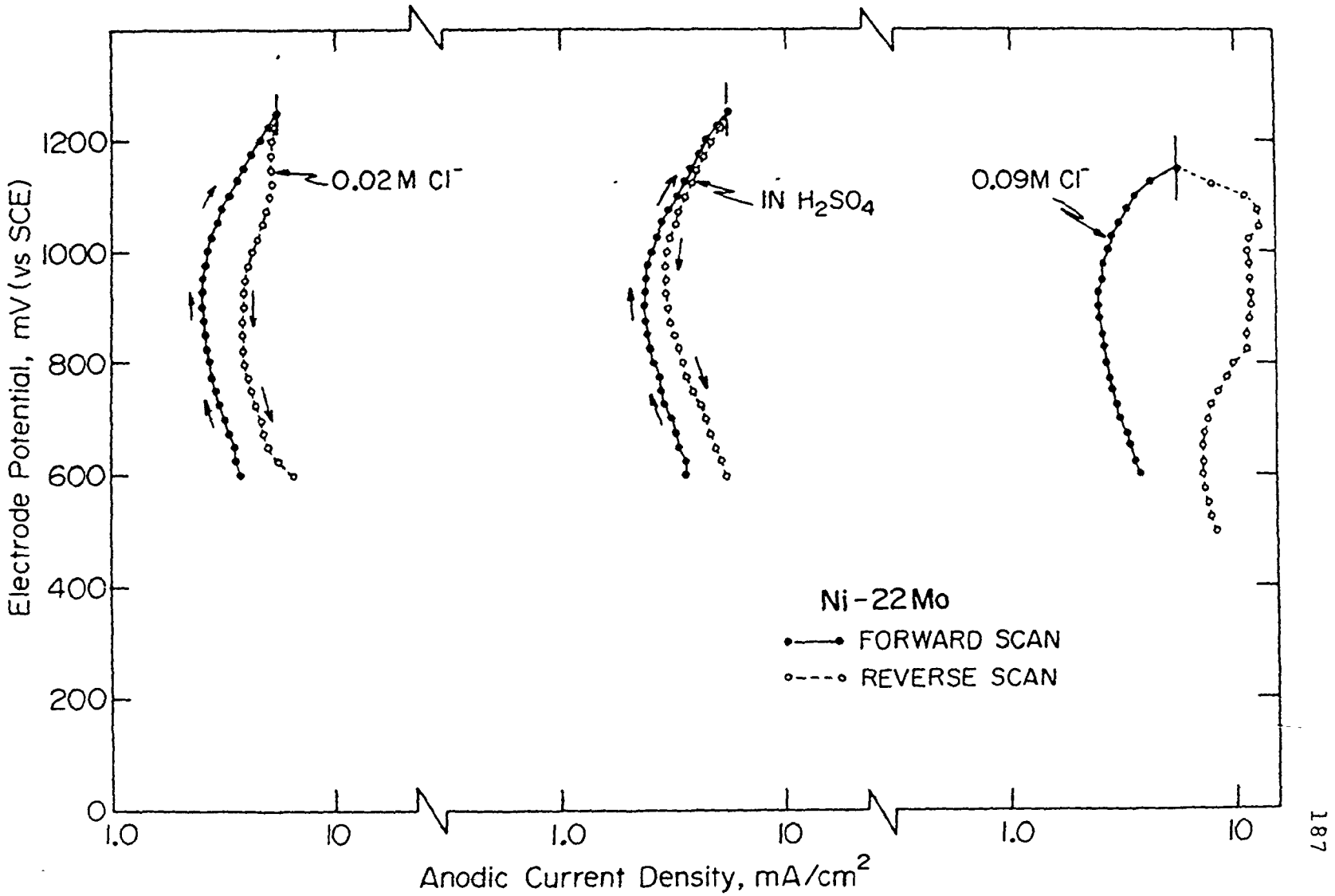

Figure 5-36. Effect of Cl^--ion concentration on the anodic current density during the potentiostatic forward and reverse scan for Ni-22Mo alloy.

is so high that the current density never returns to its earlier value. Nickel, Ni-15Mo and Ni-22Mo alloys perform remarkably well in 0.02 M Cl^- solution. Except for a slight hysteresis, the reverse curve lies very close to the forward scan curve.

When the Cl^--ion concentration was increased to 0.09 M, the passive current density for the Ni-5Mo alloy was found to be greater than 3.0 mA/cm^2 (current density chosen for reversal of potentiostatic scan) and hence a curve for comparison purposes could not be obtained. The curve shown in Figure 5-33 is merely to demonstrate the decreasing trend in the anodic current density. A hysteresis effect also exists for Ni-10Mo alloy (Figure 5-34). Although the current density values for this alloy in 0.09 M Cl^- are lower than those in 0.02 M Cl^-, it is to be remembered that the potential of scan reversal is also 250 mV less anodic. The Ni-15Mo and Ni-22Mo alloys show considerable hysteresis but at significantly lower potentials, the reverse scan curve lies very close to the forward one, especially for Ni-15Mo alloy where at +300 mV the current density during the forward scan is 0.85 mA/cm^2 and the reverse scan is 1.45 mA/cm^2 (Figure 5-35). It is emphasized that in every alloy and for all concentrations of Cl^--ions employed, there is a tendency for the decrease of the anodic current density, this tendency being the highest for the Ni-15Mo alloy. In direct contrast to this fact, the curve for nickel in 0.09 M Cl^- (Figure 5-32) shows no decrease of the anodic current density during the reverse scan. Instead, the current density increases

despite a step-wise decrease in potential.

In-situ microscopic observations were not performed during repassivation studies. Hence, the remarks on the morphological state of the surface pertain to their condition after removal of the specimen from the corrosion cell. The corrosion morphology of the materials was as follows.

1N H_2SO_4 - Nickel and Ni-15Mo alloy exhibited an etched surface with no localized corrosion at all. There was some intergranular attack in Ni-5Mo alloy and much less in Ni-10Mo alloy. The Ni-22Mo alloy showed extensive intergranular corrosion.

0.02 M Cl^- - Except for the Ni-15Mo alloy, all others showed localized attack. There was pitting at the grain boundaries of pure nickel, almost complete intergranular corrosion with attack in the grains for Ni-5Mo and Ni-10Mo alloys and continuous intergranular corrosion for the Ni-22Mo alloy, indistinguishable from that in 1N H_2SO_4.

0.09 M Cl^- - Nickel showed intense intergranular corrosion coupled with considerable corrosion of the grain interiors. The Ni-5Mo alloy presented an extremely corroded and dull surface where individual grains could not be distinguished. The Ni-10Mo alloy exhibited continuous intergranular attack with some corrosion in the grains. The Ni-15Mo alloy showed very little corrosion, but exhibited a few large pits. The extent of overall intergranular corrosion in Ni-22Mo alloy was unchanged from the previous two cases, although a few large pits were also formed.

A comparison of the electrochemical data with the corresponding corrosion morphology reveals that a hysteresis in the curve is always associated with corrosion, mostly localized, and that whenever the hysteresis is high the extent of corrosion is also extensive.

5.2.2.5 Weight Loss Measurements

Apart from cathodic protection, a material is rarely caused to corrode by impressed current or potential. In an attempt to correlate the free corroding situation with the electrochemical studies, weight loss of the specimens was determined using a conventional immersion test. These tests were conducted in a manner similar to those of Uhlig et al[33]. Hence, the reported corrosion rates are steady-state values determined from the slopes of the metal loss-time data. Although the initial corrosion rate, in general, was higher, the steady state set in about 3 days, after which the rate did not change.

The results of this study are presented in Figure 5-37. The beneficial effect of molybdenum on decreasing the corrosion rate of nickel is evident. Microscopic examinations conformed to visual observations of the specimens where only the nickel and Ni-5Mo alloy appeared attacked. The attack on nickel was mostly general although some randomly distributed pits were formed. The Ni-5Mo alloy showed intergranular corrosion, though not very intense. The other alloys were unchanged and no particular attack pattern could be observed.

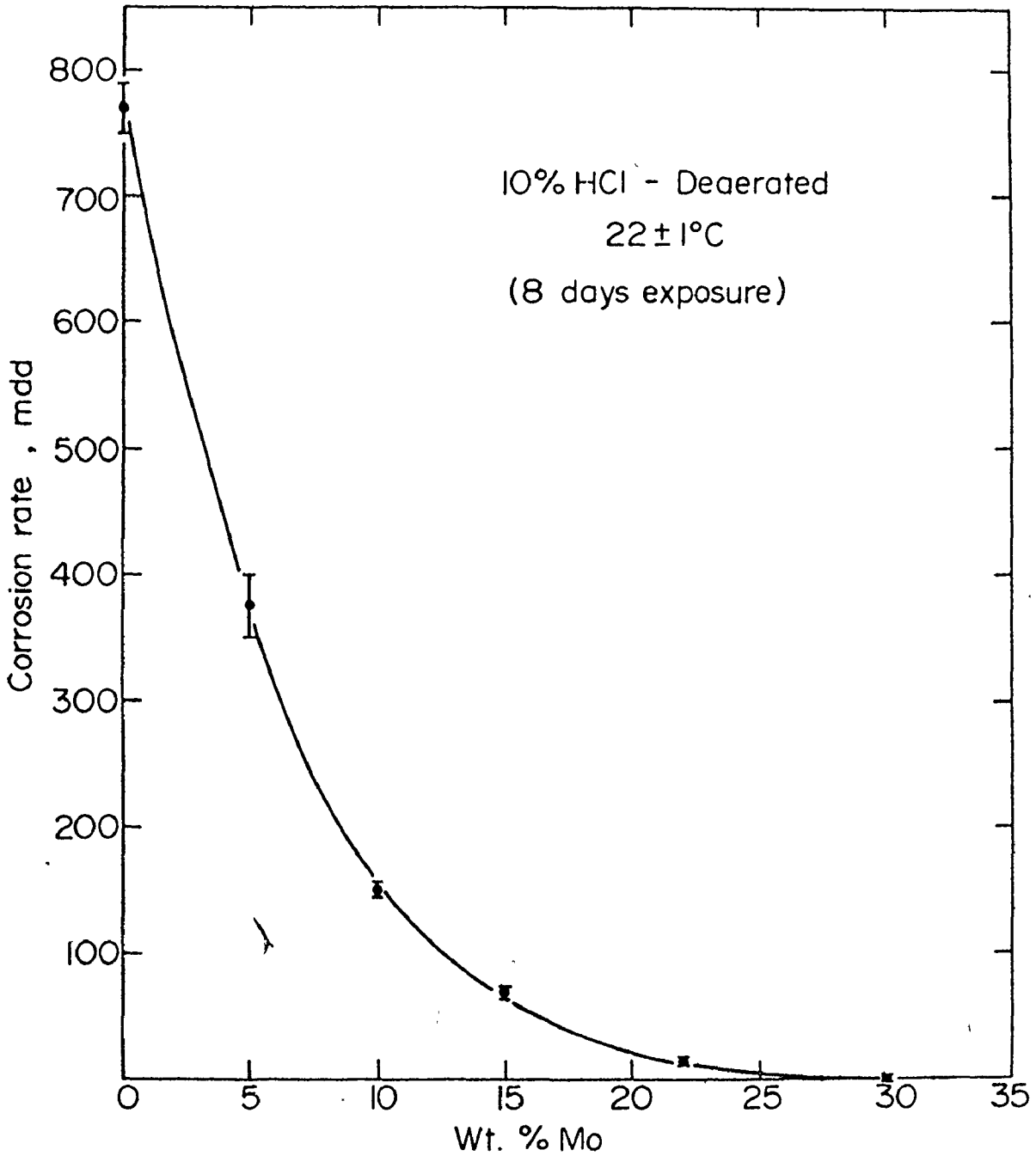

Figure 5-37. Weight loss of Ni and Ni-Mo alloys as a function of molybdenum content in 10% HCl (8 day exposure).

5.2.2.6 Effect of Metallurgical Structure

The Ni-30Mo alloy was tested in three metallurgical conditions - a supersaturated α with β and γ precipitated at the grain boundary (designated as Ni-30Mo-1 alloy), a three phase structure where β and γ were present at the α grain boundaries (designated as Ni-30Mo-2 alloy) and a structure consisting mostly of β and γ with some retained α (designated as Ni-30Mo-3 alloy). Three types of tests were performed on the alloys. They were potentiostatically polarized in 1N H_2SO_4 and three solutions containing 0.02 M, 0.09 M and 0.20 M Cl^--ions respectively; potentiostatically activated in 0.02 M Cl^--containing solution and their weight loss determined in 10% HCl solution.

The Ni-30Mo alloys did not passivate in any of the environments used for the other alloys. The polarization curves in the various solutions are shown in Figure 5-38. Although the experimental points for the three conditions of heat treatment fall within a narrow band, it can be seen that at high potentials (> 100 mV), the corrosion rate follows the order

$$\text{Ni-30Mo-1} < \text{Ni-30Mo-2} < \text{Ni-30Mo-3}$$

for all solutions. In-situ microscopic observation failed to provide any information on the corrosion morphology due to an almost sudden surface darkening at current densities of about 25 mA/cm^2. However, it did reveal the presence of a bluish-black film, similar to the one noted for Ni-5Mo and Ni-10Mo alloys in 0.33 M and 0.50 M Cl^--containing solutions. The tendency for the formation of this film was lowest for Ni-30Mo-1

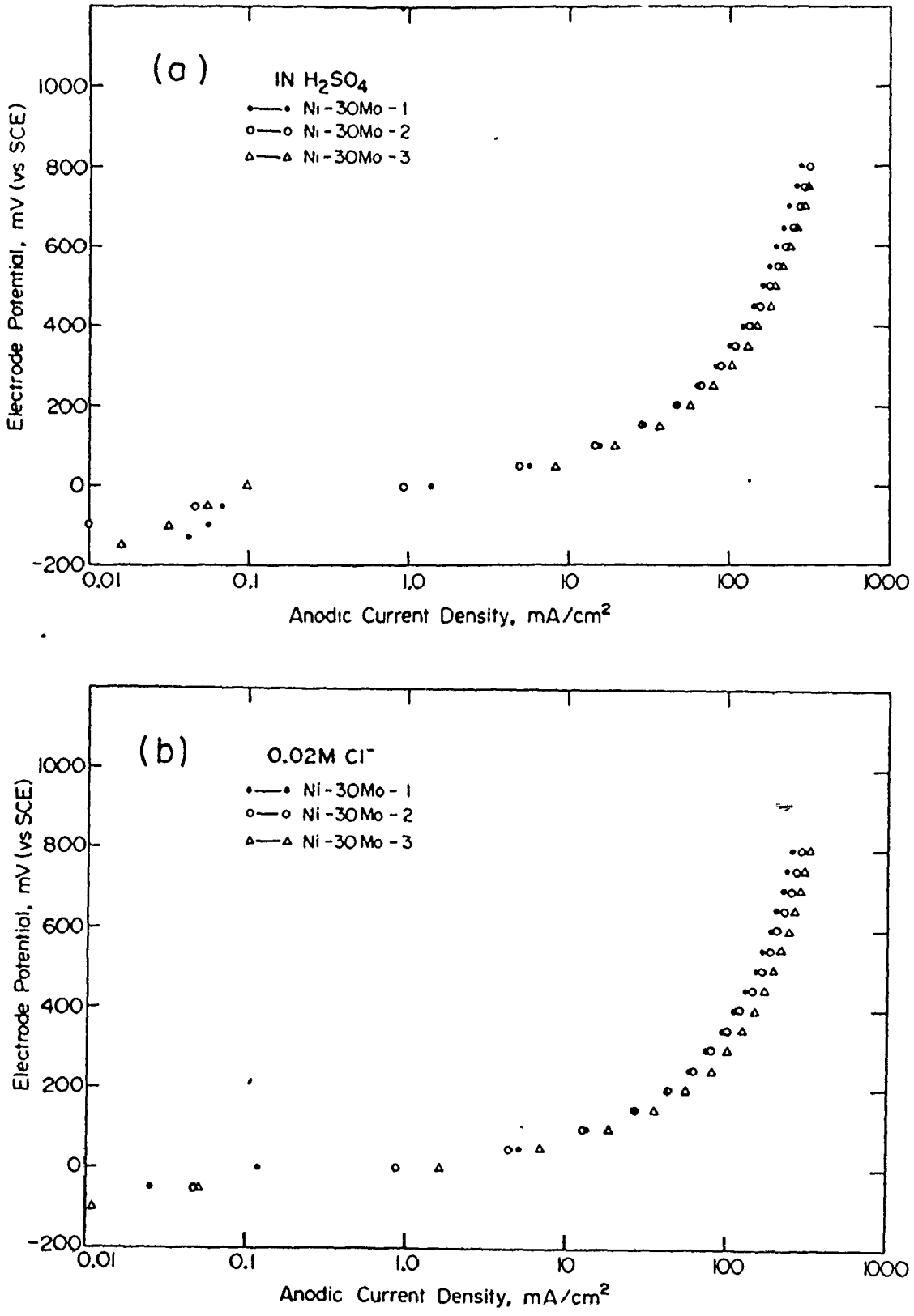

Figure 5-38. Anodic polarization curves for Ni-30Mo alloys in various heat treated conditions and Cl^--ion concentrations
(a) 1N H_2SO_4 (b) 0.02 M Cl^-

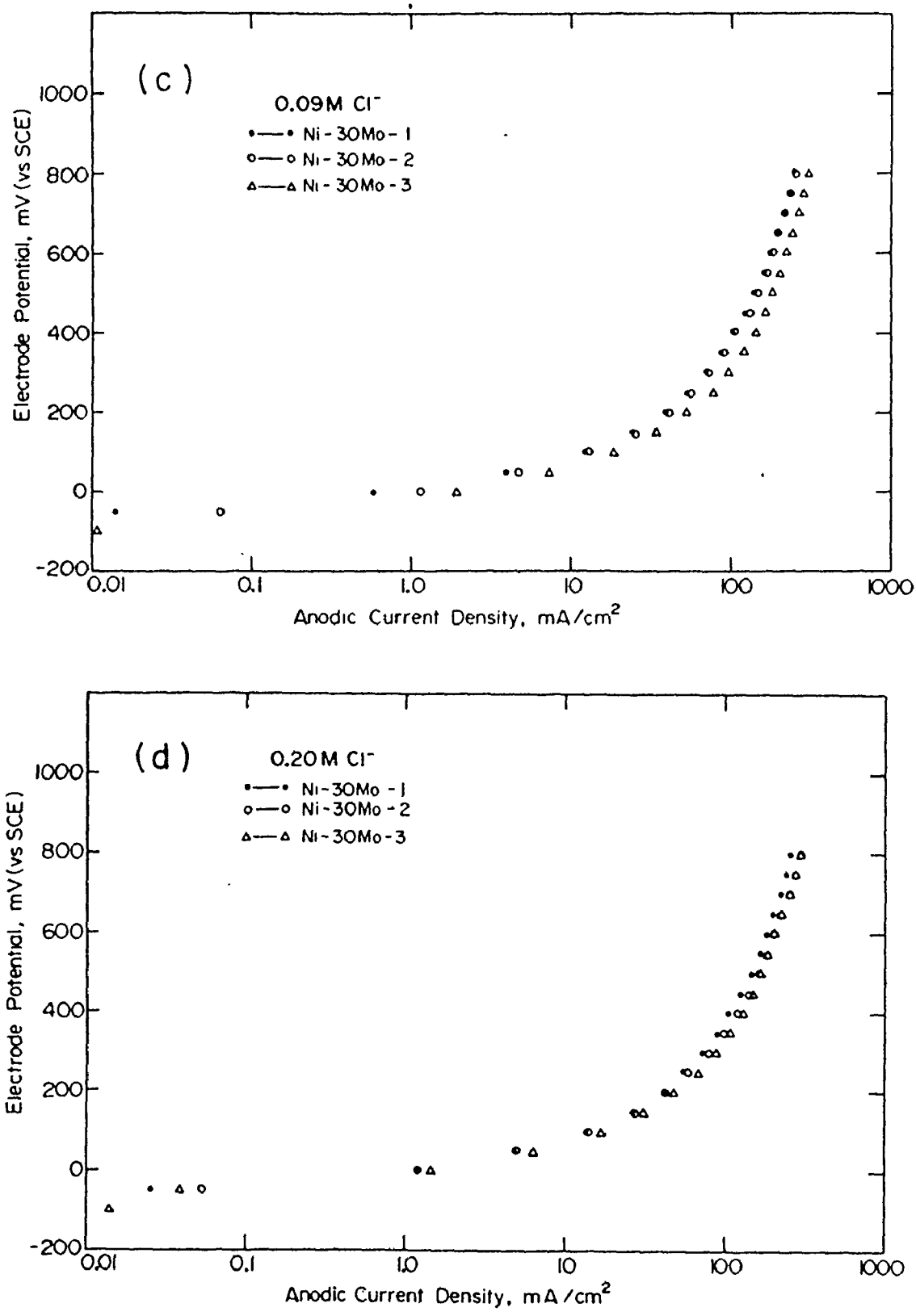

Figure 5-38. Anodic polarization curves for Ni-30Mo alloys in various heat treated conditions and Cl^--ion concentrations
(c) 0.09 M Cl^- (d) 0.20 M Cl^-.

alloy and highest for Ni-30Mo-3 alloy. It also increased with Cl^--ion concentration. Specifically, no film was observed on the Ni-30Mo-1 alloy in 1N H_2SO_4 and 0.02 M Cl^- solutions; even in 0.20 M Cl^- solution, the film was very patchy and discontinuous. In all cases there was strong hydrogen evolution at the cathode. Microscopic observations performed on specimens after the polarization and removal of the black film by scrubbing with acetone revealed general attack in all cases, except for the Ni-30Mo-2 alloy where intergranular corrosion was very distinct, particularly in 0.09 M Cl^- solution.

When the Ni-30Mo alloy was subjected to a potential of +400 mV in 1N H_2SO_4, the current density stabilized within 5 mins at a value which varied from 110 to 140 mA/cm^2 depending upon the heat treatment (being lowest for the Ni-30Mo-1 alloy and highest for the Ni-30Mo-3 alloy). The addition of Cl^--ions after 30 mins resulted in an immediate drop in the current density and a dark film was seen forming on the specimen surface. The current density continued to decrease with time while the film became more continuous and thick. Results of this experiment for 0.02 M Cl^--ion concentration are shown in Figure 5-39. It can be seen that the trend for corrosion is reversed at longer times, the Ni-30Mo-3 alloy dissolving at the lowest rate. A black film was present on the surface of this alloy in 1N H_2SO_4 even before the addition of Cl^--ion In the case of the other alloys (Ni-30Mo-1 and Ni-30Mo-2) little

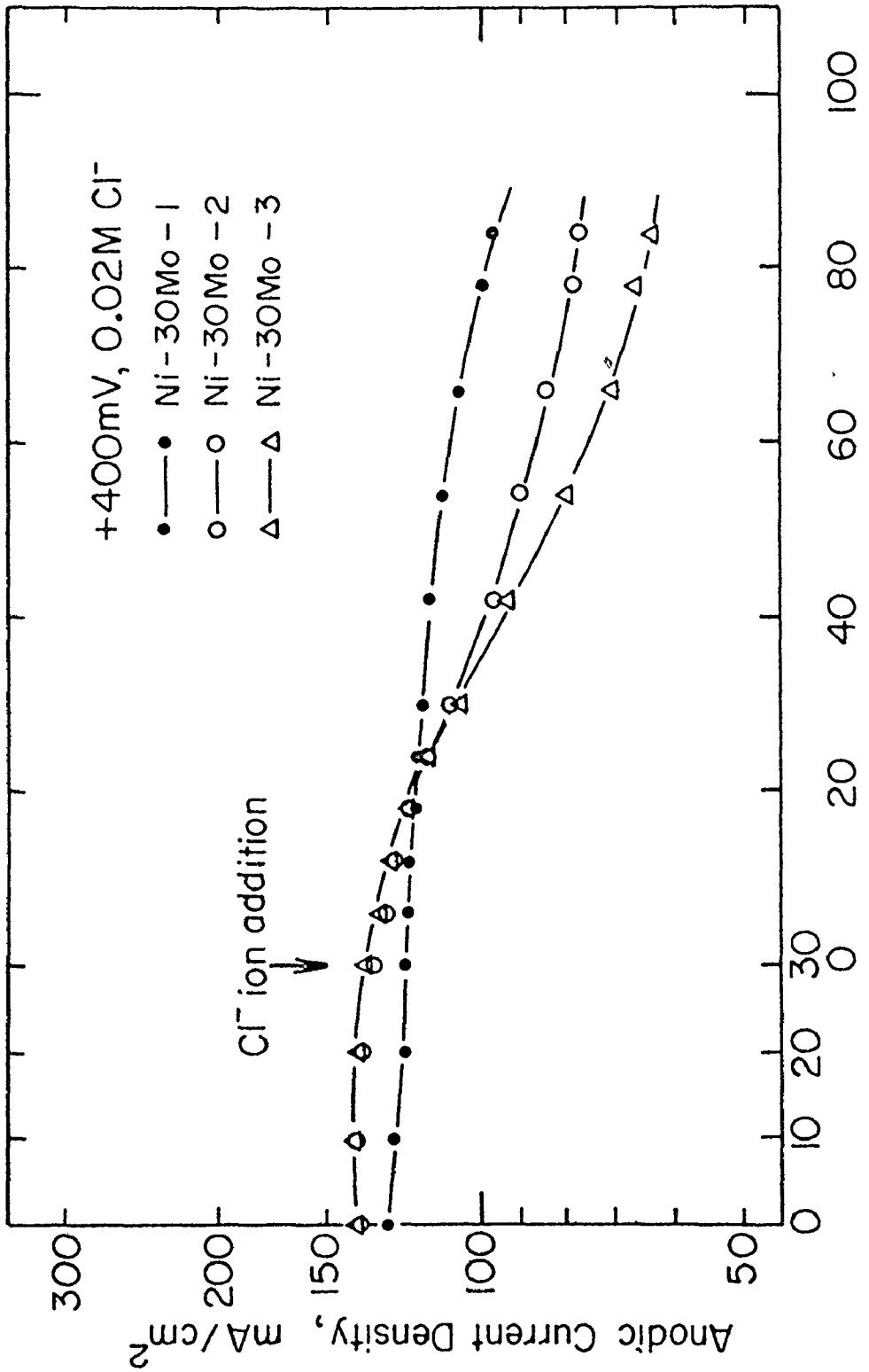

Figure 5-39. Variation of the anodic current density as a function of time for Ni-30Mo alloys in the three conditions of heat treatment in 0.02 M Cl^- solution (pH = 0.4).

or no film was observed optically on the specimen surfaces after 30 mins at +400 mV in 1N H_2SO_4 and the addition of Cl^--ions produced a film which grew with time. It is emphasized that the formation of a black film which inhibits corrosion seems to be linked with the presence of Cl^- ions.

The results of weight loss measurements in 10% HCl solution and the final corrosion morphology are given below.

Alloy	Corrosion Rate mdd	Corrosion Morphology
Ni-30Mo-1	1.8 ± 1.8	No visible corrosion
Ni-30Mo-2	251 ± 56	Intergranular corrosion
Ni-30Mo-3	754 ± 55	Etched surface, general corrosion

5.2.2.7 The Polarization Characteristics of Molybdenum

The polarization was performed in solutions with Cl^--ion concentrations ranging from 0 to 0.5 M. The results are shown in Figure 5-40. It is seen that there is no tendency for passivation in any solution and the dissolution rate is high. Although the various plotted points fall within a narrow band, it is interesting to note that the anodic current density at any potential decreases as the Cl^--ion concentration increases. A black film was formed on the surface of every specimen. In solutions with low Cl^--ion concentrations, pieces of this film tended to flake off and collect below the specimen in un-stirred solutions. However, as the Cl^--ion concentration increased, this flaking tendency decreased and in 0.50 M Cl^-

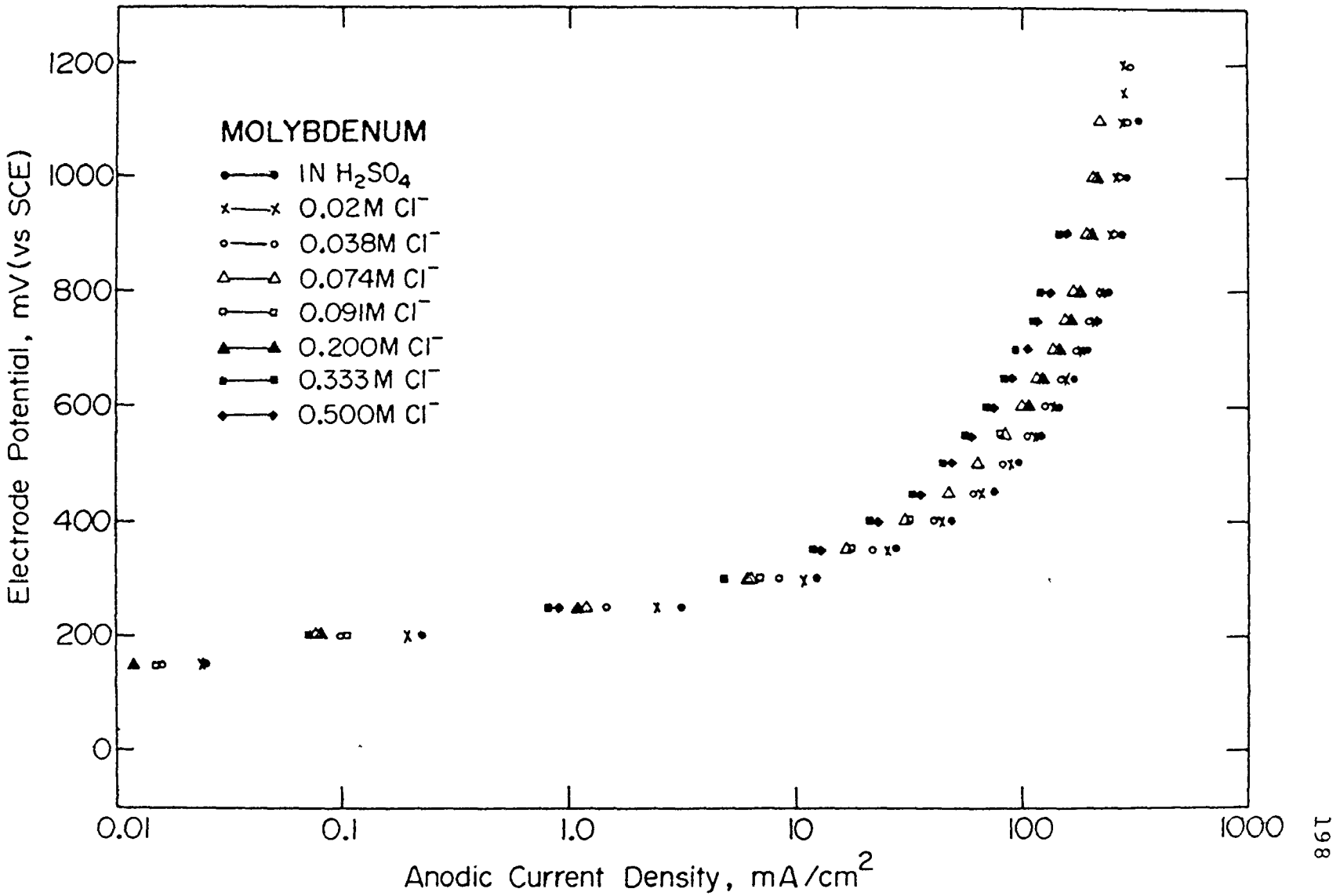

Figure 5-40. Anodic polarization curves for Mo in various solutions.

solution, the film was very adherent to the specimen surface and dissolution was low (as evidenced by visual observations of specimen thinning). Evidently the addition of Cl^--ions has a beneficial effect on the corrosion rate of molybdenum. The corrosion potentials were positive in all the solutions ranging between +42 mV in 1N H_2SO_4 to +22 mV in 0.50 M Cl^- solution. The weight loss of molybdenum in 10% HCl was found to be 9.9±3.5 mdd.

5.2.2.8 Polarization Behaviour in Synthetic Sea Water

One of the most important environments to which an alloy is subjected is sea water. In an attempt to study the performance of the Ni-Mo alloys in sea water and to correlate the electrochemical polarization behaviour in sea water to that in Cl^--containing environments all materials were anodically polarized in synthetic sea water.

The synethetic sea water was not deaerated and all alloys up to 22% Mo were electropolished prior to polarization while the Ni-30Mo alloys were tested after mechanical polishing up to 1 μm diamond. Specimens were potentiostatically polarized from -300 mV. The results obtained are shown in Figure 5-41. Except nickel, which showed an anodic maximum at -50 mV with a current density of 1.28 mA/cm^2, none of the alloys exhibited any drop in the anodic current density. The curves for Ni-30Mo-1 alloy, Ni-22Mo alloy and molybdenum are especially interesting. The Ni-30Mo-1 alloy holds very well at lower potential range

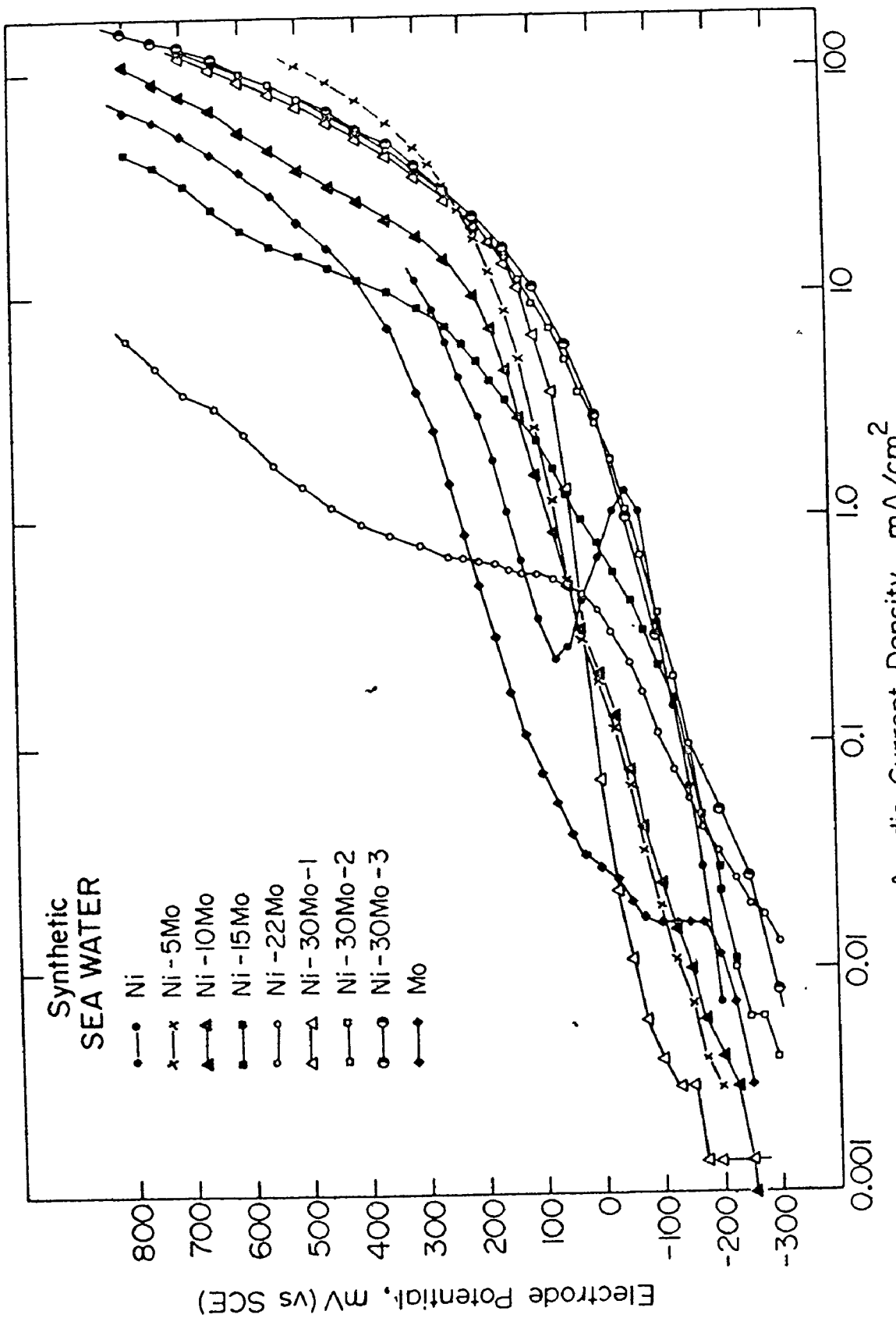

Figure 5-41. Anodic polarization curves for Ni, Mo and Ni-Mo alloys in synthetic sea water.

(-300 mV to -50 mV). Molybdenum is also particularly effective in resisting corrosion in the same potential range in that a polarization of 125 mV (from -175 mV to -50 mV) results in an extremely small change in current density (increasing from 0.016 mA/cm^2 to 0.020 mA/cm^2). The polarization curve for Ni-22Mo alloy is the best from a corrosion viewpoint where an order of magnitude increase in the current density (from about 0.1 mA/cm^2 to 1.0 mA/cm^2) occur over a potential range of about 500 mV (from -100 mV to +400 mV).

The resultant corrosion attack was interesting and completely non-related to the electrochemical behaviour. The nickel electrode was etched showing the grain structure with no observable corrosion. The Ni-5Mo alloy showed corrosion and a black film at the edges as did the Ni-10Mo alloy which also exhibited a few large pits. The surface of Ni-15Mo alloy was shiny and completely un-attacked. The Ni-22Mo alloy was also un-attacked although its surface exhibited a yellowish color. The Ni-30Mo-1 alloy showed a dark surface with a thin discontinuous black film. The Ni-30Mo-2 and Ni-30Mo-3 alloys exhibited a thick black film which covered the entire specimen surface. The molybdenum electrode had a dark surface although no real corrosion could be observed.

In correlating the electrochemical polarization behaviour with the resultant corrosion morphology, it is apparent a relative rating of the alloys is neither fair nor possible. It is nevertheless pointed out that Ni-15Mo and Ni-22Mo alloys are materials quite suitable for sea water applications.

5.2.2.9 Immersion Test

Having performed so many different electrochemical tests on the alloys in various environments, it was felt that a knowledge of their corrosion behaviour in an actual corroding situation would be useful. Hence, all specimens were subjected to a 30-day immersion test in two solutions - synthetic sea water and a 0.50 M Cl^--containing solution of pH = 0.4. Specimens were mounted in bakelite mechanically polished up to 1 μm diamond, introduced in 1000 ml of the test solution in a conical flask and then sealed. The corrosion morphology after 30 days of immersion in 0.50 M Cl^- with no stirring is shown in Figure 5-42 for all materials. Visually all the alloys exhibited dark corroded surfaces and the optical micrographs of Figure 5-42 confirmed it. Nickel, Ni-5Mo, Ni-10Mo and Ni-15Mo alloys showed extensive corrosion, particularly deep intergranular attack. The Ni-22Mo alloy exhibited deep intergrandular corrosion although attack within the grains was rather low. The Ni-30Mo alloys offered an interesting study of solid solution effects on corrosion. The Ni-30Mo-1 alloy showed some arbitrarily distributed pits and little intergranular attack. As has already been pointed out, this alloy is a supersaturated α with some precipitation of β and γ along the grain boundaries. That the β and γ are more susceptible to attack than the α is evident by comparing figures 5-42(g) and 5-42(h). Whereas in Figure 5.42(g) the β and γ are attacked and the α is not, in Figure 5-42(h) the surface appears generally corroded.

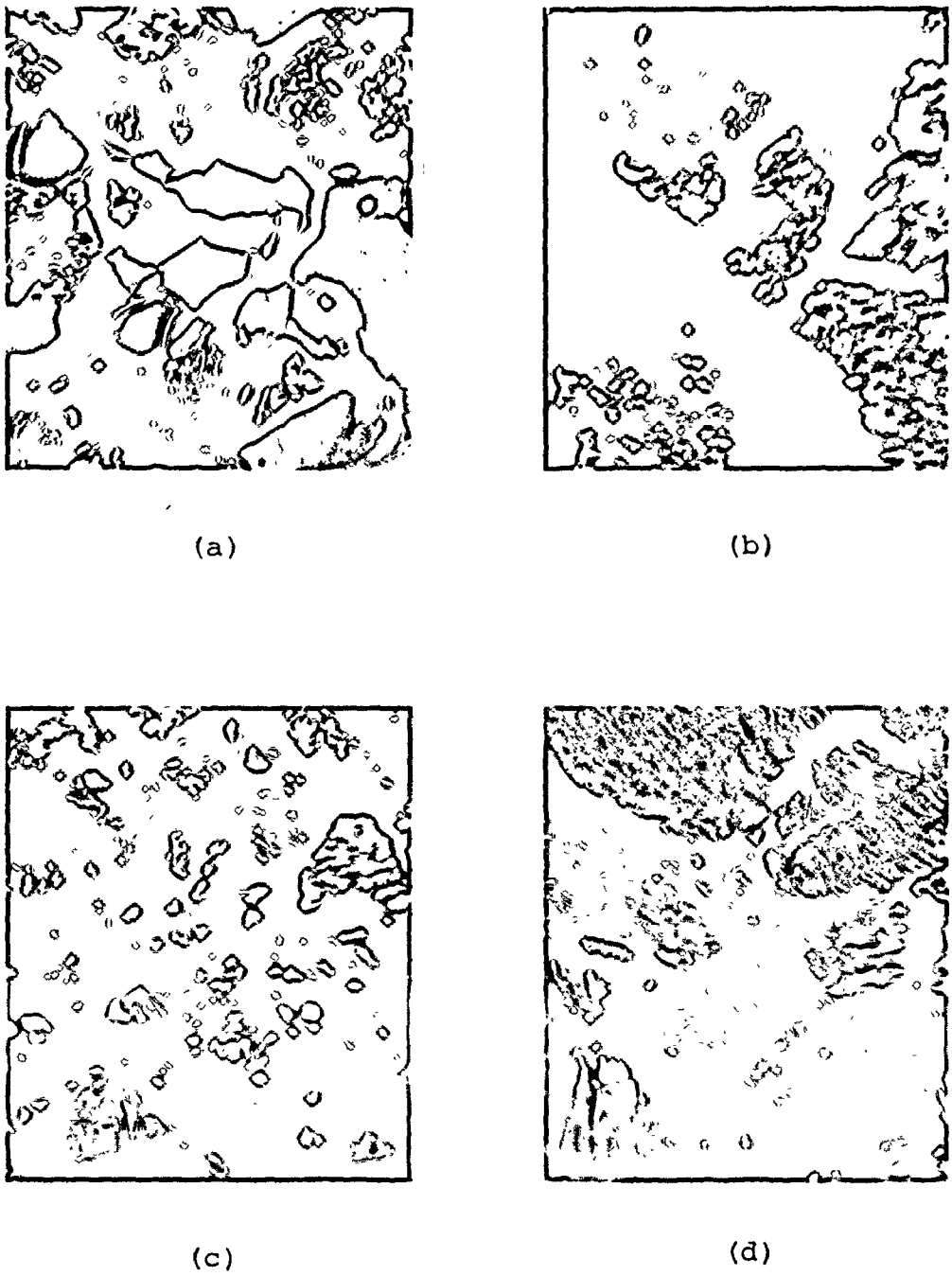

Figure 5-42. Corrosion morphology after 30 day immersion in 0.05 M Cl^- solution (pH=0.4). (a) Ni, 300× (b) Ni-5Mo alloy, 600× (c) Ni-10Mo alloy, 600× (d) Ni-15Mo alloy 600×. Specimens were polished up to 1 μm diamond prior to immersion.

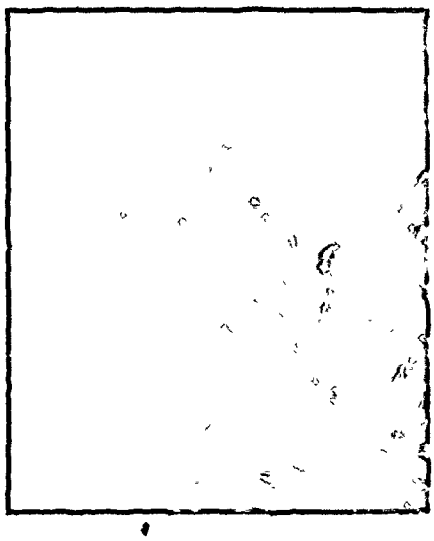

(e)

(f)

(g)

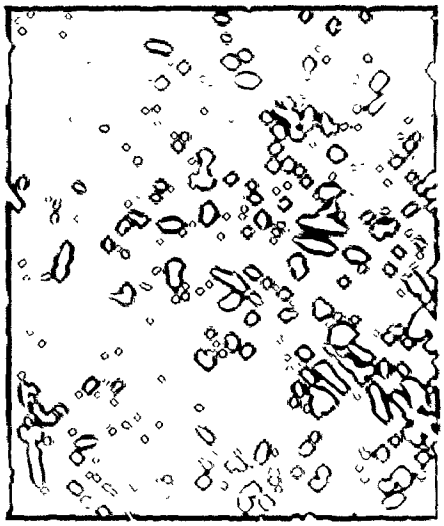

(h)

Figure 5-42 (cont'd) Corrosion morphology after 30 day immersion in 0.50 M Cl^- solution (pH=0.4) (e) Ni-22Mo alloy,600× (f) Ni-30Mo-1 alloy, 300× (g) Ni-30Mo-2 alloy, 300× (h) Ni-30Mo-3 alloy, 300×. Specimens were polished up to 1 μm diamond prior to immersion.

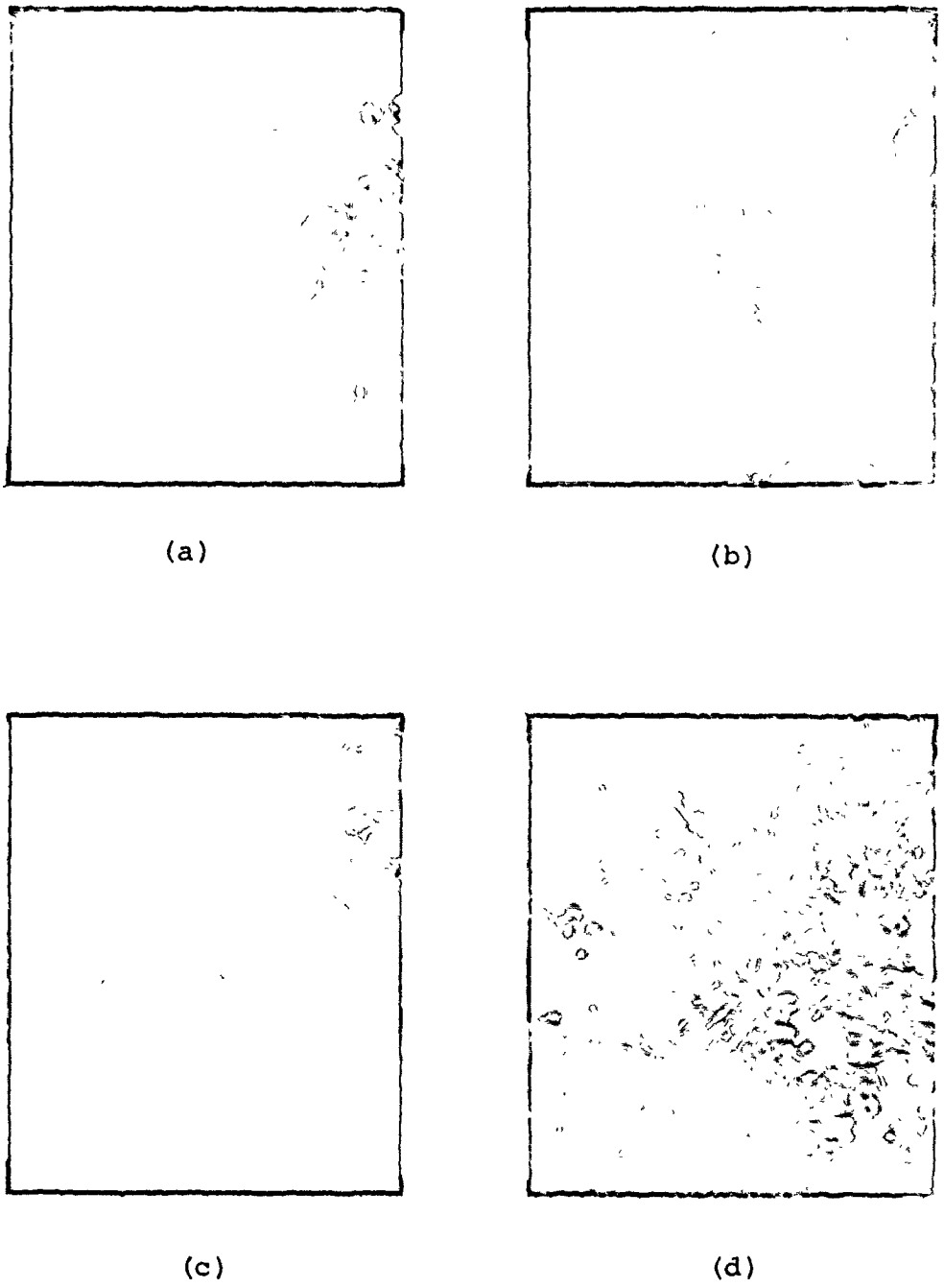

Figure 5-43. Corrosion morphology after 30 day immersion in synthetic sea water (a) Ni-5Mo alloy, 150× (b) Ni-30Mo-1 alloy, 300× (c) Ni-30Mo-2 alloy, 300× (d) Ni-30Mo-3 alloy, 300× . Specimens were polished up to 1 μm diamond prior to immersion.

The corrosion morphology in synthetic sea water was completely different from that in 0.50 M Cl^- solution. Nickel and all alloys up to 22% Mo did not exhibit any attack. The original surface remained shiny and unchanged. There was extensive corrosion around a crack in the Ni-15Mo alloy (Figure 5-43(a)). Although the crack was not intentionally introduced and its presence was a mere chance, it demonstrated the extreme importance of avoiding crevices in engineering structures involving sea water applications. The corrosion attack for the Ni-30Mo alloys is shown in Figure 5-43(b)-(d). It is very different to the attack which was observed in any solution tested so far. The attack is localized and may be imagined as large pits. A comparison of the three figures indicates that there is no correlation between the origin of the pits and the metallurgical structure. Although the corrosion morphology in 0.50 M Cl^- solution and synthetic sea water do not show any similarities, this study along with the previous one demonstrates a very important point - nickel alloys containing 15% and 22% Mo are materials very suitable for sea water applications.

5.3 Summary

Alloys containing up to 15% Mo are single phase structures of the α-solid solution while the Ni-22Mo alloy exhibits a two-phase structure containing β(Ni_4Mo) coherently precipitated in the α-matrix. The Ni-30Mo alloy can be heat treated to obtain different metallurgical structures. The addition of

molybdenum to nickel has a beneficial effect on the mechanical properties of the alloys.

The charge required to reduce the film on the alloys decreases with increasing molybdenum content and, in general, decreases even further when films are grown in the presence of chloride ions.

Alloys containing up to 15% Mo show a typical active-passive transition. The addition of molybdenum increases the corrosion rate in the passive region in 1N H_2SO_4. However, increasing molybdenum content has a beneficial effect on the corrosion rate of the alloys in chloride containing environments. This is borne out by potentiostatic polarization measurements, potentiostatic activation studies and weight loss determinations.

A black film forms on the surface of the alloys in chloride containing environments. This film was found to contain nickel, molybdenum and sulfate ions and was indexed as MoO_3 by the aid of electron diffraction. Analysis of solutions after potentiostatic polarization in chloride containing environments reveals that the proportion of molybdenum present in solution is lower than that present in the alloy, further supporting the molybdenum enrichment of the film.

All alloys up to 22% Mo exhibit a decrease in the anodic current density when the potential sweep is reversed from the transpassive region in chloride containing environments. This, however, is not true for pure nickel.

A Ni-30Mo alloy exhibits the lowest corrosion rate in

a supersaturated single phase condition. The equilibrium structure has a corrosion rate almost equal to that of pure nickel. The electrochemical behaviour of Ni-30Mo alloys is similar to that of pure molybdenum in that they do not exhibit an active-passive transition shown by the single phase α alloys. The corrosion rate of pure molybdenum decreases with increasing chloride concentration.

CHAPTER VI

DISCUSSION

6.1 Introduction

The bulk alloy compositions studied have shown that a dramatic decrease in the corrosion rate of nickel occurs upon the addition of molybdenum. Also, the single phase supersaturated alloy has a much lower corrosion rate than the equilibrium duplex structure alloy. The Ni-Mo alloys (at least those existing as the single phase α solid solution) are also capable of passivation. However, in nickel and also the alloys, dissolution is a major part of the passivation process since only a fraction of the total anodic charge is involved in film growth. In the sections to follow the kinetics of the passivation process of nickel in 1N H_2SO_4 along with the significance of the Flade potential (E_F) will be considered, the concept of the critical potential (E_c) for characterization of metals and alloys and its validity for nickel and Ni-Mo alloys will be dealt with, the validity of film thickness measurements from a solid-state physics view point will be presented and the effect of molybdenum on the corrosion properties of nickel will be discussed.

6.2 Kinetics and Mechanism of the Passive Film Formation on Nickel

The results for the galvanostatic oxidation of nickel in 1N H_2SO_4 yielded a straight line when the potential (E) was plotted against the charge stored in the film (Q_f) (Figure 4-3). As has been pointed out earlier (and more clearly in Appendix B), this implies that the electric field is constant during film growth. The equation for the growth of the film under galvanostatic conditions may be written as

$$E = E_1 + KQ_f \qquad (6\text{-}1)$$

where Q_f = charge stored in the film and is given by Eqn. (4-8)

E_1 = constant whose implications are discussed in Appendix B.

$K = \frac{\partial E}{\partial Q_f}$ and is the slope of the $E\text{-}Q_f$ curve.

Assuming that the growth of the film obeys Ohm's law, then,

$$E = i_g R = i_g \rho x \qquad (6\text{-}2)$$

where R = resistance of the film

ρ = resistivity of the film

i_g = growth current density

x = film thickness.

But,

$$x = \frac{M \cdot Q_f}{nFDr} = \lambda Q_f \qquad (6\text{-}3)$$

where, M = molecular weight of the film

D = density of the film

F = Faraday constant

n = oxidation number

r = surface roughness factor.

$$\therefore E = i_g \rho \omega Q_f \qquad (6\text{-}4)$$

and from Eqn. (6-4)

$$K = \frac{\partial E}{\partial Q_f} = i_g \rho \omega \qquad (6\text{-}5)$$

which implies that $K \propto i_g$. However, this is not experimentally true since K vs i_g does not yield a straight line. Thus, the growth of the passive film does not follow a simple ohmic behaviour.

Conway[111] has pointed out that the current-potential (i-E) relation is usually not of the simple form $\frac{\partial E}{\partial i}$ = constant indicating an ohmic behaviour, but is generally of the form $\frac{\partial E}{\partial \ln i}$ = constant, implying a non-ohmic Tafel behaviour.

If the results of the galvanostatic oxidation are plotted as E vs $\log i_g$, at constant Q_f, straight line plots are indeed obtained (Figure 6-1). In its simplest form the equation to the line may be taken as

$$\log i_g = \log\alpha + \frac{1}{\beta} E \qquad (6\text{-}6)$$

where α = constant

$\beta = \frac{\partial E}{\partial \log i_g}$ = Tafel slope.

Let $\frac{1}{\beta} \propto \frac{1}{R}$

$$\therefore \frac{1}{\beta} = \frac{k}{R}$$

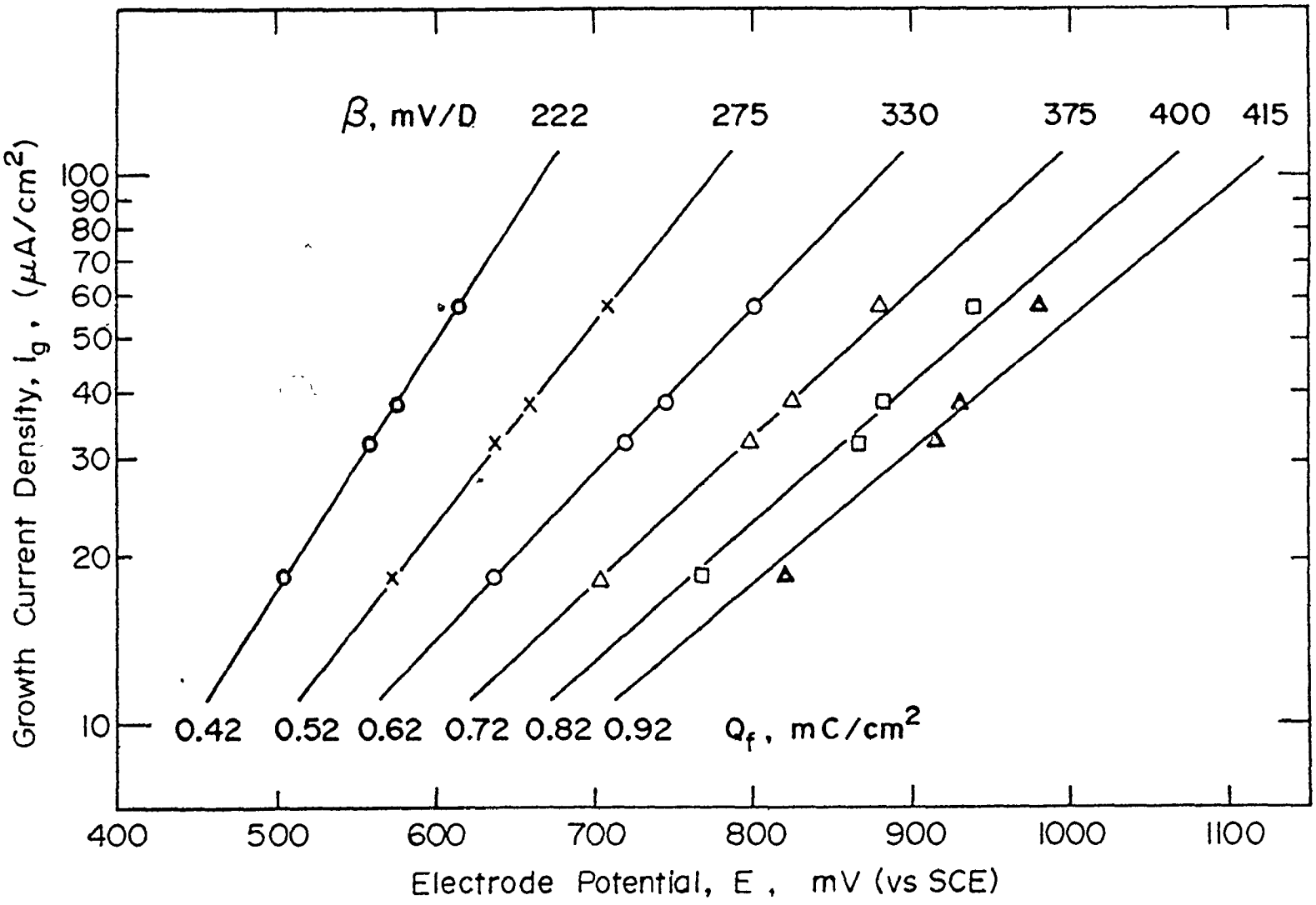

Figure 6-1. Tafel plots (E-logi) for the galvanostatic oxidation of nickel in 1N H_2SO_4 at various film thicknesses.

where, R = resistance of the film

k = proportionality constant.

From Eqns. (6-2) and (6-3), $R = \omega Q_f$

$$\therefore \frac{1}{\beta} = \frac{k}{\rho\omega Q_f} \qquad (6\text{-}7)$$

and, $$\log i_g = \log\alpha + \frac{k}{\rho\omega Q_f} E, \text{ or}$$

$$E = \frac{\rho\omega}{k} (\log i_g - \log\alpha) Q_f$$

and, as before,

$$K = \frac{\partial E}{\partial Q_f} = \frac{\rho\omega}{k} (\log i_g - \log\alpha) \qquad (6\text{-}9)$$

and this implies that $K \propto \log i_g$, which is experimentally found to be true (Figure 6-2).

Again, from Eqn. (6-7)

$$\frac{\rho\omega}{k} = \frac{\beta}{Q_f}$$

and,

$$K = \frac{\beta}{Q_f} (\log i_g - \log\alpha)$$

$$\therefore \frac{\partial K}{\partial \log i_g} = \frac{\beta}{Q_f} . \qquad (6\text{-}10)$$

The values of β can be known from Figure 6-1 at different values of Q_f. Hence, $\frac{\partial K}{\partial \log i_g}$ can be calculated from Eqn. (6-10). These values are tabulated below.

Q_f mC/cm^2	β mV/decade	$\frac{\beta}{Q_f}$ mV/decade/mC/cm^2
0.42	222	527
0.52	275	528
0.62	330	531
0.72	375	520

Average, $\frac{\partial K}{\partial \log i_g} = 527$, mV/decade/mC/cm^2

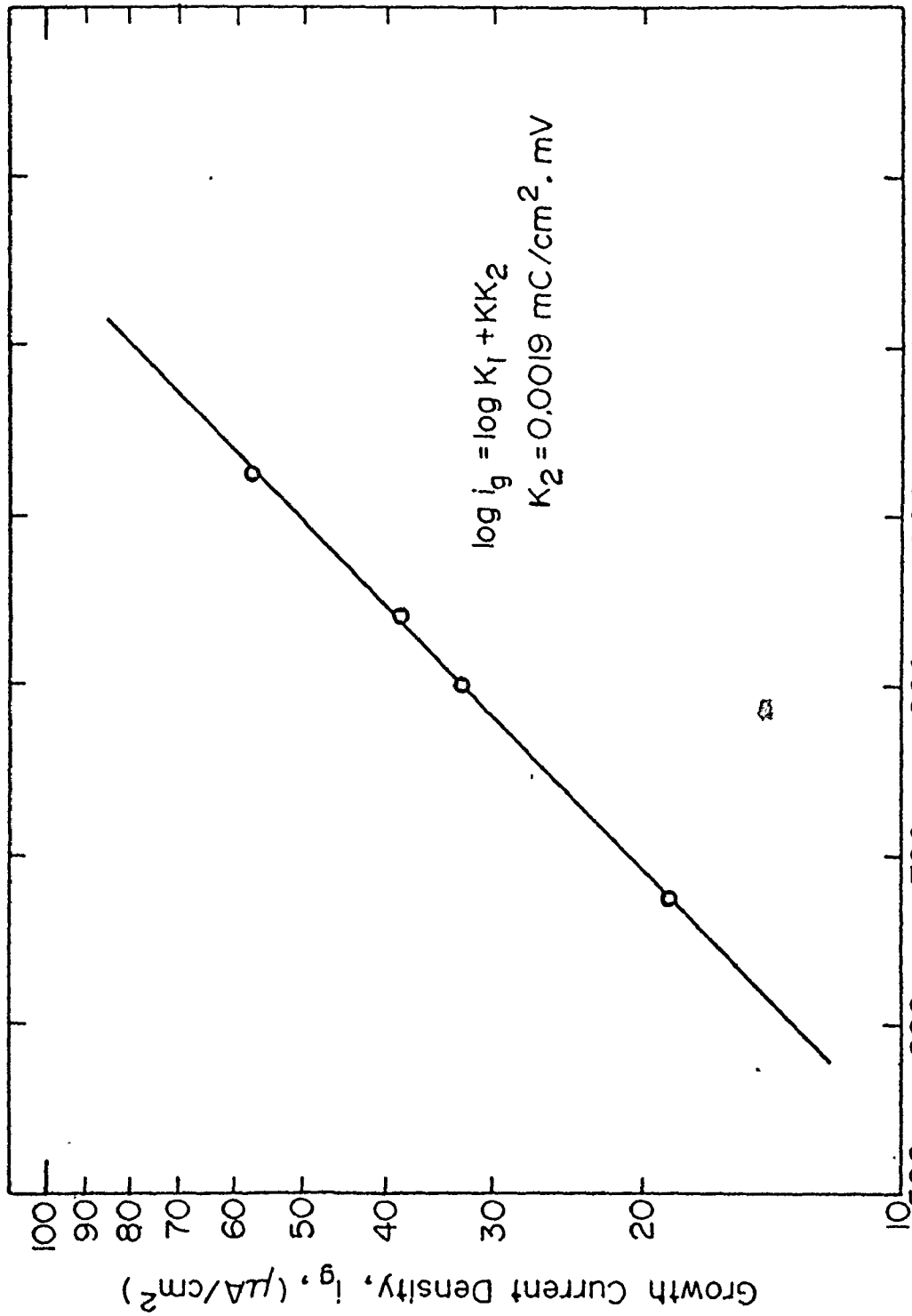

Figure 6-2. K - logi_g plot for the galvanostatic oxidation of nickel in 1N H_2SO_4.

From the K-$\log i_g$ graph (Figure 6-2)

$$\frac{\partial K}{\partial \log i_g} = 517, \text{ mV/decade/mC/cm}^2$$

The equation to the line in Figure 6-2 may be written as -

$$\log i_g = \log K_1 + K K_2 \qquad (6\text{-}11)$$

where K_1 = constant

K_2 = slope of $\log i_g$-K curve.

Substituting from Eqn. (6-1) for K into Eqn. (6-11),

$$\log i_g = \log K_1 + (E - E_1)\frac{K_2}{Q_f}$$

$$\therefore \log i_g = \log K_1 - \frac{E_1 K_2}{Q_f} + \frac{K_2}{Q_f} E \; . \qquad (6\text{-}12)$$

Comparing Eqns. (6-6) and (6-12), we have

$$\text{Tafel slope, } \frac{\partial E}{\partial \log i_g} = \beta = \frac{Q_f}{K_2} \qquad (6\text{-}13)$$

and from the K-$\log i_g$ graph (Figure 6-2),

$$K_2 = 0.0019, \text{ mC/cm}^2 \cdot \text{mV} \; .$$

The values of the Tafel slope, β, observed in Figure 6-1 and calculated from Eqn. (6-13) at various values of Q_f are given below

Q_f mC/cm^2	$(\beta)_{obs}$ mV/decade	$(\beta)_{calc}$ mV/decade
0.42	222	222
0.52	275	274
0.62	330	327
0.72	375	379
0.82	400	432
0.92	415	485

The agreement between the observed and the calculated values of the Tafel slopes is excellent. The discrepancy occurs at high values of Q_f where the variation of film thickness with potential is not linear (Figure 4-3) and the present analysis does not hold good since Eqn. (6-1) is no longer valid. Rewriting Eqn. (6-12) in an exponential form, we have,

$$i_g = K_1 \exp\{\frac{2.303(E-E_1)K_2}{Q_f}\}. \qquad (6\text{-}14)$$

The equation for the growth current density assumed by Sato et al[74] is -

$$i_g = i_o \exp(\frac{bV}{Q_f}) \qquad (6\text{-}15)$$

where i_o and b are constants and $V = E-E_1$ = potential difference across the passive oxide film. Comparing this equation with that derived in the present case [Eqn. (6-14)] it is found that they are identical. Let us now examine Eqn. (6-14) more closely. In its present form it implies that at a constant current density, as film thickness increases, the potential across the film increases. In other words, the field across the film remains constant. This is the basic premise of the present analysis and is the central factor outlining the derivation of Eqn. (B-5) from which Eqn. (6-14) has been derived.

Let us now proceed to derive the conventional rate law from Eqn. (6-14).

$$\text{Let } \frac{dQ_f}{dt} = K_3 i_g$$

where t is the time and K_3 is a proportionality constant

$$\therefore \frac{dQ_f}{dt} = K_1K_3 \exp\{\frac{2.303(E-E_1)K_2}{Q_f}\} \qquad (6\text{-}16)$$

Under galvanostatic condition, substituting from Eqn. (6-1) for $E-E_1 = KQ_f$, we have

$$\frac{dQ_f}{dt} = K_1K_3\exp\{\frac{2.303KQ_fK_2}{Q_f}\}$$

$$\therefore \quad dQ_f = K_1K_3\exp\{2.303KK_2\}dt \ .$$

Integrating,

$$Q_f = K_1K_3\exp\{2.303KK_2\}t + \text{constant}$$

$$\text{or} \quad Q_f = C_1t + C_2 \qquad (6\text{-}17(a))$$

where C_1 and C_2 are constants. Thus, integration of Eqn. (6-16) yields a linear rate law under galvanostatic conditions. However, Eqn. (6-16) can be integrated under the potentiostatic condition and a conventional rate equation of the type

$$\frac{1}{Q_f} = C_1' \ell nt + C_2' \qquad (6\text{-}17(b))$$

as suggested by Sato et al[74] can be derived. It is pointed out that the central assumption in the traditional Mott-Cabrera[112] equation for inverse logarithmic rate law of the type given by Eqn. (6-17(b)) is that the potential drop across the film is constant.

A few words need to be said regarding the application of the inverse logarithmic rate law. Although originally observed

during the growth of barrier films on the valve metals[113] (eg. Ta, Zr, Al etc), these films being poor electronic conductors, it was later applied to thinner, apparently good electron conducting films found on the 'active-passive' metals[11,114,115]. According to this law, film growth occurs by high-field (10^6 V/cm) conduction of the metal ions, the activation barrier being at the metal/oxide interface. If Eqn (6-14) is taken to represent a modified form of the inverse logarithmic law, then the current should depend on the field applied and hence it would be expected that a plot of $\log i_g$ vs $1/Q_f$ at constant potential should be linear. This is indeed found to be true from the present experimental results as is shown in Figure 6-3.

Sato et al[74] also found that the anodic film growth kinetics of potentiostatic oxidation of nickel in 0.3 N sodium carbonate solution of pH = 11.49 was inverse logarithmic in nature in that $\log i_g$ vs $1/Q_f$ yielded a linear plot. It is pointed out that no derivation of the kinetic rate law was presented. Instead, the potentiostatic oxidation data was arbitrarily plotted and it was found that a good fit to the inverse logarithmic law rather than the direct logarithmic law was obtained.

If $V = E-E_1$ = potential difference across the film, then Eqn. (6-12) can be rewritten as

$$\log i_g = \log K_1 + \frac{VK_2}{Q_f} . \qquad (6\text{-}12(a))$$

Thus, as $\frac{1}{Q_f} \to 0$, $\log i_g \to \log K_1$, and mathematically in the

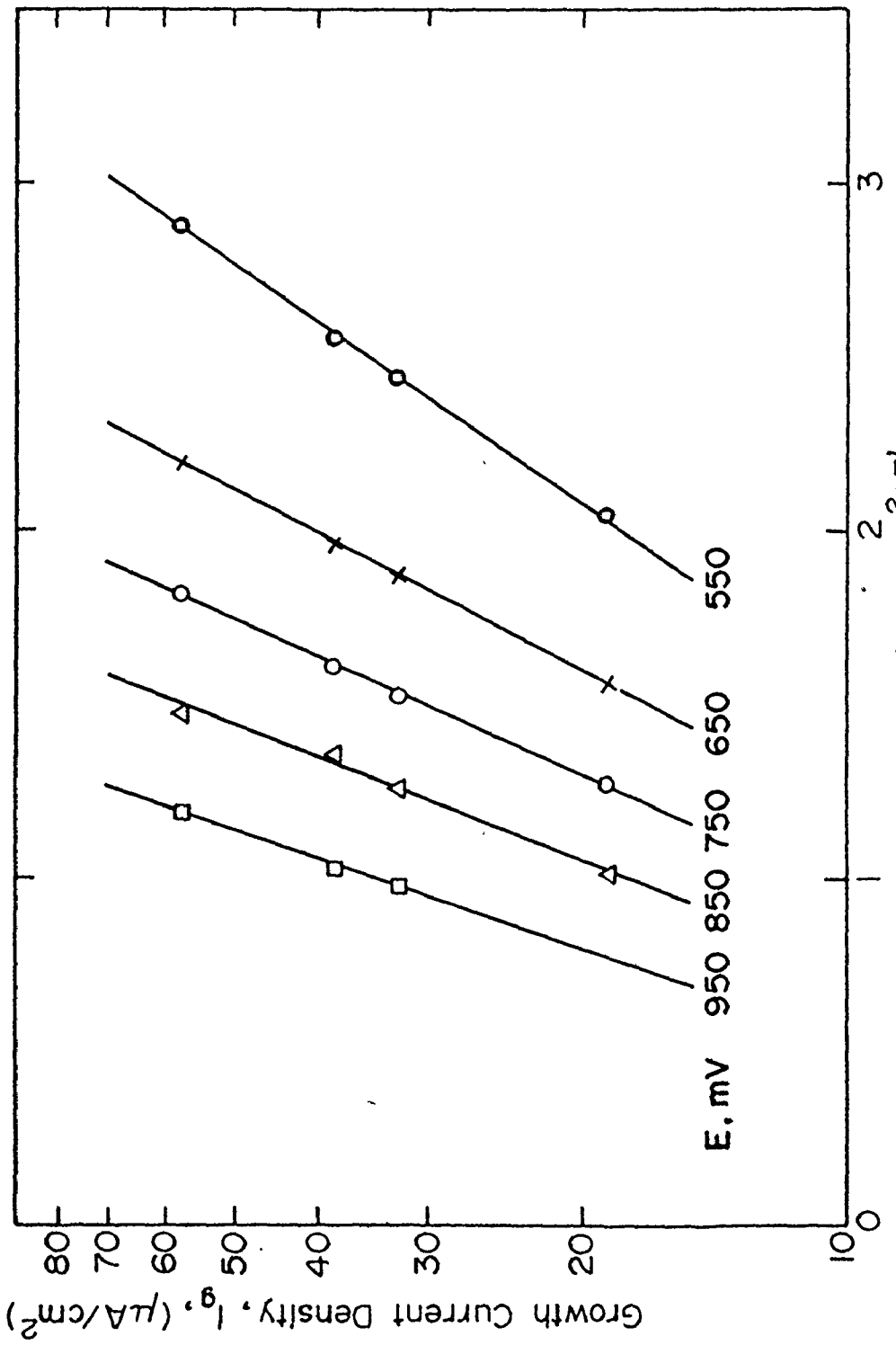

Figure 6-3. $\log i_g$ - $1/Q_f$ plot for the galvanostatic oxidation of nickel in 1N H_2SO_4

limit when $\frac{1}{Q_f} = 0$, $\log i_g = \log K_1$ and $i_g = K_1$. If the straight lines of Figure 6-3 are extrapolated to $\frac{1}{Q_f} = 0$, they converge at $i_g = K_1 = 1.3\ \mu A/cm^2$.

Rewriting Eqn. (6-12(a)) we have,

$$V = \frac{Q_f}{K_2} \log\left(\frac{i_g}{K_1}\right) . \qquad (6\text{-}12(b))$$

The resistivity of the film can now be calculated on the lines of Sato et al[74]. Let the resistance be defined as -

$$R = \frac{\partial V}{\partial i_g} .$$

Then, from Eqn. (6-12(b)), we have,

$$R = \frac{Q_f}{K_2} \cdot \frac{1}{K_1} .$$

Define resistivity as -

$$\rho = \frac{R}{Q_f} = \frac{1}{K_1 K_2} . \qquad (6\text{-}18)$$

Examining the units on the RHS of Eqn. (6-18), we have,

$$RHS = \frac{cm^2 \cdot mV}{mC} \cdot \frac{cm^2}{\mu A}$$

$$= \left(\frac{cm^2}{mC}\right) \cdot \left(\frac{V}{A} \times 10^3\right) \cdot cm^2 .$$

But, a charge of 1 mC/cm^2 is equivalent to an NiO film of thickness 5.67 $\mathring{A} = 5.67 \times 10^{-8}$ cm

$$\therefore \quad RHS = \frac{10^{11}}{5.67} , \ \Omega\text{-cm} .$$

Hence,

$$\rho = \frac{1}{K_1 K_2} \times \frac{10^{11}}{5.67} \ , \ \Omega\text{-cm}$$

$$= \frac{10^{11}}{1.3 \times 0.0019 \times 5.67} \ , \ \Omega\text{-cm}$$

$$= 7.1 \times 10^{12} \ \Omega\text{-cm} \ .$$

This value of the resistivity of the film is in good agreement with that of Sato et al[74] ($\rho \approx 10^{12}$ Ω-cm) calculated for nickel in 0.3 N sodium carbonate solution of pH = 11.49 from potentiostatic oxidation data and that mentioned in literature[116] ($\rho \approx 10^{13}$ Ω-cm) for pure and almost stoichiometric NiO.

Different views exist on the cause and the nature of the passive layer on nickel. Among the earliest to present a coherent picture of the phenomenon were Bockris and coworkers[98]. According to them a prepassive film is formed by a 'dissolution-precipitation mechanism', and this film starts becoming an electronic conductor at the primary passivation potential. The essential cause of passivity is neither a monolayer nor a multilayer of oxide. It is the conversion in the multilayer from ionic to electronic conduction at the passivation potential probably by the introduction of non-stoichiometry. The development of electronic conductivity prevents high field ion transport through the film and thus prevents metal dissolution. Recently however, MacDougall and Cohen[64] found that the passive oxide on nickel in neutral sulfate solution (pH = 8.4) is the stoichiometric NiO. Their conclusion, which was based on extensive electron diffraction studies along with coulometric and X-ray

emission spectroscopy of passivated nickel electrodes is also supported by the results of Sato et al[74] and the present investigation. This conclusion would tend to rule out Bockris et al's[87] contention that electronic conductivity of the film is caused by the introduction of non-stoichiometry.

6.3 Significance of the Flade Potential of Nickel

Sato and Okamoto[77] found the value of the Flade potential (E_F) of nickel in 1N H_2SO_4 at 40°C to be +435 mV (SHE). Later, the pH dependence of the Flade potential was given by Okamoto and Sato[117] as -

$$E_F = 0.48 - 0.060\ pH\ ,\ V(SHE)\ \text{at}\ 25°C \qquad (6\text{-}19)$$

which for the present 1N H_2SO_4 solution (pH = 0.4) yields,

$$E_F = +456\ mV\ (SHE) = +214\ mV(SCE).$$

The value of the Flade potential as determined in the present investigation is +467 mV (SHE) or +225 mV (SCE) and is therefore in good agreement with the value of Okamoto and Sato[77].

The significance of the Flade potential for nickel has remained subject to question. Okamoto and Sato[117] had suggested that the potential-determining redox reaction for the Flade potential was

$$3NiO + H_2O \rightleftharpoons Ni_3O_4 + 2H^+ + 2e \qquad (6\text{-}20)$$

for which

$$E_F(calc) = \frac{1}{2F}(\mu^o_{Ni_3O_4} + 2\mu^o_{H^+} - 3\mu^o_{NiO} - \mu^o_{H_2O}) - 0.059\ pH,\ V(SHE)\ \text{at}\ 25°C \qquad (6\text{-}21)$$

where μ^{o} designates the standard free energy of formation. Although Okamoto and Sato[117] did not provide any numerical value to the μ^{o} values in Eqn. (6-21), they had concluded that the Flade potential is not the formation potential of NiO but the transformation potential from NiO to the higher valence oxide Ni_3O_4. However, according to the Electrochemical Atlas[66], the electrode potential corresponding to Eqn. (6-20) is given by -

$$E = 0.897-0.059\ pH\ ,\ V(SHE)\ at\ 25°C \qquad (6-22)$$

which at pH = 0.4 yields,

$$E = +873\ mV\ (SHE) = +631\ mV\ (SCE)\ .$$

It is therefore apparent that the Flade potential does not correspond to the redox reaction given by Eqn. (6-20) since Ni_3O_4 is thermodynamically unstable at the observed Flade potential.

In view of the present experimental data, a slightly different interpretation will be accorded to the Flade potential. The present results have shown that the film on nickel in 1N H_2SO_4 is NiO, the formation potential of which has been found to be -170 mV (SCE). Thus, when passivity sets in, the surface of the nickel electrode is presumably covered with NiO. A potential value of +225 mV (SCE) on the anodic potentiostatic polarization curve of nickel in 1N H_2SO_4 is at the beginning of the passive region (Figure 5-8). It is, therefore, suggested that the Flade potential corresponds to that potential, more noble than E_{pp}, at which the surface of nickel is covered with a pore-free film of NiO and passivation is complete. This

interpretation of the Flade potential is also capable of explaining the data of Okamoto and Sato[77,117].

6.4 The Concept of the Critical Potential:

It has generally been believed[105-107] that metals undergo pitting corrosion only beyond a certain critical potential (E_c). This potential has served as one of the fundamental electrochemical criteria characterizing the susceptibility of metals to pitting corrosion. It is believed[118] that at more negative potentials than E_c the metal exits in a passive state, while above E_c, active and passive states coexist on the metal surface giving rise to pitting corrosion. Thus, the more positive is E_c, the more resistant is the metal to pitting corrosion.

Pourbaix et al[119] have distinguished two types of critical potential: breakdown potential (E_c), the potential corresponding to a rapid increase of the current due to pit nucleation, and protection potential (E_p), the potential corresponding to the current drop during the reverse potential sweep, caused by the repassivation of the pits. According to Pourbaix, within the range E_p to E_c propagation of already existing pits continues, but nucleation of new pits is restrained, occurring only when $E \geq E_c$. However, Wilde[2] has shown that E_p is not a unique property of a metal and depends on the length of time a pit has been growing. Therefore, in order to afford a proper basis for comparison of the repassivation ability of metals and alloys, pit growth should be allowed to occur to the same extent. In

other words, the potential sweep must be reversed from the same current density value.

The existence of anodic and cathodic sites is not a new concept and is basic even to Wagner and Traud's mixed-potential theory[120]. The distribution of such sites may be assumed[121] random over the entire specimen surface with both types of sites being present along the grain boundaries as well as within the grains. Which of these sites becomes activated depends on the conditions existing at the metal/solution interface during polarization. Grain size, cold work, and other aspects of metallurgical condition could all possibly affect the anode/cathode site distribution and, therefore, have a significant effect on the corrosion characteristic of a metal.

The results presented show that it is inappropriate to suppose that the critical potential, E_c, can be used to predict the pitting corrosion characteristics of nickel in sulfuric acid solutions containing chloride ions. Also, the anodic Tafel slopes (Table 4-4) show little difference over the entire range of grain size. Electrochemically, this fact may be taken to mean that the primary dissolution mechanism, and possibly the characteristics of the passive film, are similar in each case. It is therefore concluded that a variation in grain size from 0.025 to 0.330 mm has no effect on the pitting corrosion characteristics of nickel. It has been found[87] that cold working up to 40% also has no effect on the value of E_c for nickel in 0.02 M Cl^--solution. This invariance of E_c with cold

work is consistent with instances reported in the literature for austenitic steels[122] and Fe-Cr alloys[123].

The slopes in the transpassive region do not provide any specific information. They cannot be regarded as a measure of the growth rate of the pits because of the multiple events occurring on the surface. Pits that had nucleated grow, new ones might nucleate, and some of the older ones passivate. However, the transpassive slopes, β_t, do provide an idea of the overall corrosion of the specimen in that potential range. Within limits of computational error (±10 mV/decade), it may be seen that β_t does not significantly change with either grain size or cold work[87]. This is consistent with the observation that neither variation in grain size nor cold working have any effect on the pitting corrosion characteristics of nickel.

Referring to Figure 4-8, if one does consider the point of the change of the slope of the curves to have the same significance as the critical potential, it is around +950 to +975 mV, even though pit formation is observed to occur much earlier. The transpassive slopes for these curves are much higher (ranging between 215-235 mV/decade) which indicates a lower over-all corrosion rate. This is because the pit density in these cases is much lower than in the instance where the specimen is polarized from the beginning in a Cl^--containing solution.

The formation of pits in the active region is consistent with the concept of 'balance' between film formation and solu-

tion discussed elsewhere[82], but is in direct conflict with the idea that pitting corrosion cannot occur at potentials more active than some critical potential[105-107]. The critical potential thus does not adequately describe the electrochemical conditions required for the pitting corrosion of nickel in sulfuric acid solutions containing chloride ions.

The critical potential may be dependent on two factors: (a) internal factors, such as grain size, cold work, inclusions and compositional inhomogeneity, and (b) external factors such as chemistry of the solution or the passive film. Since E_c is independent of the internal factors, it is inferred that the critical potential is chemistry controlled. That the chemistry of the solution affects E_c of nickel has already been demonstrated[82].

The potentiostatic polarization results on the Ni-Mo alloys are similar to those on nickel. Initiation of the attack occurs in the active region in the presence of Cl^--ions and increasing the Cl^--ion concentration increases the passivation potential (E_{pp}) and decreases the critical potential (E_c) thereby decreasing the passive region. In view of these observations, it is suggested that the conclusions made on the nature of E_c for nickel are essentially true for the alloys. Thus, considerable caution must be exercised in interpreting data based on critical potentials to assess the pitting susceptibility of metals and alloys.

One point of caution however needs to be made. The effect of internal factors on E_c of the alloys has not been

investigated and therefore to assume that E_c is independent of these factors is incorrect. In fact, the behaviour of the alloys would greatly depend upon the internal factors. The depletion of molybdenum at the grain boundaries of the Ni-22Mo alloy and the subsequent intergranular attack is one example of of the effect of compositional inhomogeneity. It is possible that the intergranular corrosion of Ni-15Mo alloy is also due to a similar depletion effect, with the difference that the depletion is small and therefore undetectable by the technique employed for detection.

6.5 Validity of Film Thickness Measurements

Aside from the defect nature of the passive film which has a significant effect on the corrosion characteristics of a metal, the thickness of the passive film is also important as it provides the physical barrier between the metal and the corrosive medium. In determining the validity of the film thickness measurements in the present work, two questions need to be answered. First, is it possible to completely reduce the film electrochemically? Secondly, is it justified to assume a 100% current efficiency for reduction? These questions will be considered for nickel first since data on the system for comparison and analysis is readily available and then the concepts extended in a broader framework to include the alloys.

In dealing with the reducibility of the film, a search through the literature reveals that during his ellipsometric studies in 1933, Tronstad[124] found that when nickel (and iron)

were made anodic in acid and alkaline solutions, the optical parameters changed signifying film formation. However, upon cathodic reduction, the optical parameters did not revert back to those of the original surface suggesting that not all the film was removed. In fact, after a few successive anodic/cathodic sweeps, Tronstad was able to obtain interference colors on the specimen surface. He concluded that the passive films on nickel (and iron) are not completely reducible. More than 30 years later, Bockris et al[98], studying the passivity of nickel in 1N H_2SO_4 by ellipsometry, found that an anodically oxidized and cathodically reduced surface yielded the same optical parameters as pure nickel. They concluded that the film on nickel is capable of complete reduction.

It is, perhaps, pointless to speculate on the reasons for Tronstand's observations. For cathodic reduction techniques have been extensively employed to determine the thickness and nature of passive films on both iron and nickel[74,85,125-127]. Tokuda and Ives[85] employed galvanostatic cathodic reduction to determine the thickness of the passive layer on nickel single crystals and polycrystalline nickel in 1N H_2SO_4 in an attempt to correlate the pitting susceptibility with the physical barrier provided by the passive film. Sato et al[74] employed galvanostatic reduction techniques to determine film thickness on nickel in neutral solutions. They found that to obtain a bare surface, cathodic reduction has to be carried out in sulfuric acid for anodically oxidized surfaces and either in acid or

in neutral solution for electropolished surfaces. Recently, MacDougall and Cohen[64] determined film thickness on nickel in neutral sodium sulfate solution (pH = 8.4) by chemical analysis and x-ray emission spectroscopy. The results of film thickness measurements of Sato et al[74], MacDougall and Cohen[64] and the present work are presented below.

Investigators	Film Thickness Range	Method of Estimation
Sato et al[74]	6 to 16 Å	Galvanostatic reduction
MacDougall and Cohen[64]	9 to 12 Å	Chemical analysis and x-ray emission spectroscopy
Present work	6 to 16 Å	Chemical analysis and galvanostatic reduction

Two of the methods mentioned above do not require the reduction of the film for determination of film thickness. Chemical analysis involves the determination of the charge equivalent to the quantity of nickel present in solution which when subtracted from the total anodic charge yields the charge stored in the film (and consequently film thickness - refer to section 4.2). X-ray emission spectroscopy determines the amount of oxygen on the anodically oxidized electrode surface which can be converted to film thickness. In view of the fact that electrochemical reduction methods yield film thickness values similar to those obtained from other methods not involving film reduction, it is concluded that the passive film on nickel is capable of complete reduction in 1N H_2SO_4.

The assumption of a 100% current efficiency during

reduction is a simple justification from an electrochemical point of view. Since there is no other redox system[66] (Figure 2-4) between the hydrogen and the oxygen electrode for nickel in 1N H_2SO_4, all the current is involved in film growth and film dissolution during anodic oxidation. Since there is no film formation during cathodic reduction, a 100% current efficiency for film reduction is justified.

However, if the problem is attacked from a solid-state physics point of view, the situation becomes somewhat more complex. The passivated electrode may be considered as a metal-semiconductor system. NiO is a p-type oxide where conduction is primarily by holes. The potential barrier across the metal-semiconductor junction will depend upon the work function of the metal (ϕ_M) and the semiconductor (ϕ_S) which in turn will fix the Fermi level (E_f). The work function of nickel is 4.96 eV[128] while the band gap (E_g) in NiO is 3.9 eV[116]. In the absence of a knowledge of the exact position of the Fermi level of NiO and under the assumption that space-charge effects are negligible, two obvious cases arise[129].

a) When $\phi_{Ni} > \phi_{NiO}$ implying that the Fermi level lies lower in the metal than in the semiconductor (Figure 6-4(a)). When contact is made, electrons flow from the semiconductor to the metal until the Fermi levels coincide, thereby charging the metal negative and leaving additional holes on the semiconductor side of the junction (Figure 6-4(b)). When a potential difference is applied, conduction will

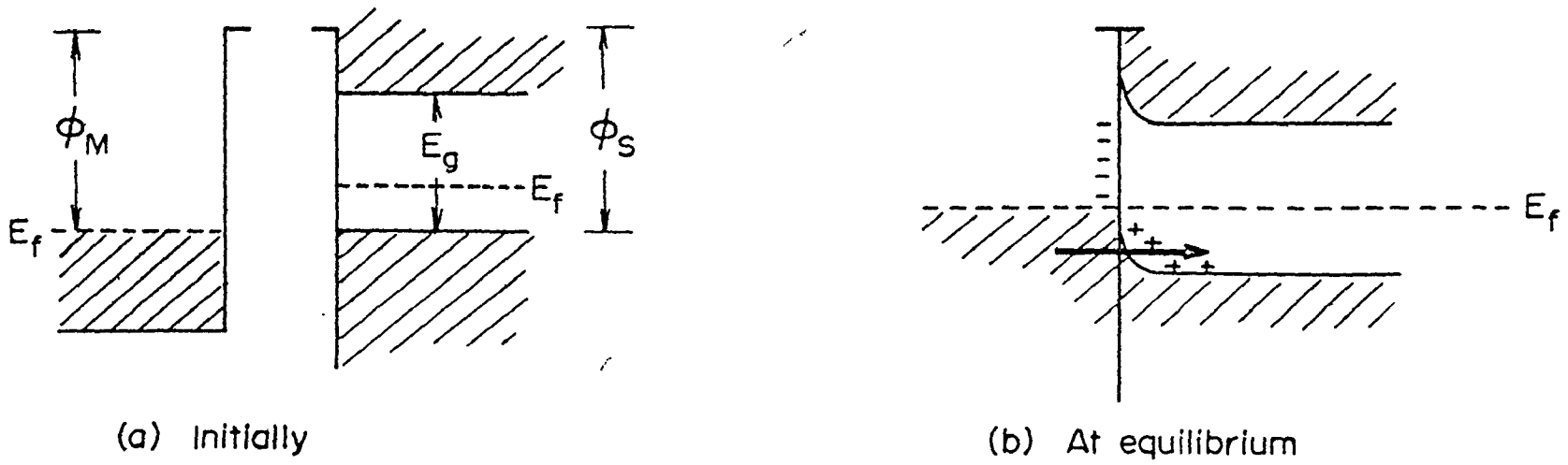

Figure 6-4. Energy level diagrams for nickel-nickel oxide interface assuming $\phi_M > \phi_S$.
(a) Initially, before contact. (b) at equilibrium, after contact.

occur only if there are impurity states present since the electrons from the metal cannot enter the forbidden gap in the semiconductor.

b) When $\phi_{Ni} < \phi_{NiO}$ implying that the Fermi level in the metal lies above that in the semiconductor (Figure 6-5(a)). When contact is made, electrons from the metal fill the holes at the junction thereby producing a negative depletion layer of ionized acceptors. When equilibrium is achieved, the metal surface bears a positive charge and the semiconductor bears a negative charge (Figure 6-5(b)). When a voltage is applied at the junction, it does nothing about the height of the barrier on the metal side - that is determined entirely by the nature of the metal and of the semiconductor. Because the depletion layer has reduced conductivity, most of the potential difference appears across it. For a reverse bias (metal negative-semiconductor positive, which is the case during cathodic reduction), the energy of the electrons in the semiconductor is lowered by $V \cdot e$ (where V is the applied potential difference and e is the electron charge) (Figure 6-5(c)). The electrons from the metal cannot move into the valence band of the semiconductor since it is full and their only possible movement is by climbing over the barrier into the conduction band of the semiconductor.

Although the movement of electrons over energy barriers is evident, when the electric field across the semiconductor is high and the semiconductor sufficiently thin, the electrons

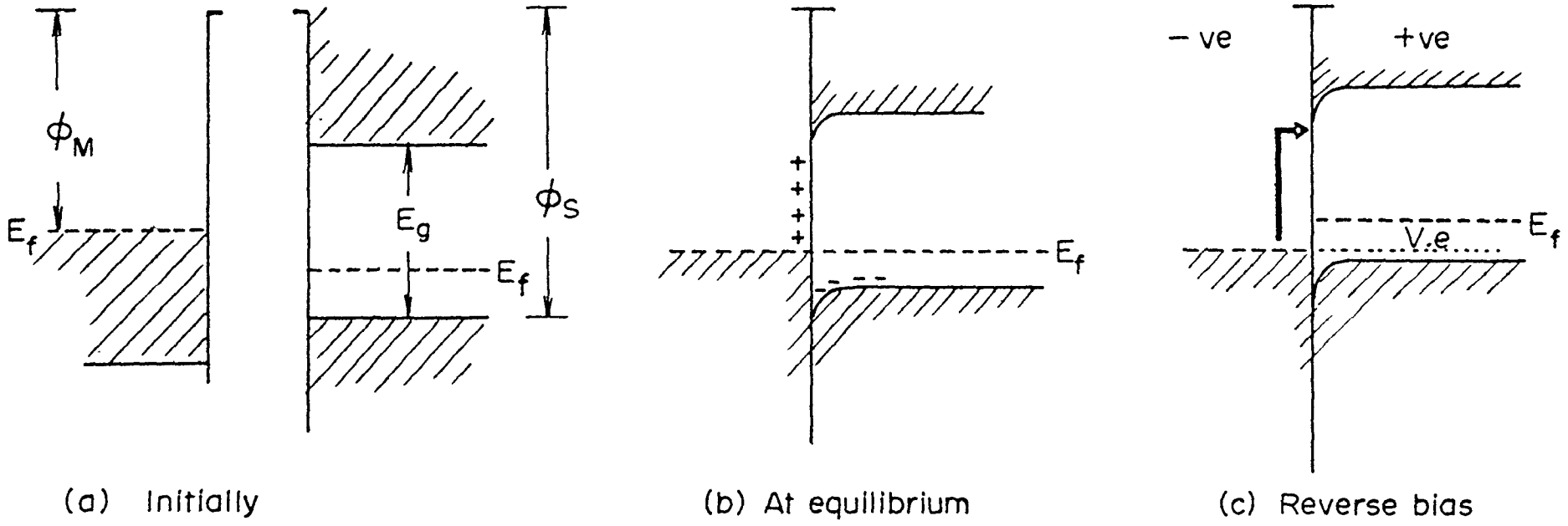

Figure 6-5. Energy level diagrams for nickel-nickel oxide interface assuming $\phi_M < \phi_S$
(a) Initially, before contact. (b) At equilibrium, after contact.
(c) On application of reverse bias.

have a finite probability of tunneling through the energy barrier[130]. In either case not all the electrons are involved in the reduction process and hence a 100% current efficiency cannot be justified. Either barrier mounting or tunnelling would result in the evolution of hydrogen on the electrode surface according to the reaction -

$$2H^+ + 2e \rightarrow H_2\uparrow$$

However, no hydrogen evolution was visually observed which would suggest the absence of barrier mounting or tunneling. In order to provide a firmer basis to the contention that barrier mounting or tunnelling does not occur, the current due to electron transfer can be calculated for each of the cases described above and then compared with the time for ion transfer during anodic oxidation. Such an estimation follows.

Let us first determine the time for ion transfer during anodic oxidation under the premise that the film grows by the movement of Ni^{2+} cations. This value of the time for ion transfer (τ_{ion}) can be calculated on the assumption that the ion starts from zero velocity, attains its maximum possible velocity for the given energy and travels through the film without encountering any resistance. This, then, implies that the value of τ_{ion} calculated on the above assumption will be the lowest possible time of ion transfer and, if resistance to motion is encountered or maximum velocity is not attained, τ_{ion} could be higher. The velocity of a free Ni^{2+} ion and the time of ion

transfer across the oxide (15 Å) can be calculated as follows -

$$\text{Velocity, } v = \sqrt{\frac{2E}{m}}$$

where, E = energy imparted to the ion and m = mass of the ion.

$$\therefore v = \sqrt{\frac{2\times 0.6\times 1.602\times 10^{-19}}{58.71\times 1.66\times 10^{-27}}} \text{ , m/sec}$$

$$= 1.4\times 10^{3} \text{ m/sec}$$

$$\therefore \text{time of ion transfer, } \tau_{ion} = \frac{\text{film thickness}}{\text{velocity}} = \frac{15\times 10^{-10}}{1.4\times 10^{3}} \approx 10^{-12} \text{ sec}$$

Let us now calculate the time for electron transfer in each of the cases discussed earlier.

a) Electrons can be transferred from the metal through the forbidden gap provided there are impurities present which act as acceptor states. Although it has been shown earlier on the basis of resistivity calculation of NiO that the oxide is pure and almost stoichiometric which would suggest the absence of impurity levels, in practice however, the level of impurity needed is so small as to leave the NiO effectively pure.

The current is

$$i = \sigma\varepsilon \text{ , amp/m}^2$$

where σ = conductivity of NiO

$$= \frac{1}{7.1\times 10^{12}\times 10^{-2}} \Omega^{-1}\text{-m}^{-1} \quad \text{(from the present results -section 6.2)}$$

ε = electric field $= \frac{V}{\epsilon x}$ (V = potential difference; x = film thickness, ϵ = dielectric constant of NiO = 11[131]).

$$= \frac{0.6}{15\times10^{-10}\times11} \text{ , V/m}$$

$$\therefore i = \frac{1}{7.1\times10^{12}\times10^{-2}} \times \frac{0.6}{15\times10^{-10}\times11} \text{ , amp/m}^2$$

$$= 5.1\times10^{-4} \text{ amp/m}^2 \text{ (or } 5.1\times10^{-8} \text{ amp/cm}^2\text{)}$$

which turns out to be negligible compared with any current density encountered in this investigation. The time of electron transfer can now be calculated since, amp×sec = Coulomb, electronic charge = 1.602×10^{-19} coul. and atomic size = 2.5×10^{-10} m.

$$\therefore \text{current} = \frac{5.1\times10^{-4}}{1.602\times10^{-19}} (2.5\times10^{-10})^2 \text{ , } \frac{\text{charge}}{\text{sec. surface atom}}$$

$$= 19.9\times10^{-5}/\text{sec}$$

$$\therefore \text{time of electron transfer, } \tau_e \approx 5\times10^3 \text{ sec.}$$

b) The net current for the electron transfer from the metal over the energy barrier into the conduction band of the NiO can be derived in the following manner.

$$\text{Conductivity, } \sigma = Ne\mu$$

where N = electron density, e = electron charge and

μ = mobility of the electrons = $\frac{\text{velocity}}{\text{electrical field}} = \frac{v}{\varepsilon}$.

Also,

$$\text{Current, } i = \sigma\varepsilon$$

$$\therefore i = Nev.$$

The velocity of the electrons can be calculated on the same basis as that of the free Ni^{2+} ions. The upper limit to the value of v is $\sqrt{\frac{2E}{m_e}}$ and in general

$$v \leq \sqrt{\frac{2E}{m_e}}$$

where E is the energy imparted to the electrons and m_e is their mass. It is acceptable to choose $v = \sqrt{\frac{2E}{m_e}}$ for the main reason that in a thin film (as the one being considered) diffusion presents no problems.

Now

$$N = N_e \exp(-\frac{\Delta E}{kT})$$

where $N_e = 2(\frac{2\pi m_e^* kT}{h^2})^{3/2}$, ΔE = energy barrier that the electrons need to overcome, m_e^* = effective mass of the electrons, h = Planck's constant, k = Boltzman's constant, T = absolute temperature.

Hence,

$$i = e\sqrt{\frac{2E}{m_e}}\ 2(\frac{2\pi m_e^* kT}{h^2})^{3/2} \exp(-\frac{\Delta E}{kT})\ ,\ amp/m^2\ .$$

In calculating i, m_e^* will be taken equal to m_e (although it may differ by a factor of 10) and ΔE will be taken equal to $(\frac{1}{2} E_g)_{NiO}$ on the assumption that at equilibrium the Fermi levels coincide and the Fermi level in NiO is midway between the band gap (E_g). In reality however, $\Delta E > \frac{1}{2} E_g$ since the Fermi level in a p-type semiconductor

is lower than half the band gap.

Now,

$e = 1.602\times10^{-19}$ C $E = 0.6$ V

$m_e = 9.11\times10^{-31}$ kg $T = 25°C = 298°K$

$k = 1.39\times10^{-23}$ J/°K $E_g = 3.9$ eV

$h = 6.63\times10^{-34}$ J sec $E_f = 4.96$ eV

$kT = 0.026$ eV

$$\therefore\ i = 1.602\times10^{-19}\sqrt{\frac{2\times0.6\times1.602\times10^{-19}}{9.11\times10^{-31}}}\times2\left\{\frac{2\pi\times9.11\times10^{-31}\times1.38\times10^{-23}\times298}{(6.63\times10^{-34})^2}\right\}^{3/2}$$

$$\times\ \exp\left(-\frac{\frac{1}{2}\times 3.9}{0.026}\right)$$

$= 2.4\times10^{-21}$ amp/m^2 (or 2.4×10^{-25} amp/cm^2).

As calculated in the previous case, time of electron transfer, $\tau_e = 1.1\times10^{21}$ sec.

Although the case against electron transfer merely on the basis of time required for the process is rather sound, one could neglect the cases discussed above and attempt to calculate the tunnelling current assuming the case of field emission. The emission current density is given by the Fowler-Nordheim Eqn.[132] -

$$i = 1.6\times10^{-6}\ \frac{\varepsilon^2}{\phi_M}\ \exp\left\{-\frac{7\times10^9\ \phi_M^{3/2}}{\varepsilon}\cdot u\right\},\ \text{amp/m}^2$$

where ϕ_M is the work function of the metal in eV, ε is the electric field in V/m and $u \cong 1 - 14\times10^{-10}\ \frac{\varepsilon}{\phi_M^2} \approx 1$.

The potential barrier encountered by the electrons is of the type

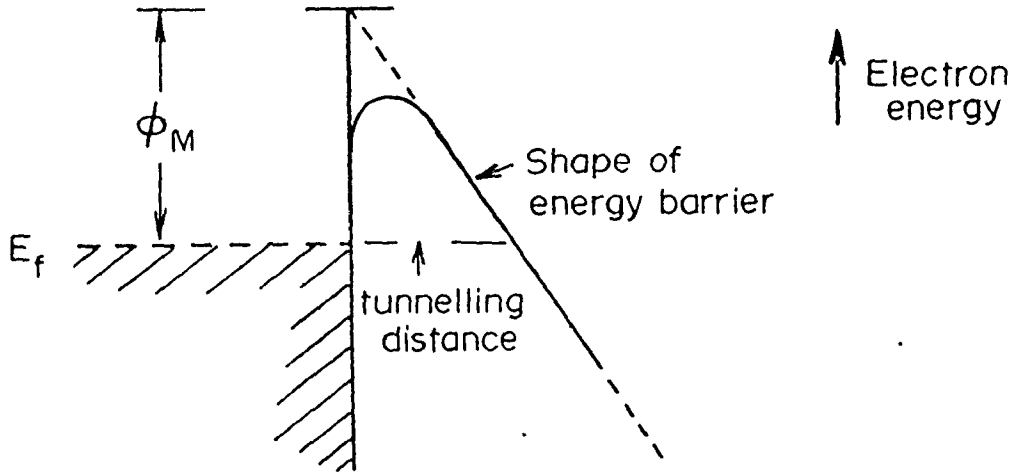

In view of the case under consideration, let us assume that the potential barrier is entirely across the semiconductor (NiO). The electrons encounter a field,

$$\varepsilon = \frac{V}{\epsilon x} \quad \text{(as before)}$$

$$= \frac{0.6}{15\times10^{-10}\times11} = 3.6\times10^{7},\ \text{V/m}$$

$$\therefore\ i = 1.6\times10^{-6}\ \left(\frac{3.6\times10^{7}}{4.96}\right)^{2} \exp\left\{-\frac{7\times10^{9}(4.96)^{3/2}}{3.6\times10^{7}}\right\}$$

$$= 6.2\times10^{-927}\ \text{amp/m}^2\ (\text{or } 6.2\times10^{-931}\ \text{amp/cm}^2)$$

which is a ridiculously small value suggesting that under the present conditions tunneling due to field emission is impossible. The reason for this is that in field emission the energy barrier in the absence of a field is almost infinite. The appli-

cation of the field bends the barrier thereby decreasing the tunnelling distance. The extent to which the barrier bends depends upon the electric field; the greater the field, the larger the bend in the barrier and consequently the lower is the tunnelling distance. In the present case, the field is low and therefore the barrier does not bend sufficiently resulting in a large tunnelling distance and consequently yielding such a small value for the emission current

In retrospect, one realizes that tunnelling poses no problem since times of electron transfer are very large especially when compared with the time of ion transfer during anodic oxidation. Aside from this conclusion, the thickness of the passive film estimated in the present investigation employing galvanostatic cathodic reduction assuming complete reduction of the film with a 100% reduction current efficiency is in good agreement with that of other workers obtained by methods other than the one used in this investigation. From a narrowed view point, the results themselves then are sufficient justification of the assumptions involved in their estimation. If this be so, then the entire exercise of calculating the times of electron transfer becomes futile. However, one point worth mentioning is that the experimentally determined value[133] for resonance electron transfer is typically of the order of 10^{-19} sec. This is many orders of magnitude lower than that estimated for ion transfer, making tunnelling a distinct possibility. It is, therefore, suggested that the situation be analyzed from a solid-state physicist's point of view before the possibility of tunnelling is ruled out. It is pointed out that the electro-

chemists should develop a greater awareness of the solid-state implications of simple electrode processes.

Although enough justification has been provided for the validity of film thickness measurements on nickel, nothing has been said about the alloys. There is no existing data on the charge required for the reduction of the anodic film on the nickel-molybdenum alloys. Cathodic reduction experiments fail to provide any information on the nature and composition of the films since the reduction curves do not exhibit any plateaus which may provide any clue to the reducing species (Figures 5-10 and 5-11). As will be discussed in detail in section 6.8,it is suggested that the film on the alloys is a mixed oxide (molybdenum doped NiO). If this be so, then the addition of molybdenum increases the vacancy concentration in the oxide but decreases the electrical conductivity[134]. For the nickel rich α-solid solution alloys, it is reasonable to assume that the oxide is still a p-type semiconductor. The work function of molybdenum is 4.24 eV[128] which is not very different from that of nickel (ϕ_{Ni} = 4.96 eV) and its presence in the oxide would be expected to change the band gap. If it is assumed that this change in the mixed oxide is not drastic so that the band gap is not very different from that of NiO, then the principles outlined in the previous pages for NiO apply to the mixed oxide as well. It would then be reasonable to infer that films on nickel-molybdenum alloys are reducible with a 100% efficiency for the reduction current.

6.6 General Discussion of the Results

6.6.1 Comparison of the Results with Those in Literature

The corrosion rates obtained in 10% HCl solution in this investigation, although following the same order as those of Uhlig et al[33] in the same solution, are much higher in magnitude especially for the low molybdenum alloys. A possible reason for this discrepancy is that the alloys used by Uhlig et al[33] were pickled in warm 6N HNO_3 following mechanical polishing to remove the disturbed metal layer. The alloys in this investigation were only mechanically polished up to 600 grit silicon carbide paper, which could account for a higher weight loss.

The potentiostatic polarization results for all the alloys in 1N H_2SO_4 are in good agreement with those of Greene[94] who noted that the current density in the passive region increases with increasing molybdenum content. This observation is also true for the present results (Figure 5-8). Greene[94] further pointed out that at 25% molybdenum, the material demonstrates very little of the original electrochemical behaviour of nickel. Referring to Figure 5-8 it is found that at 22% Mo the alloy has no real passive region and at 30% Mo, the alloy exhibits no similarity with the electrochemical behaviour of nickel but is completely akin to that of molybdenum (Figure 5-40). The potentiostatic polarization of molybdenum emerges as an activation controlled process from both studies. It is this property that the molybdenum imparts to the alloys upon alloying.

6.6.2 Anodic-Cathodic Polarization

The thermodynamic hydrogen evolution potential ($E^{o}_{H_2}$) in a solution of pH = 0.4 as obtained from the potential-pH diagram[66] is about -280 mV (SCE). The corrosion potential of nickel and all the alloys is nobler than this value of $E^{o}_{H_2}$. It, therefore, appears that some other cathodic reaction instead of hydrogen evolution would be present between the corrosion potentials and $E^{o}_{H_2}$. This in fact is found in every case as is evident from the discontinuity in the cathodic segment of the polarization curves (Figure 5-13(a)). The discontinuity appears, at approximately the same potential and current density for every alloy. It is suggested that the cathodic reaction is due to an adsorption of positively charged ions in solution, possibly the H^{+}-ion being the major absorping species.

6.6.3 Corrosion of the Alloys

There has been some speculation on what causes molybdenum to improve the corrosion resistance of nickel. Uhlig[7] has suggested that this is either due to a sluggish anodic reaction caused possibly by a slow hydration of the metal ions or to the presence of a porous diffusion barrier film of molybdenum oxide. Another view has been advanced by Taube[135] and Vijh[136] where metals have been divided into two categories based on the stability of the chloride complex. In general, a metal reacts with the chloride ion according to -

$$M + nCl^{-} \rightarrow M(Cl)_n + ne$$

followed by the dissolution, partial or complete, of the chloride according to -

$$M(Cl)_n \rightarrow M^{n+} + nCl^- \ .$$

The M^{n+} which is now in solution undergoes complex formation by the Cl^- present -

$$M^{n+} + mCl^- \rightarrow (M_nCl_m)^{(m-n)-}$$

where m is the coordination number of the metal.

Metals such as Ni, Fe, Cr, Al etc. are placed in one category where the complexes are unstable and favour dissociation by -

$$(M_nCl_m)^{(m-n)-} \rightarrow M^{n+} + mCl^- \ .$$

Such a reaction makes the Cl^--ions available to participate again in the entire reaction sequence. Metals such as Mo, Ti, Zr etc are placed in a second category where the chlorocomplex is so stable that it effectively scavenges the chloride ions and prohibits them from participating in the reaction sequence.

The results of this investigation do not support all of the above contentions. The electron diffraction pattern of the film from a Ni-5Mo alloy did not match with any of the known chlorides of molybdenum and was found to match with MoO_3 (Table 5-10). Also, chemical analysis of the film from a Ni-10Mo alloy revealed the complete absence of the chloride ion.

Metallic chlorides are known to hydrolyze[6] and the presence of MoO_3 as the film appears possible when the hydrolysis

of $MoCl_6$* is considered from a thermodynamic view point.

$$MoCl_6 + 3H_2O \rightarrow MoO_3 + 6HCl$$

$$\Delta F^o = -122 \text{ kcals/mole.}$$

The hydrolysis of $NiCl_2$ is not possible thermodynamically.

$$NiCl_2 + H_2O \rightarrow NiO + 2HCl$$

$$\Delta F^o = +7.7 \text{ kcals/mole .}$$

Another point in favour of the presence of MoO_3 appears when the potential-pH diagrams for nickel-water and molybdenum-water systems[66] are superimposed. It turns out that in the acidic region (pH = 0.4), the only stable species predicted is MoO_3. Finally, as Bullman and Tseung[102] have pointed out, if it is assumed that the dissolution rates at the oxide-solution interface show the same trends as those of the pure oxide of each metal, then the order of dissolution rates in an acid solution is[66] -

$$MoO_3 << NiO.$$

From the diffusion coefficients of the cations in their respective pure oxide it may be implied that the order of mobilities is[102] -

$$Mo(MoO_3) > Ni(NiO) .$$

Since the corrosion potentials of the alloys, let us say in 1N H_2SO_4, vary between -180 mV and -102 mV (SCE) (Table 5-2)

---

*Molybdenum is known to dissolve in the hexavalent state during anodic polarization in HCl acid solutions[66]

while that of molybdenum and nickel are +42 mV and -220 mV (SCE) respectively, it is evident that upon anodic polarization, the alloy becomes richer in MoO_3 and depleted in NiO. This could be considered as a form of leaching where the nobler constituent (molybdenum) remains behind while the active one (nickel) is leached out. Analysis of the solution after anodic polarization has shown that indeed the proportions of molybdenum in solution is less than that present in the alloy (Table 5-11).

6.7 Mechanism of Corrosion of the Alloys

In an attempt to determine the mechanism by which the nickel-molybdenum alloys corrode upon anodic polarization, two possibilities will be examined.

a) The alloys corrode as active-passive alloys.

b) The alloys corrode under anodic control through a barrier-type film.

A subtle distinction is implied between these two modes. Anodic control is not the point of distinction since it (anodic control) is typical of all materials that exhibit an active-passive transition. The aspect that distinguishes the two modes is the 'nature' of the surface film. In case (a) the anodic reaction is inhibited by the presence of a protective passive film whereas in case (b), the surface film that forms as a result of corrosion in the active region is not of the same protective nature (as that formed in the passive region).

In order to determine which of the above mechanisms is valid, a comparison will be made of the corrosion order ob-

tained from the freely corroding system (Figure 5-37) and that determined from the above modes. To this end, the potentiostatic polarization data will be plotted in two ways and the corrosion sequence at a chloride concentration of 0.4 M noted.

a) The passive circuit density at an arbitrarily chosen potential of +600 mV (SCE), $(i_p)_{+600}$ vs Cl^- ion concentration (Figure 6-6). The corrosion order in terms of the current density is -

$$(i)_{Ni-5Mo} > (i)_{Ni} > (i)_{Ni-10Mo} > (i)_{Ni-22Mo} > (i)_{Ni-15Mo} .$$

b) The critical current density (i_c) vs Cl^- ion concentration (Figure 6-7). The corrosion order in terms of the current density is -

$$(i)_{Ni} > (i)_{Ni-5Mo} > (i)_{Ni-10Mo} > (i)_{Ni-15Mo} > (i)_{Ni-22Mo} .$$

The freely corroding order of the allys is -

$$Ni > Ni\text{-}5Mo > Ni\text{-}10Mo > Ni\text{-}15Mo > Ni\text{-}22Mo .$$

A comparison of the corroding order from the freely corroding system and that from the $(i_p)_{+600}$ vs Cl^--ion concentration plot reveals that there is no similarity between them. It is thus evident that nickel-molybdenum alloys do not corrode as active-passive alloys in the same sense as do the Fe-Cr alloys or the stainless steels. Hence, the improved resistance to corrosion of Ni-Mo alloys is not linked to a passive state as suggested by Chassaing and Kinh[95].

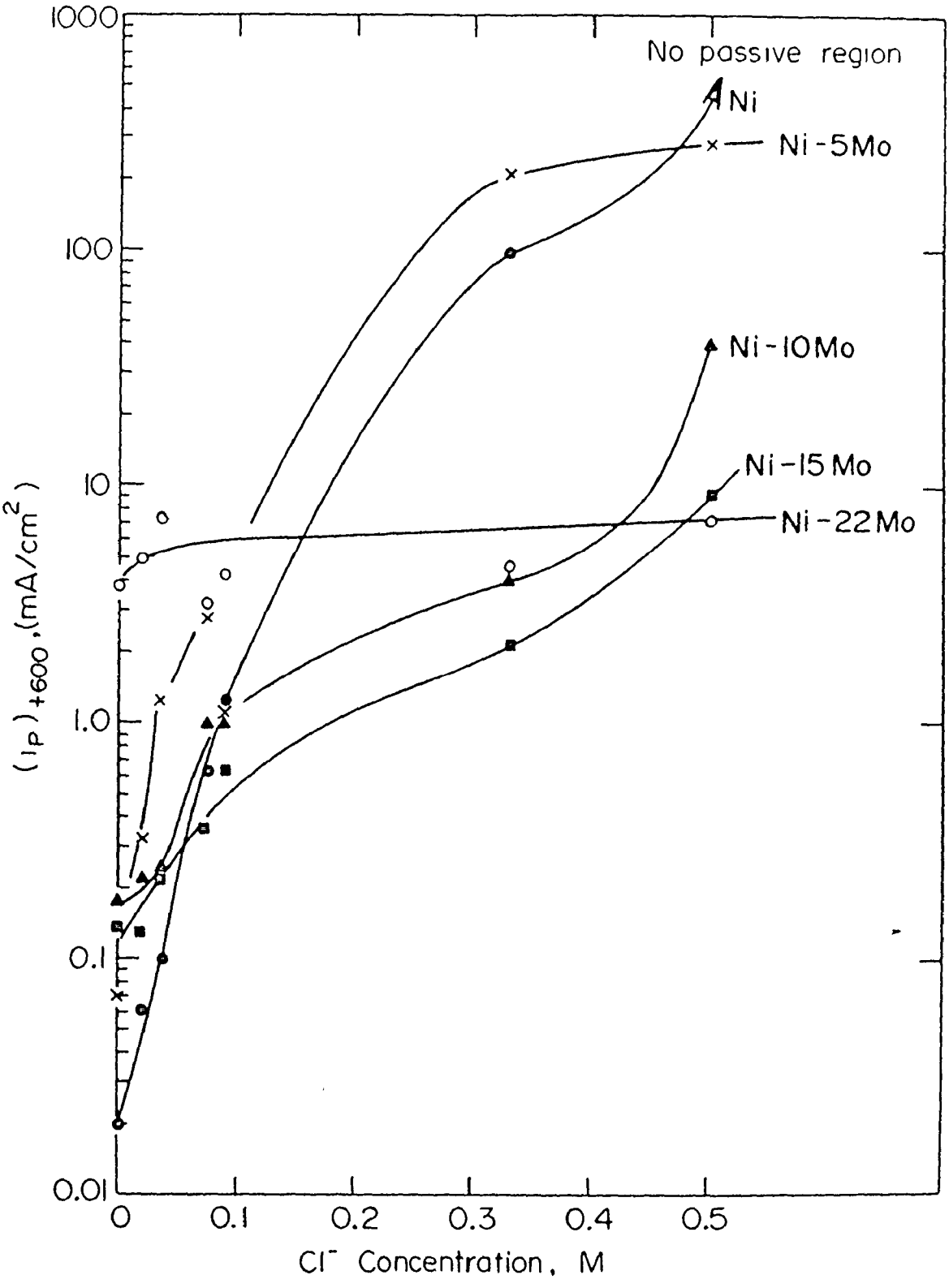

Figure 6-6. Passive current density at +600 mV as a function of the Cl^--ion concentration for Ni and Ni-Mo alloys.

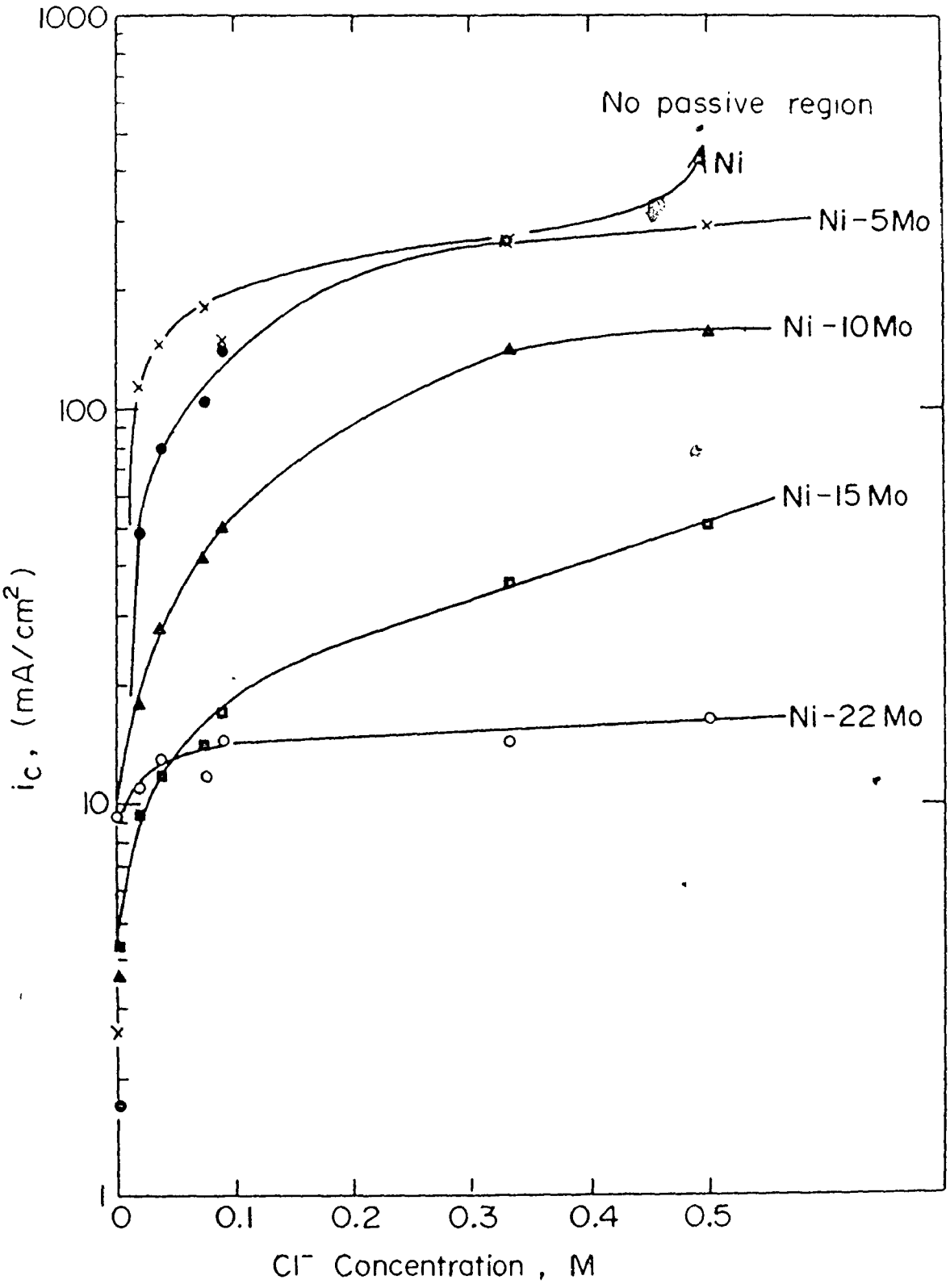

Figure 6-7. Critical current density as a function of the Cl^--ion concentration for Ni and Ni-Mo alloys.

A comparison of the freely corroding order and that from the (i_c) vs Cl^--ion concentration graph reveals that they are similar. Since the critical current density has been plotted, it implies that considerable anodic polarization of the alloys is required to produce the same corrosion trend as that of a freely corroding situation. It is thus concluded that nickel-molybdenum alloys corrode under anodic control through a barrier film. The importance of the film will become apparent in the next section. For the moment, it is pointed out that the same conclusion was made by Uhlig[7] who found that the addition of molybdenum to nickel did not change the hydrogen overvoltage but instead resulted in increased anodic polarization.

It is pointed out that at a Cl^--ion concentration of 0.33 M, no true passive region exists for Ni, Ni-5Mo and Ni-10Mo alloys. Therefore, in Figure 6-6, the current density cannot be considered as the passive current density. In fact, when the Cl^--ion concentration is 0.5 M, at +600 mV none of the alloys are truly passive and are then corroding through a barrier film. The corrosion order at 0.5 M Cl^- from Figure 6-6 is the same as that of the freely corroding situation.

6.8 Effect of Molybdenum Addition on the Corrosion Properties of Nickel

In general, the addition of molybdenum has a beneficial effect on the corrosion properties of nickel. In order to determine the mechanism of this beneficial effect, the essential features of the results outlined in the previous chapters will

be summarized below.

a) Potentiostatic polarization studies

- addition of molybdenum increases the corrosion rate in the passive region in 1N H_2SO_4

- addition of molybdenum decreases the corrosion rate at high chloride concentrations both in the passive and active regions .

b) Film thickness measurements

- the charge required to reduce the film (and consequently film thickness) decreases as molybdenum content increases

- the presence of chloride ions yields thinner films.

c) Potentiostatic activation studies

- higher molybdenum content decreases pitting susceptibility and yields a low value of b (growth rate) in the equation $i = kt^b$.

d) Repassivation characteristics

- the presence of molybdenum brings about a tendency for the decrease of the anodic current density during the reverse potential sweep.

e) Weight loss measurements

- increasing molybdenum content decreases the weight loss in 10% HCl

- the weight loss is lower for an alloy containing molybdenum in solid solution as compared to the same alloy containing a duplex structure.

Any model that is proposed to explain the corrosion behaviour of Ni-Mo alloys must be able to explain all the above experimentally observed features. The two situations that arise are - instances where the alloys corrode under no impressed current or potential and cases where the alloys are made to corrode under the influence of an applied potential.

The results presented reveal that molybdenum reduces the weight loss of the alloys in 10% HCl. Even in the actively corroding situation for the single phase alloys, the rate of increase of the current density with time (the exponent, b in the equation $i = kt^b$) decreases with increase in molybdenum content at a constant chloride concentration (Table 5-15). Further to the actively corroding situation, during repassivation studies when very high overvoltages are involved, a reversal in the potential sweep yields a decrease in the anodic current density, suggesting a real tendency for a decrease in the corrosion rate (Figures 5-33 to 5-36). Also, considerable polarization of the alloys is required to produce the same corrosion trend as that of a freely corroding situation. On the basis of these results it is concluded that the addition of molybdenum to nickel decreases the reactivity for dissolution of the alloy system. It is, therefore, suggested that at open circuit or in naturally corroding systems, the improved resistance to corrosion of Ni-Mo alloys is due to a sluggish anodic reaction due to a slow hydration of the metallic ions. The

slow hydration of the metallic ions is supported by a consideration of the metal-metal bond energy (E_{M-M}) as calculated from the heat of sublimation. Vijh[137] has suggested that metals such as molybdenum which have a high E_{M-M} value (26 kcals) do not corrode readily. On the other hand, metals such as iron with lower E_{M-M} value (17 kcals) are susceptible to corrosion.

It has been pointed out that upon anodic polarization Ni-Mo alloys corrode under anodic control through a barrier film. Chemical analysis has shown that more molybdenum is present in the film than in solution and electron diffraction has shown the film to be MoO_3. It is, therefore, suggested that under anodic polarization and in the presence of Cl^--ions, the improved resistance to corrosion of Ni-Mo alloys is due to the presence of a diffusion barrier film of MoO_3. According to Vijh[137] when a metal is covered by an oxide, any dissolution of the metal to give M^{n+} ions in solution would occur via the oxide film. He suggests that the work needed to extract an ion from the lattice of the oxide can be approximated in trend to U_L, the lattice energy per ion pair ($M^{n+} - O^{2-}$). He finds that for a corroding metal like iron, U_L = 724 kcals for $Fe^{3+} - O^{2-}$ ion ion pair while for non-corroding metals like molybdenum U_L = 1461 kcals for $M^{6+} - O^{2-}$ ion pair. Thus corroding metals not only leave their own lattice rather easily but also leave their oxide lattice more readily.

The conclusions on the mechanism of corrosion of Ni-Mo alloys will now be examined in light of the experimental obser-

vations. The passive film on nickel has been shown to be NiO. NiO is a p-type metal deficit semiconductor. It contains nickel vacancies ($\square^{=}_{Ni}$) and positive holes ($\oplus$, Ni^{3+} cations). The oxide film on nickel is almost stoichiometric NiO, the structure of which is shown in Figure 6-8(a). Let us examine what can happen when molybdenum is added to this film. The molybdenum cation (Mo^{6+}) sits on a nickel vacancy[134]. In order to conserve charge, three nickel vacancies are formed. This sequence can be represented in terms of the following equation.

$$MoO_3 \rightleftharpoons Mo^{6+}_{\square^{=}_{Ni}} + 3NiO + 3\square^{=}_{Ni}$$

where $Mo^{6+}_{\square^{=}_{Ni}}$ denotes a molybdenum cation of charge +6 on a nickel vacancy. This situation is the same as that encountered in cases of metallic oxidation[134] where the addition of a lower valence cation to NiO decreases the vacancy concentration (and oxidation rate) while the addition of a higher valence cation increases the vacancy concentration (and oxidation rate). The increased rate of oxidation manifests itself in the increased thickening of the film since the oxygen responsible for oxidation has no other chemical effect on the film. The situation in aqueous corrosion is noticably different since the solution is aggressive yielding a limiting film thickness. The effect of molybdenum addition is to form NiO which we suggest dissolves in the solution. Thus as the molybdenum content increases, film thickness decreases.

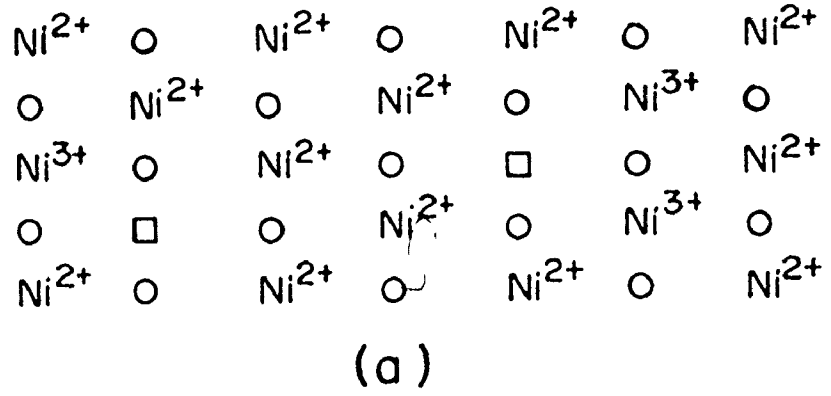

Figure 6-8. Effect of molybdenum addition on the defect structure of NiO.

The addition of a higher valence cation like Mo^{6+} to NiO also results in an increase in the vacancy concentration and a decrease in the electrical conductivity since the number of nickel vacancies is larger than that of the electron defects represented by Ni^{3+} cations. The higher the molybdenum content of the alloy, the greater the vacancy concentration. The presence of vacancies is responsible for a high diffusion rate of the alloy through the film and thus increased ionic conduction. Thus, as the molybdenum content increases, in the presence of a film, the corrosion rate increases. This is indeed found to be the case since it is experimentally observed that the passive current density in 1N H_2SO_4 increases with molybdenum content (Figure 5-8). This also suggests that films on higher molybdenum alloys would be unstable being thinner and more porous. This is also found to be experimentally true since the decrease in potential with time signifying film dissolution upon the application of a cathodic current is much faster as molybdenum content increases for the α-alloys (Figure 5-11).

The addition of chloride ions to the solution containing the alloy electrode has a significant effect on the nature of the passive film. The alloy constituents which pass into solution react with the solution to yield $MoCl_6$ and $NiCl_2$. As has been pointed out earlier, the chlorides hydrolyze according to -

$$MoCl_6 + 3H_2O \rightarrow MoO_3 + 6HCl \ , \ \Delta F^o = -122 \text{ kcals/mole}$$

$$NiCl_2 + H_2O \rightarrow NiO + 2HCl \ , \ \Delta F^o = +7.7 \text{ kcals/mole} \ .$$

It is evident that $NiCl_2$ does not hydrolyze whereas $MoCl_6$ hydrolyzes to yield MoO_3. It is suggested that this MoO_3 is formed as the outer layer on the surface of the alloy electrode. That the chloride ion is not a charge carrier but takes part chemically in the reaction is evident from the potentiostatic activation results of Ni-30Mo alloys where the anodic current density at +400 mV in 1N H_2SO_4 is constant with time and the addition of chloride ions leads to a decrease in the corrosion rate which becomes larger with time (Figure 5-39).

CHAPTER VII

CONCLUSIONS AND REMARKS

7.1 Conclusions

As a result of this investigation the following conclusions have been made -

i) A large amount of charge is consumed during the anodic oxidation of nickel in 1N H_2SO_4 solutions. However, only a small fraction, about 5%, of this charge is involved in film growth. The thickness of the passive film on nickel in 1N H_2SO_4 is between 6-16 Å for anodic oxidation times of 15-60 mins.

ii) Galvanostatic oxidation of nickel suggests that film growth occurs under the influence of an electric field which remains constant at constant current density. The kinetics of anodic oxidation of nickel in 1N H_2SO_4 are an 'inverse logarithmic' type in that the logarithm of the growth current density (i_g) is inversely proportional to the charge stored in the film (Q_f). Calculation of the resistivity of the film suggests that it is pure and almost stoichiometry NiO.

iii) The Flade potential of nickel in 1N H_2SO_4 corresponds to

that potential, more noble than E_{pp}, at which the surface of nickel is covered with a pore-free film of NiO and passivation is complete.

iv) Under potentiostatic polarization in chloride-containing solutions, the basic form of attack for Ni and Ni-Mo alloys occurs in the active region and beyond that only increases in intensity. Hence, the critical potential does not adequately describe the electrochemical conditions required for the pitting corrosion of Ni and Ni-Mo alloys in sulfuric acid solutions containing chloride ions. Thus, considerable caution must be exercized in interpreting data based on critical potentials to assess the pitting susceptibility of metals and alloys.

v) The passive film on nickel is capable of complete reduction in 1N H_2SO_4. The passive nickel electrode has been treated as a metal-semiconductor system and justification given for the assumption of a 100% efficiency for the current density during cathodic reduction. The concepts have been extended in a broader framework to include the Ni-Mo alloys.

vi) The charge required to reduce the film on the Ni-Mo alloys in 1N H_2SO_4 decreases with increasing molybdenum content and, in general, decreases even further when films are grown in the presence of chloride ions.

vii) The film formed on Ni-Mo alloys in 1N H_2SO_4 solutions containing chloride ions has been shown to be MoO_3. Ni-Mo

alloys corrode under anodic control through this barrier film.

viii) A drastic decrease in the corrosion rate of nickel occurs upon the addition of molybdenum. The improved resistance to corrosion of Ni-Mo alloys in naturally corroding systems is due to a sluggish anodic reaction imparted by a slow hydration of the metallic ions,while under anodic polarization in the presence of chloride ions it is due to the presence of a diffusion barrier film of MoO_3. These propositions are justified on the basis of a defect model for the passive film on the Ni-Mo alloys.

ix) A Ni-30Mo alloy exhibits the lowest corrosion rate in a supersaturated single phase condition. The equilibrium structure of the same alloy has a corrosion rate almost equal to that of pure nickel. The electrochemical behaviour of the Ni-30Mo alloy in various heat treated conditions is similiar to that of pure molybdenum in that neither exhibit an active-passive transition shown by the single phase α alloys.

7.2 Remarks

In rationalizing the complex processes that occur during the dissolution of binary alloys, it has generally been assumed that the individual components of an alloy system dissolve and are

present in solution in the same proportion as they are in the alloy. However, the results presented suggest that this is not true for the corrosion of Ni-Mo alloys. Surface enrichment of the nobler constituent, viz. molybdenum, occurs during anodic polarization and consequently the weight fraction of molybdenum in solution is lower than that in the alloy. Although some insight has been obtained into the passive film on the Ni-Mo alloys, a lack of detailed knowledge of the nature of the film is felt. It is suggested that future investigations aim to supplement the information reported here with detailed surface analysis of Ni-Mo alloys after various electrochemical treatments employing methods such as Auger spectroscopy.

This investigation has revealed that Ni-Mo alloys containing more than about 15% Mo are extremely promising for applications involving chloride ions, particularly sea water. It was also pointed out that the difficulties encountered in mechanically working the alloys increase with increasing molybdenum content. In an attempt to overcome this problem, it would be interesting to investigate the possibility of producing a layer of a Ni-Mo alloy on a nickel base. This could be achieved by bombarding nickel with molybdenum ions and then employing appropriate heat treatments to produce a surface layer of a Ni-Mo alloy. The composition and thickness of this layer would possibly be governed by the time and dose of bombardment.

The corrosion properties of alloy systems are known to be sensitive to the presence of other metals, notably

chromium. Investigations incorporating the presence of this element may be undertaken to study its influence on the corrosion properties of Ni-Mo alloys containing more than 15% Mo where part of the Mo and/or Ni is substituted with Cr. The extension of such an investigation to incorporate the presence of iron would be rewarding. Although this programme is rather ambitious, the knowledge obtained from it coupled with the information that already exists on the corrosion of the binary alloys of Ni, Mo, Cr and Fe would significantly add to an understanding of the phenomenon of corrosion of the Hastelloys and provide a more scientific basis for the development of alloys for the purpose of combating corrosion.

APPENDIX A

INDEXING OF X-RAY DIFFRACTION DATA

Diffraction in a crystal occurs only under the condition that Bragg's law is obeyed -

$$\text{i.e. } 2\,d\sin\theta = \lambda \qquad \text{(A-1(a))}$$

$$\text{or } 4d^2\sin^2\theta = \lambda^2 \qquad \text{(A-1(b))}$$

where d is the planar spacing, λ is the wavelength of the monochromatic x-rays incident on the crystal and θ is half of the angle between the incident and diffracted beam.

The value of d, the distance between adjacent planes in the set (hkℓ) for a cubic crystal is given by[109] -

$$\frac{1}{d^2} = \frac{h^2+k^2+\ell^2}{a_o^2} = \frac{s}{a_o^2} \,. \qquad \text{(A-2)}$$

Combining Eqns. (A-1(b)) and (A-2)

$$\frac{\sin^2\theta}{s} = \frac{\lambda^2}{4a_o^2} \,. \qquad \text{(A-3)}$$

A cubic crystal, therefore, gives diffraction lines whose $\sin^2\theta$ values satisfy Equation (A-3). Since the sum $s = (h^2+k^2+\ell^2)$ is always integral and $\lambda^2/4a_o^2$ is a constant for any one pattern, the problem of indexing the pattern of a cubic substance is one of finding a set of integers s which will yield a constant quotient when the observed $\sin^2\theta$ values are divided by s. The problem of indexing a diffraction pattern

becomes easier when it is known that the material under investigation is face-centered cubic. This implies that diffraction can only occur from un-mixed (hkℓ) index planes (odd and even).

In determining the lattice parameter of the α-solid solution for the nickel-molybdenum alloys, a suitable value of s was found so that $\sin^2\theta/s$ was a constant. Once this was done, knowing the value of λ, the value of the lattice parameter, a_o, was determined from Equation (A-3).

The value of λ used was as follows - for the single (un-split) peaks at low angles (the first two peaks in this case),

$$\lambda \text{ for Cu-}K_\alpha = 1.5418 \text{ Å since } K_\alpha = 2K_{\alpha_1} + K_{\alpha_2}$$

and for all other high angle peaks where the doublet was resolved,

$$\lambda \text{ for Cu-}K_{\alpha_1} = 1.5405 \text{ Å}.$$

In indexing the diffraction patterns for the alloys containing the β and γ phases, the value of the planar spacing, d, has been determined from Equation (A-1(a)).

Table A-1

Nickel

2θ	λ	$\sin^2\theta$	s	$\frac{\lambda^2}{4a_o^2}$	a_o (Å)	hkℓ
44.55	K_α	0.144	3	0.0479	3.522	111
51.82	K_α	0.191	4	0.0478	3.526	200
76.33	K_{α_1}	0.382	8	0.0477	3.526	220
92.89	K_{α_1}	0.525	11	0.0477	3.525	311
98.39	K_{α_1}	0.573	12	0.0477	3.525	222
121.86	K_{α_1}	0.764	16	0.0477	3.525	400
144.67	K_{α_1}	0.908	19	0.0478	3.524	331
155.68	K_{α_1}	0.956	20	0.0478	3.524	420

From the a_o vs $\sin^2\theta$ graph, at $\sin^2\theta = 1$, $a_o = 3.524$ Å.

From the ASTM card no. 4-0850 for Nickel, $a_o = 3.523(8)$ Å.

Table A-2

Ni-5Mo Alloy

2θ	λ	$\sin^2\theta$	s	$\frac{\lambda^2}{4a_o^2}$	a_o (Å)	hkℓ
44.44	K_α	0.142	3	0.0475	3.538	111
51.64	K_α	0.190	4	0.0474	3.538	200
76.00	K_{α_1}	0.379	8	0.0474	3.538	220
92.45	K_{α_1}	0.521	11	0.0474	3.538	311
97.88	K_{α_1}	0.569	12	0.0474	3.538	222
121.11	K_{α_1}	0.758	16	0.0474	3.538	400
143.28	K_{α_1}	0.900	19	0.0474	3.538	331
153.70	K_{α_1}	0.940	20	0.0474	3.538	420

Table A-3

Ni-10Mo Alloy

2θ	λ	$\sin^2\theta$	s	$\frac{\lambda^2}{4a_o^2}$	a_o (Å)	hkℓ
44.18	K_α	0.141	3	0.0471	3.552	111
51.43	K_α	0.188	4	0.0471	3.552	200
75.67	K_{α_1}	0.376	8	0.0470	3.552	220
91.98	K_{α_1}	0.517	11	0.0470	3.552	311
97.38	K_{α_1}	0.564	12	0.0470	3.552	222
120.32	K_{α_1}	0.752	16	0.0470	3.552	400
141.94	K_{α_1}	0.894	19	0.0470	3.552	331
151.85	K_{α_1}	0.941	20	0.0470	3.552	420

Table A-4

Ni-15Mo Alloy

2θ	λ	$\sin^2\theta$	s	$\frac{\lambda^2}{4a_o^2}$	a_o (Å)	hkℓ
43.99	K_α	0.140	3	0.0468	3.565	111
51.24	K_α	0.187	4	0.0467	3.561	200
75.36	K_{α_1}	0.374	8	0.0467	3.564	220
91.54	K_{α_1}	0.513	11	0.0467	3.565	311
96.90	K_{α_1}	0.560	12	0.0467	3.565	222
119.60	K_{α_1}	0.747	16	0.0467	3.565	400
140.68	K_{α_1}	0.887	19	0.0467	3.565	331
152.20	K_{α_1}	0.934	20	0.0467	3.565	420

Table A-5

Ni-22Mo Alloy

2θ	λ	$\sin^2\theta$	s	$\frac{\lambda^2}{4a_o^2}$	a_o (Å)	hkℓ
43.83	K_α	0.139	3	0.0464	3.578	111
51.01	K_α	0.185	4	0.0464	3.581	200
74.95	K_{α_1}	0.370	8	0.0463	3.581	220
91.00	K_{α_1}	0.509	11	0.0462	3.582	311
96.25	K_{α_1}	0.554	12	0.0462	3.583	222
118.63	K_{α_1}	0.739	16	0.0462	3.583	400
139.24	K_{α_1}	0.879	19	0.0462	3.582	331
148.15	K_{α_1}	0.925	20	0.0462	3.582	420

From the a_o vs $\sin^2\theta$ graph, at $\sin^2\theta = 1$, $a_o = 3.582$ Å

The three extra peaks associated with the Ni-22Mo alloy can be index as follows -

2θ	λ	$\sin\theta$	d(Å)	$d^*_{Ni_4Mo}$ (Å)
40.76	K_α	0.3482	2.214	-
43.10	K_α	0.3673	2.099	2.05
45.30	K_α	0.3851	2.002	1.99

*From ASTM card no. 3-1036 for Ni_4Mo.

Table A-6

Ni-30Mo Alloy

950°C, 8 hrs, Furnace Cooled

2θ	λ	sin θ	Observed d(Å)	ASTM Card 3-1036 (Ni_4Mo) d(Å)
22.10	K_α	0.192	4.02	3.92
29.50	K_α	0.255	3.03	2.96
31.35	K_α	0.270	2.85	2.80
43.48	K_α	0.370	2.08	2.05
50.73	K_α	0.428	1.80	1.79
56.35	K_α	0.472	1.63	1.63
61.28	K_α	0.510	1.51	1.50
64.65	K_α	0.534	1.45	1.43
74.43	K_α	0.605	1.28	1.28
90.50	K_α	0.710	1.09	1.08
95.70	K_α	0.741	1.04	1.03
116.78	K_α	0.852	0.905	0.903
137.38	K_α	0.932	0.828	0.823

From the analytical indexing method[109]

$$a_o = 5.699 \text{ Å}$$

$$c_o = 3.579 \text{ Å}, \quad c/a = 0.628$$

and from the ASTM and no. 3-1036 for Ni_4Mo

$$a_o = 5.720 \text{ Å}$$

$$c_o = 3.564 \text{ Å}, \quad c/a = 0.623$$

Table A-7

Ni-30Mo Alloy

950°C, 8 hrs, Furnace Cooled

Some of the peaks in the pattern of the Ni-30Mo alloy given in Table A-6 can be index to be a face-centered cubic α of composition Ni_4Mo. Examples of such a phase are present in the literature [52,93]

2θ	λ	$\sin^2\theta$	s	$\frac{\lambda^2}{4a_o^2}$	a_o (Å)	hkℓ
43.48	K_α	0.137	3	0.0457	3.6049	111
50.73	K_α	0.184	4	0.0459	3.5991	200
74.43	K_α	0.366	8	0.0457	3.6052	220
90.50	K_α	0.504	11	0.0459	3.6002	311
95.70	K_α	0.550	12	0.0458	3.6020	222
116.78	K_α	0.725	16	0.0453	3.6208	400
137.38	K_α	0.868	19	0.0457	3.6069	331

From the a_o vs $\sin^2\theta$ graph, at $\sin^2\theta = 1$, $a_o = 3.6075$ Å

Table A-8

Ni-30Mo Alloy

800°C, 50 hrs

2θ	λ	sinθ	Observed d(Å)	α d(Å)	β d(Å)	γ d(Å)
21.85	K_α	0.190	4.068	-	-	
29.43	K_α	0.254	3.035	-	-	3.06
31.10	K_α	0.268	2.876	-	2.80	-
43.33	K_α	0.369	2.088	2.083	2.05	-
46.10	K_α	0.392	1.969	-	-	1.969
46.45	K_α	0.394	1.955	-	-	1.951
50.20	K_α	0.424	1.817	1.804	1.79	-
64.00	K_α	0.530	1.455	-	1.43	-
73.85	K_α	0.601	1.283	-	1.28	1.28
74.53	K_α	0.606	1.273	1.275	-	-
89.70	K_{α_1}	0.705	1.092	-	-	1.094
91.08	K_{α_1}	0.714	1.079	1.088	1.08	1.085
95.38	K_{α_1}	0.740	1.042	1.041	1.03	-
116.48	K_{α_1}	0.850	0.906	0.902	-	-
135.85	K_{α_1}	0.927	0.831	-	0.829	-
137.85	K_{α_1}	0.933	0.826	0.828	-	-

Value of d for the α-phase was calculated by using a_o = 3.6075 Å, obtained from Table A-7

β-phase - ASTM card no. 3-1036 for Ni_4Mo

γ-phase - ASTM card no. 15-572 for Ni_3Mo

Table A-9

Ni-30Mo Alloy

800°C, 1200 hrs

2θ	λ	sinθ	Observed d(Å)	α d(Å)	β d(Å)	γ d(Å)
21.88	K_α	0.190	4.062	-	-	-
29.46	K_α	0.254	3.032	-	-	3.06
31.15	K_α	0.268	2.871	-	2.80	-
40.35	K_α	0.345	2.235	-	-	2.224
40.81	K_α	0.349	2.211	-	-	2.220
43.44	K_α	0.370	2.083	2.083	2.05	-
45.90	K_α	0.390	1.977	-	-	1.969
46.33	K_α	0.393	1.960	-	-	1.951
50.30	K_α	0.425	1.814	1.804	-	-
51.20	K_α	0.432	1.784	-	1.79	1.784
73.83	K_{α_1}	0.601	1.282	-	1.28	1.280
74.55	K_{α_1}	0.606	1.272	1.275	-	1.267
89.75	K_{α_1}	0.706	1.092	-	-	1.094
91.15	K_{α_1}	0.714	1.079	1.088	1.08	-
95.48	K_{α_1}	0.740	1.041	1.041	1.03	-
116.25	K_{α_1}	0.849	0.907	0.902	0.907	-
135.95	K_{α_1}	0.927	0.831	0.828	0.829	-
137.90	K_{α_1}	0.933	0.825	-	0.823	-
143.33	K_{α_1}	0.949	0.811	-	0.814	-
144.65	K_{α_1}	0.953	0.808	-	0.809	-
148.70	K_{α_1}	0.963	0.800	-	0.798	-

Values of d for the phases are from the sources of Table A-8

APPENDIX B

DERIVATION OF THE KINETIC EQUATION FOR INITIAL FILM THICKNESS

Since there is no redox reaction in the potential range between the hydrogen and oxygen electrode in H_2SO_4 solution[66], the observed anodic current of a passive nickel electrode indicates the difference between the rate of film formation and the dissolution rate of the oxide. At steady state, these rates are equal. Such a condition is fulfilled in the passive region of a nickel electrode in 1N H_2SO_4 where the anodic current density is independent of potential. Under such conditions, the rate of thickening of the oxide film is,

$$\frac{dQ_f}{dt} = (i_g - i_d) \qquad \text{(B-1)}$$

where i_g = anodic growth current density, A/cm^2

i_d = equivalent dissolution current density of oxide film, A/cm^2

Q_f = thickness of the oxide film, represented in the equivalent coulombs of metal ion, C/cm^2

t = time, sec.

Since i_d is constant in the passive region, at a constant growth current density (under galvanostatic conditions), we have integrating,

$$Q_f = (i_g - i_d)t + A$$

at $t = 0$, $Q_f = Q_i$

$$\therefore A = Q_i$$

$$\therefore Q_f = (i_g - i_d)t + Q_i \quad . \qquad \text{(B-2)}$$

Since it has been shown[75-77] that the film thickness is proportional to the potential implying that the electric field is constant during film growth, we have

$$E-E_1 \propto Q_f$$

$$\text{or} \quad E-E_1 = KQ_f \qquad \text{(B-3)}$$

where $E-E_1$ = potential difference between the metal/oxide and oxide/solution interface.

Now, $E = E_1$ when $Q_f = 0$. This condition is fulfilled at the initial instant when there is no film, implying that there is no current and consequently no potential difference either. This potential is the potential for the spontaneous passivation of nickel and is the Flade potential, E_F. Thus, in Eqn. (B-3), E_1 can be replaced by E_F

$$\therefore E - E_F = KQ_f. \qquad \text{(B-4)}$$

And combining with Eqn. (B-2),

$$E - E_F = K\{(i_g - i_d)t + Q_i\} \quad . \qquad \text{(B-5)}$$

The importance of Eqn. (B-5) lies in that all the quantities in it, except Q_i, are known and thus the initial film thickness can be calculated. A knowledge of Q_i serves to yield the percentage of the total anodic charge which is involved in film growth.

APPENDIX C

MECHANICAL PROPERTIES OF Ni-Mo ALLOYS

The mechanical properties of the Ni-Mo alloys were determined by tensile testing flat specimens by an Instron testing machine. Only one specimen was tested whose geometry is shown in Figure C-1. The results are given below.

Alloy	Yield Strength psi$\times 10^3$	Ultimate Tensile Strength psi$\times 10^3$	% Elongation in 3/4" gauge length
Ni	3.3	47.5	40
Ni-5Mo	17.3	70.0	45
Ni-10Mo	28.3	84.8	40
Ni-15Mo	39.8	103.4	40
Ni-22Mo	47.2	118.0*	45

It can be seen that the strength of Ni-Mo alloys increases with increase in molybdenum content and even with 22% Mo the alloys are very ductile.

---

*UTS calculated from the load at fracture. Specimen fractured before reaching maximum load.

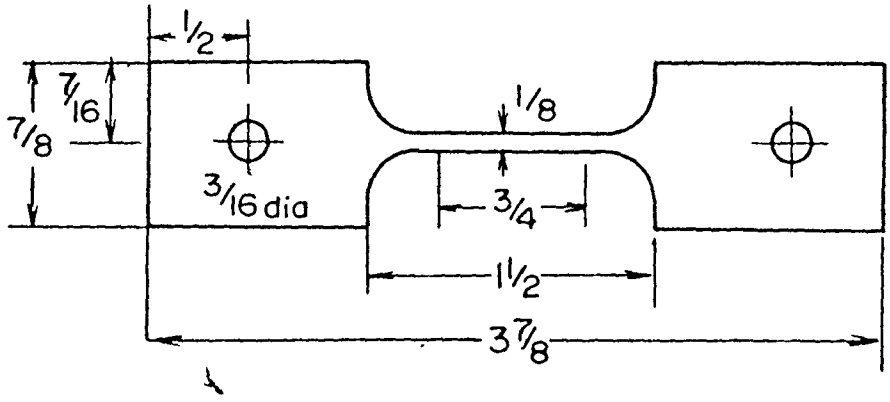

All dimensions in inches.

Figure C-1. Diagram showing the dimensions of the tensile test specimens (Appendix C)

REFERENCES

1. U.R. Evans, 'The Corrosion and Oxidation of Metals', p 3, Edward Arnold Ltd., London (1971).
2. B.E. Wilde, 'Localized Corrosion', p. 342, NACE (1974).
3. G.K. Jha, M. Eng. Thesis, McMaster University (1971).
4. M. Henthorne, 'Intergranular Corrosion in Iron and Nickel-Base Alloys', p 66, in 'Localized Corrosion - Cause of Metal Failure' ASTM Publication 516 (1972).
5. K.T. Aust and O. Iwao, 'Localized Corrosion', p 62, NACE (1974).
6. M.G. Fontana and N.D. Greene, 'Corrosion Engineering', p 31 McGraw-Hill Book Co., New York (1967).
7. H.H. Uhlig, 'Corrosion and Corrosion Control', p 353, John Wiley & Sons Inc., New York (1971).
8. H.H. Uhlig, 'Corrosion Handbook', p 253, John Wiley & Sons Inc., New York (1958).
9. B.E. Field, Trans. AIME, 83, 149 (1929).
10. J.O'M. Bockris and A.K.N. Reddy, 'Modern Electrochemistry', Vol. 2, p 879, Plenum Press, New York (1970).
11. K.J. Vetter, 'Electrochemical Kinetics - Theoretical and Experimental Aspects', p. 138, Academic Press Inc., New York (1967).
12. N.D. Tomashov, 'Theory of Corrosion and Protection of Metals, p 329, The MacMillan Co., New York (1966).
13. M. Faraday, cited in 'Passivity and Protection of Metals against Corrosion', N.D. Tomashov and G.P. Chernova, p 12, Plenum Press, New York (1967).

14. U.R. Evans, 'Metallic Corrosion, Passivity and Protection', p 4, Edward Arnold Ltd., London (1946).

15. J. Langmuir, J. Chem. Soc., 62, 517 (1940).

16. I.N. Stranski, Z. Electrochem., 45, 393 (1929); 46, 25 (1930).

17. H.H. Uhlig and J. Wulff, Trans. AIME, 135, 494 (1939).

18. H. H. Uhlig , Trans. Electrochem. Soc., 85, 307 (1944).

19. H.H. Uhlig, Z. Electrochem., 62, 700 (1958).

20. J. Osterwald and H.H. Uhlig, J. Electrochem. Soc., 108, 515 (1961).

21. G. Tammann, Z. Anorg. Chem., 169, 151 (1928).

22. H. Feller and H.H. Uhlig, J. Electrochem. Soc., 107, 864 (1960)

23. T.P. Hoar, D.C. Mears and G.P. Rothwell, Corr. Sci., 5, 279 (1965).

25. T.P. Hoar, Corr. Sci., 7, 341 (1967).

26. T.P. Hoar and W.R. Jacob, Nature, 216, 1299 (1967).

27. Ja. M. Kolotyrkin, J. Electrochem. Soc., 108, 209 (1961).

28. C. Edeleanu and W.R. Evans, Trans. Faraday Soc., 47, 1121 (1951).

29. H.J. Engell and N.D. Stolica, Z. Phys. Chem., 20, 113 (1959).

30. M.A. Streicher, J. Electrochem. Soc., 106, 161 (1959).

31. H. Coriou, J. Hure and G. Plante, Electrochim. Acta, 5, 105 (1961).

32. J.S. Armijo and B.E. Wilde, Corr. Sci., 8, 649 (1968).

33. H.H. Uhlig, P. Bond and H. Feller, J. Electrochem. Soc. 110, 650 (1963).

34. J.R. Ambrose and J. Kruger, Proc. 4th Int. Cong. on Met. Corr., p 698, NACE (1972).

35. C.L. McBee and J. Kruger, 'Localized Corrosion', p 252, NACE (1974).

36. G. Bianchi, A. Cerquetti, F. Mazza and G. Torchio, Corr. Sci., 10 19 (1970); 'Localized Corrosion', p 399, NACE (1974).

37. R. Stickler and A. Vinckier, Corr. Sci., 3, 1 (1963).

38. S. Alm and R. Kiessling, J. Inst. Metals, 91, 190 (1963).

39. C. Strawström and M. Hillert , Iron and Steel Inst., 77, Jan. (1969).

40. C.S. Tedmon, D.A. Vermilyea and J.H. Rosolowski, J. Electrochem. Soc., 118, 192 (1971).

41. G. Grube and H. Schlecht, Z. Electrochem., 44, 413 (1938).

42. G. Grube and O. Winkler, Z. Electrochem., 44, 423 (1938).

43. F.H. Ellinger, Trans. ASM, 30, 607 (1942).

44. P.V. Guthrie and E.E. Stansbury, Rept. ORNL-3078, Oak Ridge National Laboratory, Oak Ridge, Tennessee (July 1961).

45. D. Harker, J. Chem. Phys. 12, 315 (1944).

46. E. Ruedl and S. Amelinckx, Mat. Res. Bull., 4, 361 (1969) Crys. Lattice Defects, 2, 247 (1971).

47. W.B. Pearson,'Handbook of Lattice Spacings and Structures of Metals', p 753, Pergamon Press (1964).

48. E. Ruedl, P. Delavignette and S. Amelinckx, Phys. Stat. Sol., 28, 305 (1968).

49. M. Yamamoto, S. Nenno, T. Saburi and Y. Mizutani, Trans. Jap. Inst. Metals, 11, 120 (1970).

50. P.R. Okamoto and G. Thomas, Acta Met., 19, 825 (1971).

51. T. Saburi, K. Komatsu, M. Yamamoto, S.Nenno and Y. Mizutani, Trans. AIME, 245, 2348 (1969).

52. J.E. Spruiell and E.E. Stansbury, J. Phys. Chem. Solids, 26, 811 (1965).

53. K. Schwabe and W. Schmidt, Corr. Sci., 10, 143 (1970).

54. K. Schwabe and U. Ebersbach, Proc. 4th Int. Cong. on Met. Corr., p 709, NACE (1972).

55. K. Schwabe, J. Electrochem. Soc., 110, 663 (1963).
Electrochim. Acta, 3, 186 (1960).

56. R.L. Cowan and R.W. Staehle, J. Electrochem. Soc., 118, 557 (1971).

57. T.S. de Gromoboy and L.L. Shrier, Electrochim. Acta, 11, 895 (1966).

58. A.K.N. Reddy, M.G.B. Rao and J.O'M. Bockris, J. Chem. Phys., 42, 2246 (1965).
J. Electrochem. Soc. 113, 1133 (1966).

59. A.C. Makrides, J. Electrochem. Soc., 113, 1159 (1966); 109, 977 (1962).

60. W.J. Müller, Z. Electrochem. 30, 401 (1922).

61. A.K.N. Reddy and M.G.B. Rao, Can. J. Chem., 47, 2693 (1969).

62. J. Siejka, C. Cherki and Y. Yahalon, J. Electrochem. Soc., 119, 991 (1972)
Electrochim. Acta, 17, 161 (1972).

63. D. Toumi, J. Electrochem. Soc., 112, 1 (1965).

64. B. MacDougall and M. Cohen J. Electrochem. Soc., 121, 1152 (1974).

65. R. D. Armstrong and M. Henderson, J. Electroanal. Chem., 39, 222 (1972).

66. M. Pourbaix, 'Atlas of Electrochemical Equilibria in Aqueous Solutions', p 330, Pergamon Press Ltd., (1966).

67. N. Sato and G. Okamoto, J. Electrochem. Soc.,110, 605 (1963).

68. D.E. Davies and W. Barker, Corrosion,20, 47t (1964).

69. Y. Yahalom and I. Weisshauss, 'Localized Corrosion', p. 410, NACE (1974).

70. I.A. Ammar and S. Darwish, Electrochim. Acta, 13, 781 (1968).

71. L. Tronstad, Z. Phys. Chem., 142, 241 (1929).

72. K. Arnold and K.J. Vetter, Z. Electrochem., 64, 407 (1960).

73. H. Pfisterer, A. Politycki and E. Fuchs, Z. Electrochem., 63, 257 (1959).

74. N. Sato, K. Kudo and M. Miki, J. Japan Inst. Metals, 35, 1007 (1971).

75. G. Okamoto, H. Kobayashi, M. Nagayama and N. Sato, Z. Electrochem., 62, 775 (1958).

76. I.A. Ammar and S. Darwish, Electrochim. Acta, 12, 225 (1967).

77. G. Okamoto and N. Sato, J. Electrochem. Soc. Japan (Overseas Ed), 27, E125 (1959).

78. T. Koizumi and H.H. Uhlig, J. Electrochem. Soc., 121, 1137 (1974).

79. J. Postlethwaite, Electrochim. Acta, 12, 333 (1967).

80. Z. Szklarska-Smialowska, Corr. Sci., 11, 209 (1971).

81. F.G. Hodge and B.E. Wilde, Corrosion, 26, 146 (1970).

82. M. Zamin and M.B. Ives, Corrosion,29, 319 (1973).

83. Z. Szklarska-Smialowska, Corr. Sci., 12, 527 (1972).

84. M. Zamin, M. Eng. Thesis, McMaster University (1972).

85. T. Tokuda and M.B. Ives, Corr. Sci., 11, 297 (1971).

86. I. Garz and U. Häfke, Corr. Sci., 11, 329 (1971).

87. M. Zamin and M.B. Ives, J. Electrochem. Soc., 121, 1141 (1974).

88. I. Garz, H. Worch and W. Schatt, Corr. Sci., 9, 71 (1969).

89. S.W. Parr, Trans. Am. Inst. Metals, 8, 211 (1915).

90. G. Massing and G. Roth, Werkst. u. Korr., 3, 176, 253 (1952).

91. S.S. Pavlov and T.V. Svistunova, Mettaloved. Term. Obrab. Metal, 11, 13 (1968).

92. E. Ruedl, J. Mat. Sci., 7, 1342 (1972).

93. E. Ruedl, Proc. 8th Italian Congress on Electron Microscopy, Milan (1972).

94. N.D. Greene, Proc. 1st Int. Cong. on Met. Corr., p. 113, Butterworths, London (1962).

95. E. Chassaing and M. Vu Quang Kinh, C. R. Acad. Sci., 278, C, 1397 (1974).

96. K.E. Heusler, Corr. Sci., 6, 183 (1966).

97. 'Metals Handbook', Vol. 2 'Heat Treating, Cleaning and Finishing', 8th edition, p. 259, 267, ASM, Metals Park, Ohio (1964).

98. M.R. Arora and R. Kelly, J. Electrochem. Soc., 119, 270 (1972).

99. A. P. Bond and H.H. Uhlig, J. Electrochem. Soc., 107, 488 (1960).

100. R.P. Frenkenthal, J. Electrochem. Soc., 116, 580 (1969).

101. K. Nii, Corr. Sci., 10, 571 (1970).

102. G.M. Bullman and A.C.C. Tseung, Corr. Sci., 12, 415 (1972).

103. M. Okuyama and S. Haruyama, Corr. Sci.,14, 1 (1974).

104. K.G. Weil, Z. Electrochem., 59, 711 (1955).

105. Ja. M. Kolotyrkin, Corrosion, 19, 261t (1963).

106. W. Schwenk, Corrosion, 20, 129t (1964).

107. Z. Szklarska-Smialowska and M. Janik-Czachor, 'Localized Corrosion', p. 353, NACE (1974).

108. Z. Szklarska-Smialowska, Corrosion, 29, 319 (1973).

109. B.D. Cullity, 'Elements of X-Ray Diffraction', Addison-Wesley Pub. Co., Inc., New York (1959).

110. N.D. Stolica, Corr. Sci., 9, 205 (1969).

111. B.E. Conway, 'Theory and Principles of Electrode Processes', p. 140, The Ronald Press Co., New York (1965).

112. N. Cabrera and N.F. Mott, Rep. Prog. Phys., 12, 163 (1949).

113. L. Young, 'Anodic Oxide Films', Academic Press, London (1961).

114. R.V. Moshtev, Ber. Bun. Phys. Chem., 71, 1079 (1967).

115. J.L. Ord, J. Electrochem. Soc., 113, 213 (1966).

116. Z.M. Jarzebski, 'Oxide Semiconductors', p.150, Pergamon Press, Warsaw (1973).

117. G. Okamoto and N. Sato, Trans. JIM, 1, 16 (1960).

118. Z. Szklarska-Smialowska, Corrosion, 27, 233 (1971).

119. M. Pourbaix et al, Corr. Sci., 3, 239 (1963).

120. C. Wagner and W. Traud, Z. Electrochem., 44, 391 (1938).

121. S.C. Sircar, U.K. Chatterjee, M. Zamin and H.G. Vijayendra, Corr. Sci. 12, 217 (1972).

122. P. Forchhammer and H.J. Engell, Werkst. u. Korr., 20, 1 (1969).

123. Z. Szklarska-Smialowska and M. Janik-Czachor, Brit. Corrosion J., 4, 138 (1969).

124. L. Tronstad, Trans. Faraday Soc., 29, 502 (1938).

125. N. Nagayama and M. Cohen, J. Electrochem. Soc., 109, 781 (1962).

126. G. Aronowitz and N. Hackerman, J. Electrochem. Soc., 110, 683 (1963).

127. D.E. Davies, U.R. Evans and J.N. Agar, Proc. Roy. Soc., 225A, 443 (1955).

128. A.J. Dekker, 'Solid State Physics', p. 223, MacMillan and Co., London, (1967).

129. F.K. Richtmyer, E.H. Kennard and J.N. Cooper, 'Introduction to Modern Physics', 6th ed., p 628, McGraw-Hill Book Co. (1969).

130. L. Solymar and D. Walsh, Lectures on the Electrical Properties of Materials', p 112, Clarendon Press, Oxford (1970).

131. S. Kabashima, J. Phys. Soc. Japan, 26, 975 (1969).

132. R.L. Sproull, 'Modern Physics', p. 453, John Wiley & Sons, Inc., New York (1967).

133. I. Terzić and B. Perović, Surf. Sci., 21, 86 (1970).

134. O. Kubaschewski and B.E. Hopkins, 'Oxidation of Metals and Alloys', p 92, Butterworth and Co. Ltd., London (1962).

135. H. Taube, Chem. Revs., 50, 69 (1952).

136. A. K. Vijh, Corr. Sci., 11, 161 (1971).

137. A.K. Vijh, 'Influence of Solid State Properties on Electrochemical Behaviour', in 'The Anodic Behaviour of Metals and Semiconductor Series', ed. J.W. Diggle, M. Dekker, Inc., New York (1973).